AD-A110 409 TEXAS TECH UNIV LUBBOCK DEPT OF ELECTRICAL ENGINEERING F/G 20/3
COORDINATED RESEARCH PROGRAM IN PULSED POWER PHYSICS.(U)
DEC 81 M KRISTIANSEN, M O HAGLER F49620-79-C-0191
UNCLASSIFIED AFOSR-TR-82-0018 NL

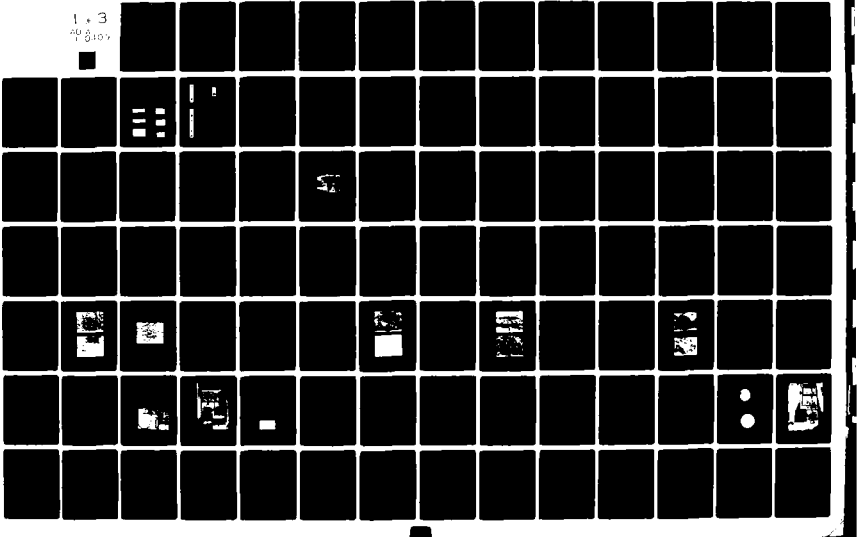

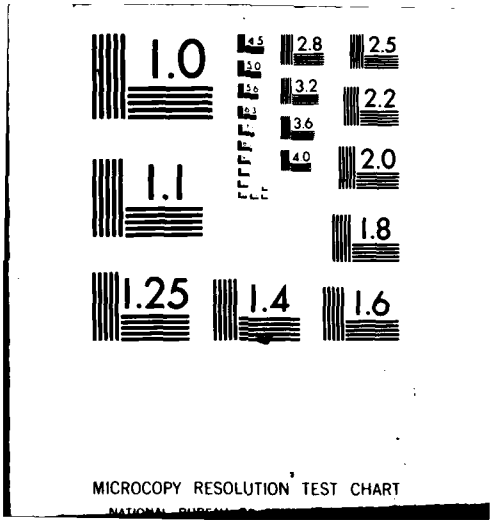
1.0
1.1
1.25
1.4
1.6
1.8
2.0
2.2
2.5
2.8
3.2
3.6
4.0
4.5
5.0
5.6
MICROCOPY RESOLUTION TEST CHART

LEVEL

(5)

SECOND ANNUAL REPORT

on

COORDINATED RESEARCH PROGRAM

in

PULSED POWER PHYSICS

December 1, 1981

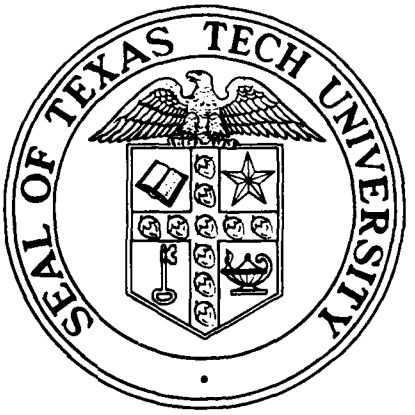

Air Force Office of Scientific Research
Contract No. F49620-79-C-0191

PLASMA AND SWITCHING LABORATORY
LASER LABORATORY

Department of Electrical Engineering
TEXAS TECH UNIVERSITY

Lubbock, Texas 79409

(8)

Unclassified

SECURITY CLASSIFICATION OF THIS PAGE (When Data Entered)

REPORT DOCUMENTATION PAGE		READ INSTRUCTIONS BEFORE COMPLETING FORM
1. REPORT NUMBER AFOSR-TR- 82-0018	2. GOVT ACCESSION NO. AD-A110 409	3. RECIPIENT'S CATALOG NUMBER
4. TITLE (and Subtitle) Coordinated Research Program in Pulsed Power Physics		5. TYPE OF REPORT & PERIOD COVERED Annual 10/1/80 - 9/30/81
		6. PERFORMING ORG. REPORT NUMBER
7. AUTHOR(s) M. Kristiansen M.O. Hagler		8. CONTRACT OR GRANT NUMBER(s) F49620-79-C-0191
9. PERFORMING ORGANIZATION NAME AND ADDRESS Department of Electrical Engineering Texas Tech University Lubbock, Texas 79409		10. PROGRAM ELEMENT, PROJECT, TASK AREA & WORK UNIT NUMBERS 2301/A7 61102F
11. CONTROLLING OFFICE NAME AND ADDRESS AFOSR BLDG 410, Bolling AFB, D.C. 20332		12. REPORT DATE December 1, 1981
		13. NUMBER OF PAGES 250
14. MONITORING AGENCY NAME & ADDRESS(if different from Controlling Office)		15. SECURITY CLASS. (of this report) Unclassified
		15a. DECLASSIFICATION/DOWNGRADING SCHEDULE

16. DISTRIBUTION STATEMENT (of this Report)

Approved for public release; distribution unlimited.

17. DISTRIBUTION STATEMENT (of the abstract entered in Block 20, if different from Report)

18. SUPPLEMENTARY NOTES

19. KEY WORDS (Continue on reverse side if necessary and identify by block number)

Pulsed Power, Switching, Electromechanical Pulse Device, Laser Triggering, Electron Beam Triggering, Surface Physics, Electrode Erosion, Spark Gap, Discharge, Spectroscopy, Opening Switches

20. ABSTRACT (Continue on reverse side if necessary and identify by block number)

Ten program elements related to pulsed power research are described. These program elements form a multi-disciplinary, coordinated program whose main emphasis is to gain improved understanding of high power, repetitive closing and opening switches. The main emphasis is concerned with triggering of discharges in gas filled spark gaps and the associated electrode erosion and insulator damage. Considerable efforts are also being made to understand the limitations and fundamental discharge phenomena in fast opening switches for inductive energy storage. A novel electromechanical pulse generator which promises to deliver fast, repetitive pulses to a load is also being investigated.

DD FORM 1 JAN 73 1473 EDITION OF 1 NOV 65 IS OBSOLETE

Uniclassified

SECURITY CLASSIFICATION OF THIS PAGE (When Data Entered)

4

Second Annual Report on

COORDINATED RESEARCH PROGRAM IN PULSED POWER PHYSICS

AFOSR Contract #F49620-79-C-0191

December 1, 1981

Program Director:	M. Kristiansen
Associate Program Director:	M. Hagler
Principal Investigators:	J. Craig M. Hagler L. Hatfield M. Kristiansen E. Kunhardt G. Schaefer K. Schoenbach F. Williams
Subcontractor:	SRI International D. Lorents L. Lee
Post Doctoral Fellow:	S. Kaplan
Associate Investigators:	H. Carper J. Marx R. Pedersen W. Fo·
Technician III:	K. Zinsmey
Secretary III:	M. Byrd
Secretary II:	C. Wang+

Graduate Students:
R. Biesele
S. Dahli
A. Donaldson
R. Dougal
H. Dunlap
L. Gordon
H. Harjes
G. Hutchinson
G. Jackson
D. Johnson
G. Leiker
R. Ness
T. Tzeng
C. Yeh*

+ Resigned effective August 14, 1981

* Paid by Republic of China (Taiwan)

TABLE OF CONTENTS

CONTRACT WORK STATEMENTS

The contractor shall furnish scientific effort during the period indicated in Paragraph 1a of Section H*, together with all related services, facilities, supplies and materials, needed to conduct the following research:

a. Transient Processes in Laser-Triggered Spark Gaps

   1) Theoretically and experimentally study initial buildup of charge and current.

   2) Measure temporally and spatially resolved electron densities.

   3) Study the importance of inverse bremsstrahlung.

b. Spark Gap Discharge and Erosion Phenomena

   1) Investigate changes in the chemical composition of various filler gases and time resolved recovery of gaps with different electrode materials, gas types, and pressures.

   2) Construct a coaxial transmission line generator

c. Pulsed Power Surface Physics and Applications

   1) Study the surface damage of dielectric materials by UV radiation.

   2) Study surfaces of dielectric and conducting materials used in an actual spark gap.

   3) Study a surface discharge switch to determine the effect of surface material on lifetime, inductance, and hold-off voltage.

d. Excited State Spectroscopy of Electrically Excited Gases

   1) Determine excited state species concentration using laser-induced fluorescence.

   2) Study species population during the gap recovery stage.

   3) Study multiphoton ionization cross sections for gases of direct interest to switching.

---

* Paragraph 1a of Section H not included here.

e. Exploratory Concepts

1) Conduct a computer analysis of gas flow dynamics in a rep-rated spark gap.

2) Study the feasibility of the field effect electrolyte switch.

3) Analyze the laser-divertor opening switch.

4) Study shock suppression in liquids.

5) Investigate arc quenching materials in opening switches.

f. Electromechanical Pulse Device

1) Perform a study to determine parameters for which this device is most useful.

2) Design a low inductance, low volume capacitance which can be mechanically varied with time.

g. Multiple Ionization Cross Section Measurements

1) Measure the absolute multiphoton cross sections at a number of rare gas halide wavelengths, including 193 and 248 nm, of several gases including Ar, H_2 and N_2.

h. Microscopic Processes in Spark Discharge Initiation

1) Study ionization processes of importance to electrical breakdown phenomena in several gases including Ar and N_2.

2) Identify the important ionizing processes and to characterize these processes in a manner suitable for use in computer modelling studies of electrical breakdown.

i. An investigation of the properties of a discharge suitable for use as an opening switch shall be initiated. The discharge will be a diffuse, volume discharge in which the gas temperature is relatively low, i.e., a "cold" discharge. Specific points to be addressed are:

1) An experimental discharge cell will be constructed. This cell will include windows for diagnostics and laser beam access.

2) The temporal stability and spatial homogeneity of a diffuse volume discharge will be studied. Relatively high pressures (up to atmospheric) will be used. Various gas mixtures will be employed including some with electronegative gases.

3) The optogalvanic effect will be used to attempt to change the conductivity of the discharge. Both increases and decreases in the conductivity through the use of a laser will be investigated. A specific goal will be to attempt to terminate the discharge in spite of a rising E/p. Particular attention will be paid to

mixtures of gases in which the electron attachment rate increases with E/p or temperature.

4) Diagnostic apparatus will be constructed to measure the voltage across the discharge and the discharge current. Time intergrated photography, time resolved optical measurements, and streak photography will be used to study the temporal evolution and spatial distribution of the discharge.

j. An investigation of the properties of electron-beam initiated and controlled switches, both opening and closing, shall be conducted. Several other opening switch concepts will be analyzed to determine their feasibility and potential for further development. Among these concepts are the dense plasma focus switch, plasma instability switches, the plasma compression or variable inductance switch, the radiation controlled switch, and others. Specific points to be addressed are:

1) Study the discharge character as a function of e-beam current for the closing switch. Determine the lower limit on e-beam current for diffuse discharge operation.

2) Determine if admixtures of SF_6 cause discharge filamentation in the e-beam closing switch.

3) Determine the polarity effects of the electrodes in the e-beam closing switch.

4) Design and construct an e-beam opening switch system.

5) Study the theoretical feasibility of the plasma instability and plasma compression switches.

SUMMARY

The Coordinated Research Program in Pulsed Power Physics is a multi-investigator program which involves eight Principal Investigators, four Associate Investigators, one Postdoctoral Fellow and 14 Graduate Students from the departments of Electrical Engineering, Physics, Chemistry, and Mechanical Engineering at Texas Tech University. It is mainly concerned with the physics of high power switching and has 10 program elements. The research is supported by AFOSR and ARO.

The study of spark gap closing switches has five program elements. The first is concerned with electron-beam initiated (triggered) discharges where the work has been aimed at understanding the e-beam parameters which control the discharge conditions. The conditions for initiating the discharge have been determined but in order to determine the conditions for sustaining the discharge a new experimental arrangement is needed. Results of this work to date are being prepared for publication.

Under the second program element we have developed a computer program to calculate the electric field in a spark gap with electric charges present. We have also studied the laser induced fluorescence of various excited species in the spark gap in order to understand the mechanism of laser-triggered breakdown of spark gaps.

In the third project we have studied the importance of electrode and insulator materials as well as gas type on electrode damage. Various surface analysis techniques as well as on-line mass and spectroscopic analysis and post chemical analysis are utilized in an effort to understand the complicated discharge-plasma chemistry processes that occur in high power discharges. Experimental facilities have also been constructed for quantitiative analysis of electrode erosion.

Project No. 4 is carried out in close cooperation with No. 3 and is concerned with the damage that occurs to insulators in high power switches and in surface discharge spark gaps. Some of the same analysis techniques that are applied in Project No. 3 are also used here. In addition there are efforts to study separately the influences of UV radiation to insulator surface flashover and to determine the best available insulator for a repetitive surface discharge switch.

In Project No. 5 we study multiphoton ionization phenomena in order to improve (better determine) the initial conditions in laser induced spark gap breakdown. We also try to develop new diagnostic techniques, such as laser induced fluorescence, to determine better the discharge evelution.

In order to evaluate new ideas that inevitably occur during the various other investigations we study, under program element No. 6, some exploratory switch concepts. Among these are optical studies of density gradients in gas blown spark gaps, the effect of various arc quenching media, field effect electrolyte switches, and others.

Project No. 7 is quite different in nature from the others since it deals with a novel electromechanical pulser concept. The advantage of this pulser is that it has a very short rise time ($\lesssim$ 10 μs) compared to other electromechanical pulse devices and that it lends itself to a modest rep-rate of more than 1000 pps. A proof-of-concept model of the pulser is ready for testing.

A subcontract was issued to SRI, International to study various multiphoton ionization cross sections and microscopic processes in spark gap discharge initiation. This work is described under Projects 8 and 9. Several interesting results were obtained, especially with regard to the increased decay rate constant for conduction current in N_2 vs E/N, by

addition of N_2O to the buffer gas. This is particularly important to the opening switch concepts described in Project No. 10 below.

In this project (#10), we have designed and nearly constructed two experimental facilities for studying possible rep-rated opening switches. Opening switches are particularly important because of a potential factor of 100-1000 weight and volume savings for inductive energy storage as compared to the conventional capactive storage. We are studying several opening switch concepts but the two which are receiving most attention are the electron beam and the optically controlled discharges, where e-beams or laser beams are used to change the conductivity of a diffuse discharge.

During the last contract period we also moved our experimental facilities into a new research building. The improved space and utility situation should greatly enhance our research capabilities since we were earlier located in extremely cramped and antiquated quarters.

Several positive efforts have also been made to establish cooperative research efforts with various national, industrial, and university laboratories. Considerable benefits from these efforts are expected during the next contract period.

Project No. 1

ELECTRON BEAM INITIATED BREAKDOWN*

(T. Tzeng, E. Kunhardt and M. Kristiansen)

A. Summary

The work on this project was stopped halfway through the contract period. The reason is that it was felt that most of the important information obtainable with the machine used up to that time had been obtained and that only a machine with considerably longer pulselength ($\tau_p >> 10$ ns) would provide significant additional insight into the problem. The experiment had, however, been quite successful and most of the results obtained up to that time are summarized in the attached paper by T. Tzeng et. al. A more complete paper is being prepared for submission to a refereed journal.

Plans have been made for continuing this work either as part of the e-beam controlled opening switch work described in Project No. 10 or by constructing a new, separate experiment. The final decision is primarily a resource allocation problem (manpower & equipment) which will be made by next summer when we can better judge the availability of new, qualified graduate students. Some equipment for constructing a new experiment has, however, been gathered together for the eventuality that we chose to go this route.

---

* Funded by ARO for part of the 1980-81 research period

THE EFFECT OF ELECTRON BEAM INDUCED SPACE CHARGE ON SPARK GAP BREAKDOWN *

Y.H. Tzeng, E.E. Kunhardt, and M. Kristiansen
Department of Electrical Engineering
Texas Tech University
Lubbock, Texas 79409 USA

A.H. Guenther
Air Force Weapons Laboratory
Kirtland Air Force Base, New Mexico, 87117, USA

Abstract

An investigation into the effect of electron beam induced space charge on the insulating property of a gas in a spark gap is presented. The characteristics of the gas transition from insulator to conductor show strong dependence on the amount and location of the space charge introduced. Investigations of the delay time and the characteristics of the conducting channel have been made. The delay time from the injection of the e-beam to the collapse of the gap voltage ranges from 10^{-9} to 10^{-3} second. From open shutter photography, we observe that the character of the conducting channel is quite varied. Dark, diffuse, filamentary, or diffuse followed by filamentary (single or multiple) channels have been observed, depending on the space charge conditions. The fundamental processes leading to the collapse of the insulating property of the gas for various experimental conditions are discussed.

I. Introduction

The development of high power switches has recently received a great deal of attention as a common and crucial area of interest for scientists working on high power laser, fusion, high current charged-particle accelerators, and weapons-effect simulators. These switches must be capable of fast and repetitive transfer or interruption of high voltage, high current from an energy storage device to various transducers. To meet these requirements a number of novel switches have been proposed.[1] In many of these approaches, switching is accomplished by causing a transition between insulating and conducting states of a gas. The various devices that operate in this fashion differ mainly in the way this transition is initiated and in the characteristics of the conducting stage, i.e. whether it be a diffuse or filamentary discharge.

The electron beam har been shown to be a powerful tool for initiating either a self-sustaining or a nonself-sustaining discharge in a high pressure gas in a spark gap.[2,3] This paper presents an investigation into the effects of the space charge induced by an electron-beam on spark gap operation. These effects are fundamental to the understanding of the e-beam switching.

In Section II of this paper, the experimental setup and procedures are described. In Section III, the results are presented. These results significantly extend those presented in a previous paper.[4] We give further discussions of the physical processes occurring in e-beam switching. Recommedations for e-beam switching applications are given in Section IV.

II. Experimental Arrangement

A diagram of the apparatus used for these investigations is shown in Fig. 1. This setup has been described in detail in references 4 and 5. Briefly, the experiment consists of an energy storage element, a gas insulated, pressurized spark gap, and a source of energetic electrons. The energy storage element and the spark gap are contained within the high pressure vessel of a Van de Graaff charged coaxial line. The line can be charged to approximately 1 MV and delivers a rectangular pulse of approximately 10 ns, full width at half maximum duration. The electron beam is generated by a cold cathode field emission vacuum diode which is located behind the electrode facing the Van de Graaff charged line. Modification to the diode described in reference 4 are discussed in reference 5. A better characterization of the e-beam has also been made (see reference 5).

The effects that we have studied include (1) The characteristics of the resulting current pulse (i.e. amplitude, length, risetime, and waveform); (2) The switch delay time and jitter; and (3) The spatial character of the discharge channel.

The parameters varied during the course of these investigations are: (1) The gap polarity (depending on how the Van de Graff is charged, the target electrode can be either positive or negative); (2) The gap voltage V_g (varied between 30 percent and 95 percent of the selfbreakdown voltage, which ranges from 40 kV to 500 kV); (3) The gas pressure (3-7 atm); (4) The type of gas (N_2, and mixtures of N_2 and SF_6); (5) The e-beam current (varied by putting a 1 mm thick aluminum mask with the desired area of uniformly distributed holes in front of the beam. The current can be varied from about 4 A to 1 kA) (6) The average e-beam energy (35 keV to 180 keV); (7) The e-beam pulse length (2-50 ns).

III. Results and Discussions

Since the parameter space investigated is large, we have chosen the type of gas and the gap voltage polarity, in reference to the direction of the electron beam, to subdivide this space. This choice is based on the similarities of the physical processes that occur in the regimes defined by these parameters. We shall first present the results obtained using pure nitrogen, followed by those obtained with mixtures of N_2 and SF_6.

*Supported by AFOSR and ARO

Because SF_6 is electronegative, the nature of the electron beam induced space charge is significantly different from that for pure N_2. This has a great influence on the subsequent evolution of the space charge in the gap, and ultimately on the characteristics of the pulse observed at the load.

In general, for pure N_2 and negative gap voltage polarity (i.e. the electron beam is retarded by the external field), the discharge current characteristics and the conducting channel luminosity are strong functions of e-beam current amplitude and pulse length, and are relatively weak functions of average e-beam energy. This is also observed for positive gap polarity. Figure 2 shows the discharge current pulses at the load as a function of e-beam current amplitude, and pulse length for both gap voltage polarities. For both gap voltage polarities, no filamentary arc channels are observed when the amount of space charge introduced by the e-beam is large. All the e-beam initiated discharge current pulses shown in Fig. 2 correspond to diffuse discharge channels. Since the discharge current source is a charged transmission line with a two-way delay time of 10 ns and the load is matched to the line, the discharge current pulse is a square pulse with a duration of 10 ns only when the gap resistance is small compared to the characteristic impedance of the charged transmission line (50 ohm in this experiment). When the gap resistance is high, the mismatching created will cause reflections, thus forming a current pulse longer than 10 ns with a smaller amplitude. Thus, from Fig. 2, we note that for the same average e-beam energy the discharge current pulse gets smaller in amplitude, has longer risetime and becomes wider as the e-beam current is lowered or made shorter in duration. This implies that the gap resistance decreases when the e-beam current increases. Using the same arguments, we find that when the target electrode is charged negative and the gas pressure is increased from 5 atm to 7 atm, the gap resistance increases considerably. The variation of gap resistance due to a similar pressure change for the positive target case is not observed. A 700 A, 60 keV, 35 ns electron beam is used for both of these gas pressure experiments. The discharge current pulse risetime was observed to range from 2.5 ns to more than 10 ns. The lower limit is the same as that for a selfbreakdown pulse. In general, the smaller the e-beam current is, the longer the risetime is. From this kind of measurements we conclude that the delay time measured from the injection of the e-beam to the appearance of a sharp rise in the discharge current is less than 1 ns (not including the delay time of the transmission line used for diagnostics). Similarly, the jitter is lower than the resolution of the experimental set-up (sub-nanosecond). In general, the variation of delay time with respect to gap voltage polarity, gap voltage, gas pressure, e-beam energy and current is not detectable. A superposition of five discharge current pulses is shown in Fig. 3.

The spatial characteristics of the e-beam initiated discharge channel is determined from open shutter photographs. Examples are shown in Fig. 4 for a positive target electrode and in Fig. 5 for a negative target electrode. For the same polarity, the conducting channel luminosity varied as we changed the experimental conditions (e.g. e-beam current amplitude, e-beam pulse length, e-beam cross section, number of e-beams, gap voltage, etc). The light distribution in the gap changes with polarity, indicating that there are different processes leading to the discharges. In general, the discharge channel is broad except when the amount of space charge induced by the beam is small. In this case, the discharge channels are filamentary (single or multiple), and large delays are observed (hundreds of ns). Figure 6 is an illustration of this condition. In this case a 4 A, 150 keV, 10 ns e-beam has been used to trigger a spark gap pressurized to 3 atm of N_2. The gap voltage is close to selfbreakdown voltage (i.e. 95 % V_{sb}). Multichannel discharges have also been achieved using multiple electron beams. Up to eight channels have been simultaneously created (see Fig. 4a).

The various results discussed in the above paragraphs may be explained as follows. When the e-beam is injected into the gap towards a negatively charged electrode, it is retarded by both the gas and the electric field. The spatial distribution of the induced space charge is thus determined by the beam energy, the gas pressure and the magnitude of the applied field. The distribution and amount of the induced space charge together with the gap conditions, determine the properties of the discharge channels and current characteristics. Simple calculation shows that the current generated in the external circuit due to the motion of the space charge induced by a 1 ns, 500 A, 60 keV e-beam injected into a gap charged to 150 kV in 3 atm N_2 is on the order of kA. This explains the short delay times observed (ns). Once the e-beam is injected into the gap, the ionized and excited gas molecules will emit photons in a short period of time. Those photons having low absorption cross section may reach the cathode. If their energy is higher than the work function of the electrode material, they can release electrons via the photoelectric effect. This constitutes a supply of electrons distributed over a large area of the cathode. In their way to the anode the photoelectrons form a number of avalanches. Since the avalanches are overlapping, the space charge enhanced field is uniform, and therefore, we see a broad discharge channel. This phenomenon is similar to that observed by Koppitz.[6] The avalanches evolve until the ion space charge resulting from the e-beam induced plasma is neutralized. This is seen in Fig. 5. If this space charge is small (for low e-beam current, for example multiple avalanches will develop, resulting in a filamentary discharge as shown in Fig. 6. When the target electrode is charged positive, the injected fast electrons can penetrate across the gap and create a conducting channel by ionizing the gas molecules. The conductivity of the channel depends on the amount of space charge introduced. The properties of this discharge are similar to the e-beam sustained discharge discussed in reference 3. This experiment shows the fast turn-on of this mode of operation and its capability of delivering a 0.5 kA/cm^2 discharge current density

When mixtures of N_2 and SF_6 are used as the gas medium, the character of the discharge is different than when pure N_2 is used. In general, when the gap voltage is higher than some threshold voltage, V_t (Fig. 7a), the discharge channel is filamentary (single or multiple) with a discharge current pulse similar to the selfbreakdown pulse. The threshold voltage, V_t, for the onset of this filamentary discharge depends on gas pressure, % SF_6, e-beam conditions, etc. When the gap voltage is lower than this threshold, no filamentary arc channel is observed. The discharge current amplitude is then very small compared to that of selfbreakdown. After the discharge stops the voltage of the charged line drops to only a fraction of its original voltage. These phenomena are observed for both gap voltage polarities.

The delay time, from the injection of e-beam to the detection of the discharge current pulse at the load, not including the delay time due to the transmission line for diagnostics, has been measured and is shown in Fig. 7 for negative target electrode and in Fig. 8 for positive target electrode. For the case of negative target electrode, the e-beam energy plays an important role in determining the delay time. From Fig. 7b, we note that for a ten fold increase in e-beam current, the delay time decreases by 70 %. Moreover, from Fig. 7c, we note that the delay time increases by 500 times when the average e-beam energy decreases to 60 % and the e-beam current decreases to 33 %. Therefore, we conclude that the delay time is a strong function of the average e-beam energy and a relatively weak function of the e-beam current. For the case of a positive target electrode, both e-beam current and average energy show important effects on the delay time. This is shown in Fig. 8a, 8b, and 8e. In Fig. 7d and 8f, the dependence of the delay time on the gas pressure is displayed. The delay time increases with increasing gas pressure for the case of a negative target electrode, while it decreases with increasing gas pressure for the case of a positive target electrode. The dependence of the delay time on the ratio of mixtures of N_2 and SF_6 is displayed in Fig. 7e and 8d.

These observations can be explained as follows. The attachment coefficient of SF_6 is high for low energy electrons and increases with decreasing ratio of electric field to gas pressure. Therefore, most of the low energy electrons produced in the gap will attach to SF_6 to form negative ions. Since the drift velocity of these ions is low, the space charge current induced in the external circuit right after the injection of the e-beam is small. When the target electrode is negative, the ionized gas close to the anode virtually extends the anode and enhances the electric field due to asymmetry and reduction of the cathode-virtual-anode distance. Since the net ionization coefficient, (the difference between ionization and attachment) is a strong function of the ratio of electric field to gas pressure, the electron number density close to the symmetrical axis of the electrodes grows faster than those at other places. When the injected e-beam has higher energy, it can penetrate farther. The electric field in the cathode-virtual-anode region determines the further development of the breakdown. Under some conditions, a filamentary arc channel may develop. Therefore, the delay time is strongly dependent on the e-beam penetration depth, which is a function of e-beam energy, gap voltage and gas pressure. When the target electrode is positive, the inhomogeneous ionization of the gas by the non-monoenergetic electron beam and the resulting nonuniform distribution of space charge are thought to be the reasons leading to the breakdown of the spark gap. When the gap voltage is lower than the threshold, V_t, the space charge enhanced electric field is not strong enough for the spark gap to break down. A diffuse discharge channel, which ceases before the charged line voltage drops to zero, is observed under this condition.

IV. Conclusions

The fundamental processes leading to the collapse of the insulating property of the gas for the various experimental conditions studied have been elucidated. It has been shown that with e-beam triggering, diffuse or multichannel discharges can be achieved. For high power switching applications, the diffuse discharge channel obtained under certain conditions provides the beneficial characteristics of nonmeasurable delay and jitter, low electrode erosion, fast recovery (because it can be operated at low % V_{sb} and the gas is not fully ionized), and low switch inductance. Moreover, multichannel discharge operation, shown possible with e-beam triggering, provides low gap resistance, low switch inductance, and low electrode erosion compared to that of a single discharge channel.

The ability to tailor the space charge induced by the e-beam to virtually create any type of discharge channel would make this scheme most desirable for spark gap operation. However, the requirements for the e-beam parameters may limit the range of applicability. These requirements have been discussed in Section III.

References

1. T.R. Burkes, M.O. Hagler, M. Kristiansen, J.P. Craig, W.M. Portnoy, E.E. Kunhardt, " A Critical Analysis and Assessment of High Power Switches," Report NP30 Submitted to Naval Weapons Center, Dahlgren, Virginia (1978).

2. A.S. El'chaninov, V.G. Emel'yanov, B.M. Koval'chuck, G.A. Mesyats, and Yu F. Potalitsyn, " Nanosecond-range Triggering of Megavolt Switches," Sov. Phys. Tech. Phys, Vol. 20, No.1. pp 51-54, July 1975.

3. R.O. Hunter, " Electron Beam Controled Switching," Proc. First IEEE International Pulse Power Conference, paper IC8-1, Nov. 1976, Lubbock, Texas.

4. K.McDonald, M. Newton, E.E. Kunhardt, M. Kristiansen, and A.H. Guenther," An Electron-beam Triggered Spark Gap", IEEE Trans. Plasma Science PS8, 181,1980.

5. Y. Tzeng," The Effect of Space Charge Induced by an Electron Beam on Spark Gap Operation", Master Thesis, Texas Tech University, August 1981.

6. J. Koppitz," Nitrogen Discharges of Large Cross Section at High Overvoltage in a Homogeneous Field", J. Phys. D: Appl. Phys 6, 1494 (1973).

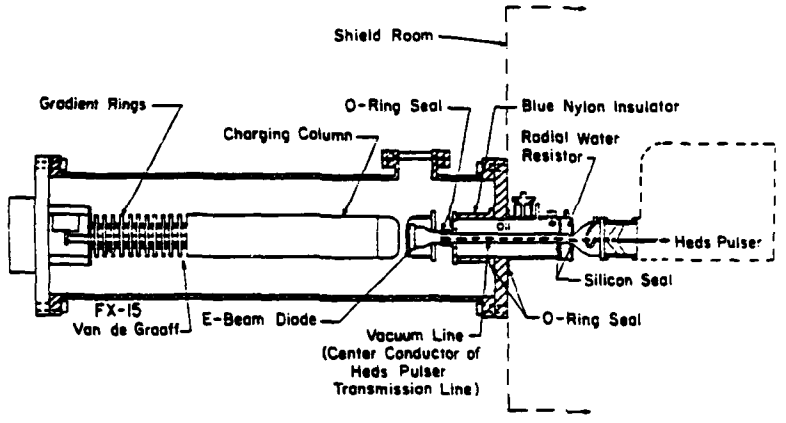

Fig. 1. Experimental Setup.

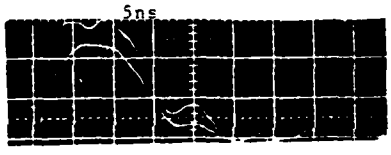

(a) Selfbreakdown (Larger Amplitude, V_{sb}=176kV); E-beam Initiated (Smaller Amplitude, V_g= 132 kV; E-beam: 700 A, 60 keV, 40 ns).

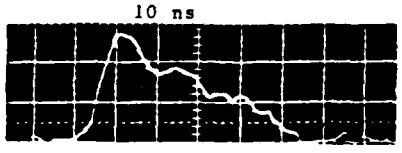

(b) E-beam Initiated (V_g= 132 kV, E-beam: 70 A, 60 keV, 40 ns).

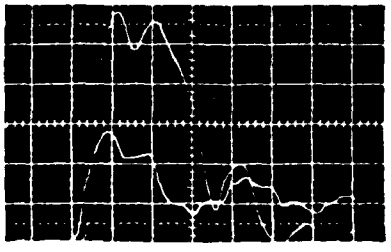

(c) Selfbreakdown (Larger Amplitude, V_{sb}=170kV) E-beam Initiated (Smaller Amplitude, V_g=140 kV; E-beam: 580 A, 70 keV, 2.5 ns).

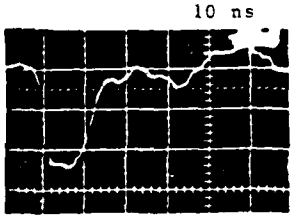

(d) E-beam Initiated Discharge Current Pulse with E-beam Current of 700 A and Average E-beam Energy of 60 keV.

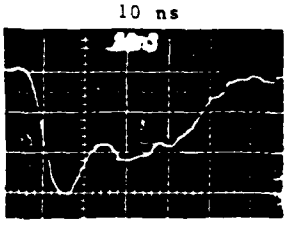

(e) E-beam Initiated Discharge Current Pulse with E-beam Current of 70 A and Average E-beam Energy of 60 keV.

Fig. 2. Discharge Current Pulses.

Fig. 3. The Delay and Jitter Measurements.

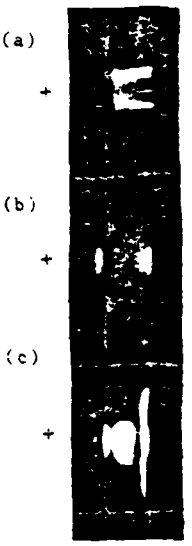

Discharge Channels Initiated by a 4 A, 150 keV, 10 ns E-beam. (A 1 mm Thick Al Mask with 8 Holes was Put in front of the E-beam, and the Gap Voltage was below 95 % V_{sb}.)

Discharge Channel Initiated by a 500 A, 35 keV, 10 ns E-beam.

Discharge Channel Initiated by a 500 A, 35 keV, 2.5 ns E-beam.

Fig. 4. Discharge Channels when E-beam was Injected from Cathode.

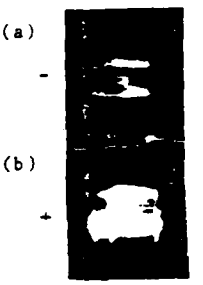

E-beam Direction

Fig. 6. Discharge Channels Initiated by a 4 A, 150 keV, 10 ns E-beam. (A 1 mm Thick Al Mask with 8 Holes was Put in front of the E-beam.)

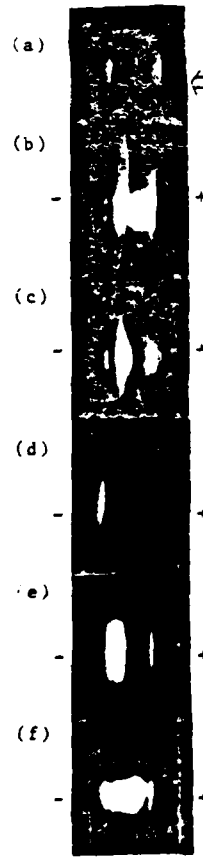

E-beam only

Discharge Channels Initiated by Two E-beams.

Discharge Channel Initiated by a 500 A, 10 ns, 35 keV E-beam.

Discharge Channel Initiated by a 440 A, 60 keV, 3 ns E-beam. (V_g = 72 kV, V_{sb} = 160 kV).

Discharge Channel Initiated by a 440 A, 60 keV, 3 ns E-beam. (V_g = 126 kV, V_{sb} = 160 kV).

Discharge Channel Initiated by a 192 A, 35 keV, 3 ns E-beam. (V_g = 156 kV, V_{sb} = 160 kV).

Fig. 5. Discharge Channels when E-beam was Injected from the Anode.

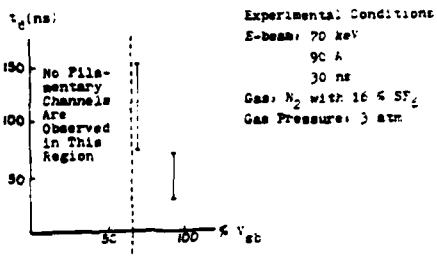

Fig. 7a. Delay Time vs % V_{sb}.

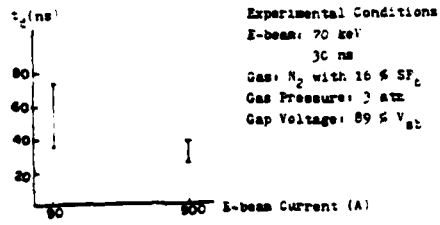

Fig. 7b. Delay Time vs E-beam Current.

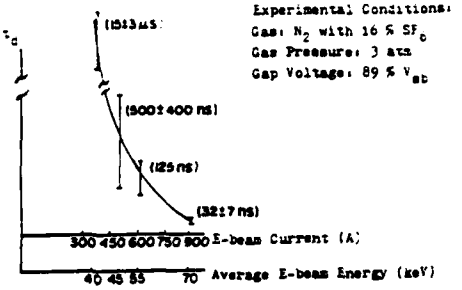

Fig. 7c. Delay Time vs E-beam Current And Energy.

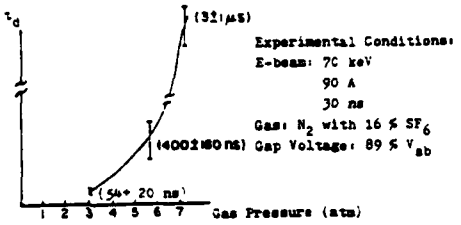

Fig. 7d. Delay Time vs Gas Pressure.

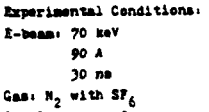

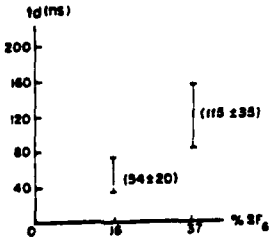

Fig. 7e. Delay Time vs % SF_6

Fig. 7. Delay Time vs E-beam and Gap Conditions.

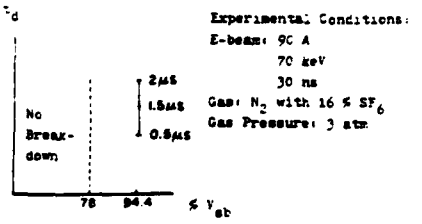

Fig. 8a. Delay Time vs % V_{sb}

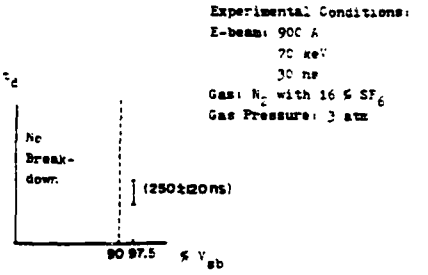

Fig. 8b. Delay Time vs % V_{sb}

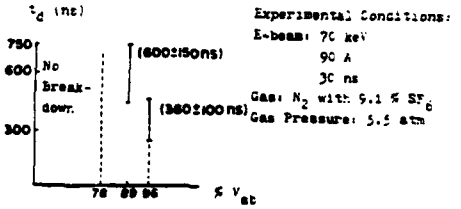

Fig. 8c. Delay Time vs % V_{sb}

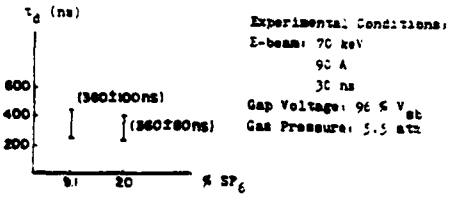

Fig. 8d. Delay Time vs % SF_6

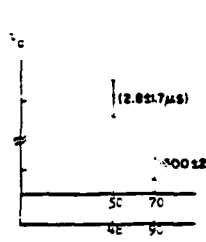

Experimental Conditions:
E-beam: 70 keV - 50keV
30 ns
Gap Voltage: 94 % V_{sb}
Gas: N_2 with 16 % SF_6
Gas Pressure: 7 atm

Fig. 8e. Delay Time vs E-beam Current And Energy.

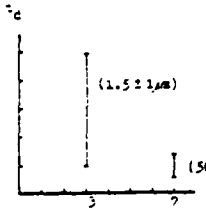

Experimental Conditions:
E-beam: 70 keV
30 ns
90 A
Gap Voltage: 94 % V_{sb}
Gas: N_2 with 16 % SF_6
Gas Pressure: 3-7 atm

Fig. 8f. Delay Time vs Gas Pressure.

Fig. 8. Delay Time vs E-beam and Gap Conditions.

Project No. 2

Transient Processes in Laser-Triggered Spark Gaps

(R. A. Dougal, R. A. Biesele, and P. F. Williams)

A. SUMMARY

Accomplishments during the contract period include 1) A computer program suitable for calculating electric fields in axially-symmetric geometries with space charge has been finished and tested. This program is essential for modelling the breakdown process in laser-triggered spark gaps. 2) Work was started on writing a computer program for solving the nonlinear continuity equations which should describe charge build-up in the spark gap leading to breakdown. This program is needed to test mechanisms and models for laser-triggered as well as more conventionally-triggered breakdown. 3) A program to study the evolution of fluorescence from the gap was initiated using a sensitive streak camera. Good data have been obtained for the spark phase of the discharge, but feedthrough during the camera retrace prevented acquisition of data for the times between the arrival of the laser pulse and the subsequent gap closure. The streak camera was being modified by the manufacturer at the end of the contract period to reduce or eliminate this problem and it is expected that work will be resumed shortly on this part of the project. 4) A considerable effort was made to observe, using laser-induced fluorescence, the presence of the excited metastable $A\ ^3\Sigma_g^+$ state of N_2 in a nitrogen filled gap during the afterglow. At the close of the contract period, this effort had not been successful. 5) We have investigated the effect of using electrode materials other than the previously used aluminum in our laser-triggered gap. Of the materials investigated to date, amorphous graphite appears to provide the most reliable, lowest jitter triggering.

6) An improved vacuum cell for housing the spark gap was constructed and has been in use for most of the contract period. The cell utilizes high vacuum technology, ceramic insulators, and oil-free pumping to provide a clean, reproducible environment. 7) Considerable effort was expended in developing the software and hardware for interfacing our PDP 11/34 computer to laboratory experiments. The bulk of this work was finished early in the contract period and the computer has been used as an integral part of several experiments.

B. ACCOMPLISHMENTS

The goal of the work in this project is to understand the physical mechanisms important in laser-triggered breakdown. A multifaceted program directed towards this end is presently underway. A major aspect of this program is the development of a numerical procedure to follow the build up of charge and current in the gap following the laser trigger. For this purpose a program is needed for computing the electric field in the gap when significant space charge is present. We have finished the development and testing of a suitable program and this work is described in Sec. B.1. Work is now underway to develop a procedure for solving the simple continuity equations describing the development of charge in the gap. This work should provide much useful insight into triggering mechanisms.

Another major facet of the program involves the gathering of experimental information about the breakdown process. Several separate efforts are underway along these lines. In Sec. B.3, we discuss the status of our work to monitor the temporal and spatial dependence of the overall luminescence from the gap during the breakdown process. This work has included high speed streak photography of the gap as well as intensity vs. time measurements taken with high speed photodiodes and photomultipliers. Since the luminescent emission from the gap is related to the physical

processes occurring there, this information will be useful in formulating and checking models of the breakdown.

In a previous report, we discussed measurements of the buildup and decay of excited state populations of molecular N_2 as well as atomic and ionized species during the spark cycle in laser-triggered discharges in N_2. The presence of the metastable A $^3\Sigma_g^+$ state of N_2 should play an important role in gap recovery and probably in gap breakdown under conditions in which long delays are experienced. The presence of this species is not easily detected with conventional spectroscopic methods because of the unfavorable selection rules associated with transitions to lower lying states. As discussed in Sec. B.4, we have used laser-induced fluorescence techniques in an attempt to detect this species in the pre- and post-spark stages of laser-triggered breakdown of N_2-filled gaps. Probably due to the poor sensitivity of the technique when used in this application, these efforts have not been successful to date.

We have briefly investigated the utility of other electrode materials in laser-triggered switching. As discussed in Sec. B.5, besides the aluminum electrodes we used initially, we have looked mostly at graphite electrodes in this application. This material provides reduced delay and jitter over the aluminum electrodes, with much shorter current rise times. We believe that this material should be seriously looked at for very fast, low jitter, switching applications.

Finally, several improvements in our experimental facilities have been made. A new reticon-based, optical multichannel analyzer with 5 ns gating capability was acquired. A new, 750 mJ, Nd:YAG laser system was delivered just after the close of the contract period, and a high energy dye laser system designed to be pumped by the YAG laser was on order, with scheduled delivery in December. These new lasers will allow us to carry

out several types of experiments which we were previously unable to attempt. As described in Sec. B.6, an improved vacuum cell for housing the spark gap was placed into operation early in the contract period. The new cell is very clean, and therefore greatly enhances the reproducibility of our experimental results. The cell is also electrically much cleaner than our previous model, with improved high frequency response. Finally, our PDP 11/34 computer system has been interfaced to the laboratory experiments and is now used routinely to acquire and analyze spectra from both of our optical multichannel analyzer systems. This work is discussed briefly in Sec. B.7.

1. Numerical Poisson Solver in 2-D.

In collaboration with Dr. E. Kunhardt of Texas Tech, work was finished during the contract period on a computer program to solve numerically Poisson's equation for cylindrically symmetric geometries. The program is fast and reasonably accurate for the space charge densities we tested.

a. Introduction

In a previous report [1] we discussed the general problem of numerically calculating the potential and/or the electric fields associated with a cylindrically-symmetric charge distribution. We chose to develop a method which makes use of Fourier transform techniques to handle z-axis derivatives, and uses a novel, cubic spline, technique to solve the resulting differential equation in the r variable. In that report, we described the spline technique for solving second order differential equations, as well as testing methods used to determine the magnitude of roundoff errors using the technique. As discussed in the report, roundoff errors were essentially eliminated by factoring the tridiagonal matrix, $\underline{\underline{U}}$ into two matrices, $\underline{\underline{L}}$ and $\underline{\underline{R}}$, containing only a diagonal and either a super or a sub diagonal, respectively.

Further investigations of the algorithm for calculating the fields carried out during the most recent contract period revealed unexpected behavior of the algorithm with some test charge densities. We therefore carried out a more thorough investigation of the truncation errors which appear with the scheme.

Using the notation of Ref. [1], the set of equations to be solved to determine the numerical solution of Eq. (6) of Ref. [1] is

$$\sum_j U_{ij}\ T_{j,0} = \sigma_i \tag{1}$$

where U_{ij} is a tri-diagonal matrix, the $\{T_{i,0}\}$ are the coefficients of x^0 in the cubic splines, and the σ_i are related to the driving function, $\rho_n(r_i)$. Specifically for $2<i<N-1$, if $f_i = \frac{1}{r_i}$, $g_i = -\left(\frac{n\pi}{a}\right)^2$, and h_i is the width of the i^{th} partition, $h_i = r_{i+1} - r_i$, the tridiagonal matrix, $\underline{\underline{U}}$, is given by

$$U_{ij} = A_{i,1}\ E_i\ \delta_{i,j+1} + (A_{i,0} + A_{i,1}\ F_i - B_{i,1}\ E_{i+1})\delta_{i,j} - (B_{i,0} + B_{i,1}\ F_{i+1})\delta_{i,j-1} \tag{2}$$

and the driving vector, $\underline{\sigma}$, is given by

$$\sigma_i = R_i + B_{i,1}\ W_{i+1} - A_{i,1}\ W_i \tag{3}$$

where

$$\begin{aligned}
A_{i,0} &= 1 - \tfrac{1}{3} h_i^2\ g_i & A_{i,1} &= h_i(1 - \tfrac{1}{3} h_i\ f_i) \\
B_{i,0} &= 1 + \tfrac{1}{6} h_i^2\ g_{i+1} & B_{i,1} &= \tfrac{1}{6} h_i^2\ f_{i+1} \\
C_{i,0} &= -\tfrac{1}{2} h_i\ g_i & C_{i,1} &= 1 - \tfrac{1}{2} h_i\ f_i \\
D_{i,0} &= \tfrac{1}{2} h_i\ g_{i+1} & D_{i,1} &= 1 + \tfrac{1}{2} h_i\ f_{i+1} \\
R_i &= -\tfrac{1}{6} h_i^2\ (\rho_{i+1} + 2\rho_i) & S_i &= -\tfrac{1}{2} h_i\ (\rho_{i+1} + \rho_i)
\end{aligned} \tag{4}$$

$$W_{i+1} = (A_{i,1}\, S_i - C_{i,1}\, R_i)/\Delta_{i+1}$$

$$E_{i+1} = (C_{i,1}\, A_{i,0} - A_{i,1}\, C_{i,0})/\Delta_{i+1}$$

$$F_{i+1} = (A_{i,1}\, D_{i,0} - C_{i,1}\, B_{i,0})/\Delta_{i+1} \qquad (5)$$

$$\Delta_{i+1} = C_{i,1}\, B_{i,1} - A_{i,1}\, D_{i,1}$$

At the endpoints,

$$U_{0,0} = D_{0,1}\, A_{0,0} - B_{0,1}\, C_{0,0} \qquad U_{1,0} = A_{1,1}\, E_1$$

$$U_{0,1} = B_{0,1}\, D_{0,0} - D_{0,1}\, B_{0,0} \qquad U_{1,1} = A_{1,0} + A_{1,1}\, F_1 - B_{1,1}\, E_2 \qquad (6)$$

$$\sigma_0 = D_{0,1}\, R_0 - B_{0,1}\, S_0 \qquad \sigma_1 = R_1 + B_{1,1}\, W_2 - A_{1,1}\, W_1 \qquad (7)$$

where

$$A_{0,0} = 1 - \frac{1}{6} h_0^2\, g_0 \qquad A_{0,1} = h_0$$

$$B_{0,0} = 1 + \frac{1}{6} h_0^2\, g_1 \qquad B_{0,1} = \frac{1}{6} h_0^2\, f_1$$

$$C_{0,0} = -\frac{1}{4} h_0\, g_0 \qquad C_{0,1} = 1 \qquad (8)$$

$$D_{0,0} = \frac{1}{2} h_0\, g_1 \qquad D_{0,1} = 1 + \frac{1}{2} h_0\, f_1$$

$$R_0 = -\frac{1}{6} h_0^2\, (\rho_0 + \rho_1) \qquad S_0 = -\frac{1}{4} h_0\, (\rho_0 + 2\rho_1)$$

and for the boundary condition $y(x) = y_N$

$$U_{N,N-1} = 0 \qquad U_{N,N} = 1 \qquad (9)$$

$$\sigma_N = y_N \qquad (10)$$

Equation (1) may then be solved to determine to the 0^{th} order spline coefficients, $\{T_{i,0}\}$. The remaining coefficients give the values of the first, second, and third derivatives of ϕ at the $\{x_i\}$, and may be determined from

$$T_{i,1} = W_i + E_i\, T_{i-1,0} + F_i\, T_{i,0} \qquad (11a)$$

$$T_{i,2} = \rho_i - g_i\, T_{i,0} - f_i\, T_{i,1} \qquad (11b)$$

$$T_{i,3} = \frac{1}{h_i} (T_{i+1,2} - T_{i,2}) \qquad (11c)$$

b. Truncation Error and Stability

Several techniques may be used to solve Eq. (1). The stability of the solution must be carefully investigated, as discussed in Ref. [1], since in unfavorable cases small, roundoff, arithmetic errors will be magnified at each step of a sequential solution procedure. We will use a uniformly-spaced partition so that $h_i=h$, and $f_i=\frac{1}{ih}$. Also, $g_i=-\left(\frac{n\pi}{a}\right)^2 = g$. In the limit of large i, our driving function will always approach zero, and Eq. (1) reduces in the limit to

$$(1 + \frac{h^2}{6} g)\ \Delta^2\ T_{i,0} + \frac{1}{h(i-1/3)}\ \Delta T_{i,0} + g T_{i,0} = 0 \qquad (12)$$

Neglecting the term in ΔT, the solutions to this equation are

$$T_{i,0} = A\xi^i + B\xi^{-i} \qquad (13)$$

where

$$\xi = \frac{1}{1+\frac{h^2}{6} g} \left[1 - \frac{h^2}{3} g + \sqrt{-h^2 g\ (1 - \frac{h^2}{12} g)} \right] \qquad (14)$$

This solution to the finite difference equations consists of exponentially growing and decaying terms. In an analytical solution, the growing term would be discarded due to the boundary condition at $r \to \infty$. For a numerical solution, however, small roundoff errors can introduce a small amount of this growing solution, resulting in large and growing errors for large i. As discussed in Ref. [1], this problem may be eliminated by factoring the tridiagonal, 2nd order, finite difference equation, Eq. (1), into two 1st order finite difference equations, each having only one homogeneous solution. If in solving the first order equations we can always choose our direction of integration such that the homogeneous solution is decaying, the problem with roundoff errors will be eliminated.

A scheme which works well with the tridiagonal Eq. (1) is to factor $\underline{\underline{U}}$ according to

$$\underline{\underline{U}} = \underline{\underline{L}}\ \underline{\underline{R}} \tag{15}$$

where

$$L_{i,j} = \delta_{i,j} + \ell_i\ \delta_{i,j-1} \tag{16a}$$

$$R_{i,j} = d_i\ \delta_{i,j} + r_i\ \delta_{i,j+1} \tag{16b}$$

and

$$r_i = U_{i,i-1} \tag{17a}$$

$$d_i = U_{ii} - \ell_i\ U_{i+1,i} \tag{17b}$$

$$\ell_i = \frac{U_{i,i+1}}{d_{i+1}} \tag{17c}$$

For $0<g<-12$, these terms approach, for large i,

$$r_i \to -(1 + \frac{h^2}{6} g) \tag{18a}$$

$$d_i \to 1 + \frac{1}{6} \sqrt{-h^2 g(h^2 g + 12)} \tag{18b}$$

$$\ell_i \to - \frac{-(1 + \frac{h^2}{6} g)}{d_i} \tag{18c}$$

We now define the vector $\underline{G}$ by

$$\underline{G} = \underline{\underline{R}}\ \underline{T_0} \tag{19}$$

Then

$$G_i + \ell_i\ G_{i+1} = \sigma_i \tag{20}$$

In the limit of large i, this equation becomes

$$G_i - \frac{1 + \frac{h^2 g}{6}}{d}\ G_{i+1} = 0 \tag{21}$$

with solution

$$G_i = A\left(\frac{d}{1 + \frac{h^2 g}{6}}\right)^i \tag{22}$$

For $-12 \le g \le 0$, this solution grows exponentially with i, and therefore Eq. (20) must be solved starting at i = N-1 and iterating inwards.

Similarly, the equation for $\underline{T_0}$ is

$$d_i\, T_{i,0} + r_i\, T_{i-1,0} = G_i \tag{23}$$

with the asymptotic homogeneous equation

$$dT_{i,0} - (1 + \frac{h^2}{6} g)\, T_{i-1,0} = 0 \tag{24}$$

and solution

$$T_{i,0} = \left(\frac{1 + \frac{h^2}{6} g}{d}\right)^i \tag{25}$$

This is an exponentially decaying solution, so the equation must be solved by starting at i = 0 and iterating outwards.

By factoring the tridiagonal matrix and then solving for $\underline{T_0}$ in this way, we were able to completely eliminate inaccuracies due to roundoff error, as demonstrated in Ref. [1]. The discussion shows, however, that the truncation error with this algorithm may be significant. In the limit of large i, the tridiagonal Eq. (1) reduces to Eq. (12), with solutions given by Eqs. (13) and (14). For $|h^2 g| << 1$, these solutions reduce to the expected exponential solution of the original differential equation. For larger values of $h^2 g$, the discrete solution deviates significantly from the continuous solution, and for $h^2 g < -6$, $\xi < 0$ so that the sign of the discrete solution alternates at consecutive points.

The quantity $h^2 g$ is given by

$$h^2 g = -\left(\frac{n\pi h_r}{a}\right)^2 = -\pi^2 \left(\frac{h_r}{h_z}\right)^2 \left(\frac{n}{N_z - 1}\right)^2 \tag{26}$$

where h_r and h_z are the r-axis and z-axis partition widths, respectively, and $a = N_z h_z$. If we take $h_r \sim h_z$, then for the larger values of n, the quantity $h^2 g$ will be less than -6 and erroneous results may be produced.

c. Computer Program and Test Results

Using these ideas a Fortran computer program was written which calculates numerically the potential and electric fields for a given, cylindrically symmetric charge density, ρ. For each value of r, $\rho(r,z)$ is Fourier transformed in the z dimension yielding the functions $\rho_n(r)$ in Eq. (6) of Ref. [1]. The Fourier transform is accomplished using a standard fast Fourier transform algorithm. For each value of n, this equation is solved for the $\phi_n(r)$, using the cubic spline techniques just discussed. For each n, Eq. (11a) is used also to determine the coefficients $\{T_{i,1}\}$ which are just the values of $\frac{\partial \phi_n}{\partial r}$ at each point, i. The z-component of E is determined by fast inverse cosine-transforming the set $\{\frac{n\pi}{a} \phi_n\}$ and the r-component is obtained by fast inverse sine-transforming the set $\{\frac{\partial \phi_n}{\partial r}\}$.

In order to test this numerical procedure, we used a test charge density consisting of a set of spheres, each of uniform charge density centered on the gap axis. The position on the axis, the radius, and the charge density of each were independently variable. This charge density was then used as input to the field calculator routine. The field from a charge distribution of this type can also be calculated readily by the method of images, although many images are needed to ensure proper convergence. A separate program was written to calculate the field using this method, and the results compared with our field calculation routine.

The results we obtained in these tests depended on the charge density used, but they were generally good. The most completely studied charge distribution was that of a single uniform sphere of charge. In most tests, h_r/h_z was approximately one so that significant truncation errors may be ex-

pected for high frequency Fourier components. Nonetheless, as long as the diameter of the sphere was at least several times the partition spacing, the spline algorithm produced answers which agreed with the image charge routine to within 2%. A pathologic case in which ρ was non-zero only on the axis was discovered which would drive the algorithm into an unstable region, resulting in a wildly oscillating result. Otherwise, the performance of the program with single, solid spheres of charge was quite good.

The program also proved to be quite fast. Operating on a VAX 11/780 system, the program completed the calculation of the potential and both components of the field on a (N_r=51 x N_z=32) dimensioned partition in $\approx$ 10 sec. In contrast, calculating the same fields using the method of images required several minutes of computer time.

The performance of the subroutine with multiple sphere test charge densities is less well investigated. These tests provide a somewhat more stringent test of the algorithm than do the sphere tests. The case of equally, but oppositely, charged spheres of the same radii, but displaced slightly from each other, simulates the dipole fields set up by the shielding charges of a neutral plasma sphere in an external field. In this case, the charge density is zero everywhere, except in a thin shell where the two spheres fail to overlap. If the thickness of this shell is of the order of a partition spacing, we would expect the numerical procedure to provide incorrect results.

We compared the accuracy of the program when used with equal but oppositely charged spheres displaced by $\frac{1}{2}h_r$ and by $\frac{5}{2}h_r$ where h_r is the partition dimension in the r-direction. For the $\frac{1}{2}h_r$ case, the program produced results which were in error by as much as 75%. The calculated results were, however, everywhere of reasonable value, and we believe that the error was primarily a sampling error caused by the rapid variation of ρ. In other words,

the program was correctly calculating the fields, but it was calculating them for a ρ which has the same values at the sampling points as the intended ρ, but is elsewhere rather different.

As a test of this hypothesis, we numerically calculated the total charge in the gap by numerically integrating ρ and compared this value with the flux of E through the electrode surfaces, again calculated numerically from our spline solution results. These numerically determined quantities satisfied Gauss' Law to within 10-15% in the worst cases.

2. Solution of Continuity Equations

The particle conservation equation describing the growth of ionization in the pre-breakdown state are of the form [2]

$$\frac{\partial \rho_i}{\partial t} = - \vec{\nabla}\cdot(\rho_i \vec{W}_i) + \sum_j c_{ij} \rho_j |\vec{W}_j| \qquad (27)$$

where ρ_i is the density of particles of type i, $\vec{W}_i$ is the mean velocity of these particles, and the c_{ij} are coupling coefficients between the particle types, describing effects such as primary ionization, attachment, detachment, etc. Assuming $\vec{W}_i$ may be written in terms of a mobility, $\mu(E)$,

$$\vec{\nabla}\cdot(\rho_i \vec{W}_i) = \mu_i(E)\vec{E}\cdot\vec{\nabla}\rho_i + \rho_i\mu_i(E)\vec{\nabla}\cdot\vec{E} + \rho_i \frac{\partial \mu_i}{\partial E} \vec{E}\cdot\vec{\nabla}|\vec{E}| \qquad (28)$$

In solving Eq. (27) numerically, the spatial derivatives are potentially troublesome in that they may introduce sizable numerical errors due to the small differences of large numbers involved in evaluating the derivatives. The term in $\vec{\nabla}\cdot\vec{E}$ is easily handled by using the first Maxwell equation to equate it to ρ/E_0. Following Davies, et. al. [2], the term in $\vec{\nabla}\rho_i$ may be eliminated by solving the equation in a continually distorting reference frame, moving locally at velocity $\vec{W}_i$. In the initial efforts we will take μ to be independent of E, thereby eliminating the term in $\vec{\nabla}|\vec{E}|$. More accurate models will likely require the inclusion of the effects of the E de-

pendence of μ. In this case, the spatial derivatives involved in $\vec{\nabla}|\vec{E}|$ will have to be dealt with in some way. The term should be large only in regions of high field gradients, and the small errors introduced by the spatial derivatives should not be important.

3. Streak Photography of Fluorescent Emission

Several workers using streak and/or framing cameras have reported observation of the later stages of avalanche growth as well as other fast, wave-like, phenomena in over-volted breakdown [3-9]. In order to try to tie their work in with our work on laser-triggered breakdown of under-volted gaps, we have obtained streak photographs of the emission from the gap during laser-triggered breakdown. We have obtained several clear photographs of the very late stages of the breakdown process, but at the close of the contract period, we were awaiting the modification of our streak camera (by the manufacturer) to allow observation of the weak emission during the earlier stages of breakdown.

Two streak cameras were used in this work, One was a TRW Model 1D and the second a Hamamatsu C979 Temporal Dispenser unit. All data reported here were obtained with the Hamamatsu camera since it has much greater sensitivity than the TRW camera. A typical streak photograph is shown in Fig. 1. This is a photograph of the onset of a laser-triggered spark in N_2. The lower electrode is the one struck by the trigger laser and it is charged with a negative polarity. The emission was attenuated by about 10^3 with a neutral density filter, and the system optics were such that emission with wavelength shorter than about 3500 Å was not detected. The feature shown here starts approximately 90 ns after the arrival of the laser trigger and is essentially coincident with the sharp rise in gap current. The vertical lines are used as time markers and are separated by $\approx$ 10 ns. The gap spacing was 0.5 cm and the voltage applied to the gap

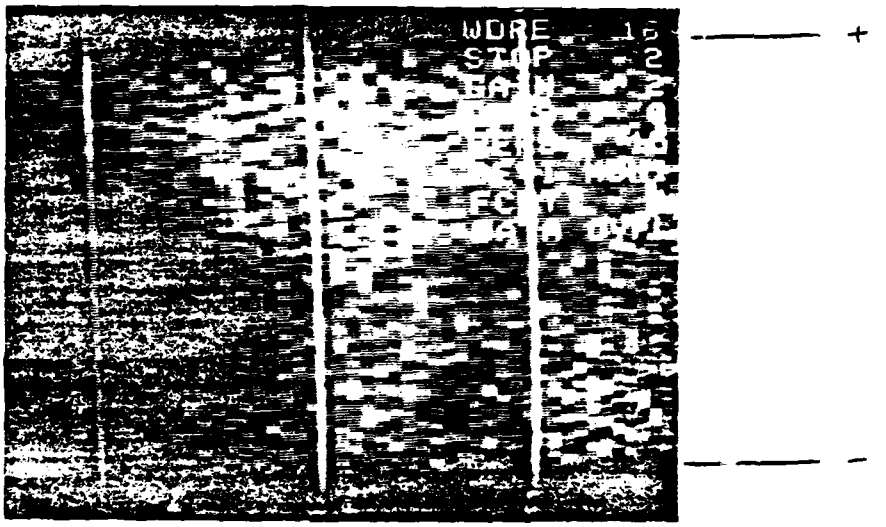

Fig. 1 Streak photograph showing the formation of the luminous arc channel. The negatively charged electrode was struck by the laser trigger. The vertical lines are separated by 10 ns, and the electrode spacing is 0.5 cm.

12 kV.

From this photograph it is clear that two waves of luminescence can be associated with the final transition to the spark phase. One wave starts at the anode and the second starts about 5 ns later at the cathode. The waves propagate toward the gap center with about equal speeds of $\sim 3 \times 10^7$ cm/sec. These results differ significantly from streak photographs obtained from conventional over-volted gaps in N_2 in that in conventional breakdown the luminosity grows from a point between the two electrodes first toward the anode, and then toward the cathode. Also, more structure is generally observed at later times in the conventional breakdown photographs.

These differences are consistent with differences observed between current waveforms observed with conventional over-volted and laser-triggered breakdown. Figure 2 shows current oscillograms obtained on the same spark gap for the two types of breakdown. The current in the laser-triggered case is notable for the lack of structure. This difference in behavior is not understood currently, but it is clearly important, technologically, in that it forms the basis for the very fast risetimes which can be obtained from under-volted gaps using laser triggering.

In order to obtain more information about the early stages of breakdown, we removed the neutral density filters from the Hamamatsu streak camera. Efforts at recording emission from these times were hampered by some type of feedthrough mechanism of the intense light from the spark such as to provide a low-level background signal. At the close of the contract period the camera was being modified to reduce the problem.

We also looked at the time dependence of the emission from the gap using a high speed vacuum photodiode (Hamamatsu R1328U-02, $\tau_r < 100$ ps) and later a fast photomultiplier (EMI D279B, $\tau_r \sim 0.8$ns). Typical results

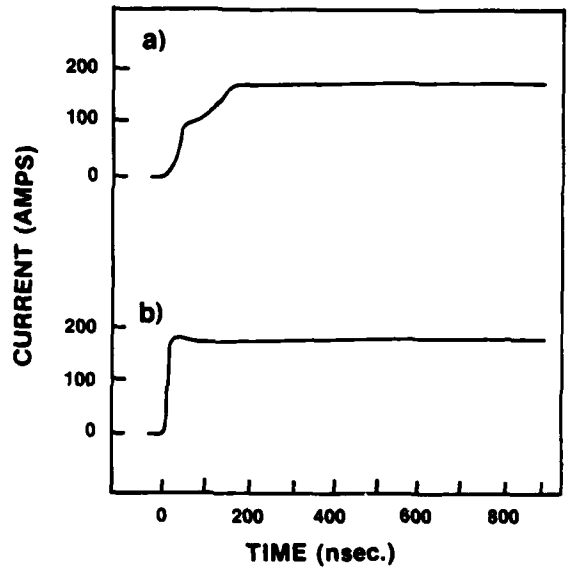

Fig. 2 Current waveforms for a) conventional over-volted breakdown, and b) laser-triggered breakdown. Data was obtained in N_2 at 600 torr with a gap spacing of 0.5 cm. The electrodes were made of graphite and the voltage was approximately a) 101% and b) 98% of the static breakdown voltage.

obtained with the photodiode for conventional over-volted and for laser-triggered breakdown are shown in Figures 3 and 4. Also shown in these figures are the corresponding current wave-forms. The differences between the two types of breakdown are striking in these figures.

4. Metastable A $^3\Sigma_u^+$ in N_2 Breakdown

As we pointed out in a previous report [1], in nitrogen breakdown delays of almost 1 ms can be observed in laser-triggered breakdown. These long delays seem to imply that the build up of the population of N_2 molecules in the metastable A $^3\Sigma_u^+$ state can play an important role in the breakdown of the gap [10]. Accordingly, we have attempted to monitor the population of this state both before the spark channel formation and after the spark was extinguished. The scheme we used to detect the presence of the spark is illustrated in Figure 5. The output of a tunable dye laser is used to excite the A species to the v = 3 level of the $B^3\Pi_g$ state. Subsequent emission from transitions back to the v = 1 level of the A state was monitored to detect the presence of the A species.

In our experiments we were unable to detect any laser-induced emission attributable to metastable A. This scheme for detection of the A state molecules is relatively insensitive due to the long radiative lifetime for transitions between levels of the A and B state. We estimate the minimum density level of detectivity, using this technique, to be 10^{12} - 10^{14} cm^{-3}. This is a rather large value, and the presence of an energetic species, such as the A state, with density less than this value, could significantly affect the breakdown process.

5. Effects of Electrode Material

We have investigated the behavior of amorphous graphite electrodes

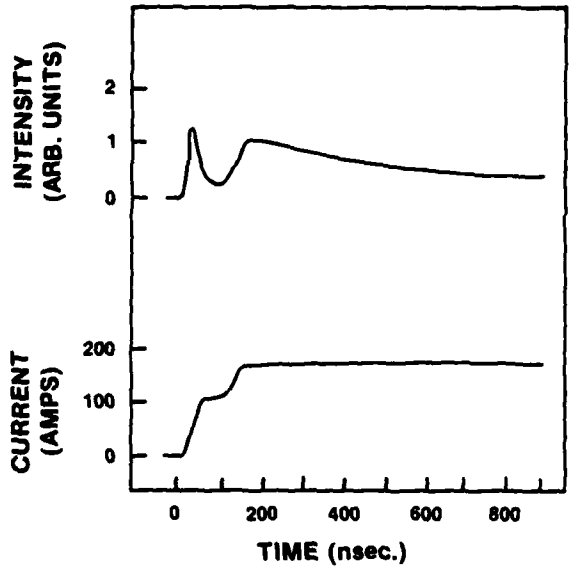

Fig. 3 Oscillograms showing light emission intensity and gap current for over volted breakdown. The conditions were the same as in Fig. 2a.

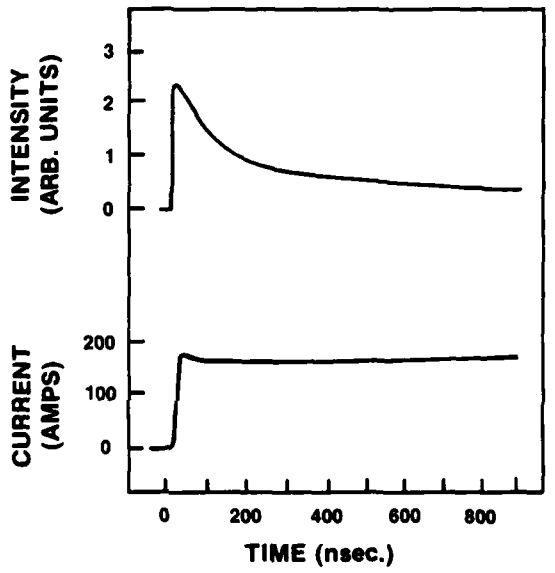

Fig. 4 Oscillograms showing light emission intensity and gap current for laser-triggered breakdown. The conditions were the same as in Fig. 2b.

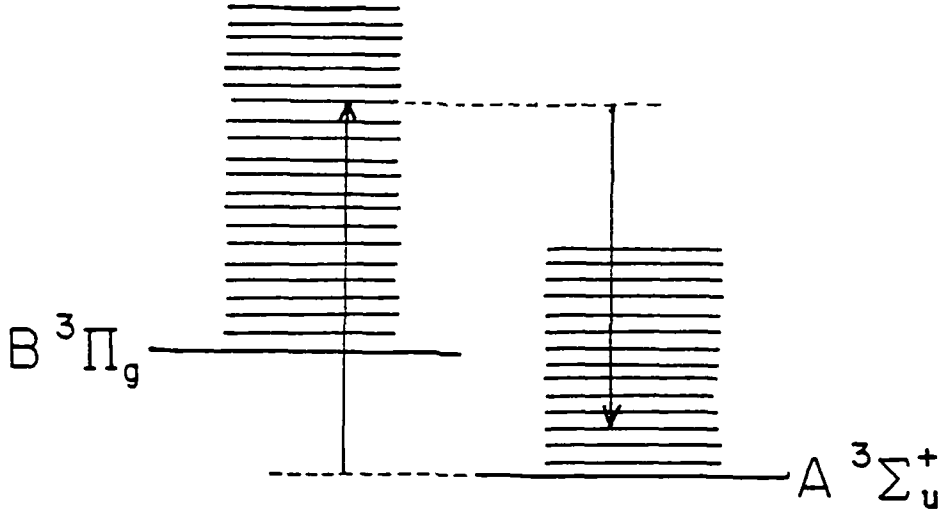

LASER-INDUCED FLUORESCENCE IN N_2

Fig. 5 Schematic diagram of energy level structure of N_2 relevant to laser-induced fluorescence studies of the metastable A $^3\Sigma_u^+$ state.

in our spark gap and found that they provide much improved performance in laser-triggered gaps over the aluminum electrodes we had been using previously. The reasons for this improved performance are not clear, but several effects are apparent. The trigger laser produces a more intense plasma fireball with the graphite electrodes than with other materials we have used. This stronger fireball results in faster, lower jitter triggering. The flat black surface of the electrode would provide up to an order of magnitude greater absorption of laser energy than would a metallic surface. Graphite electrodes have also been demonstrated to provide reduced jitter and risetime in over-volted gaps [11]. We speculate that this behavior may be the result of unusually large secondary emission or field emission coefficients for graphite. The only unfavorable characteristic we have observed with the graphite electrodes is that they seem to erode more readily than metallic electrodes. This observation is inconsistent with reports of erosion in conventional over-volted spark gaps where graphite is found to offer superior erosion characteristics [12]. We believe the difference is due to the greater vaporization of graphite by the triggering laser. In repetitive operation we also see fine particulate material in the gap. Although we have not had any difficulties as a result of these particles, they could be responsible for degradation of gap hold-off voltage either as a direct result of the particles in the gap, or due to coating of the insulators after prolonged operation.

6. An Improved Vacuum Cell

An improved vacuum cell for housing the laser-triggered spark gap was placed into operation early in the contract period. A cross-sectional drawing of the cell is shown in Fig. 6. The primary goal of the cell

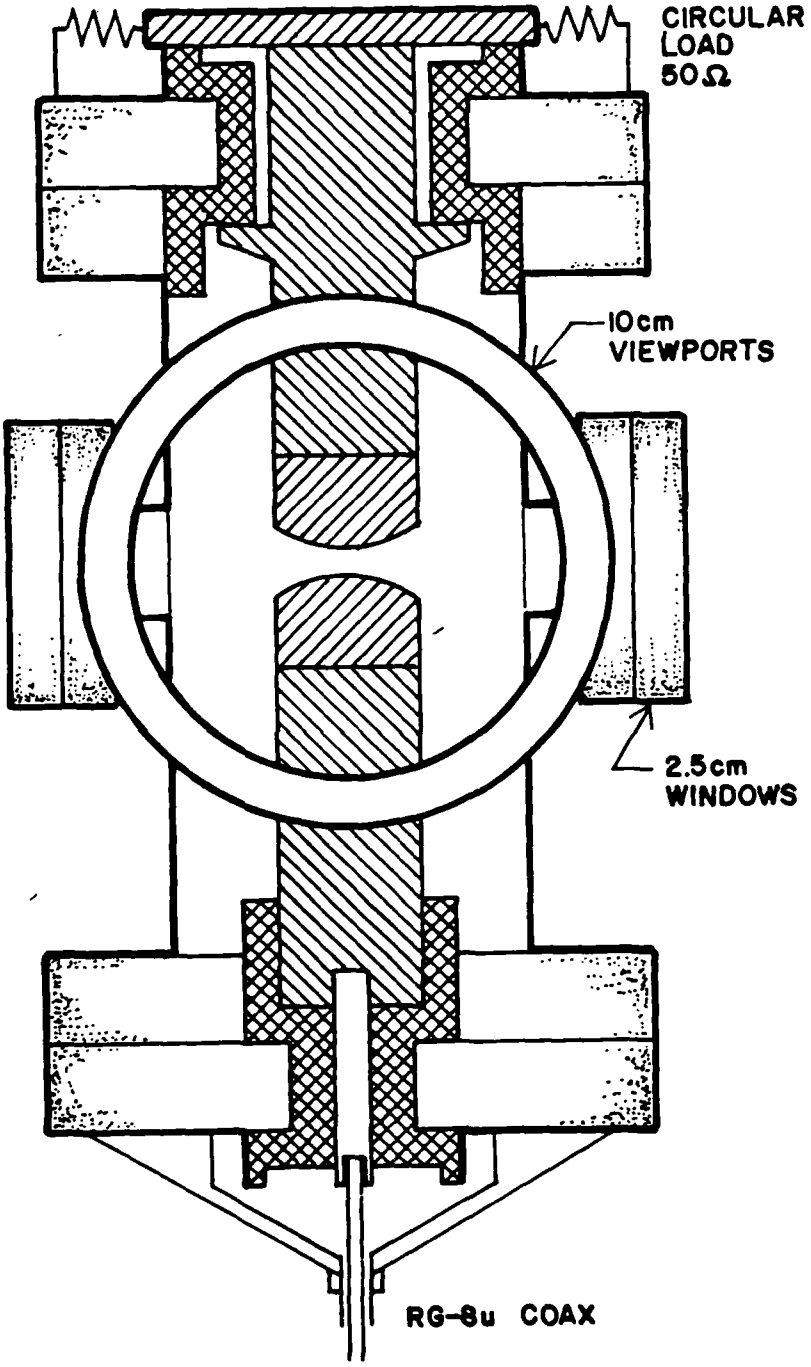

Fig. 6 Simplified cross-sectional drawing of the vacuum cell used to house the spark gap.

design was to provide a clean, reproducible environment for the spark gap. Electrical insulation is provided by Macor machinable ceramic parts. Six Viton O-rings are the only organic material in the system. All other seals are of the copper gasket type, and pumping is accomplished with sorption and ion pumps to further ensure cleanliness.

Electrically the system is fairly well matched. The system is completely coaxial with nominal 50 Ω impedance, although dimensions in the vacuum feedthroughs deviate considerably from the 50 Ω values. A 10 cm quartz viewing port, transverse to the gap axis, provides optical access to the gap. Two 2.5 cm diameter windows transverse to both the gap axis and the viewing direction of the viewing port provide access for a probe laser beam for laser-induced fluorescence and other studies. The electrodes are easily interchangeable, and the gap spacing is variable to more than 5 cm, although the cell must be disassembled to change the gap separation.

7. Integration of the PDP 11/34 Computer System into the Laboratory

Considerable effort was expended during the contract period to adapt our PDP 11/34 computer system to our laboratory needs. We are now operating under the UNIX operating system [13], a versatile, multitasking system which is very well suited to use in applications involving control and data collection from laboratory experiments. Programs were written and debugged to control the system RL01 hard disks, to control the Tektronix IEEE 488 GPIB interface card, and to control and collect data from our PAR optical multichannel analyzer (OMA) systems. An existing interface unit for interfacing these OMA's was modified for use with the 11/34 computer system, and work continued on a microprocessor-based interface unit which will allow convenient acquisition of two-dimensional data from our vidicon-based OMA.

C. REFERENCES

1. First Annual Report on Coordinated Program in Pulsed Power Physics, AFOSR Contract No. F49620-79-C-0191, Project No. 2, pp 31-37, December 1980.
2. A. J. Davies, C. J. Evans, P. Townsend, and P. M. Woodison, "Computation of Axial and Radial Development of Discharges Between Plane Parallel Electrodes," Proc. IEEE. 124, 179 (1977).
3. E. Marode, "The Mechanism of Spark Breakdown in Air at Atmospheric Pressure Between a Positive Point and a Plane. I. Experimental: Nature of the Streamer Track," J. Appl. Phys. 46, 2005 (1975).
4. J. Koppitz, "Image Converter and Intensifier Investigations on Luminous Fronts (Ionizing Waves) in Nitrogen Discharges in a Homogeneous Field," Z. Naturforsch. 26, 700 (1971).
5. A. A. Doran, "The Development of a Townsend Discharge in N_2 up to Breakdown Investigated by Image Converter, Intensifier, and Photomultiplier Techniques," Z. for Phys. 208, 427 (1968).
6. M. Kekez, M. R. Barrault, and J. D. Craggs, "Spark Channel Formation," J. Phys. D: Appl. Phys. 3, 1886 (1970).
7. V. H. Tholl, "Zur Entwicklung einer Elektronen Lawine bei Uberspannung in N_2 Teil 1 : Generationaufbau," Z. Naturforsch. 19a, 346 (1964).
8. M. Bayle, P. Bayle, and M. Crokwert, "The Development of Breakdown in a Homogeneous Field at High Overvoltages in Helium-Neon Mixtures and Nitrogen," J. Phys. D: Appl. Phys. 8, 2181 (1975).
9. I.D. Chalmers, H. Duffy, and D. J. Tedford, "The Mechanism of Spark Breakdown in Nitrogen, Oxygen, and Sulphur Hexafluoride," Proc. R. Soc. Lond. A. 329, 171 (1972).
10. S. C. Haydon and O. M. Williams, "Combined Spatial and Temporal Studies of Ionization Growth in Nitrogen," J. Phys. D: Appl. Phys. 9, 523 (1976).
11. E. E. Kunhardt, Private Communication.
12. D'Affinite, E. Bar-Auraham, and A. Fisher, "Design and Structure of an Extended Life, High Current Spark Gap," IEEE Trans. Plasma Sci. PS-7, 162 (1979).

13. D. M. Ritchie and K. Thompson, "The UNIX Time Sharing System," Bell Sys. Tech. J. 57, 1905 (1978), and other articles in the same issue.

Project No. 3

Spark Gap Erosion and Discharge Phenomena

(L. Gordon, A. Donaldson, C. Yeh, R. Ness
M. Hagler, and M. Kristiansen)

A. SUMMARY

A spark gap subjected to 40 kV, 650 J, 0.03 C pulses is being used to compare the performance of graphite and K-33 (a tungsten-copper composite) electrodes, Lexan and "Blue Nylon" insulators, and N_2 and SF_6 filler gases. Diagnostics include off-line electron spectroscopy for chemical analysis (ESCA), scanning electron microscopy (SEM), and mass spectroscopy and chemical analysis of deposits in the gap, as well as on-line optical spectroscopy of the discharge and mass spectrometry of the filler gas. The results indicate that the erosion process is quite different for different combinations of filler gas and electrode material. Graphite electrodes used with N_2 filler gas, for example, suggest two possible erosion mechanisms. An extremely fine grain structure (less than 0.1 μm) is apparently caused by sublimation at the discharge point. Large, widely scattered craters suggest accelerated chemical reactions at impurity sites. In graphite electrodes used with SF_6, on the other hand, a uniform high density of craters (5-10 μm diameter and hemispherically shaped) implies that chemical erosion occurs during the discharge. Placing an insulator material near the discharge in a gap does not affect the electrode erosion mechanism appreciably. The electrodes do become covered with organic molecules, however, except for the graphite-SF_6 combination.

Voltage recovery measurements in N_2, SF_6 and a mixture of N_2 and

SF_6 show that the recovery rate decreases with gap spacing and pressure and that N_2 has a faster recovery rate than SF_6 at the same pressure. The 0.1 SF_6 + 0.9 N_2 mixture (500 torr, 8.3 mm spacing) has an intermediate recovery rate until 5 ms, after which it shows the fastest recovery rate. A lumped transmission line generator (60 kV, 40 kA, 12 μs) for study of gaps at higher charge transfer (~ 0.5 C) per shot and a PFN (20 kV, 25 μs, 0.4 C/shot, 4 kJ/shot, 1.5 pps) for more quantitative erosion studies have been completed.

B. SPARK GAP CHEMICAL STUDIES WITH THE SINGLE CAPACITOR GENERATOR

1. System Changes

A description of the spark gap assembly and the single capacitor generator was given in the First Annual Report pp. 61-74, Ref. [1]. Several problems arose and corresponding design changes have been incorporated. Some of these design modifications are briefly described below.

a) Spark Gap

Each electrode material is shrunk-fit into an aluminum holder. The holder is threaded to screw into an aluminum support, permanently installed in the gap. The contact created by the shrink fit of the electrode piece into the holder was successful and caused no trouble. The threaded connection between the aluminum holder and the aluminum support created, however, two severe problems. First, aluminum threads against aluminum threads have a high tendency toward seizing. This problem is especially aggravated by the expansion and contraction of

the metal due to the temperature changes in a continuously operated gap, and by the "dirt" or discharge products that build up after many shots. Several holders and supports were destroyed by such thread seizures.

A second problem with the aluminum holders and supports arose while studying SF_6. Fluorine generated in the gap caused the aluminum threads on the holder to deteriorate. The resulting poor connection caused arcing which, accelerating the production of fluorine, led to total loss of the threads. After about 15,000 shots, the upper holder would drop from the upper support, allowing the electrodes to touch and short the gap. Details on the chemical processes involved are described later. A simple and quick solution was to pin the upper electrode holder into the support to prevent thread loosening and to maintain good electrical contact. A more permanent solution was to make the holder and support out of one piece of aluminum. This approach, however, increases electrode replacement time and aluminum usage. A better solution for both thread problems probably would be to make the holder and/or supports out of another material, such as brass, copper, or stainless steel.

Another problem encountered during the study of SF_6 was destruction of the glass diagnostic windows on the chamber ports by the SF_6 decomposition products. A window could be repolished after several hundred shots (being clouded) but was totally destroyed after several thousand shots (being deeply etched). The windows were normally removed except for during optical spectroscopic or photographic studies. Using a nonreactive salt (e.g. MgF_2) as a window material is being

considered but may present problems at pressures of several atmospheres.

Tracking and premature breakdown occurred along the lower, 2.5 cm thick acrylic insulating plate that separates the aluminum containment cylinder from the bottom header plate. The tracking was between the lower electrode support (high voltage) and the cylinder (at ground potential). High electric fields between the cylinder and the lower header plate, through the acrylic insulator, caused the triple point at the metal-insulator-gas interface to be a strong source of corona. Tracking was reduced by rounding the bottom edge of the cylinder, recessing the cylinder 0.3 cm into the insulating plate, cutting 0.6 cm deep, 0.6 cm wide circular grooves in the top surface of the plate and cutting the plate 1.2 cm back from the electrode support. Although the situation was greatly improved, the gap voltage was still limited to about 45 kV in N_2 and 60 kV in SF_6.

Possible solutions for future gaps include using a dielectric material for the cylinder (although how this will affect chemical studies is unclear) or redesigning the lower header plate to eliminate the high field stresses at the triple point.

b) High Voltage Network

Originally the brass support rods surrounding the cylinder served as the sole current return path. The resulting current pulse was 3 to 4 μs long. Including the gap chamber as part of the return path decreased the circuit inductance and reduced the risetime to give a shorter duration (2 μs) and higher amplitude current pulse. The cylinder is held at ground potential.

The solid discharge load, composed of four ceramic-carbon resistors, now has withstood about 1.5×10^6 shots. Although the resistors show some signs of deterioration and aging, they have withstood use for nine months at rep rates up to 2 pps and for continuous operating periods up to 12 hours. The load resistors do get very hot during continuous operation and are forced air cooled. Due to the good performance on the single capacitor generator, these solid carbon-ceramic resistors were chosen as the load element for the lumped transmission line and the "Coulomb pusher" line which will be used for erosion studies.

The 2.1 MΩ air-cooled charging resistor network mentioned in the previous report was redesigned to increase the rep-rate capability (from .2 to 2 pps), to decrease corona and resistor tracking problems, and to improve cooling. The charging resistor and the safety dump are now immersed in oil and the oil container is forced air cooled. The RC charging network is inefficient and generates large amounts of waste heat. Even though the resistors are submerged in oil, after 6 to 8 hours of operation problems are caused by heat buildup. These remaining problems should solved by using constant current charging techniques and/or designing better cooling for the charging resistors.

c) Vacuum and Diagnostic Systems

Originally the high vacuum pumping system was used both for the mass spectrometer sensing head and for evacuation of the cylinder for possible vacuum gap studies. However, the present gap design will not allow vacuum gap operation due to internal corona and subsequent tracking along the lower acrylic insulator (even with the improvements

discussed earlier). The high-vacuum glass connections to the cylinder were very difficult to maintain in the shock environment of the gap. Thus, the high-vacuum turbomolecular pump is, for the present, dedicated solely to the mass spectrometer. The pressure converter roughing pump is now used on a time-shared basis to evacuate the gap chamber to 10^{-2} Torr before filling it with a gas.

Several problems were encountered in the use of the residual gas analyzer in a high-pressure, pulsed power environment. As a result, the vacuum and gas sampling systems have been rearranged considerably to shorten the sample path length to improve the gas monitoring sensitivity. The pressure converter has been mounted directly on the sensing head and the sampling capillary tube connected directly to the cylinder.

Noise generated by the gap discharge was coupled into the mass analyzer sensing amplifier and microprocessor through the grounding between the sensing head and the vacuum system, despite careful grounding and shielding techniques. During an accidental high voltage fault, several integrated circuits and transistors were destroyed. The sensing head has now been completely isolated from the vacuum system by a 15 cm long section of Pyrex pipe and the noise problems are greatly reduced.

New accessories for the residual gas analyzer have improved its usefulness. A specially designed baking jacket for the sensing head keeps a constant, elevated temperature inside the sensing unit and thus reduces sample absorption by the metal surfaces. A new copier produces a hard copy of the mass spectrometer output and greatly speeds data acquisition and reduces film consumption.

2. Diagnostic Development

a) Mass Spectrometer for Gas Analysis

The on-line mass spectrometer used for gas analysis has been an extremely difficult instrument to use. The large background spectrum due to the high pressure gas makes it very difficult to detect the relatively small changes in the gas after a discharge. Also the pressure converter necessary to reduce the gas sample from 2 Atm to 10^{-5} Torr results in a long sample time (approximately 2 s) and hence reduces the possibility of measuring highly reactive (short-lived), ionized species, molecules of low volatility, or readily absorbed molecules. The mass spectrometer is also highly susceptible to the noise created in the pulsed power environment. Several system changes made to improve the mass spectrometer operations were described in the previous section. Maintaining good calibration and accurately measuring background spectrum, sample delay time, and line drift has been necessary to obtain reproducible results from the gas analysis.

It is also imperative to know, before-hand, what changes to look for in order to use the mass spectrometer productively. Thus other techniques are necessary to give an indication of possible chemical reactions occurring in the gas.

b) Spectroscopy

Optical spectroscopy on the pressurized gas discharge is difficult because the high temperature, high pressure discharge leads to a very complex spectrum. A large continuum level, highly broadened lines and many emission lines (especially for SF_6) make spectroscopy highly unreliable for quantitative measurements. A few qualitative observa-

tions (line identifications) are possible, especially on the simpler gases (N_2).

c) Current and Voltage Probes

Discharge current measurements are made with a Pearson current transformer, without difficulty. Voltage measurements, however, have proven to be more difficult. The original goal was to measure the voltage drop across the gap by using capacitive dividers within the cylinder, without perturbing the electric field sufficiently to alter the breakdown characteristics. These two requirements, however, are somewhat mutually exclusive. To build a capacitive voltage probe with enough surface area and relative spacing (cylinder-ground-to-probe/probe-to-electrodes) to overcome the tremendous signal-to-noise problem in the high-current, fast discharge, without significantly perturbing the electric field between the electrodes, may be unattainable. Resistive voltage dividers attached to the electrodes at their exit from the gap chamber are used instead, since the time scales involved are long (microseconds).

d) ESCA

Electron spectroscopy for chemical analysis (ESCA)* has proved to be a very useful surface analysis technique for identification of atomic species present on the electrode surfaces, Ref. [2]. Samples, approximately 1 cm^2, are cut from two regions on each electrode surface. As shown in Fig. 1, the inner region is the discharge region which undergoes erosion and thus is the site of any anode spots caused

---

*Work has been done, on a contract basis, by SCR Labs in Houston, Texas.

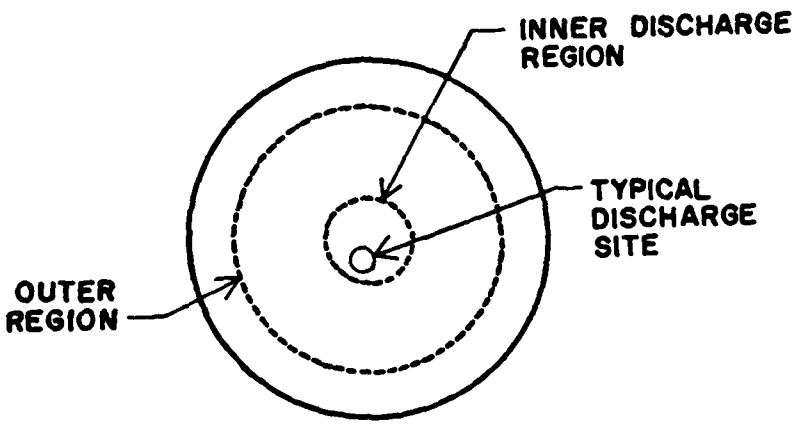

Fig. 1 Electrode Region (to scale)

by the arc channel. The outer region immediately surrounds the discharge region and shows evidence of chemical reactions or deposits. From ESCA, quantitative results (± 15% at best) and emitted electron energy shifts aid in determining the chemical bond structure on the surface. This technique provides an excellent starting point from which to begin interpretation of results from other surface and gas analysis techniques.

e) SEM

Scanning electron microscopy (SEM)* has produced excellent results, especially in comparing electrode deterioration under different conditions. Scanning electron photomicrographs are taken of the same samples as cut for the ESCA analysis. Metallurgists or graphite specialists must be consulted for much of the interpretation of the surface features. X-ray emission scans of different metal contents of the electrode surfaces can sometimes give a crude picture of metal distributions.

f) Fluorescence

The absorption and emission spectrum in the optical range promise to give some information on graphite surfaces, especially concerning possible organic deposits.

g) Mass Spectroscopy of Deposits

Deposits from several places in the gap, as well as those from the electrode surface and the gas, have been analyzed. Mass spectroscopy has yielded some useful information on solid samples taken from

---

*Work has been done, on a contract basis, by SCR Labs in Houston, Texas.

the bottom of an SF_6 filled gap. The solid sample (a very small amount) is heated and the volatilized species are analyzed. This technique should prove to be very useful in examining further deposits.

h) Chemical Analysis

A few analytic chemical techniques have been used to estimate qualitatively the deposit contents. Results obtained by these techniques are mentioned in the next section.

3. Results

Spark gap materials studied and described in this report are graphite and K-33 (a tungsten-copper composite) electrodes, Lexan and "Blue Nylon" insulators, and N_2 and SF_6 filler gases. The number of materials studied initially is limited in order to speed the development of the on-line diagnostics and to refine the surface analysis techniques before attempting the study of a more complete range of materials. Even with this reduced parameter space there are (including the no-insulator case) twelve different combinations to be studied. The materials chosen represent some of the most promising materials currently being used in spark gaps. This section of the report deals primarily with analysis of the anode (bottom electrode) and the gas. The interaction of the insulators with the electrodes and gas is discussed but detailed analysis of the insulator surface is given in the Project No. 4 part of this report.

The SEM and ESCA analyses were done by Spectrochemical Research Corp. in Houston, Texas. Interpretation of the ESCA results was aided by Mike Foster of the Spectrochemical Research Corp. During the writing phase of this paper help in analyzing the ESCA results and

SEM photographs has been received from Ken Rachocki, Dennis Dimiduk and Larry Matson from WPAFB and from personnel from Poco Graphite Co., the manufacturer of the graphite electrode material. Frazer Williams (Projects No. 2 & 5) is aiding with the optical spectroscopy of the gas and Dr. John Marx of the TTU Chemistry Department is helping with the chemical analysis techniques, including mass spectroscopy and fluorescence, and with interpretation of the gap chemistry.

a) Graphite

The graphite being used is ACF-10Q made by Poco Graphite of Decatur, Texas. It is a very dense, fine grain graphite with a maximum particle size of less than 0.02 mm. The hemispherical electrodes are made on a lathe with a steel bit and under magnification show a surface structure representative of fine grained graphite. No chemical agents are used and no machining marks are visible. The surface of the virgin electrode is 94% carbon and 6% oxygen. The oxygen is adsorbed O_2, CO and CO_2 on the graphite surface. Hydrocarbons are also invariably adsorbed on the surface but are difficult to detect on the carbon background.

Different erosion processes are apparent in the SEM photographs of the electrode surfaces. Figures 2 & 3 compare virgin, N_2 exposed, and SF_6-exposed samples. The latter two were each subjected to 50,000 shots in their respective gases without an insulator present. At 40 kV, each shot contains about 650 J and passes .03 C, giving a total transferred charge of 1.5×10^3C.

b) Graphite - N_2

The erosion mechanism occurring in N_2 is most likely sublimation.

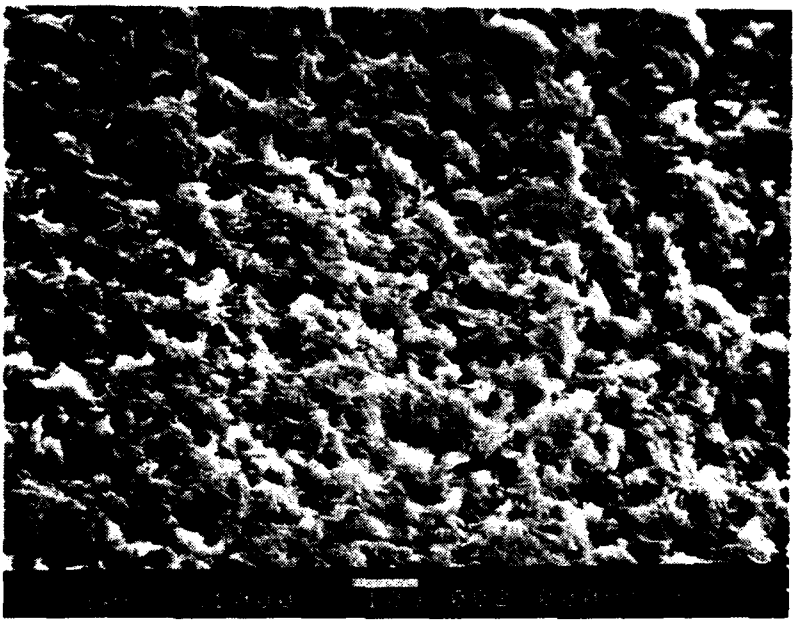

a. Virgin - 0 shots (scale x 1000)

b. N_2 - 50,000 shots (scale x 1000)

Fig. 2 Graphite Electrodes (Inner Region)

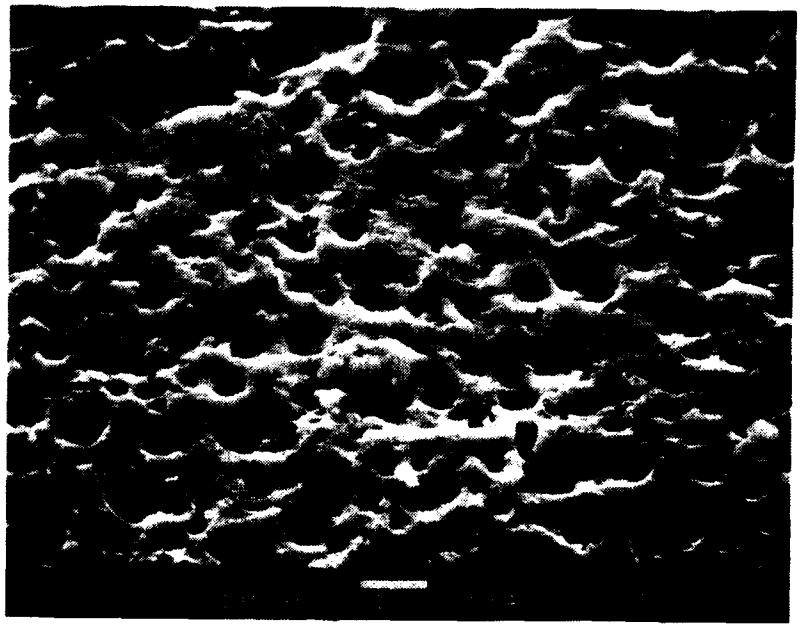

Fig. 3 Graphite Electrode (Inner Region) in SF_6 - 50,000 shots (scale x 1000)

Graphite does not have a molten state at the pressures found in the gap, although it reaches a flowing stage at 2800°C, and will sublimate at 3700°C. The inner region discharge surface (Fig. 2b) is very smooth, with extremely fine grain structure (less than .1 μm) and apparently was eroded at the point of the discharge by sublimation at a surface temperature in excess of 3700°C. The surface also contains a few craters, 2-3 μm in diameter. A few thermally induced cracks are visible. The smooth, fine-grain structure and the few large craters indicate two possible mechanisms of erosion. The large craters are too few and widely scattered to be the major erosion mechanism. Instead of being formed by ejection of pieces of material (since the graphite does not melt) the craters probably occur at impurity sites which were subject to accelerated chemical reaction (with O or N). Further analysis of the crater walls with an electron microprobe or Auger electron microscopy is necessary.

From ESCA analysis, the virgin surface (94% C, 6% O) changes to 52% C, 14% O and 31% N in the inner region and 70% C, 11% O and 16% N in the outer region. Also a small amount of fluorine contamination (less than 2%) was present due to system contamination from previous SF_6 studies. Several conclusions were reached from the ESCA analysis. First, the change in O on the surface (after allowing for about 6% adsorbed O) is due to an increase in oxides (CO and CO_2) formed on the surface. The oxygen is obtained from the water released by all surfaces in the gap during firing. The gap was not baked under vacuum in order to remove water prior to firing since this would not be representative of a real spark gap usage. The residual gas analysis in-

dicates an increase in CO_2 in the gas directly proportional to any increase in H_2O (discussed further later). Also NO_2 has been detected by other chemical means. Optical spectroscopy indicates the presence of C and O ions in the graphite-N_2 discharge.

The second significant chemical process occurring on the electrode is the nitrogen attachment to the surface. In the inner region, N accounts for 31% of the surface atoms. The increases in both N and O are higher in the inner region, indicating either that the inner region (higher temperature) is the site of more chemical reaction (very likely) or that the outer region is being covered by deposited carbon. The energy spread of the carbon line (ESCA) after firing indicates the presence of a carbon bond with another atomic species. The exact nature of the C-N bond, or if it has any effect on the erosion, is not yet understood.

Continued study of the graphite-N_2 combination will include spectroscopy, looking for NO and CN compounds (Cyanogens), polished cross-section analysis to study crater depth, chemcial analysis of the black powder deposited throughout the gap (probably amorphous carbon and not graphite) and detailed measurement of the erosion rates.

c) Graphite-SF_6

Graphite in SF_6 seems to undergo a completely different erosion process. (Fig. 3). The surface shows a uniform, high density of holes (craters), 5 to 10 μm in diameter and hemispherically shaped. The uniform density and shape imply that a chemical erosion is occurring in the discharge. ESCA shows that the graphite surface is composed of several forms of carbon. Some of the C bonds can be identified as CF_x

compounds formed on the surface.

Study of the graphite surface in SF_6 is complicated by another chemical process taking place in the gap. Fluorine generated in the discharge from the decomposition of SF_6 reacts with aluminum in the spark gap chamber to form AlF_3. The AlF_3 (a whitish powder) covers all surfaces and collects at the bottom of the gap. The Al comes from occasional misfires between the bottom electrode and the outer cylinder (1 in 1000 shots) or from poor electrical contact in the upper electrode holder (generating sparks at the threads). The inner electrode region shows a composition of 40% C, 32% AlF_3 and 20% other F. The 20% extra F is bonded to the graphite surfaces in the form of CF_x compounds.

The outer region is composed of 77% AlF_3, 16% C and 6% O. Since the C and O probably result primarily from surface adsorption of oxides and hydrocarbons after removal from the gap, the outer electrode region is probably 100% covered by AlF_3. This conclusion is verified by analysis of a removed flake of material under x-ray map analysis of Al (see Fig. 4), showing virgin graphite beneath the chemical crust. The AlF_3 crust has the appearance of a hot chemical deposit which has been cooled, leading to cracking and curling (10 μm diameter flakes).

The constant O content (6%) in the virgin, inner and outer SF_6 samples is most likely all due to surface adsorption after removal from the gap. Thus there may be no oxygen available for reaction with the graphite surface, as occurred in nitrogen. Any H_2O released during discharge probably rapidly reacts with F or other SF_6 derivatives.

After 50,000 shots in SF_6, the bottom of the gap is covered with

a. SEM photograph (scale x 2000)

b. Al metal map of same region (scale x 2000)

Fig. 4 Graphite Electrode (Outer Region)

up to 2 mm of powder. Chemical analysis so far has detected elemental sulfur, AlF_3 and some elemental aluminum.

d) K-33

The metal electrode studied is a composite composed of 66% W and 33% Cu (designated as K-33) developed and manufactured by Metallwerk Plansee of Austria and distributed by Schwarzkopf Development Corporation. It is made by forming a porous tungsten substrate from a sintered tungsten (W) powder, then infiltrating molten copper. The W gives good erosion properties and the Cu gives good thermal and electrical conductivity. Figure 5a shows an SEM photograph of the machined electrode surface. Machining marks are highly visible and ESCA shows the surface to be composed of 61% Cu, 3.6% W and 36% hydrocarbon contaminants. The machining process turns over the soft copper and masks the W. The metal electrode samples show a high surface contamination content under ESCA (typically 50% hydrocarbon, 40% oxides) after removal from the spark gap and exposure to the atmosphere. To reduce this masking contamination, all metal samples are exposed to a weak argon ion beam, which sputters away adsorbed surface molecules. On the virgin sample, for instance, hydrocarbons are reduced to 36% and all of the oxides are removed. As with graphite, K-33 appears to undergo different chemical processes in N_2 and SF_6.

e) K-33 - N_2

In the inner region (discharge region) in N_2, the resulting K-33 surface is very rough (Fig. 5b). The material appears to have been melted and splattered. The material surrounding the many pores is probably the original tungsten matrix because of its similarity in

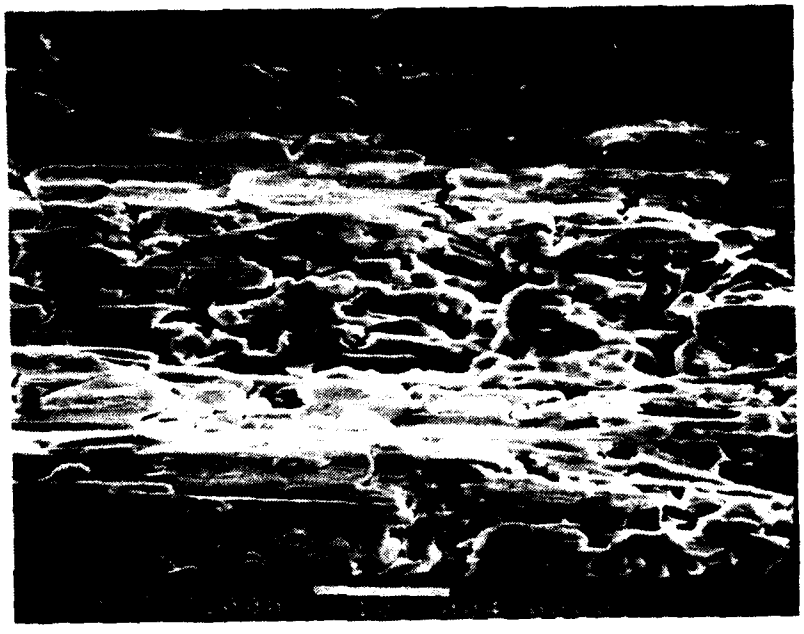

a. Virgin - 0 shots (scale x 2000)

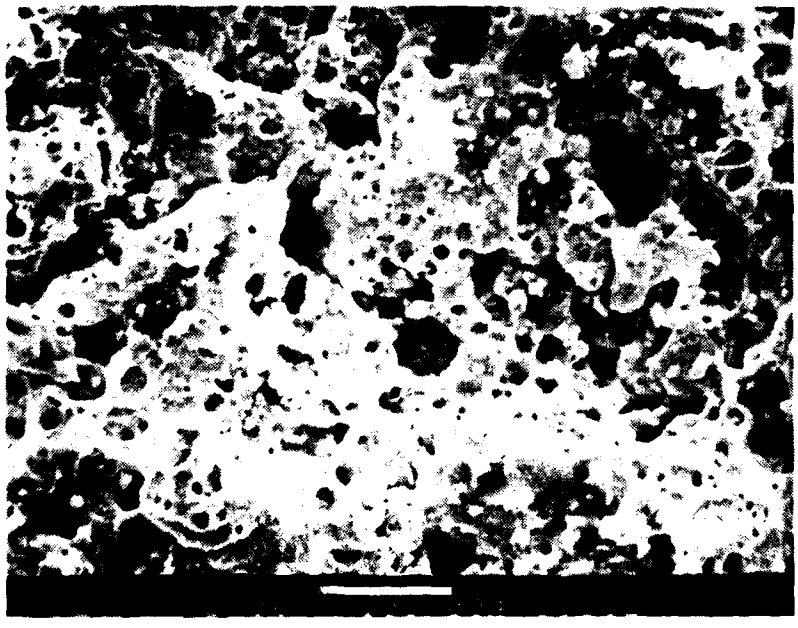

b. N_2 - 50,000 shots (scale x 2000)

Fig. 5 K-33 Electrodes (Inner Region)

appearance to a polished cross-section view of a virgin sample. ESCA indicates a relative decrease in Cu and some increase in W (28% Cu, 4.8% W, 36% O, 25% hydrocarbons). The copper has probably been drawn to the surface and boiled off or ejected in molten particle form. All W exposed on the surface has been oxidized (probably WO_2 and WO_3). The surface of the K-33 has no smooth, vaporized characteristic like the graphite, but appears to have undergone melting and violent boiling. This circumstance is plausible since W, and especially Cu, have lower melting temperatures than C.

The outer region is covered entirely with vapor redeposited metal crystals. The vertical crystalline growth is composed of dendrites, 1-4 μm in diameter, 2-8 μm tall, which are primarily tungsten oxides and metallic Cu. The tungsten has a lower oxidation potential at high temperatures than copper and thus oxidizes much more readily.

Details of the damage mechanisms and the recrystallation processes are not clear and necessitate further study. To determine the damage depth and the tungsten-copper profile depth, three new techniques should be employed. First some polished electrode surfaces need to be subjected to a single shot to determine the extent of damage per shot. Second, cross-section slices should be cut, polished and examined with SEM. Finally, more accurate surface probing techniques, such as an electron microprobe or Auger electron spectroscopy, need to be employed to study crystal growth and material distribution.

f) K-33 - SF_6

The processes involved with K-33 in SF_6 are interesting and quite complex. This combination is the first to show a definite effect of

each individual discharge. In graphite, for instance, detailed analysis of the surface shows no distinct change caused by the most recent shots to the immediate surrounding material. In K-33, however, each of the last few shots has masked the effects of the previous, underlying shots. Two distinct regions are apparent within the inner discharge region. The center of a single discharge, 3 mm diameter, appears to have been a molten pool of material which underwent rapid cooling from the bottom up (Fig. 6a). During cooling, recrystallization of the material produced a large scale (400 μm across) cellular pattern. The region immediately outside the individual discharge site (still within the inner electrode region) is composed of two materials, of different melting points (Fig. 6b). This was determined by noting how one material flowed around the other. At least one of these materials was thrown out from the center of the discharge site.

Since ESCA analysis covers a relatively large spatial area (1 mm^2), it is not selective enough to study each of the two regions at a discharge site, but gives an average of the surface content. Analysis with an electron microprobe or with Auger electron spectroscopy is needed. Although resolution is poor, ESCA does show a very broad F line indicating several fluorine compounds, including CuF_2 and CF_2. There are two forms of carbon on the inner electrode region indicating the normal hydrocarbons plus some other carbon compounds (probably CF_2). The carbon available for chemical reactions in the discharge comes from prior hydrocarbon contaminants or from impurities within the metal. It is very likely that WF_6 is formed in the discharge but

a. Inner Region (scale x 200)

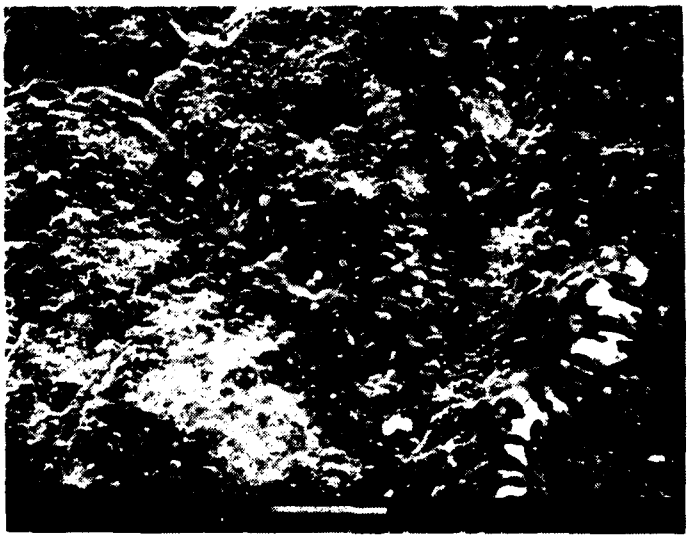

b. Outer Region (scale x 200)

Fig. 6 K-33 Electrodes in SF_6 (50,000 shots)

none is detected on the electrode surface due to its high volatility (boiling point 19.5° C). The inner region is composed of 28% F and although some CuF_2 is formed, most of the copper is still in metallic form. Again in SF_6, as for the graphite electrodes, very little oxygen is found on the surface.

The outer region (outside all discharges) is composed of a redeposition of material in a flake pattern, characteristic of chemical deposits. It is composed of 43% F with very little metal content (less than 20%). Detailed analysis of the K-33 electrode regions used in SF_6 are needed with the same techniques previously mentioned: one-shot study, cross-section analysis,and electron microprobe or Auger electron spectroscopy.

g) Exposure to Insulators

Square insulator samples (20 cm x 20 cm x 8 mm thick) were placed 5 cm from the discharge region to (1) produce discharge-exposed insulator samples to be studied in Project #4 and (2) to study the effect of the insulator presence on the electrode and the gas. Several studies with Lexan have been made and preliminary studies of blue nylon have begun. The electrode analysis reveals some similar characteristics of almost all electrode surfaces exposed to either insulator. These will be discussed first.

When comparing an electrode sample taken after 50,000 shots,without an insulator,with one taken after 50,000 shots,with an insulator, it is apparent that the erosion mechanisms for the electrode material is basically the same. The electrode sample exposed to the insulator, however, is invariably highly masked with organic molecules (except for

the graphite-SF_6 case), most likely deposited after the electrode surface has cooled. The erosion detail, holes and cracks seen previously without an insulator are now filled and covered, although their outline can sometimes be seen. In all cases (all combinations of K-33, graphite, N_2 and SF_6), ESCA shows a higher surface content of organic carbon compounds on the surface. Since both inner and outer areas are covered and since most organic molecules have a low melting point it is thought that the material is deposited after the discharge.

In N_2, an increase in H_2O is observed in the gas, a small increase with Lexan present, and a larger increase with blue nylon. This result is consistent with the fact that Lexan absorbs 3% water and blue nylon absorbs 6% water by weight.

h) Lexan

In the graphite-N_2 system, a thick organic deposit is formed on the electrode surface. Besides an increase in organic carbon, the oxygen concentration is 23% as opposed to 14% without an insulator. On K-33 surfaces in both N_2 and SF_6, the organic layer shows a somewhat crystalline, star-shaped pattern. It is more prominent in N_2. In SF_6, organic F compounds were formed and deposited on the surface.

The only visibly odd case was the graphite in SF_6 which showed no distinct visible difference between the insulator and the non-insulator cases.

i) Blue Nylon

Two important differences are observed when blue nylon is present in the discharge. First, more visible deposits are left and more H_2O is released (leading to increased sources of O for the production of CO_2

in graphite and WO_2 in K-33). The second major difference between the blue nylon and Lexan cases is that after exposure to blue nylon, silicon is found on the electrode surfaces. The exact chemical nature of the Si on the electrode surface is not yet known, nor its source, although it is suspected to come from the mold release for the blue nylon.

4. Further Studies

The preliminary analysis generated many unanswered questions. Improvement to the current on-line diagnostics, refinement of the surface analysis techniques and some new analysis approaches are all needed. Many of these have been mentioned but will be briefly reviewed.

Two important on-line diagnostics for chemical analysis should be improved. The optical spectrum could be more effectively studied by using an optical multichannel analyzer (OMA) in conjunction with the 0.5 m monochromator. Not only would this allow study of the complete spectrum in one shot, but by gating the OMA, the cooler stages of the discharge can be studied by avoiding detector saturation during the arc phase. The selectivity and sensitivity of the mass spectrometer could be greatly improved for gas analysis by using it in conjunction with a gas chromatograph. The background gas, N_2 for instance, could be separated, allowing for more sensitive detection of the small percentage gas constituents.

Some new surface analysis techniques need to be employed to resolve chemical structure on the electrode surfaces. Auger electron spectroscopy and an electron microprobe will give better spatial resolution. Single shot studies and cross-section analysis will give

information on damage depth and single shot damage mechanisms. The electrode surfaces should be prepared in different manners, polishing the K-33 and grinding the graphite, to give a more uniform initial surface. More analytic chemical analysis is needed, including vaporization and mass spectrometer scans of electrode scrapings and other gap deposits.

Erosion and recovery measurements are currently in progress and will give needed data on how the different chemical processes and erosion mechanisms discussed will affect the properties of the spark gap operation.

5. Lumped Transmission Line Generator

The construction of the lumped transmission line generator (60 kV, 40 kA, 12 μs) has been completed and is shown in Fig. 7. This line will be used for detailed diagnostic studies of spark gap processes at higher charge transfer per shot. The design of a new test gap for such studies is nearly completed. The gap will be able to operate at modest vacuum levels or at high pressure and will have two sets of through ports to allow for a variety of optical diagnostics including inteferometry and absorption spectroscopy.

The line was tested by being resonantly charged with a triggerable Marx bank (60 kV, 18 kJ) shown in Fig. 8, and discharged into a portable spark gap and load test assembly. The output pulse given by the computer code SCEPTRE and the current pulse viewed by a current transformer were in close agreement, as seen in Fig. 9.

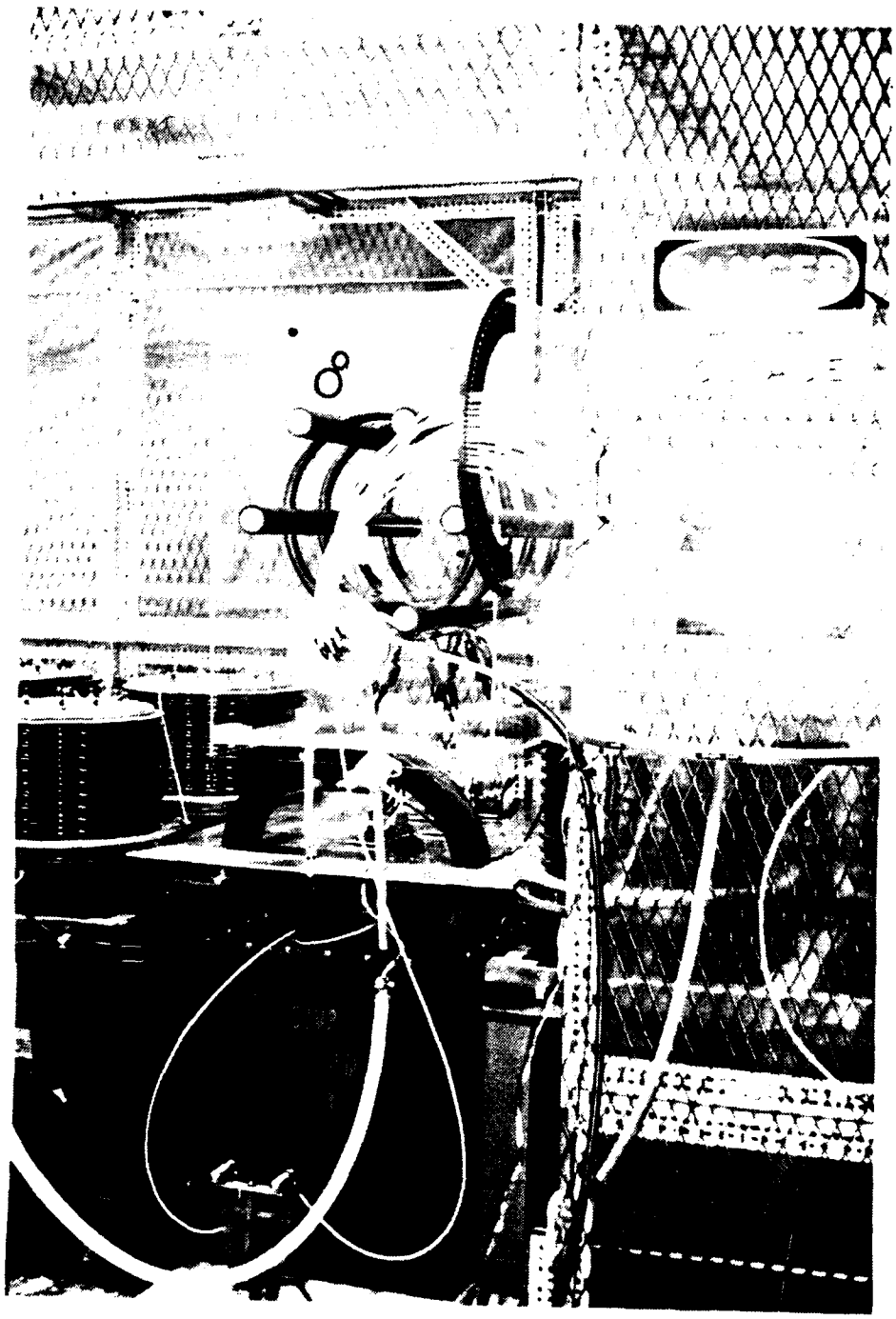

FIG. 7 LUMPED TRANSMISSION LINE GENERATOR

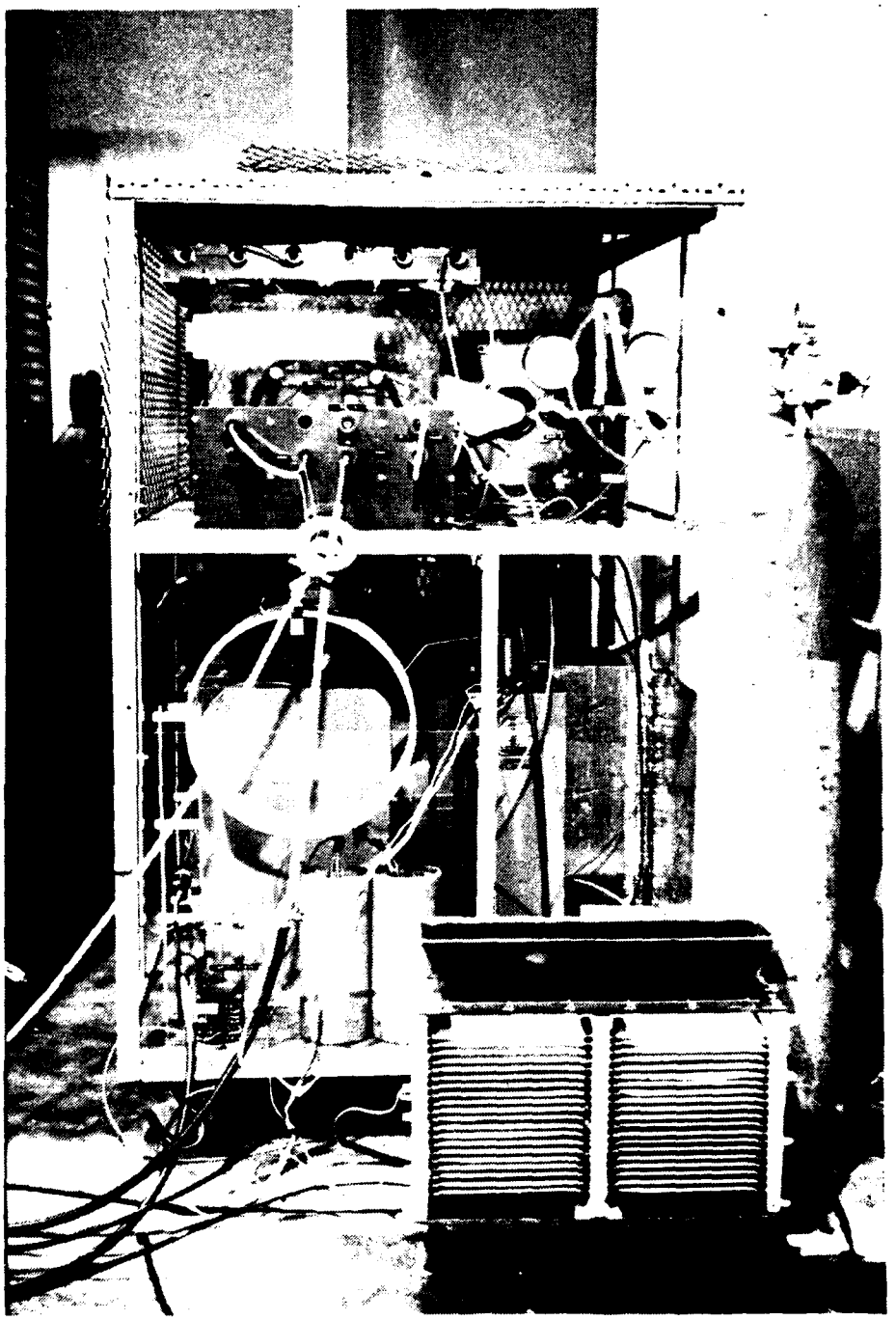

FIG. 8 MARX BANK

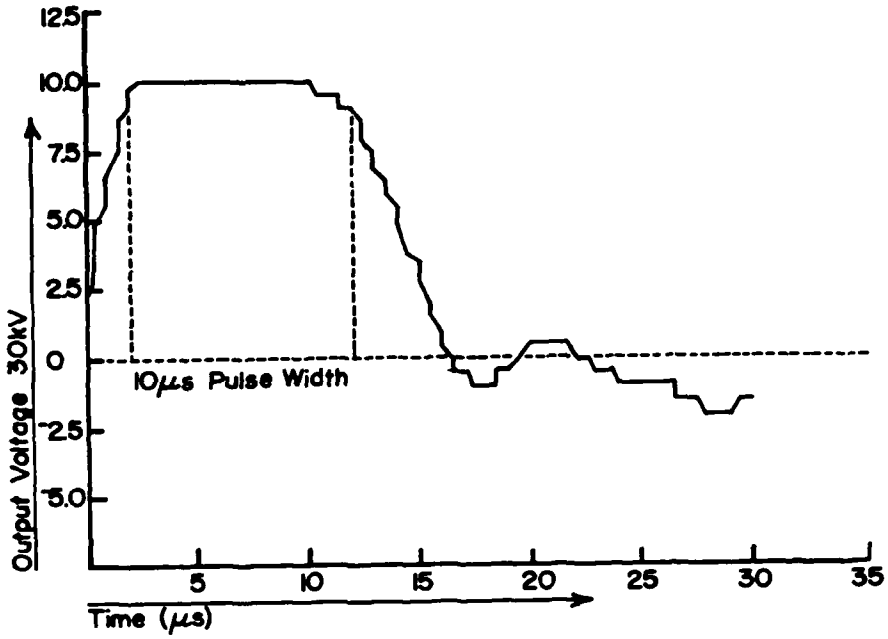

FIG. 9a
PREDICTED OUTPUT WAVEFORM

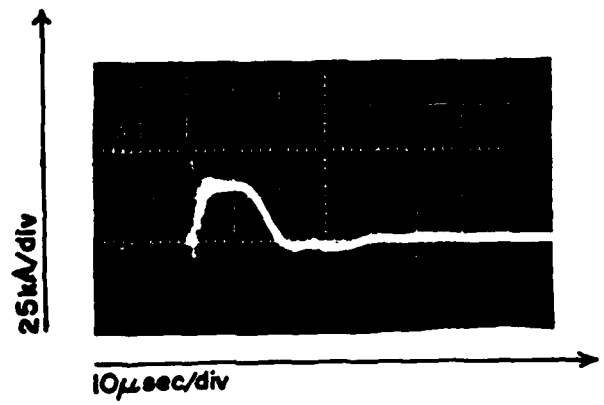

FIG. 9b
ACTUAL OUTPUT WAVEFORM

C. SPARK GAP RECOVERY STUDIES WITH THE SINGLE CAPACITOR GENERATOR

Preliminary studies of the voltage recovery processes in spark gaps are underway. Fig. 10 shows the schematic of the recovery test circuit. The main circuit consists of the capacitor C (0.82 μF), the spark gap chamber, and the 1Ω load. The capacitor charges from the 75 kV power supply through the 1 MΩ charging resistor. When the gas in the chamber breaks down, C discharges through the spark gap chamber and the 1Ω load. The Rogowski coil picks up the discharge current to trigger the delay generator. After a suitable delay time, the output signal from the delay generator triggers the ignitron generator circuit which in turn fires the Marx bank. Power supply #2 (30 kV) charges the Marx bank capacitors.

The erected Marx bank charges capacitor C through an adjustable resistor (1 - 25 kΩ). The adjustable resistor changes the charging rate of capacitor. The first breakdown current and second restrike breakdown current are measured by a Rogowski coil and recorded by a pulse height analyzer (KIDL, 400 channels, model 34-12B) or a storage oscilloscope (Tektronix type 549). It is assumed that the peak current is nearly proportional to the capacitor charging voltage, since $R_L >> R_{spark}$.

The test parameters in the spark gap chamber for recovery study are:

1. electrode separation: 0.1 - 1.0 cm
2. electrode materials: graphite, brass, K-33
3. filler gases: N_2, SF_6, mixture of N_2 and SF_6
4. pressure: 150 torr - 3 atm
5. restrike charging rate: 0.3 kV/ms - 7.5 kV/ms

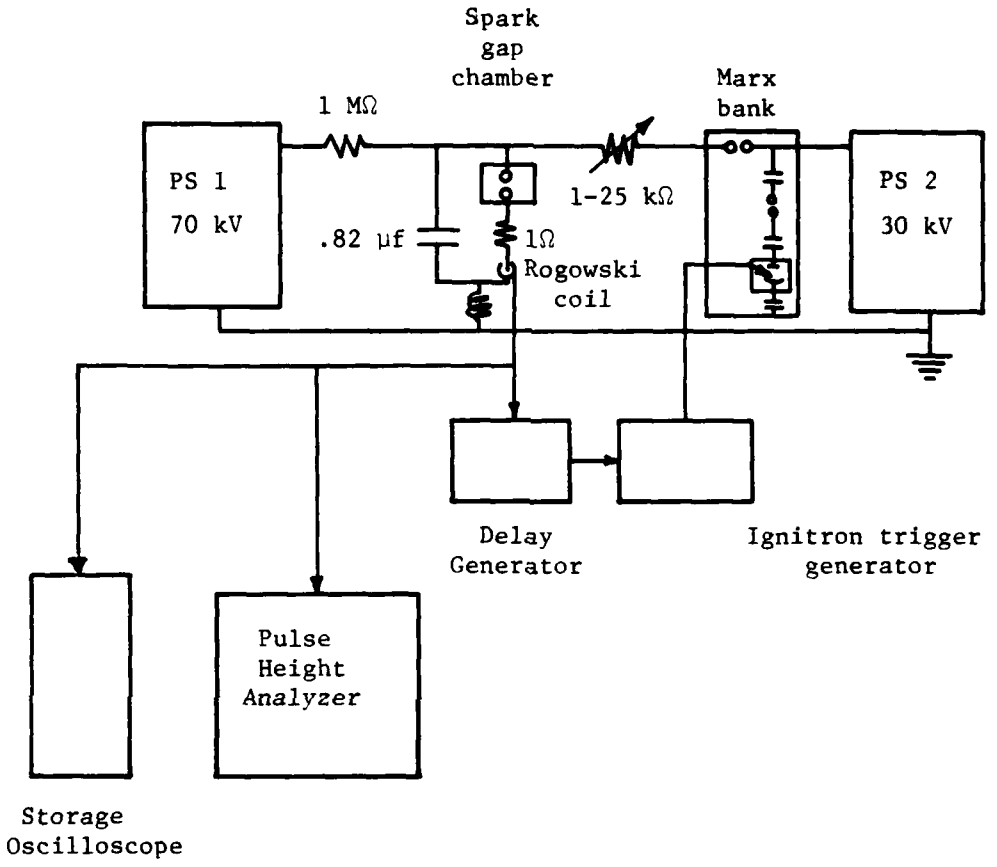

Fig. 10 Schematic of Recovery Test Circuit

The recovery rate in N_2 with 2 different gap spacings is shown in Fig. 11. Note that the recovery rate decreases with gap spacing. The recovery rate in N_2 and SF_6 with different pressures is shown in Fig. 12. The N_2 has a faster recovery rate than SF_6 at the same pressure. Figs. 11 and 12 also show that the recovery rate decreases with pressure. The recovery rates in the N_2, SF_6 and N_2 - SF_6 mixture at the same pressure are shown in Fig. 13. At 1 atm and d - 3.3 mm, pure N_2 has a faster recovery rate than 0.1 SF_6 + 0.9 N_2. Pure SF_6 has the lowest recovery rate. At larger gap spacings (d - 8.3 mm, P - 500 torr), pure N_2 has a faster recovery rate the first 5 ms. After 5 ms, 0.1 SF_6 + 0.9 N_2 has a faster recovery rate than pure N_2, as shown in Fig. 14.

The graphite electrodes after several hundred recovery shots are shown in Fig. 15. Tracks on the bottom electrode suggest that the restrike may occur near the edge of the electrode, presumably through the hot gasses, and then move toward the electrode center. We plan to use a MgF_2 window and a streak camera to observe the extinction and restrike of the arc.

D. ELECTRODE EROSION

1. PFN for Erosion Studies

A new PFN, shown in Fig. 16, has been designed, built, and tested in order to perform erosion studies requiring a large amount of total charge transfer. The equivalent circuit model in Fig. 17 was calculated and a comparison of SCEPTRE results and the initial test results are shown in Fig. 18. The design is flexible to allow for changes in voltage, pulse width, charge per shot, and energy per shot, over the

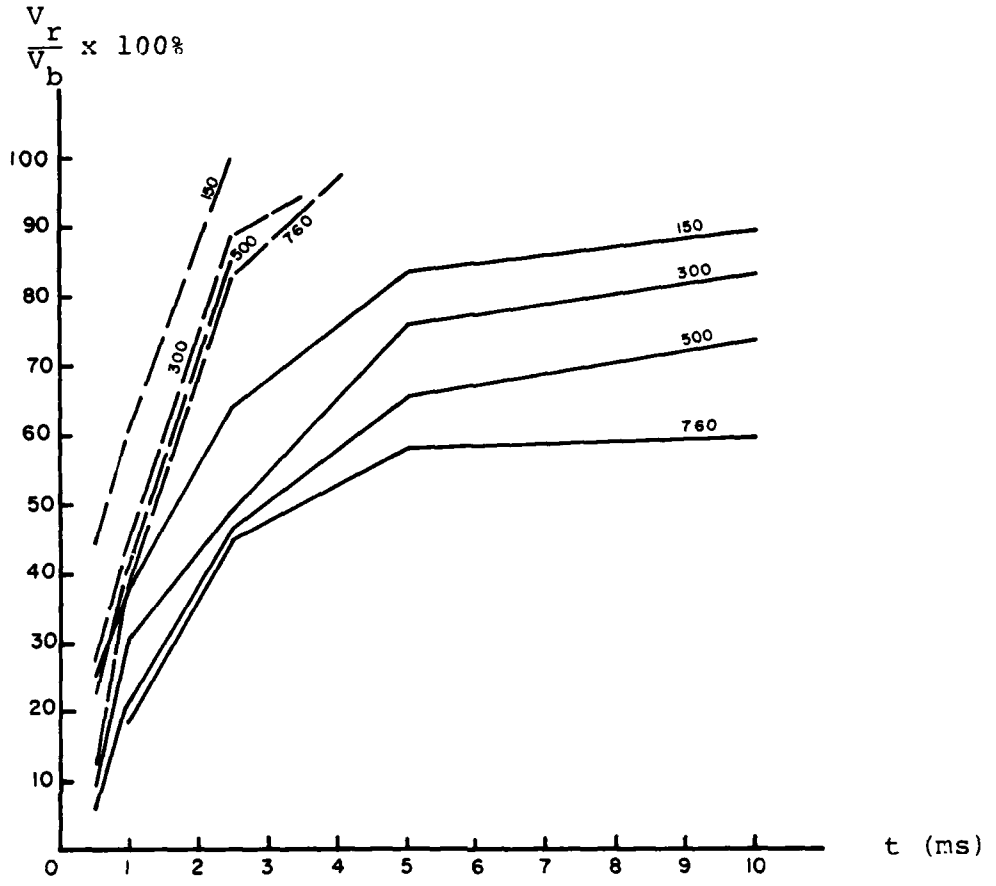

d = 8.3 mm ————— All Pressures in Torr

d = 3.3 mm — — —

Fig. 11 Recovery Rate in N_2 With Two Different Gap Distances

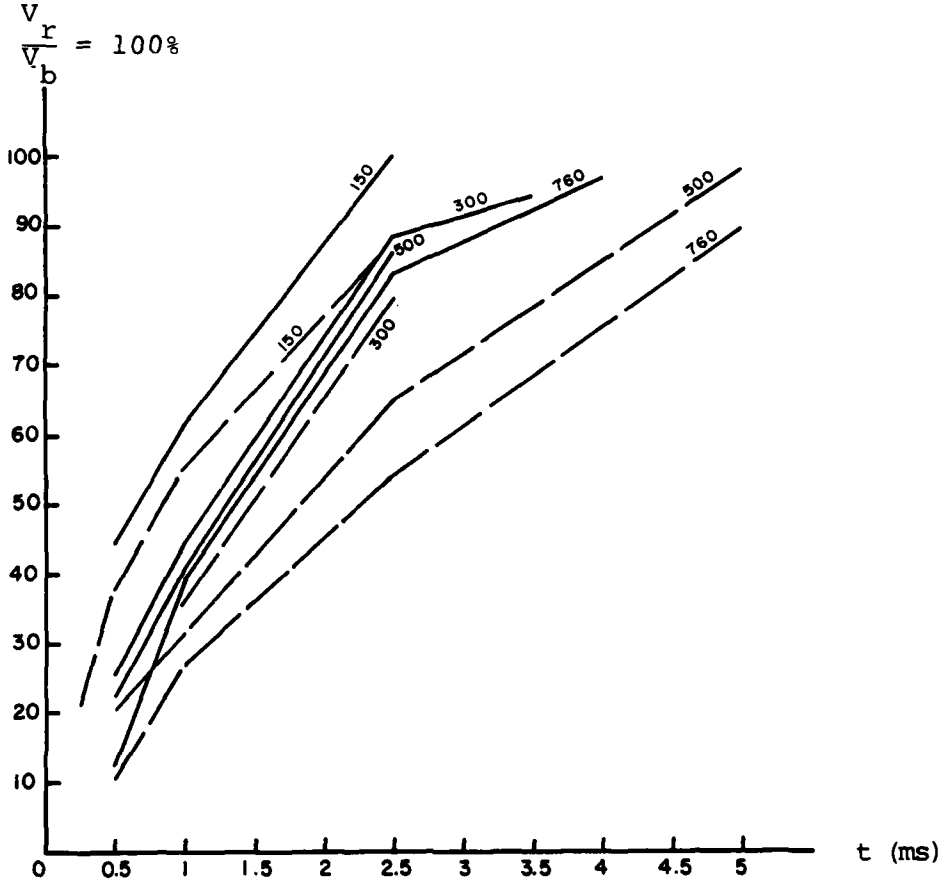

Fig. 12 Recovery Rate in N_2 and SF_6 With Different Pressures (d=3.3 mm)

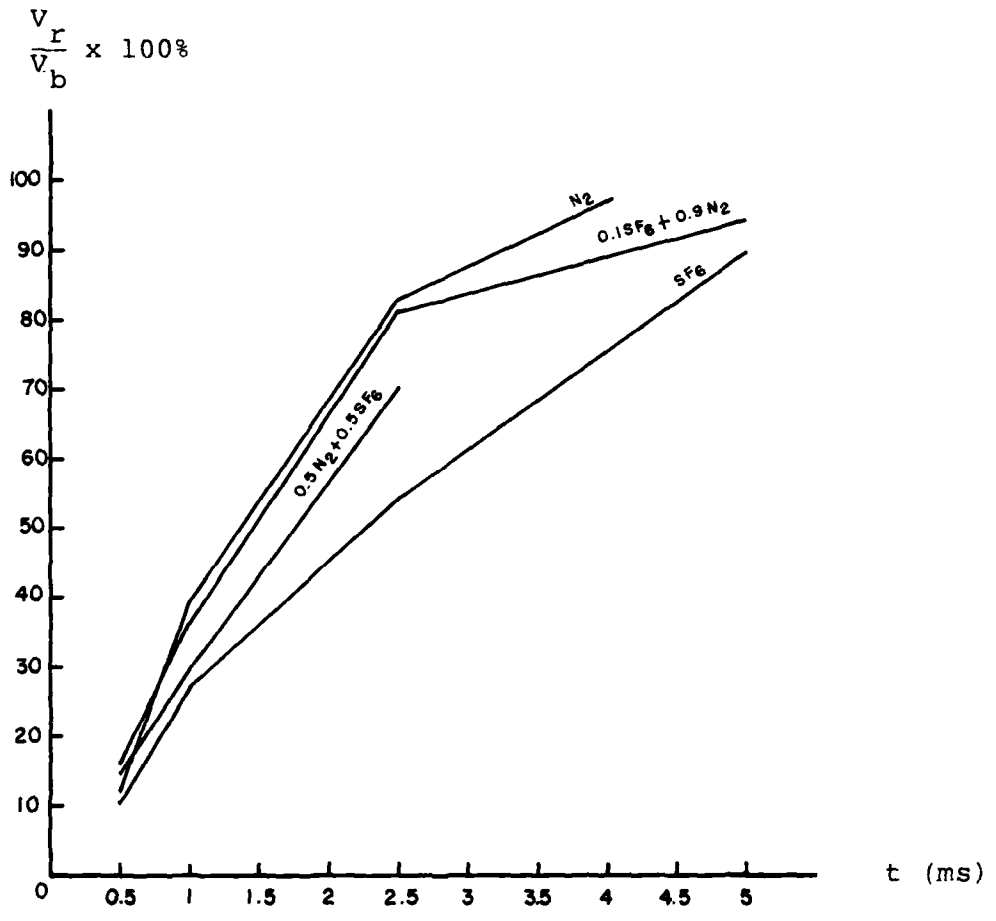

Fig. 13 Recovery Rate in N_2, SF_6 and N_2-SF_6 Mixture (d = 3.3 mm, P = 1 atm)

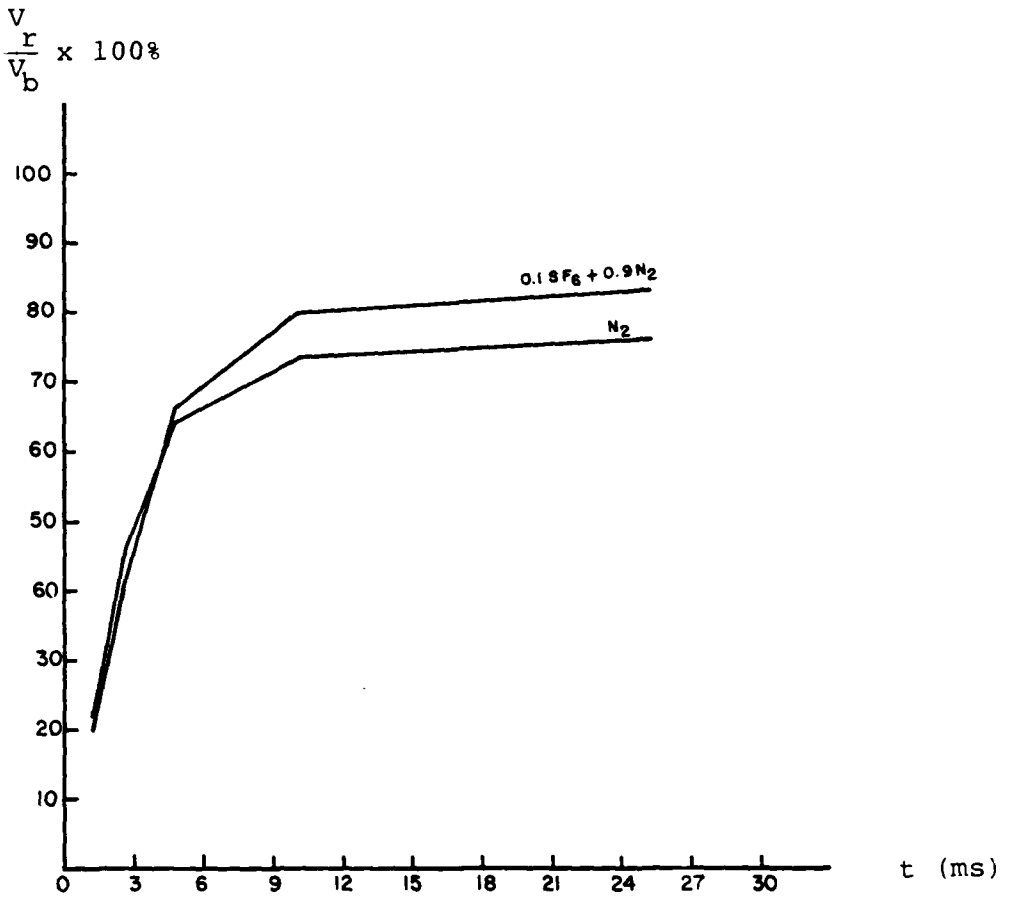

Fig. 14 Recovery Rate in N_2 and N_2-SF_6 Mixture With Larger Gap Distance (P-500 torr, d = 8.3 mm)

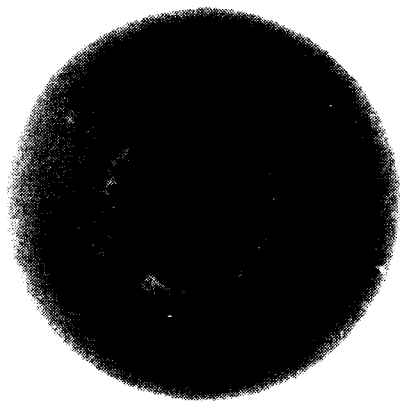

a. Upper Electrode

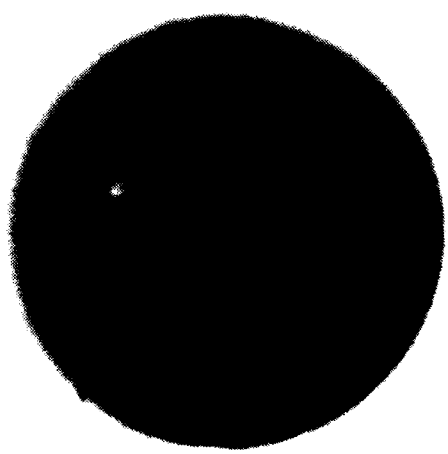

b. Lower Electrode

Fig. 15 Graphite Electrodes After Several Hundred Shots

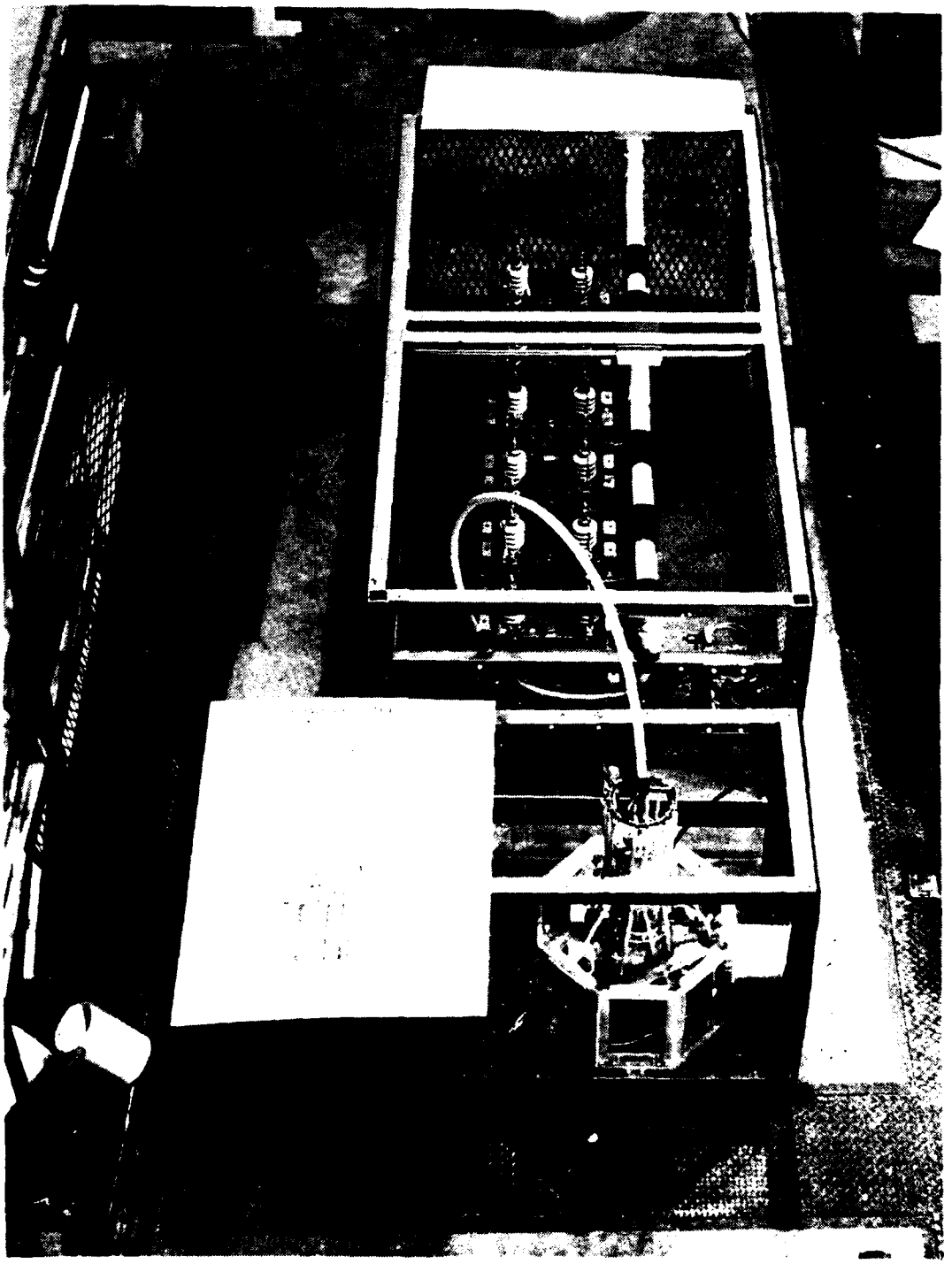

FIG. 16 PFN CONNECTED TO PORTABLE TEST ASSEMBLY

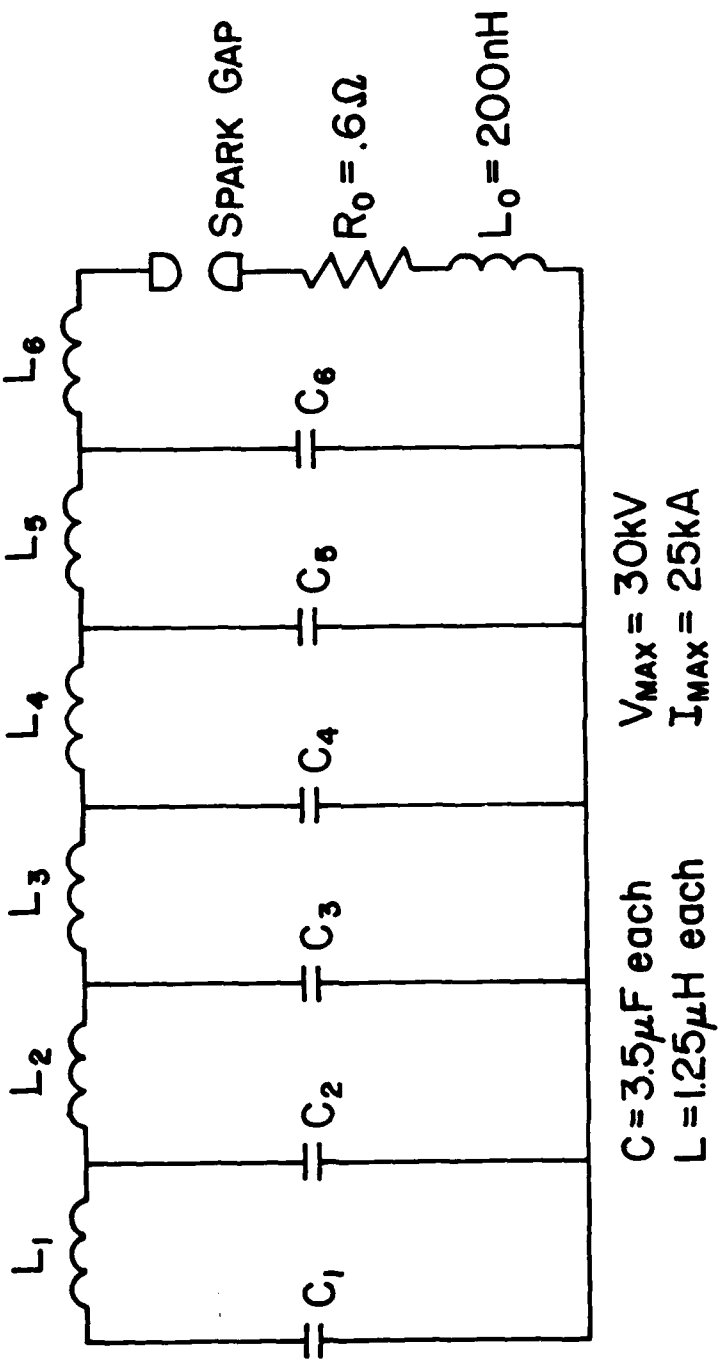

FIG. 17 PFN EQUIVALENT CIRCUIT

ranges shown in Fig. 19. At present the PFN operates at 20 kV, 25 μs, 0.4 Coul/shot, 4 kJ/shot, and 1.5 pps.

To accommodate the large average power required for erosion studies, a portable test assembly consisting of a flexible spark gap designed for easy electrode replacement and a low inductance, solid state load (0.6 Ω, 60 kV, 30 kW) was designed, built, and tested. Fig. 16 shows the test assembly connected to the PFN and Fig. 20 shows the details of the spark gap.

2. Plans for Erosion Tests

In order to provide a means of comparing our erosion results with other work, hemispherical 1" diam. brass electrodes have been machined for initial testing in static air. Eventually K-33, a copper tungsten alloy, and Poco graphite (ACQ-10) will be tested under static and flowing air conditions.

E. REFERENCES

1. First Annual Report on Coordinated Research Program in Pulsed Power Physics, December 1, 1980, AFOSR Contract #F 49620-79-C-0191.

2. Technical Report on Application of Surface Analysis Techniques to Pulsed Power Problems, G.L. Jackson, March 23, 1981, AFOSR Contract #49620-79-C-0191, Department of Electrical Engineering, Texas Tech University, Lubbock, Texas.

Circuit* #	V charge (kV)	I load (kA)	Z load (Ω)	C pfn (μF)	Q/shot (coul)	τ rise (μS)	τ pulse (μS)	Energy (kJ)
1	20	17	.60	21	.41	2.1	25	4.1
2	30	25	.60	15	.45	2.3	18	6.8
3	30	25	.60	30	.90	2.3	36	14
4	15	12	.60	45	.68	4.6	54	5.1
5	15	12	.60	105	1.6	4.6	126	12

* Different Circiut #'s correspond to series and/or paralleling available capacitors

Fig. 19 Sample Parameter Ranges for PFN

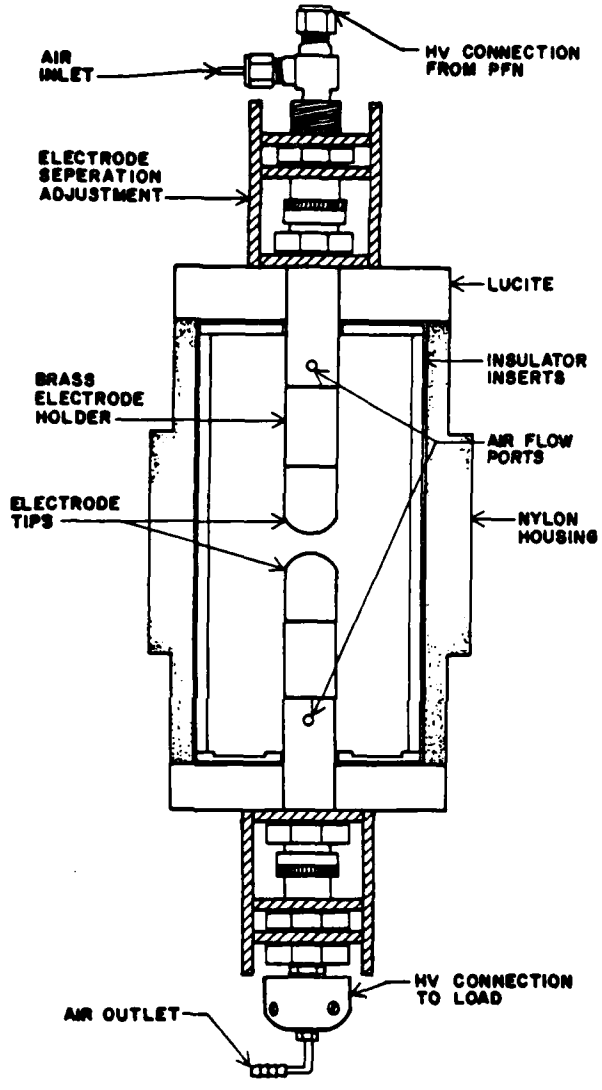

FIG. 20
SPARK GAP FOR EROSION STUDIES

Project No. 4

Pulsed Power Surface Physics and Applications

(G. Jackson, D. Johnson, L. Hatfield, and M. Kristiansen)

A. SUMMARY

Considerable progress has been made in the understanding of the damage to the surface of insulators inserted in the spark gap of Project No. 3. Some of the results are described in this report. Most of our resources, however, were committed to a study of the surfaces of the graphite and K-33 electrodes. Much more information about the insulators is available in the form of damaged samples awaiting surface analysis. These samples will be analyzed during the current contract period. The surface flashover experiment has yielded unexpectedly high flashover voltages for damages samples, forcing us to increase the applied voltage significantly and thereby slowing our progress.

The surface discharge switch investigations are on schedule. The basic switch assembly is complete and various dielectric flashover surfaces are ready for testing. Multichannel switching with up to 170 channels/meter has been demonstrated.

B. ANALYSIS OF INSULATORS EXPOSED IN THE SPARK GAP

1. Experimental Results

As part of the investigation of the damage to insulators used in high voltage spark gaps, Lexan insulators were placed inside of the spark gap described in Project No. 3. These insulators were 15 cm by 15 cm rectangles placed 1.5 cm away from the 5 cm diameter cylindrical electrodes. The composition of the electrodes and the gas used in the gap were changed in order to understand better how these parameters affect an insulator. During these experiments Lexan insulators were subjected to 5000 shots at about 40 kV with approximately 1 kJ of energy transferred per shot, in either 2 atmospheres of N_2 or SF_6 gas and with either graphite or K-33* electrodes. Afterwards the insulators were analyzed with Electron Spectroscopy for Chemical Analysis (ESCA) to determine what changes occurred to the surface of these insulators. Figure 1 shows the ESCA spectrum of an undamaged Lexan insulator. The spectrum shows that the surface of Lexan is composed of 86% Carbon and 14% Oxygen, obtained by the methods described in reference 1. This stoichiometry is in good agreement with that of virgin Lexan ($C_{16}O_3H_{18}$). It should also be noted that Lexan exhibits negative surface charging when exposed to the x-ray beam used in the ESCA spectrometer (as observed by the negative shift in the binding energy of the C_{1s} line). This phenomenon is extremely rare in ESCA [2]. However, for polymers such as Lexan which have an aromatic benzene ring it is possible to observe a negative charge accumulation on the surface.

---

* A brand name of Schwarzkopf Development Corporation for a cintered tungsten matrix with 33% infiltrated copper.

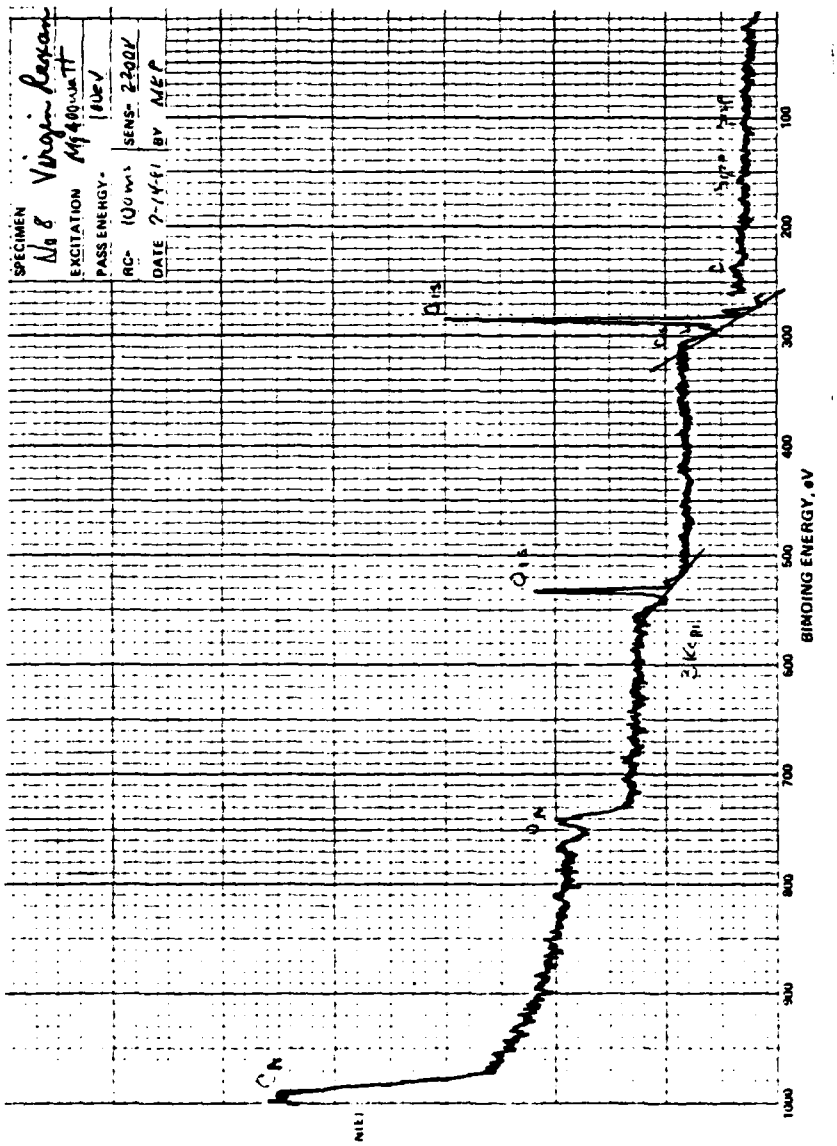

Fig. 1 ESCA Spectrum of an Undamaged Lexan Insulator

The Lexan insulator which was exposed to 5000 shots in the spark gap with graphite electrodes in 2 atmospheres of N_2 also exhibits negative charging in the ESCA spectrometer. The ESCA spectrum for this particular sample shows a marked decrease in the amount of carbon and a large increase in the amount of oxygen present on the surface. An expanded scale spectrum of the C_{1s} peak shows it to be considerably broadened compared to the expanded scale spectrum of the virgin sample, probably due to some form of C-N or C-O bonding, since there is some N_2 seen on the surface of this sample. However, the resolution of this peak is not adequate to identify the different forms of carbon bonding present on the surface. Scanning Electron Microscope (SEM) micrographs of this sample show the surface to be imbedded with small microparticles (the largest of which is approximately 2 microns in size). These microparticles cannot be indentified through the use of ESCA. However, it is probable that these microparticles are carbon from the graphite electrodes.

Another Lexan insulator was inserted into this gap with 2 atmospheres of SF_6 and graphite electrodes. The ESCA scans of this sample showed some surprising results, as seen in Fig. 2. The amounts of carbon and oxygen seen on this insulator are extremely small compared to the virgin sample, and there is a large amount of aluminum and fluorine seen on the surface. In addition, the surface no longer demonstrates negative surface charging but instead exhibits positive charging. The expanded scale spectrum of the aluminum 2p peak shows a shift in the binding energy of this line, which corresponds exactly to AlF_3, and the stoichiometry of the aluminum to fluorine in the spectrum is almost exactly 3:1. An SEM micrograph of this sample showed that there was a heavy coating of a powdery material on the surface. An x-ray dot map of the surface showed that this powder

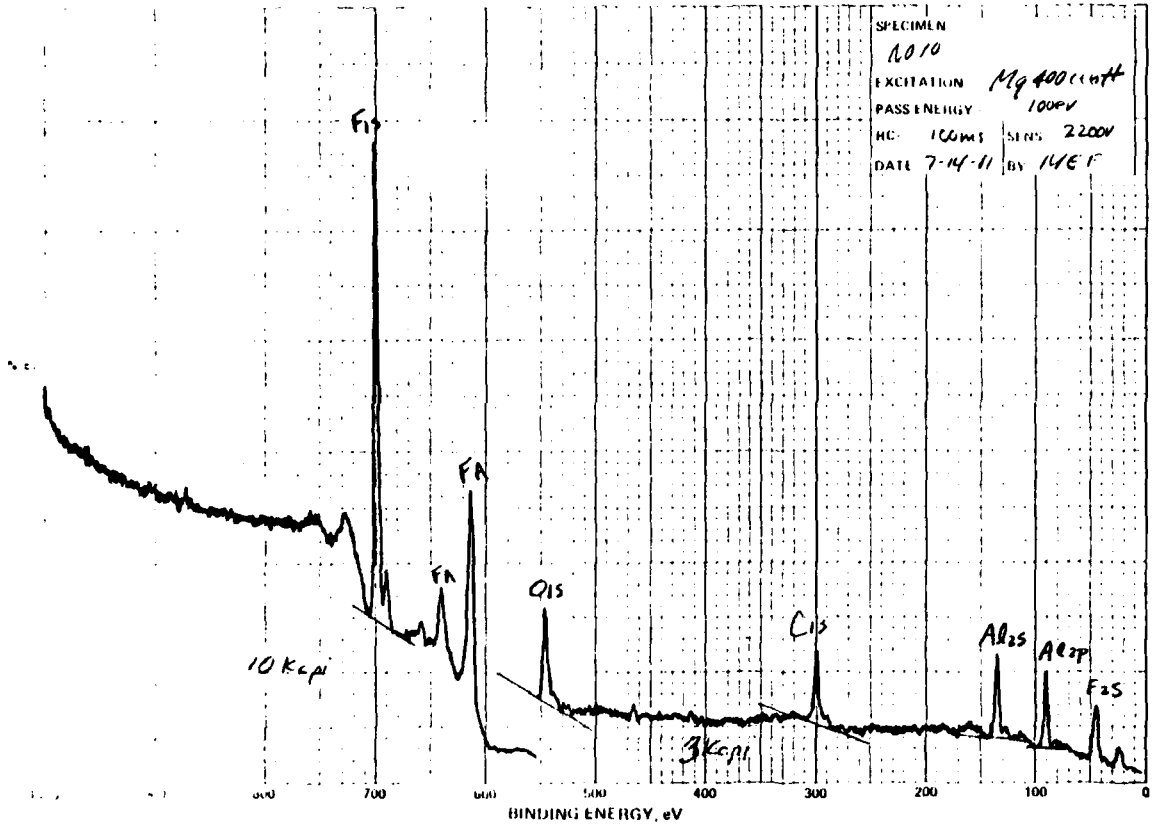

Fig. 2 ESCA Spectrum of a Lexan Insulator Exposed to 5000 shots in the Spark Gap of Project 3 with Graphite Electrodes and 2 Atmospheres of SF_6

was composed of aluminum, consistent with the ESCA indication of aluminum fluoride. The fact that the surface was covered with a thick powdery material explains why the concentration of carbon and oxygen is so small on the surface and why the surface of this particular sample exhibits positive surface charging, whereas the two previous samples show the opposite effect. The presence of the aluminum on the surface of this sample was somewhat of a surprise; however, the spark gap vessel is composed of aluminum. Several times during the experiment, misfires to the walls of the chamber could have liberated metallic aluminum which reacted with the fluorine in the gas and subsequently was deposited inside the spark gap. Such misfires have been observed to occur occasionally.

For a Lexan insulator exposed to 5000 shots in this same spark gap, with 2 atmospheres of N_2 and K-33 electrodes, the ESCA spectrum indicates that the surface of the sample is covered with a very thin layer of copper and tungsten. An expanded scale spectrum of the carbon 1s peak indicates that there is more than one form of carbon present on the surface; however, the resolution of this peak is not sufficient to identify all the forms of carbon present. Expanded scale spectra of the copper and tungsten peaks indicate that the tungsten exists in some form of oxide; however, the copper spectrum shows pure metallic copper on the surface. Experts at Wright Patterson Air Force Base, Dayton, Ohio believe that the copper and tungsten from the electrodes are deposited on the insulator with similar deposition rates. The tungsten, which has a rapid rate of reduction compared to copper, is oxidized on the way to the insulator (by the oxygen in the spark gap in the form of water). This process yields a deposited layer of copper and tungsten oxide on the insulator, and therefore the copper in this layer never has an opportunity

to oxidize even after the insulator is removed from the spark gap. SEM micrographs of the surface show that it is covered with a thin, discontinuous layer of a metallic-looking substance. X-ray dot maps of tungsten and copper on several large conglomerations of apparently molten material are inconclusive as to whether it is tungsten or copper. Additional analysis of these particles is being performed by x-ray fluorescence to determine the composition of this molten looking material. However, this information is not available at this time.

ESCA analysis of Lexan insulators exposed to 5000 shots in 2 atmospheres of SF_6 with K-33 electrodes shows a significant increase in the amount of tungsten (from 4% to 13.3%) present on the surface, as compared to the previous situation in N_2. There is also a large decrease in the concentration of carbon on the surface. However, this may be attributed to a masking of the carbon originating from the Lexan insulator by a surface coating of copper and tungsten, which are both present in large amounts on the surface. Another alternative to the reduced concentration of carbon on the surface, relative to the virgin sample, is that the carbon is from a hydrocarbon contamination by the air (after the sample is removed from the gap) and not from the insulator. The validity of this hypothesis can be checked through the use of FT-IR (Fourier Transform Infrared Spectroscopy) or possibly some technique which can determine the thickness of the deposited layer on the sample (such as Rutherford Backscattering Spectroscopy [3]). SEM micrographs of the surface indicate a large concentration of a powdery material on the surface, which copper dot maps indicate to be some form of copper. These dot maps are inconclusive as to the form of the copper; however, due to the large concentration of fluorine present on the surface it is possible that this

powder is a copper fluoride. The detailed scan of the copper by ESCA does not give an unambiguous answer. The broadness of the detail scan of the fluorine 1s peak, however, seems to indicate that there is more than one form of fluorine on the surface (either a copper fluoride or a carbon fluoride). More work needs to be done in order to understand better the composition of this powdery material.

Similar experiments were performed in this spark gap using a "Blue Nylon" insulator. The ESCA spectrum of the virgin sample indicates that the insulator is composed of carbon, oxygen, nitrogen and silicon. Blue Nylon is a insulator which is cast in a mold with a blue dye (and not extruded as are most insulators used in high voltage spark gaps). This casting process leads to a larger percentage of cross-linking in the polymer and consequently more strength. The usual composition of Nylon used in high voltage spark gaps is $C_6H_{11}ON$; however, for the Blue Nylon insulator the ESCA data give a concentration of nitrogen in the material that does not agree with this stoichiometry and the presence of silicon in the material was somewhat of a mystery. However, a company representative of The Polymer Corporation informs us that the silicon is a result of the use of a silicon product in the mold release, which may penetrate as much as 1/4" into the material. When a Blue Nylon insulator was inserted into the spark gap with graphite electrodes and 2 atmospheres of N_2, the ESCA spectrum shows that the nitrogen in the sample has disappeared after 5000 shots. This is a very surprising result and it may be necessary to rerun this experiment to attempt to verify this result.

The Blue Nylon insulator inserted in the spark gap with graphite electrodes and 2 atmosphere of SF_6 appears to be covered with a powdery

substance. An ESCA spectrum of this sample indicates a large concentration of aluminum and fluorine. An expanded scale spectrum of the aluminum 2p peaks indicates that the aluminum is in the form of AlF_3, which is consistent with results discussed earlier in this report. SEM micrographs and aluminum x-ray dot maps verify this result. The carbon 1s peak indicates some form of CF bonding on the surface, however, the resolution of this peak is not sufficient to determine which CF compound is responsible.

ESCA spectra of the Blue Nylon insulator from the spark gap with K-33 electrodes and 2 atmospheres of N_2 indicate that the amount of carbon on the surface has been greatly reduced (from 78% to 47%) and that the amount of oxygen and silicon have been increased considerably. The data also indicate that there is no copper or tungsten on the surface. SEM micrographs of this sample also indicate that copper and tungsten are not present on the surface. This difference, compared to results on the Lexan insulator, could possibly be due to the silicon mold release, which leaves the surface "slick" so that metal vapor will not deposit and adhere to the surface. However, it is impossible to verify this result with the present data. The data for the Blue Nylon insulator in the spark gap with K-33 electrodes and 2 atmospheres of SF_6 show results similar to those for Blue Nylon with K-33 electrodes and N_2. This indicates that the lack of metal films on the surface is not related to the use of SF_6. Further tests are necessary to determine the role of the silicon on the surface.

C. SURFACE FLASHOVER MEASUREMENTS

1. Experimental Results

During the past year the apparatus used to measure the surface flashover potential of an insulator has been changed. Originally we attempted to measure the flashover potential in the millisecond region with voltages of approximately 50 kV; however, private communications from various experts in pulsed power research suggested that a more realistic time region for measuring the surface flashover potential was .5 - 5 μs. Consequently, the apparatus was redesigned to accommodate the change in time scale and also for the anticipated increase in voltage necessary to cause a surface flashover. Figure 3 shows a schematic representation of the new ultraviolet irradiation chamber. A Marx bank is used to ramp the voltage up across the sample in a time which is determined by the RC time constant of the Marx Bank output resistor and the capacitance of the parallel plate electrodes. The maximum voltage obtainable to this date across the samples is approximately 110 kV, which is limited by the geometry of the vacuum chamber. If higher voltages are needed to cause a surface flashover, it will be necessary to build a larger vacuum chamber.

Figure 4 is an oscilloscope trace of the flashover potential of a cylindrical, unexposed, Lucite sample which is 5 cm in diameter and 1 cm in height. The vertical scale of the trace is 43,600 volts/div. and the horizontal scale is .5 μs /div. From this figure the flashover potential is about 87,000 volts in 2 μs. Figure 5 is an oscilloscope trace of the flashover potential of the same Lucite insulator after it has been exposed to 80,000 shots from the surface discharge ignitor plug seen in Fig. 3. Again the vertical scale of each trace is 43,6000 volts/div and the horizontal scale is .5 μs/div. The three traces indicate that within 4.5 μs

AD-A110 409 TEXAS TECH UNIV LUBBOCK DEPT OF ELECTRICAL ENGINEERING F/G 20/3
COORDINATED RESEARCH PROGRAM IN PULSED POWER PHYSICS.(U)
DEC 81 M KRISTIANSEN, M O HAGLER F49620-79-C-0191
UNCLASSIFIED AFOSR-TR-82-0018 NL

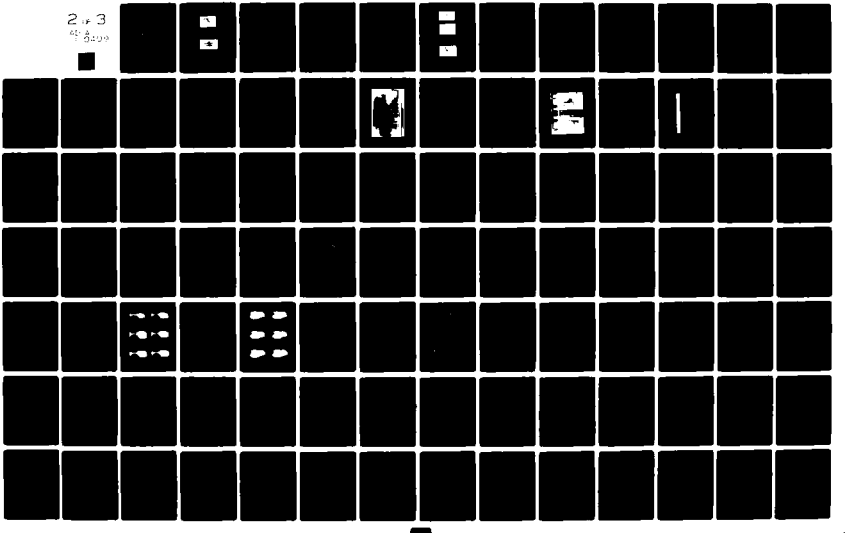

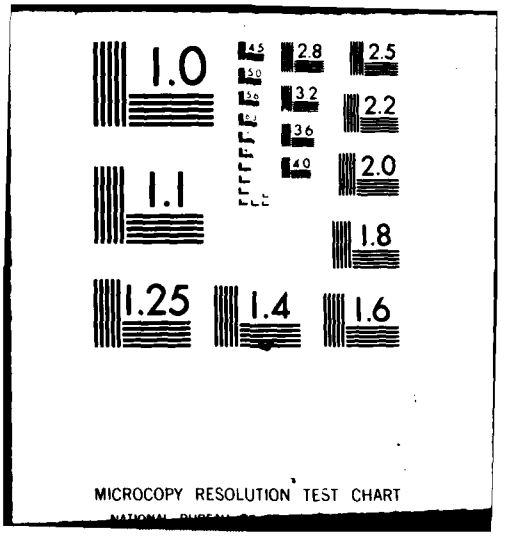
1.0
1.1
1.25
1.4
1.6
1.8
2.0
2.2
2.5
2.8
3.2
3.6
4.0
4.5
5.0
5.6
MICROCOPY RESOLUTION TEST CHART

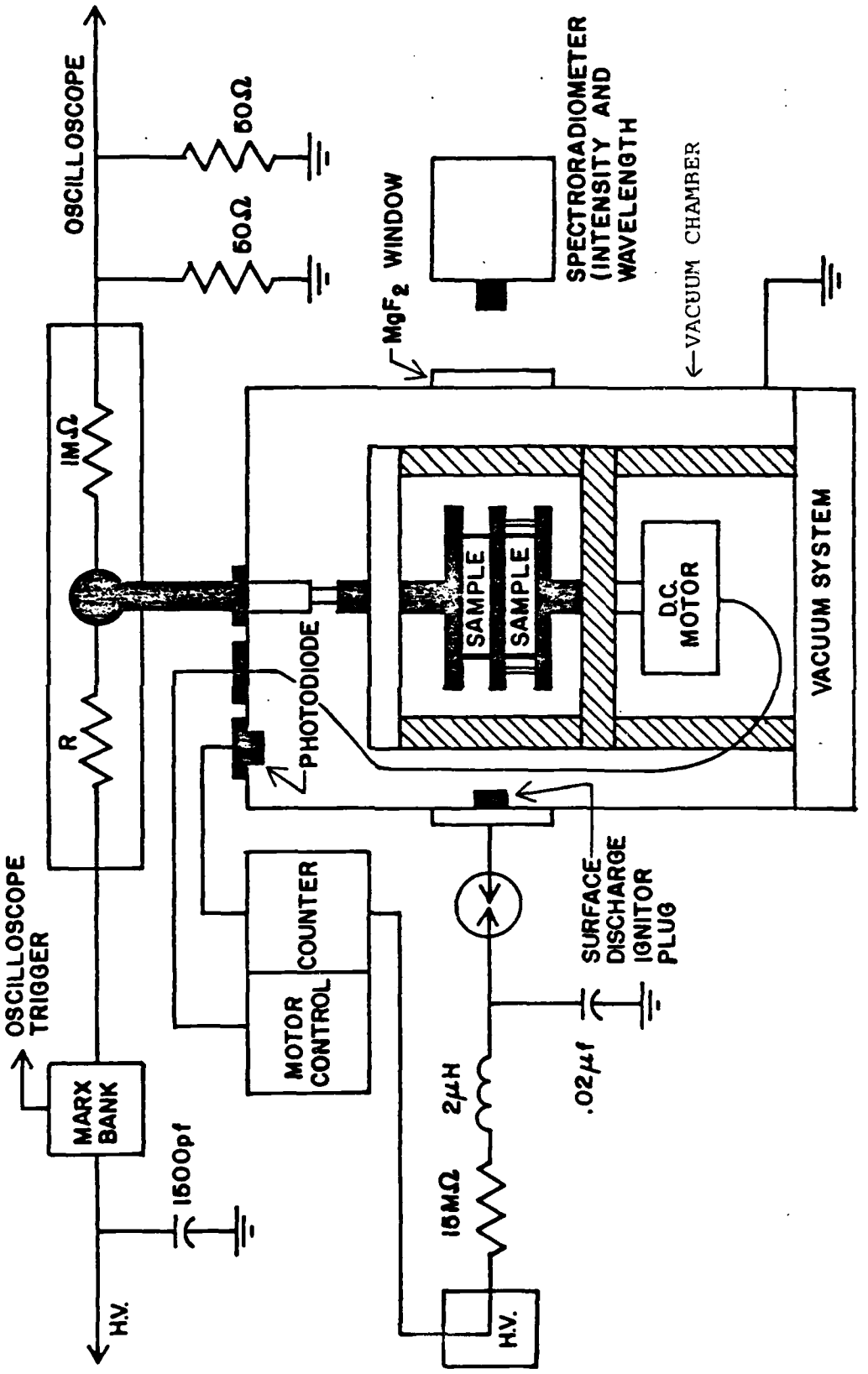

Fig. 3 Ultraviolet Irradiation Chamber

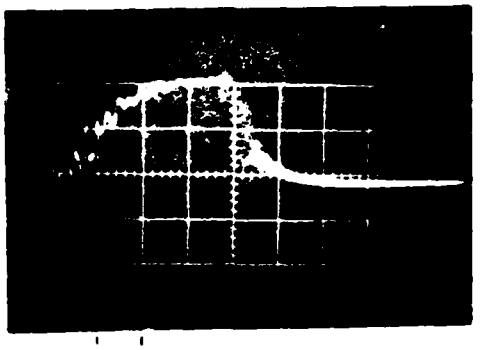

Figure 4 Oscillogram of surface flashover potential across a 1 cm high, 5 cm diameter Lucite insulator.

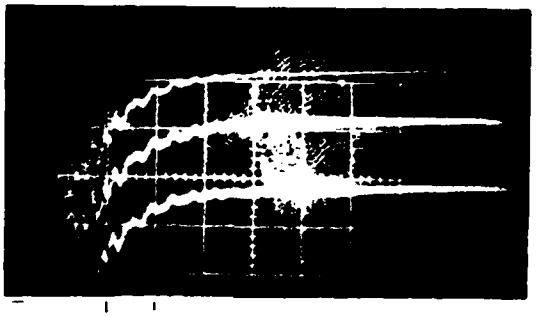

Figure 5 Oscillogram of surface flashover potential across the same Lucite insulator after exposure to 80,000 shots in the ultraviolet irradiation chamber.

there was no flashover across the sample, however a flashover did eventually take place as observed visually through a viewing port. The fact that the electric field across the sample reached 110 kVcm without a flashover is significant.

The flashover voltage of this same sample was then tested by backfilling the vacuum system with 1 atm of N_2. Figure 6 shows the oscilloscope trace of the flashover which occured at about 60 kV/cm. When the flashover was tested again in 1 atm of N_2 it appeared to require no voltage to cause flashover of the sample. The sample was then removed from the vacuum system and examined.

Physical inspection of the sample showed that the surface of the sample was visibly discolored, possibly due to ultraviolet and soft x-ray radiation damage from the spark or from a deposition of some material onto the sample from the spark source. It also showed that a track had developed along the surface of the insulator. This track is probably due to the flashover across the surface in N_2 which caused local heating of the sample in the region of the surface arc, leading to crazing of the surface. This track probably explains why the flashover in N_2 required no voltage after the initial attempt.

One hypothesis that might explain the large increase in flashover voltage in vacuum after irradiation of the sample is that a layer of carbon from the radiation source is deposited on the sample, causing a grading of the field along the surface, which results in an increase in the flashover potential, or it is possible that the radiation from the spark source has changed the surface composition of the insulator causing it to exhibit a larger flashover potential. At this time no attempt has been made to determine which of these hypotheses is correct. How-

ever, using ESCA with grazing angle incidence or perhaps FT-IR it should be possible to distinguish between a carbon coating from the spark source and changes in the surface due to radiation damage. The problem with distinguishing between these two forms of damage is that since the Lucite sample is composed mainly of carbon, any carbon deposited on the surface would be difficult to distinguish from the carbon in the sample. Since the major effort thus far in the analysis of the materials has been to analyze the electrodes used in Project No. 3, the analysis of this sample has been postponed until a later date.

A change from rectangular and then trapezoidal samples to cylindrical samples to measure the flashover potential was made because with the rectangular samples the surface flashover always occurred along an edge of the sample, which caused ambiguous values of the flashover potential due to inconsistencies in the machining of the samples. With cylindrical samples this problem was eliminated. However another critical problem arose. The voltage required to cause flashover is higher than anticipated but the sample height should not be decreased further due to the area effect first observed by J.C. Martin at Aldermasten, England [4]. The area in question is the surface area across which the electric field is applied, and according to empirical results by J.C. Martin there is a critical area at which the electric field necessary to cause flashover begins to become larger as the area gets smaller. This critical area for different insulating materials is not well defined; however, while experimenting with the flashover potential for various thickness of the same cross-sectional area we believe that it is possible to come up with a "ball park" figure for this critical area, depending upon the particular insulator being tested. As mentioned earlier, the flashover field for a virgin sample, 1 cm in height, was approximatedly 87 kV/cm. whereas

the flashover field for one that is 7 mm high is approximately 125 kV/cm, (as shown in Fig. 7). Consequently, decreasing the height of the sample, which lowers the surface area, causes an increase in the electric field necessary to cause flashover. Therefore, our intentions are to increase the height of the sample, while keeping the cross-sectional area constant, or increasing the cross-sectional area while keeping the height nearly constant, to ensure that the samples have a large enough surface area to overcome this critical area effect.

D. SUMMARY OF SECTIONS B AND C

The most important effect observed for all dielectric samples analyzed so far is the coating of the surface by materials generated in the arc. As reported above, some of the coatings are evaporated electrode material while others are dielectric compounds such as AlF_3. Microparticles from the electrodes are also found embedded in the surfaces of the insulators. Even the samples used in the surface flashover apparatus may have a coating of material from the spark source, however, this remains to be analyzed quantitatively.

The apparent loss of nitrogen from the surface of the Blue Nylon samples and the lack of coatings on these surfaces are somwehat surprising. Further analysis is needed before confidence can be placed in these results.

This leads to some qualitative conclusions which help determine the future course of this investigation. Metal coatings on the insulators may actually reduce the probability of failure through flashover and tracking, as long as the coating is thin. Since the coating thickness increases with each shot, the conductivity of the surface must increase

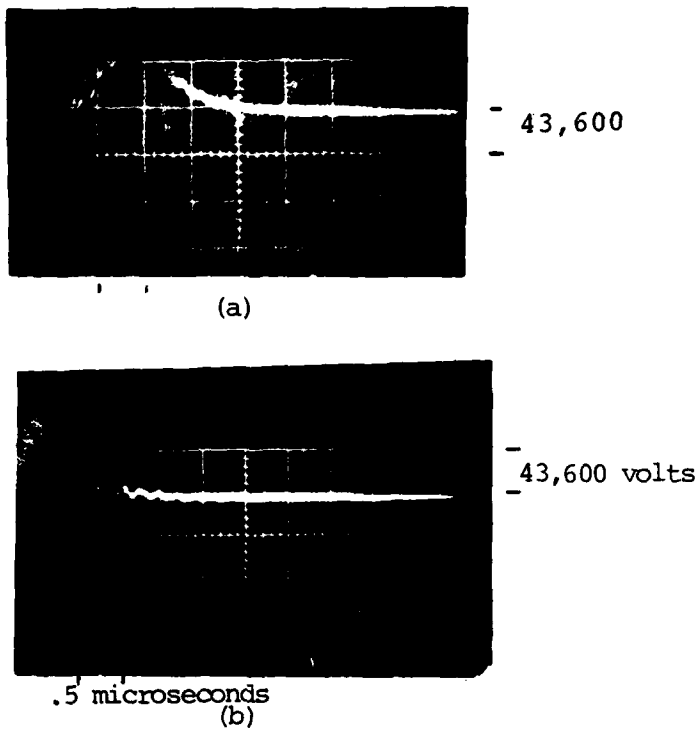

Figure 6 Oscillogram of surface flashover potential across the same Lucite insulator in 1 atmosphere of N_2 after exposure to 80,000 shots in the irradiation chamber.

(a) flashover potential for initial test,
(b) flashover potential for subsequent tests.

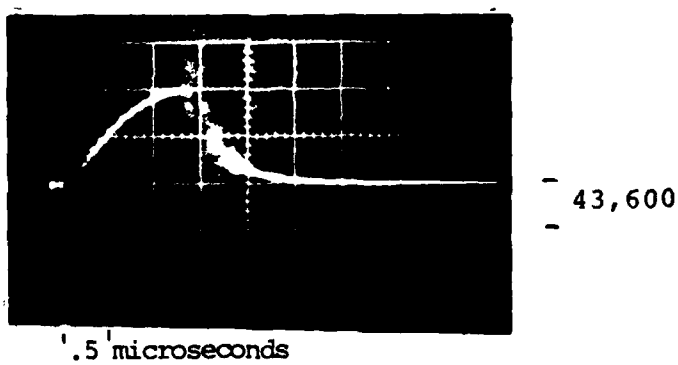

Figure 7 Oscillogram of surface flashover potential across a 7 mm high, 5 cm diameter Lucite insulator.

until the spark gap fails due to conduction along that surface. Clearly, the rate of deposition of these coatings under various conditions must be determined. Also, the mechanism by which the coating forms must be investigated to see if a vapor shield might be effective in protecting the insulator.

The dielectric coatings, such as AlF_3, could actually be beneficial. Such materials could shield the insulator surface from U-V radiation and microparticles. These possibilities need further investigations. It may be that such coatings, applied to insulators to be used in spark gaps, could reduce the surface damage rate but this is presently not well enough documented.

The surface coatings have, so far, prevented us from observing any structural damaged to the surfaces of the dielectric materials. Removal of the coatings and analysis of the surface underneath is the next obvious step in this work.

Mass spectroscopic analysis of powder deposits from the spark gap has been performed in the Chemistry Department at Texas Tech (see Project No. 3 report). The results indicate that material is removed from the insulator and deposited as residue in the spark gap chamber. No estimate of the amount of material removed is available but none of the other techniques used for insulators analysis shows significant structual damage. It is possible, however, that dielectric material is displaced by the microparticles from the electrodes when they strike the surface.

E. ANALYSIS TECHNIQUES NOT REVIEWED IN PREVIOUS REPORTS

1. Fluorescence

Measuring and identifying the spectral bands of the fluorescence spectrum from a material can give information about the surface contaminants and corrosion products within a few 1000 Å of the surface. Therefore, fluorescence can help identify some of the products formed on the electrodes and insulators used in high voltage spark gaps.

Fluorescence is a phenomenon that occurs when radiation is emitted by an excited molecule as the result of a transition between quantum-mechanical states of the same multiplicity, either singlet-singlet transitions or triplet-triplet transitions. The processes of absorption, fluorescence, and phosphorescence (the radiation emitted in a transition between states of different multiplicity) are shown in Fig. 8 [5]. Internal conversion is the radiationless loss of energy from excited states without a change in multiplicity, intersystem crossing is the radiationless loss of energy from excited states with a change of multiplicity. The higher excited states rapidly lose their absorbed energy (10^{-11} s) and decay to the lower excited states. Therefore fluorescence, which occurs in about 10^{-9} s, arises from the radiative transitions from the lowest vibrational levels of S_1 to the various levels of S_o. The phosphorescence lifetimes are on the order of 10^{-3}s up to minutes, due to the low probability of transitions between states of different multiplicity. The phosphorescence spectrum is much weaker that the fluorescence spectrum because there is more time for energy to be lost through intersystem crossing, and phosphorescence is also a low probability event.

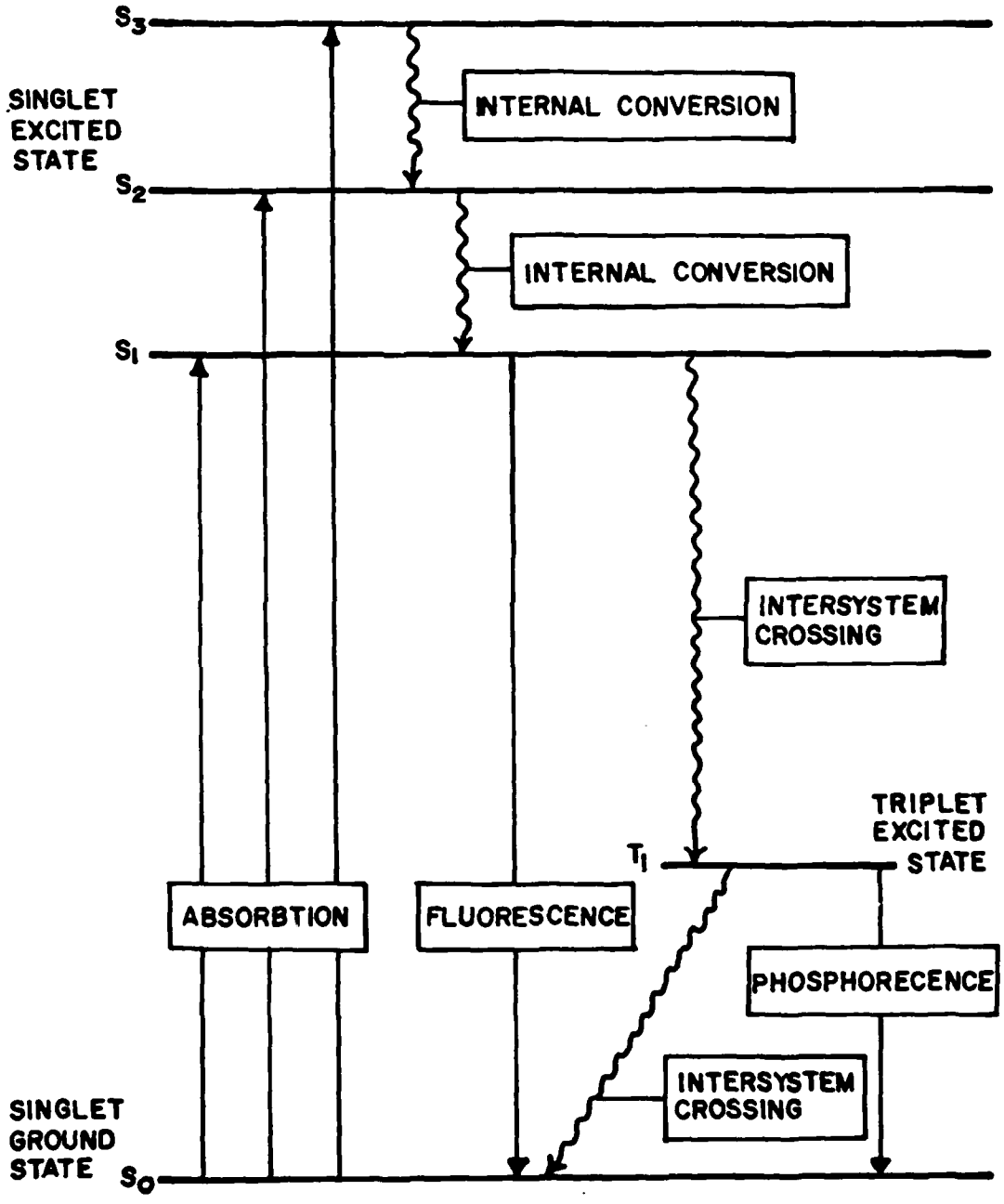

Fig. 8 Schematic representation of changes in molecular energy levels which may occur upon absorption of radiation. Nonradiative processes are represented by squiggly arrows and radiative processes are represented by straight arrows (Ref. 5)

The fluorescence experiment is performed by shining a laser of a certain frequency into the sample and measuring the frequency of the emitted radiation. However, relatively few light absorbing organic compounds are strongly fluorescent because of intersystem losses, internal conversion, collisions with other molecules that result in loss of energy through heating, or because the chemical bonds of the molecule are disrupted by the incident beam. The fluorescence process in organic molecules will be preferred, however, if the excited singlet state is stable with an approximate half life of 10^{-8}s or if the excited singlet and triplet states are well separated, reducing the probability of intersystem crossing, or if certain structural requirements are met. These structural requirements include the geometrical arrangement of the molecule, the type and position of the substituents, and the nature of the carbon structure. These requirements are explained in much greater detail in reference [6]. Some of the other factors which affect the fluorescence probability, such as the instrument employed, the pH of the material, the temperature, and the stability of the compound in the exciting light are also discussed in this reference.

Another problem associated with the fluorescence experiment which causes difficulties in the analysis of most insulating materials deals with the use of lasers. When a laser is used to activate the fluorescence of a sample, local heating of the sample can cause damage to the sample which may obscure the measurement of any damage due to exposure to a high voltage discharge. Also the spectrum which is obtained is often complicated and difficult to interpret unless there is some prior knowledge of the sample. Quantitative analysis with fluorescence is extremely complicated due to these problems.

The use of fluorescence as an analytical technique for the analysis of the constituents of spark gaps could prove to be extremely valuable. For example, when graphite electrodes are used in a nitrogen atmosphere one possible reaction by-product is a nitrite (C ≡ N) which is fluorescent as a substitute in a benzene ring. The use of fluorescence in conjuction with ESCA can thus help identify some of the observed peak shifts in ESCA.

2. Fourier Transform Infrared Spectorscopy (FT-IR)

Fourier Transform Infrared Spectroscopy (FT-IR) is a nondestructive optical technique which can be used for analysis of the molecular structure of insulators used in high voltage spark gaps. Infrared spectroscopy is a commonly used technique for the analysis of polymers and FT-IR is one particular method of obtaining the infrared absorption spectrum. The use of infrared spectroscopy was previously not recommended as a method of analyzing the components in high voltage spark gaps because it is not a surface sensitive technique. In addition, the particular method of obtaining the infrared absorption spectrum, Attenuated Total Reflection (ATR), had many obvious problems with respect to its intended use [7]. However, FT-IR has many advantages over ATR for the analysis of materials.

The use of FT-IR for the analysis of the insulators used in high voltage sparks gaps was suggested by Paul Predecki [8]. It was proposed that the soft x-rays emitted from high voltage spark gaps are a very important process in the deterioration of these insulators. The use of the FT-IR therefore could be an important technique for the analysis of the bulk and surface damage due to these soft x-rays.

The basic optical component of an FT-IR spectrometer is a Michelson interferometer, as shown in Fig. 9. It consists of two plane mirrors, which are mutually perpendicular to each other, and a beam splitter. One of the mirrors is stationary and the other is free to move along an axis perpendicular to its plane. If a collimated monochromatic beam of radiation of frequency ν is incident upon the beam-splitter it will be divided into two rays. One ray travels to the fixed mirror and returns to the beam-splitter, while the other ray travels to the movable mirror and returns. The two rays are then recombined at the beam-splitter and interfere due to their optical path difference. Translation of the moveable mirror results in changes in the optical path difference of the beams, and causes either constructive of destructive interference depending upon the path difference. The output of the interferometer (the interferogram) is measured as a signal intensity, $I(\delta)$, where δ is the optical path difference. If the interferometer is illuminated with a white light source and a translation of the moving mirror is made, an interferogram is produced which is characteristic of the source and beam-splitter. If the output of the interferometer is passed through a sample, the sample will absorb certain components of the incident radiation, depending upon the characteristics of the sample. The emerging signal from the sample is an interferogram of the sample, beam-splitter and source. The spectrum, $S(\nu)$ is related to the emergent intensity $I(\delta)$ by the Fourier integral [9]

$$S(\nu) = C \int_{-\delta}^{\delta} [I(\delta) - I(0)/2] e^{-i2\pi\nu\delta} d\delta \qquad (1)$$

where C is a constant and $I(0)$ is the intensity at $\delta = 0$.

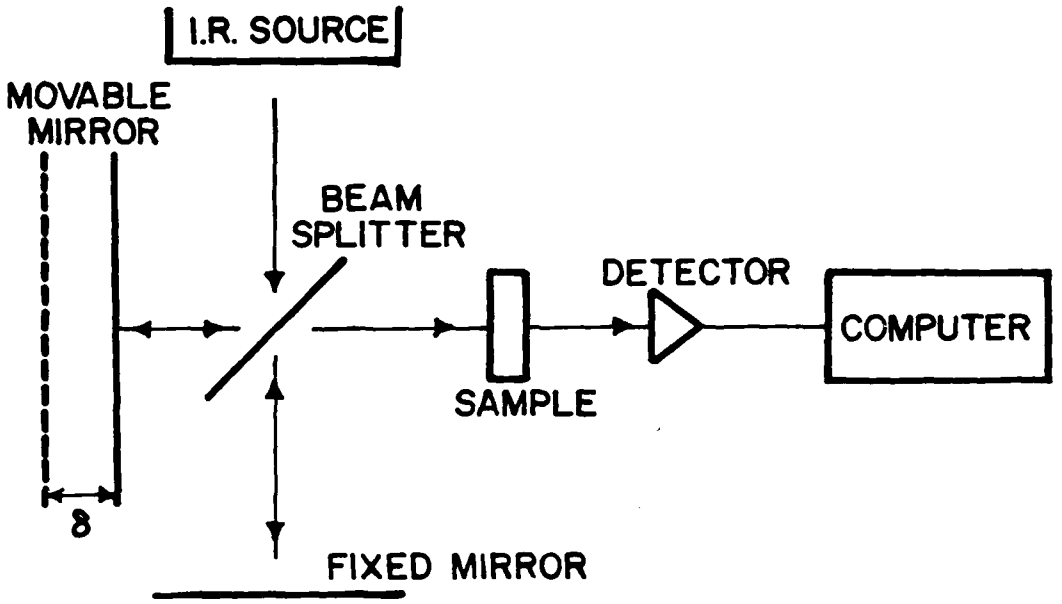

Fig. 10 Experimental apparatus for measuring the Fourier Transform Infrared spectrum of a sample

In order to obtain the spectrum which is characteristic of the sample only, a white source of radiation is passed through the interferometer and the moveable mirror is translated through a displacement $-\delta$ to δ. The output from the interferometer is continuously passed through the sample and the resulting interferogram is measured with an appropriate IR detector. The signal produced by the detector is sampled at certain intervals of δ, depending upon the highest frequency contained in the incident radiation. The spectrum of the sample is then obtained from the interferogram by calculating the real part of the Fourier integral of Eq.(1). To obtain the spectrum which is characteristic of only the sample it is possible to measure the spectrum of the sample, beamsplitter and the source and then subtract the spectrum of the beamsplitter and the source, thus obtaining a difference spectrum which is characteristic of only the sample. This is an important advantage of FT-IR spectrometers because the difference spectrum of a virgin sample and a sample which has been damaged by some method can be obtained. Therefore the changes in the sample, caused by some mechanism, can be investigated with FT-IR. The method by which difference spectra are obtained is demonstrated in Ref. [10].

The use of the difference techniques in FT-IR spectrometers makes it an extremely important technique for the analysis of organic and some inorganic materials. The purpose of obtaining difference spectra is to isolate changes that occur in the molecular structure due to different interactions. If a chemical interaction introduces a new functional group in a material, or reduces one, the absorption bands may be weak and overlapped by bands which correspond to similar chemical bonding present in the virgin sample. Difference spectra effectively subtract

from the spectra absorption bands which correspond to chemical bonding from the virgin sample. This eliminates interference from the virgin sample.

Some of the changes that occur due to chemical or physical interactions, such as changes in hydrogen bonding, or other changes in the intermolecular forces, are seen as shifts in the absorbing frequency or a change in the absorptivity of the bands. If physical or chemical interactions result in a shift of an absorbing frequency then the change in the difference spectrum will show a structure similar to a differentiation peak. For changes in absorptivity there is a positive or negative absorbance shown relative to the baseline. A positive absorbance relative to the baseline indicates an increase in a particular chemical species, while a negative absorbance relative to the baseline indicates a decrease in a particular chemical species. The use of difference spectroscopy in FT-IR for the analysis of the insulators used in high voltage spark gaps is described in Ref. [11]. In this particular paper the use of FT-IR is discussed along with ESCA, AES, SEM, and XRF for the analysis of the insulators and conductors used in high-voltage spark gaps.

There are many advantages and disadvantages associated with the use of FT-IR spectrometers compared to conventional grating infrared spectrometers [9]. The two most important advantages of FT-IR spectrometers are referred to as "Fellgett's advantage" and "Jacquinot's advantage". These deal with the measuring time required to obtain an appreciable signal to noise ratio using FT spectrometers compared to grating spectrometers and with the energy throughput that can be used before the spectral resolution is degraded, respectively. Some of the disadvantages of

FT-IR spectrometers deal with the use of a movable mirror and the drive mechanism that must be used and also with the use of nonideal beam splitters. However, the advantages of FT-IR spectrometers make the use of them far superior to conventional spectrometers, when high resolution is required in a short time.

Quantitative analysis by FT-IR is basically achieved by Beer's Law that states

$$\log \frac{I_o}{I} = A = \varepsilon c l$$

where I_o is the incident intensity, I is the emerging intensity, A is called the absorbance, c is the concentration of molecules present in the sample, l is the path length and $\varepsilon = k/2.303$ which is referred to as the molar absorption coefficient. Many of the problems associated with quantitative analysis by FT-IR are discussed in Ref. [12].

FT-IR spectroscopy is a method of obtaining qualitative information about the functional groups present in materials and the identification of organic and some inorganic materials. By itself FT-IR is a technique which gives some detailed information about the bulk and surface structure of materials; however, when used in conjunction with other techniques such as ESCA, that give only surface structural information, it can become an extremely valuable tool for the analysis of insulators used in high voltage spark gaps. This is especially the case if the soft x-rays generated in spark gaps cause significant changes to the bulk structure of these insulators.

F. SURFACE DISCHARGE SWITCH

1. Experimental Setup

The initial construction of the surface discharge switch is complete and tests of the dignostic systems are underway. A block diagram and a photograph of the present switch system is shown in Fig's 10and 11, respectively. The system consists of a 60 kV, 10 mA power supply which charges a 0.1 μF, 0.1 μH, capacitor bank. The capacitors are connected to a 6 ohm stripline through a railgap and the surface discharge switch is placed in series with the upper conductor of the stripline. The line is terminated in a matched, 6 ohm load which is constructed with 60, 2-watt, carbon composition, resistors placed so that they approximate the stripline geometry.

The surface switch is designed for ease of changing electrodes and dielectric substrates. A top and side view of the switch portion of the line, showing the major switch dimensions, is given in Fig's. 12 and 13, respectively. The line plates are held together by a number of phenolic clamps situated along the line.

2. Instrumentation

Instrumentation consists primarily of voltage measurements, open shutter photography, and streak photography. Open shutter photography is used to count accurately the number of discharges paths. One such photograph of a discharge across Delrin, in air, at 45 kV and an electrode separation of about 1.8 cm is shown in Fig. 14 In the future, a streak camera will be used to determine simultaneity of channel closure across what we determine to be viable dielectric substrates.

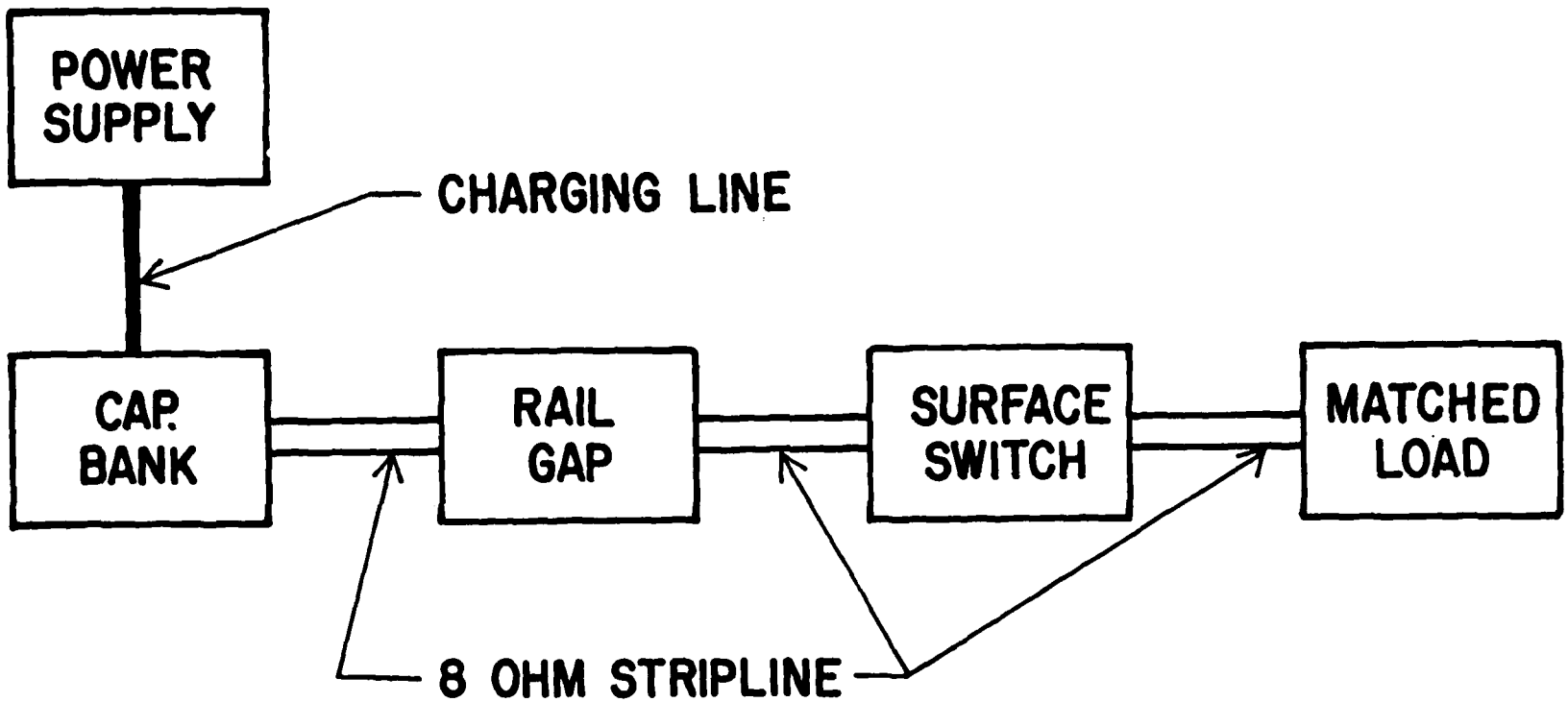

Fig. 10 Surface Discharge Switch Block Diagram

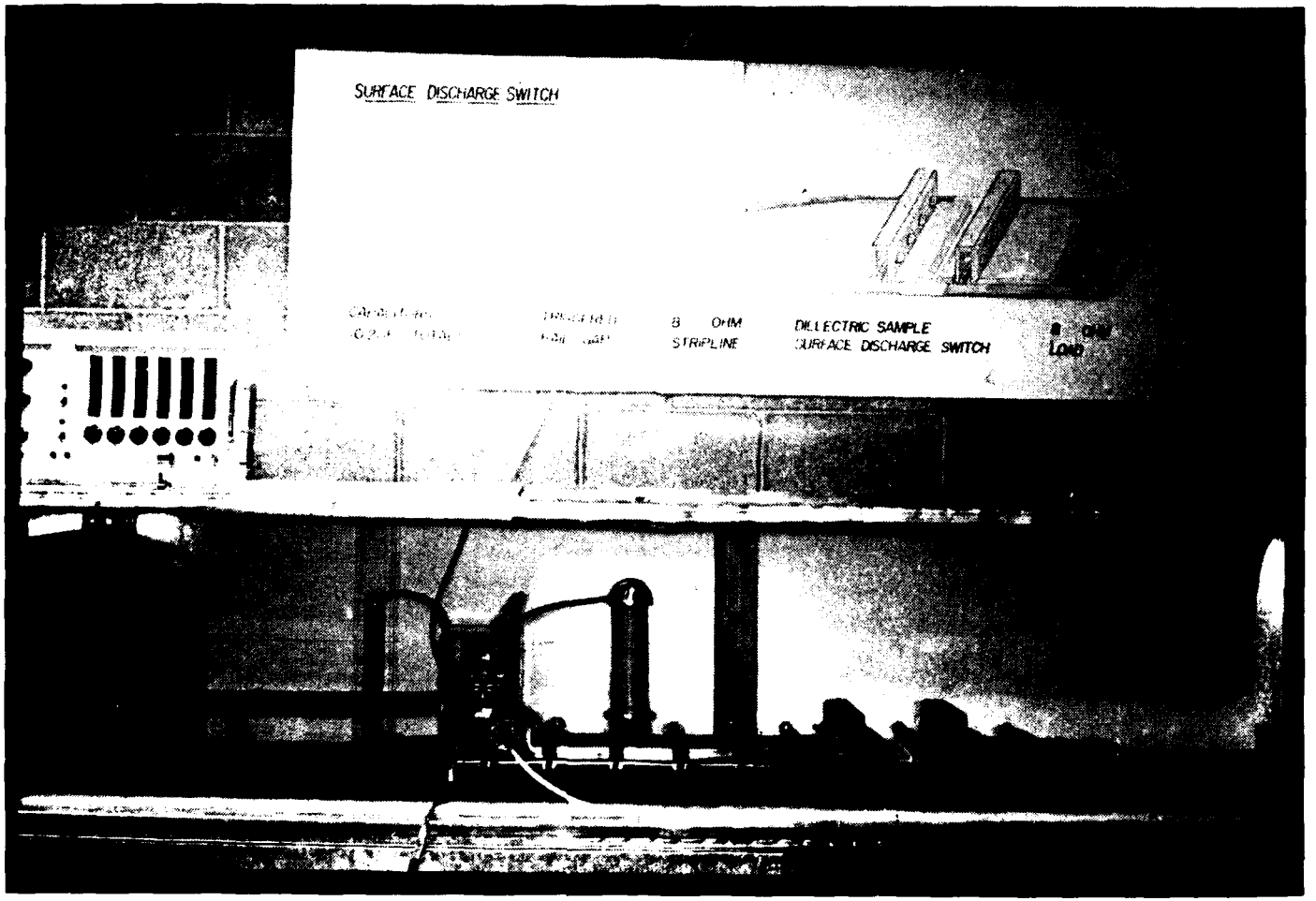

Fig. 11 Surface Discharge Switch System

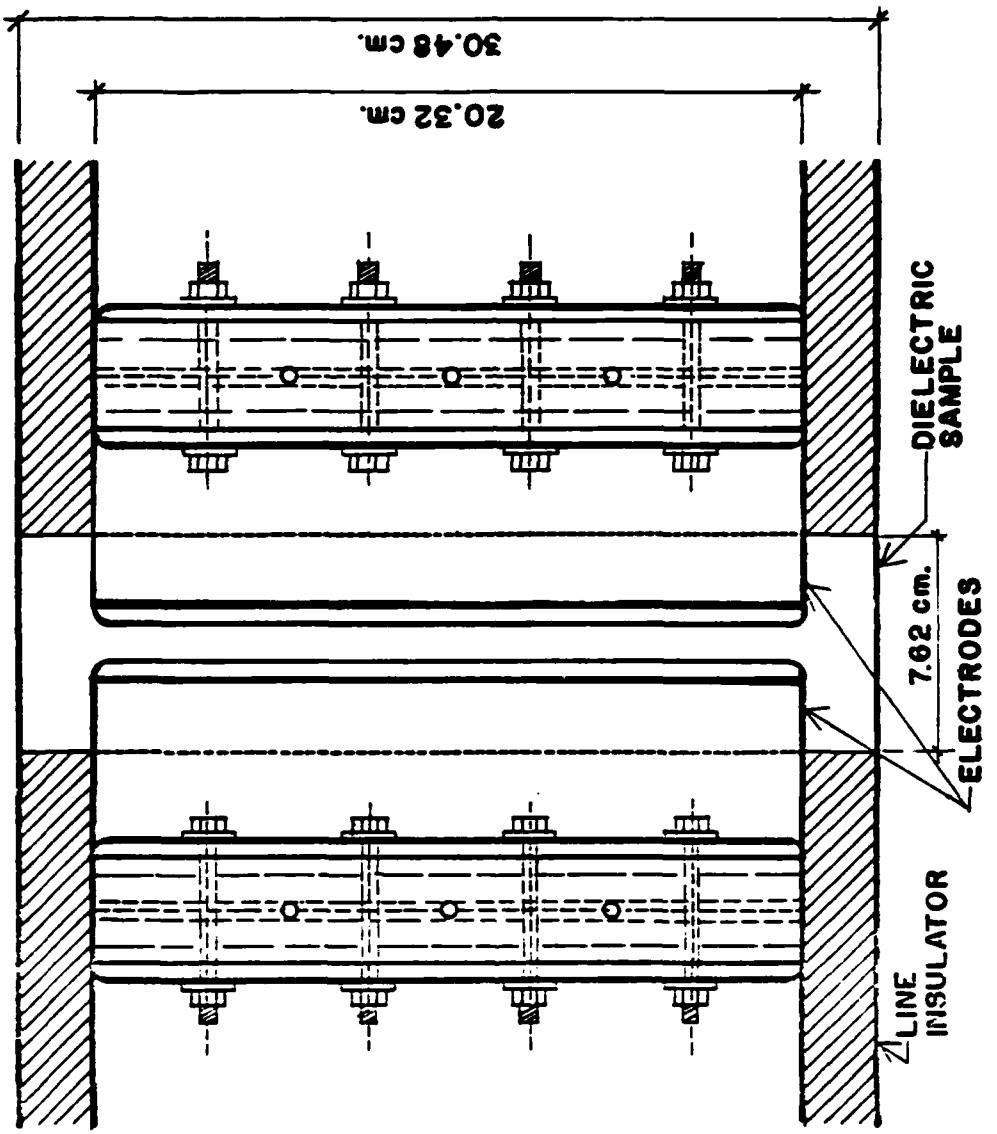

Fig. 12 Top View of Switch Assembly

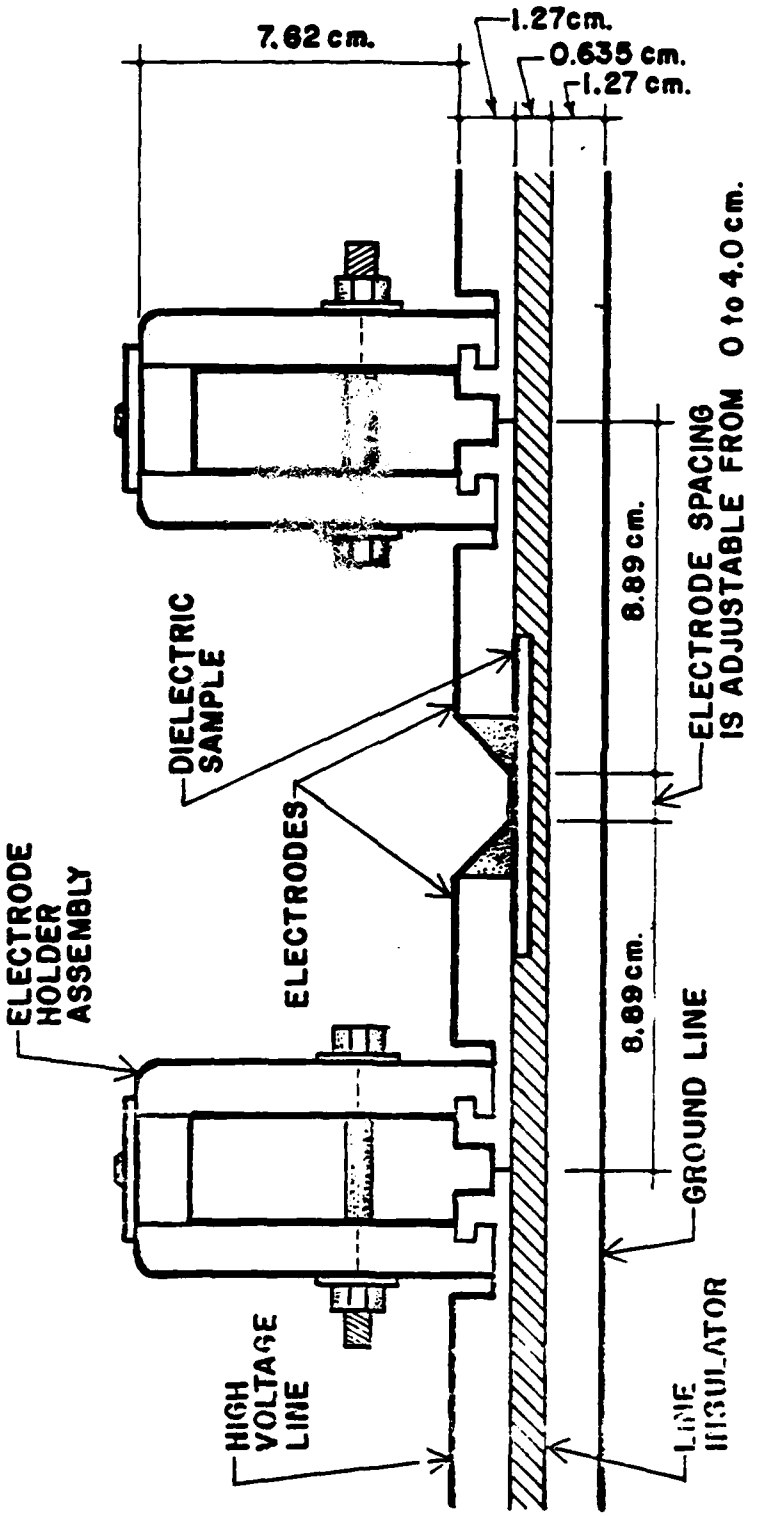

Fig. 13 Side View of Switch Assembly

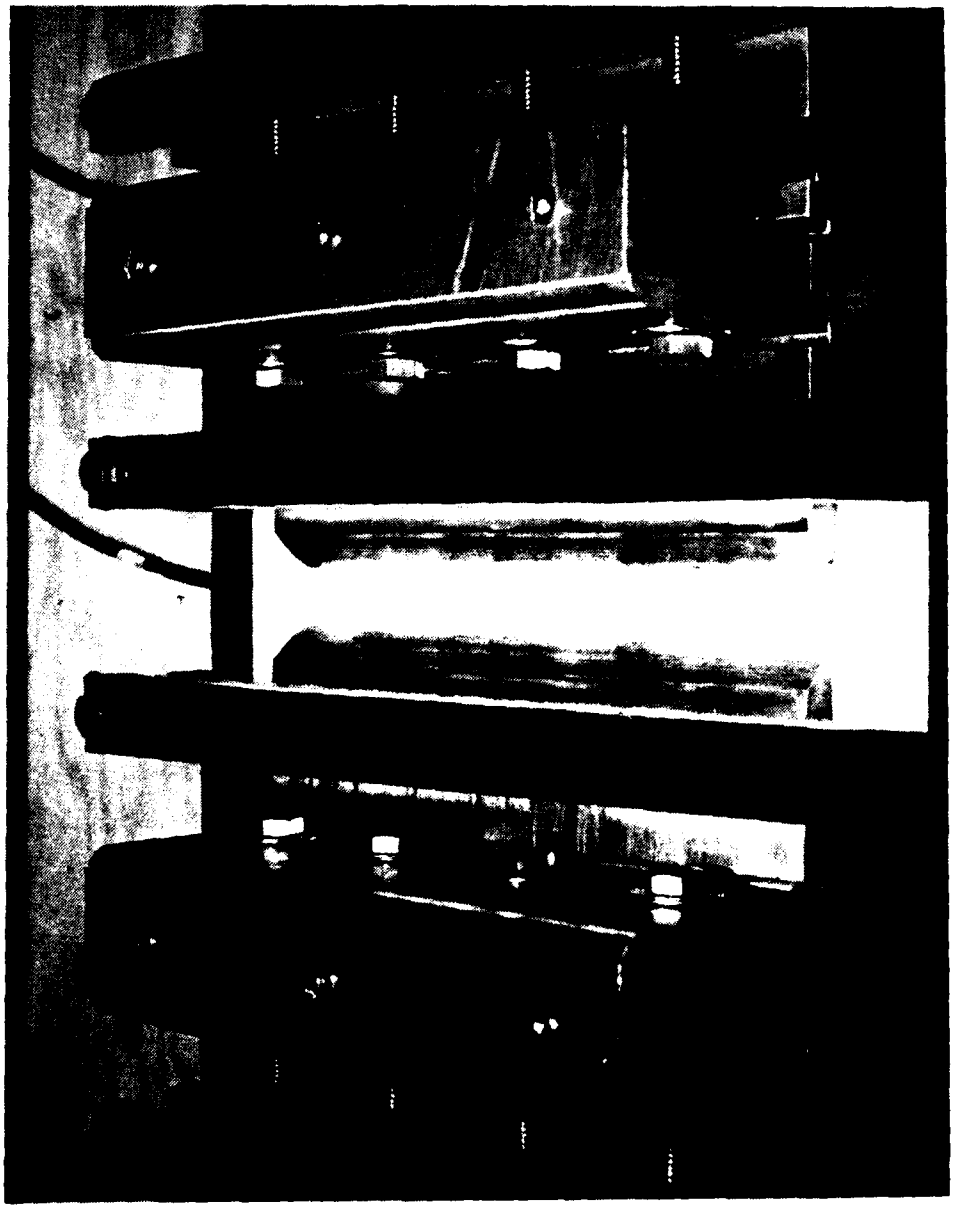

Fig. 14 Discharge Across Delrin, in air, at 45 kV

Voltage measurements are taken at 4 places in the system. The charging voltage is monitered across the capacitor bank and the voltage at both switch electrodes is measured, in the stripline, with capacitive dividers that feed directly through the ground line plate. A resistive divider is used to measure the voltage at the load.

3. Initial Operation

The system operates at voltages up to 45 kV at a rep-rate of about 2 pps. The rail gap is pressurized so that its selfbreak voltage is 45 kV and the electrode spacing adjusted so that the selfbreak of the surface switch is about 25 kV. In this manner the surface switch is over-volted by about 100% which causes dense multichanneling. Events with 75 to 175 discharges per meter have been observed with 1/3 to 1/2 of the channels appearing quite luminous and pressumed to be conducting the major portion of the current. This compares reasonably well with the results W.J. Sarjeant achieved in multiatmosphere switches [13]. A photograph of a Lucite sample, which clearly demonstrates visible damage after less than 100 shots, is shown in Fig. 15. Other surfaces, such as Delrin, show considerably less damage even after 1000 shots.

Triggering of a surface discharge switch is not a trivial problem but has been successfully demonstrated [13-15]. By not triggering and instead using overvoltage we are able to investigate damage to the dielectric and electrode with a much less complicated system. By measuring hold-off voltage, switch-on time, and the number of channels per meter, we will ultimately be able to make qualitative recommendations as to which combinations of dielectric material, electrode material, and flow gas is most appropriate for a particular application. The analysis and

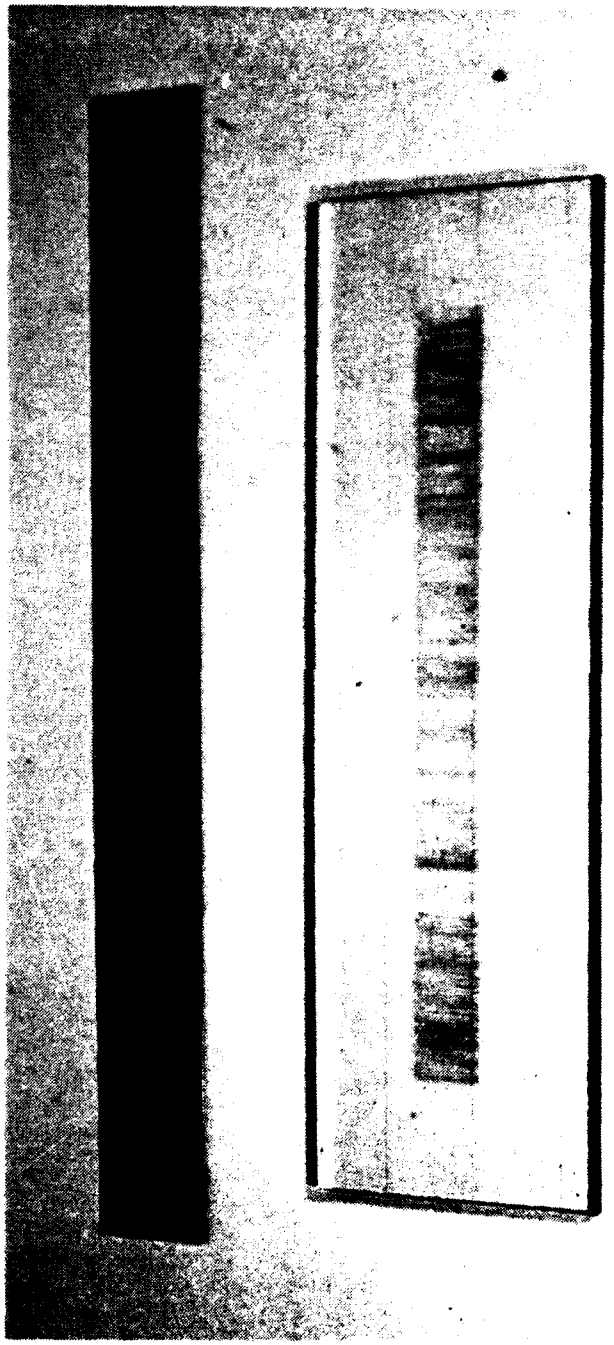

Fig. 15 Lucite Sample After 100 shots in air at 45 kV (12 inch ruler for scale)

study of the damage mechanism will also depend heavily on techniques learned in our experiments on the damage of insulators in gas filled spark gaps (Sec's. B-E). Likewise, we expect the damage studies done on the surface switch materials to aid in the understanding of the gas filled spark gap insulator damage.

We plan to compare the erosion damage of several insulator materials. We have acquired approximately ten different dielectric substrates to investigate. These will initially be tested in ambient air and with brass electrodes. The dielectrics include 3 forms of boron nitride which has been shown to be a good substrate in work done by J.W. Sarjeant [13]. Some mica impregnated epoxy combinations will also be tested since epoxy insulators are working well in several high voltage applications [16,17] Other available insulator samples include Delrin, "Blue Nylon", regular nylon, Kapton, and Lucite.

Before spending extensive time on electrode shape calculations we feel that it is essential to gain working experience with the switch to limit further research to a few dielectric samples that perform substantially better than the others. This will enable us to establish a general understanding of the main damage mechanisms in the switch so that the importance of electrode shape and dielectric mounting, for instance, can be accurately evaluated. The design of the removable electrodes and dielectric sample allows us to modify the electrode shape and material with ease. This decision is supported by J.C. "Charlie" Martin whose experience prompted him to suggest that we start with any reasonable electrode shape since it might not affect the switch performance at all [15].

After gaining experience with the various surfaces in ambiert air we plan to enclose the switch structure so as to determine the importance of various gases and pressures. This will, however, complicate the replacement of electrodes and dielectric surfaces and will only be implemented after we have narrowed the choice of suitable materials.

G. REFERENCES

1. G.L. Jackson, "Technical Report on Application of Surface Analysis Techniques to Pulsed Power Problems", Report No. AFOSR-PP-1, 1981 pp 17-18.

2. C.D. Wagner, "Energy Calibration of Electron Spectrometers", Applied Surface Analysis, STP 699,(T.L. Batt, and L.E. Davis, eds.), American Society for Testing and Materials, Philadelphis, Pa (1980), pp 140-142.

3. Carl J. Maggiore, "Materials Analysis with a Nuclear Microprobe", Scanning Electron Microscopy (1980), I (SEM. Inc., AMF O'Hare, Chicage, Il.) pp. 439-454.

4. J.C. Martin, "Volume Effect of the Pulse Breakdown Voltage of Plastics", SSWA/JCM/6511A (reprinted as Dielectric Strength Note No. 3).

5. F. Daniels and R.A. Alberty, Physical Chemistry, (John Wiley & Sons, Inc., New York, NY, 1975) Ch. 18,pp 584-601.

6. J.W. Bridges,in Luminescence in Chemistry,(E.J. Bowen, ed.) (D. Van Nostrand Company Ltd., London, England, 1968), Ch. 6, pp 77-115.

7. G.L. Jackson, "Attenuated Total Reflection (ATR)", Technical Report No. AFOSR-PP-1 on Applications of Surface Analysis Techniques to Pulsed Power Problems, 1981, Ch. 11, pp 101-103.

8. Private Communications with Dr. Paul Predecki at the University of Denver, Denver, Colorado.

9. P.R. Griffiths, Transform Techniques in Chemistry,(P.R. Griffiths, ed.)(Plenum Press, New York, N.Y., 1978) Ch. 5, pp 109.

10. J.L. Koening, "Applications of Fourier Transform Infrared Spectroscopy to Chemical Systems", Applied Spectroscopy 29, 293 (1975).

11. L.E. Murr, F.L. Williams, D.M. Smith, P. Predecki, and S.H. Wong, "A Preliminary Survey of High-Energy Switch Materials Degradation: Spectroscopic and Microscopic Characterization," Proceedings of the Third IEEE International Pulsed Power Conference, Albuquerque, N.M., 1981.

12. J.R. Ferraro, and Louis J. Basile, eds., Fourier Transform Infrared Spectroscopy Applications to Chemical Systems, (Academic Press, New York, N.Y., Vol. 2, Ch. 6, pp 193-242.

13. W.J. Sarjeant, "High Pressure Surface-Discharge Plasma Switches", IEEE Trans. Plasma Science PS-8, 216 (1980).

14. T.R. Burkes, et. al., "A Critical Analysis and Assessment of High Power Switches", Naval Surface Weapons Center (Dahlgren, VA) Rept. NP 30/78, p. 354 (1978).

15. Private Communication with J.C. (Charlie) Martin, May, 1981.

16. E.J. Stefanides, "Cast Epoxy Excels as High-Voltage Insulator", Design News, 80 (1978).

17. D. Affinito, E. Bar-Avraham, and A. Fisher, "Design and Structure of an Extended Life High Current Sparkgap", IEEE Trans. Plasma Science PS-7, 162 (1979).

Project No. 5

Excited State Spectroscopy of Electrically Excited Gases

(S. K. Dhali and P. F. Williams)

A. SUMMARY

Accomplishments in this project during the contract period October 1, 1980 through September 30, 1981 include the following 1) Multiphoton ionization involving the $5d(3\frac{1}{2})$ intermediate state in Xe has been observed and carefully studied. The absolute multiphoton ionization cross section for this transition was determined, and careful measurements of the dependence of the ionization efficiency on laser power were carried out. Extrapolation of these results indicates that with commercially available dye laser sources substantial ionization of tailored volumes can be achieved with this technique. We anticipate that it will be useful in fast, low jitter triggering applications as well as in fundamental studies of space-charge-controlled breakdown. 2) Multiphoton ionization (MPI) in N_2 has been studied. We find a flat, essentially featureless continuum in the MPI spectrum throughout the spectral range 3600 Å to 4500 Å, except in the vicinity of 3850 Å where a regular, highly structured spectrum is observed. Since low-jitter laser triggering of spark gaps appears to depend on laser-induced ionization in the gap region, and since N_2 is often a major constituent of the fill gas for switch gaps, these measurements are important for understanding fast, low-jitter triggering. 3) We have investigated the feasibility of using laser-induced fluorescence to follow the migration of electrode material into the gap region during and after an electrical spark, The results of the study were quite encouraging, and we report the results of a preliminary

measurement of the migration of Al vapor under these conditions.

B. ACCOMPLISHMENTS

The goals of the work in this project are to develop diagnostic techniques for use in studying electrical discharges and to study basic physical problems such as multiphoton ionization which are of direct importance to studies of electrical discharges.

In reports of studies of laser-triggered breakdown, as well as conventional over-volted breakdown, it has been frequently suggested that some mechanism must be producing small amounts of free charge in the gap as a prelude to the rapid current rise which signals gap closure. Prominent among the mechanisms suggested for this charge production is some type of multiphoton ionization process. Accordingly, we have invested significant effort in an on-going study of the multiphoton ionization process in several gases. The construction, testing, and calibration of a proportional counter cell suitable for use in detecting the weak ionization effects of multiphoton ionization are described in the previous annual report. In section B.1 of this report, the study of the four-photon ionization of xenon via a three-photon transition to the excited 5d state is discussed. The results of this study indicate that with a more powerful dye laser than was available to us, this process should be useful in fast, low-jitter spark gap triggering applications, and as a clean source of free charge for studies of space-charge-controlled breakdown. A suitable dye laser for these applications is on order, and experiments in both areas are planned.

We have also carried out multiphoton ionization studies in N_2, since there is evidence that multiphoton ionization plays an important

role in fast laser-triggered switching, as well as in conventional overvolted breakdown in N_2 and N_2 mixtures. This work is ongoing and is described in section B.2.

In the previous annual report we discussed the use of conventional, temporally and spatially resolved, emission spectroscopy techniques for monitoring relative excited state species concentrations. During the most recent contract period, we have studied the usefulness of laser-induced fluorescence techniques to extend this capability to include ground state species concentration. As discussed in section B.3, we have found the technique very useful in monitoring the migration of Al vapor from our electrodes after the spark has extinguished, and it appears that it could be applied equally well to monitoring other species.

1. Multiphoton Ionization in Xenon

Multiphoton ionization is an attractive technique for producing cleanly tailored volumes of ionization in a gas for switching purposes and for fundamental studies of electrical breakdown. Recent work suggests that with lasers of moderate power, substantial ionization can be produced [1,2]. Although multiphoton ionization spectroscopy has been used to study a number of atomic and simple molecular systems, in most studies published to date the measurement of the absolute ionization efficiency of the process has been of only secondary interest [3-11]. Because of the potential utility of the processes, we were interested in determining as accurately as possible what the strength of an ionization process is, and what degree of gas ionization can be produced. Accordingly, we have carefully carried out experiments to deter-

mine the number of charges produced in the multiphoton ionization of xenon via a ground to 5d state intermediate transition.

We chose xenon for our initial studies because 3-photon intermediate transitions to excited levels of the atom are possible and have been reported [3,8] with laser frequencies within the range of our dye laser, and because the non-reactive character of xenon makes it an acceptable additive to other gas mixtures for experiments in which multiphoton ionization is to be used to produce free charges. For the laser frequencies we used, four photons are needed to ionize the xenon atom. The initial transition to a 5d level involves a 3-photon process, with none of the intermediate steps being resonant. The final transition from the 5d level to an ionic state can be accomplished with a single photon, and this transition is believed to be saturated. Thus the rate-determining step is that involving the initial transition to a 5d level, and although the overall process requires 4 photons, the ionization efficiency is expected to behave like a 3 photon process.

a) Experimental Arrangement

Our experimental set-up is shown in Fig. 1. A Molectron DLII dye laser pumped by a Molectron UV400 nitrogen laser was used as the source. With a PBD dye, this system produced 4-8 kW pulses over the 363-372 nm wavelength range we investigated. The output of the dye laser was focused using a 10 cm focal length lens into the proportional counter described in Ref. [12], filled with with pure xenon, or a mixture of xenon, argon, and methane. The signal from the proportional counter was amplified, gated, filtered, and then recorded. For a Gaussian cross section beam, the minimum beam diameter at the focus of the lens would be about 25 μm. Since the output of our dye laser is only approximately

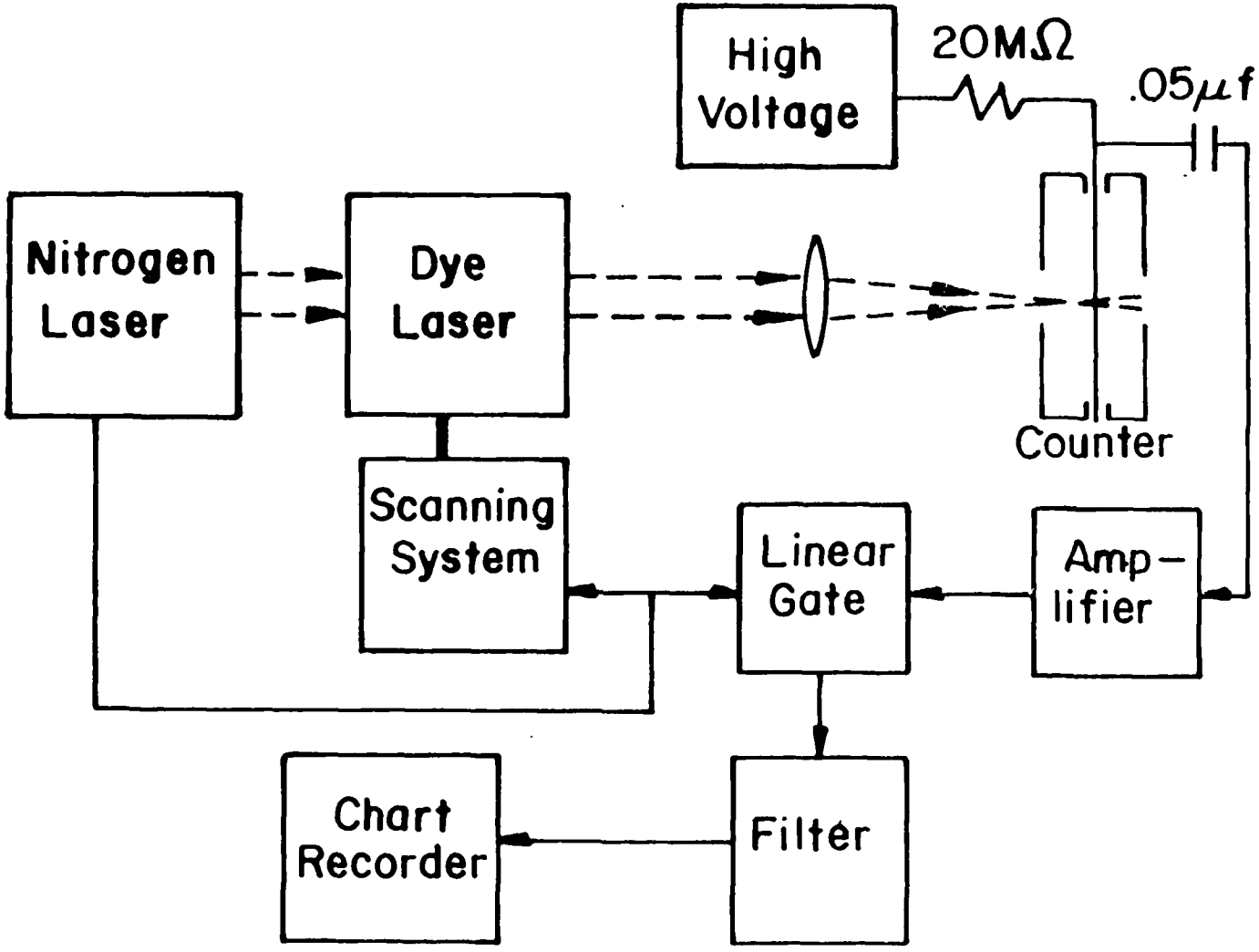

Fig. 1 Experimental setup for multiphoton ionization spectroscopy.

Gaussian, the actual waist diameter is probably somewhat larger.

The construction, testing, and calibration, of our proportional counter system are described in a previous report [12]. Briefly, the procedure consists of using it and a multichannel pulse height analyzer to obtain the x-ray emission spectrum of a ^{57}Co sample. In the low energy region, ^{57}Co emits 6.4 and 14.4 keV x-rays [13]. To a good approximation, the number of free charges produced in an x-ray absorption event is given by the ratio of the x-ray photon energy to the ionization energy of the fill gas atoms. Therefore, the gain of the proportional counter may be readily determined under a given set of conditions, and the linearity of the system can be checked by monitoring the relative positions of the 6.4 and 14.4 keV peaks. Over a gain range of more than 10^2, the gain was accurately an exponential function of the proportional counter voltage, and the linearity was excellent.

b) Results

After calibrating our proportional counter cell in this manner, we proceeded to acquire multiphoton ionization spectra. Figure 2 shows the spectrum obtained in the vicinity of the lines resulting from transitions to the 5d states, 5d [3½] J=3, and 5d [2½] J=3. These results are similar to those of Aron and Johnson [3]. At the peak of the 3638 Å line, with 150 torr of Xe, and peak laser power of 8 kW (intensity ≈ 1.6×10^9 W/cm^2) we found a total multiphoton ionization charge production of 2.2×10^7 charges (excluding the gain in the proportional counter).

For a 3-photon process, the ionization efficiency would be expected to scale as I^3, where I is the laser intensity. Dye lasers with 10^3 greater output power than ours are readily available, so that if the

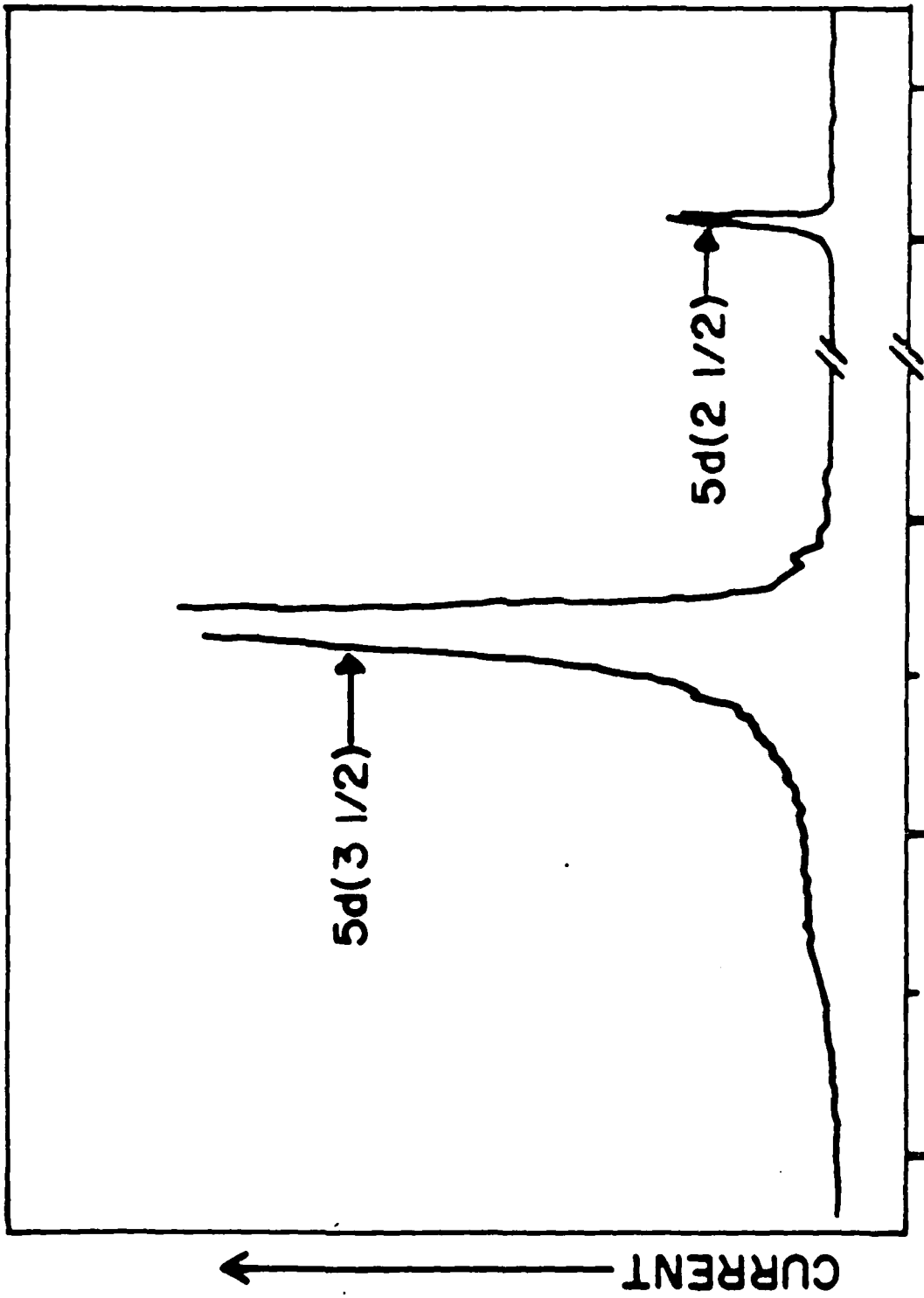

Fig. 2 Multiphoton ionization spectrum of Xe at 150 Torr pressure.

cubic intensity dependence holds, very substantial gas ionization could be accomplished with this process. Figure 3 shows the results of a series of experiments designed to determine this intensity dependence. The laser intensity was varied by inserting neutral density filters in the dye laser beam.

In the uncorrected data, there is clear evidence of saturation at higher laser intensities. Several experiments involving measurement of signal strength vs. laser power for reduced proportional counter voltages have made it evident, however, that the effect is largely the result of the saturation of the proportional counter and not of the ionization process. Dalby, et. al. have reported a similar effect for multiphoton ionization in I_2 [11]. The data points labeled "corrected" in Fig. 3 were obtained with reduced proportional counter voltage and corrected by using the gain curve measured previously. We conclude, therefore, that over the laser power range we studied the ionization efficiency obeys a cubic power dependence, except perhaps at the highest powers, where the curve may be starting to saturate.

Briefly, the experiments for testing the saturation of the proportional counter consisted of determining the magnitude of the ionization signal from the counter as a function of laser energy in the high energy region for a number of different voltages applied to the counter cell. Although there was some scatter in the data, for laser energies above $\sim$20 μJ, the data points for a given counter voltage fit roughly on a straight line on a logarithmic plot. The slope of the line increased with decreasing counter voltage, changing from a slope of 1.4 with 1400 V on the counter to 2.7 at 600 V, the lowest counter voltage we looked at. This behavior provides clear evidence that substantial,

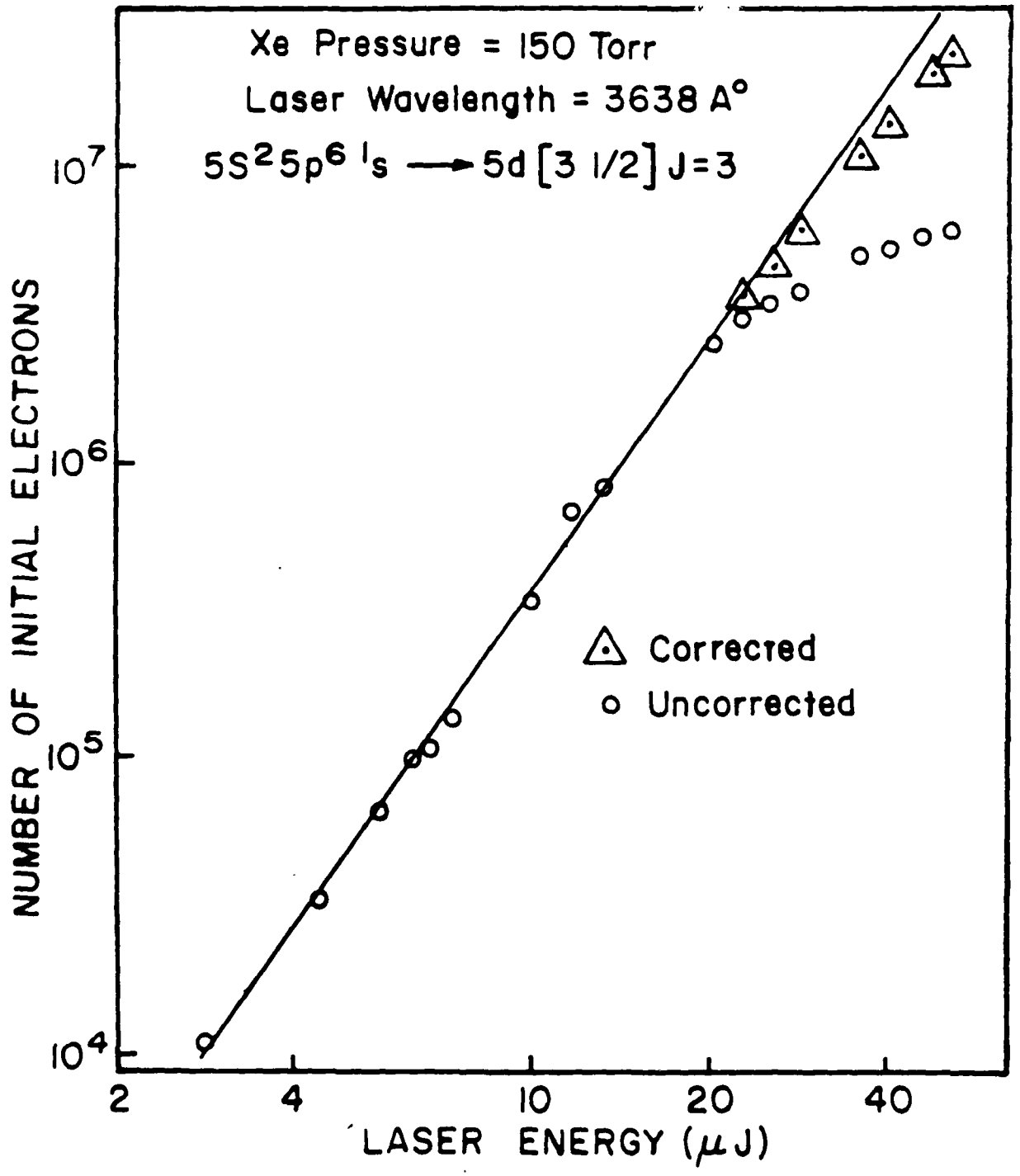

Fig. 3 Plot showing the apparent number of electrons produced by M.P.I. in Xe at the peak of the 3638 Å line as a function of laser energy. Points labelled as corrected were corrected for the saturation of the proportional counter as discussed in the text. The straight line has a slope of 3 as would be expected for a 3-photon process.

space-charge-induced, saturation of the counter is occurring in our high power experiments.

Even after accounting for this effect, there appears to be a slight de iation from a cubic intensity dependence at the highest laser powers. In 2-photon ionization studies of several organic molecules Lee and Bischel reported a strong saturation effect which they attributed to recombination [2]. In their model some of the ionization produced is not detected by the proportional counter because it recombines before being collected at the electrodes. This explanation seems the most likely cause of any residual saturation effects in our experiments. We estimate that there are more than 10^{11} Xe atoms in the volume sampled by the most intense portion of our laser beam. Since the laser induces only 10^{7} ionization events, depopulation of the ground state level does not appear to be a likely cause for saturation.

Because the spatial dependence of the laser intensity is not well known, it is difficult to obtain an accurate, generally useful measure of the ionization efficiency. In order to estimate this quantity we will assume that we have a Gaussian-shaped beam and that the beam focusing lens is diffraction-limited. Deviations from these assumptions will result in a larger diameter focus, and our efficiency estimate therefore represents a lower limit.

The coefficient describing a three-photon transition can be defined in several ways. We choose:

$$N = \alpha n \int\int I^3(r,t) d^3r dt \qquad (1)$$

Here N is the number of transitions induced by a laser pulse, α is the efficiency coefficient for the process, n is the number density of gas

atoms and $I(\vec{r},t)$ is the laser intensity. Under the Gaussian assumption above, the integral in Eq. (1) may be evaluated, with the result that

$$\alpha = \frac{N}{n} \frac{6\sqrt{3t_o^2\lambda^3 f^2}}{\pi d^2 E^3}, \qquad (2)$$

where t_o is the full width at the 1/e points of the laser pulse, λ is the laser wavelength, f is the focal length of the focusing lens, d is the 1/e diameter of the laser beam at the focusing lens, and E is the pulse energy of the laser. For our system, t_o = 6 ns, λ = 364 nm, f = 10 cm, d = 1 mm, and E = 20 μJ. We observed 2.9×10^6 charges with a number density of Xe atoms of 4.8×10^{18} cm^{-3}. With these values, we obtain an estimate for α of $\alpha = 4\times10^{-24}$ $cm^6/s\text{-}W^3$.

The ionization coefficient is also sometimes defined by introducing a factor of $1/h\nu$ into the right hand side of Eq. (1). This alternate definition results in a coefficient, α', related to our coefficient α, by $\alpha' = h\nu\alpha$. From our result for α, we obtain $\alpha' = 2\times10^{-42}$ cm^6/W^2.

Due to the uncertainty in the spatial dependence of the laser intensity, this estimate of the ionization coefficient may be significantly in error. Since the actual beam waist diameter will be larger than that predicted by our assumption of a Gaussian profile, our estimate should represent an approximate lower limit for the value of α. The correct value for α could be as much as a factor of 10 larger than our estimate.

The obvious continuation of this work is to use a higher power dye laser to measure the ionization efficiency with substantially higher peak powers, and, if the predicted large ionization is observed, to make use of the technique to trigger a spark gap or as a source of

charge for studies of space-charge dominated electrical breakdown. A dye laser with more than 10^3 greater peak power than the one currently available to us is on order, and we expect these studies to be initiated shortly after receipt of the laser.

2. Multiphoton Ionization in N_2

In light of the utility of N_2 as a component in gas fill mixtures for spark gap switches and of the suggested role of multiphoton ionization in electrical breakdown mechanisms [14], we have studied multiphoton ionization in N_2. Throughout most of the spectral range we investigated (3600 Å to 4500 Å), we observed a broad, featureless continuum in the ionization efficiency spectrum. Within an approximately 100 Å wide band centered around 3850 Å, however, a spectacular, regular, highly structured spectrum is observed. The multiphoton ionization spectrum observed in this region is shown in Fig. 4. The regularly-shaped peaks in this spectrum seem similar to rotational structure, and the peak spacing is of the right order of magnitude to be of rotational origin, but there are much too many peaks to be explained by rotational structure from a gas at 300°K.

To illustrate this point, we show in Fig. 5 a synthetic spectrum calculated using "typical" values for the rotational and vibrational constants of excited states of N_2, lying within roughly one photon energy of the ionization continuum. Since at these wavelengths five photons are needed to ionize N_2, we have assumed that the overall ionization process results from a four-photon transition to an excited state followed by a one photon ionizing transition. The intensity of a par-

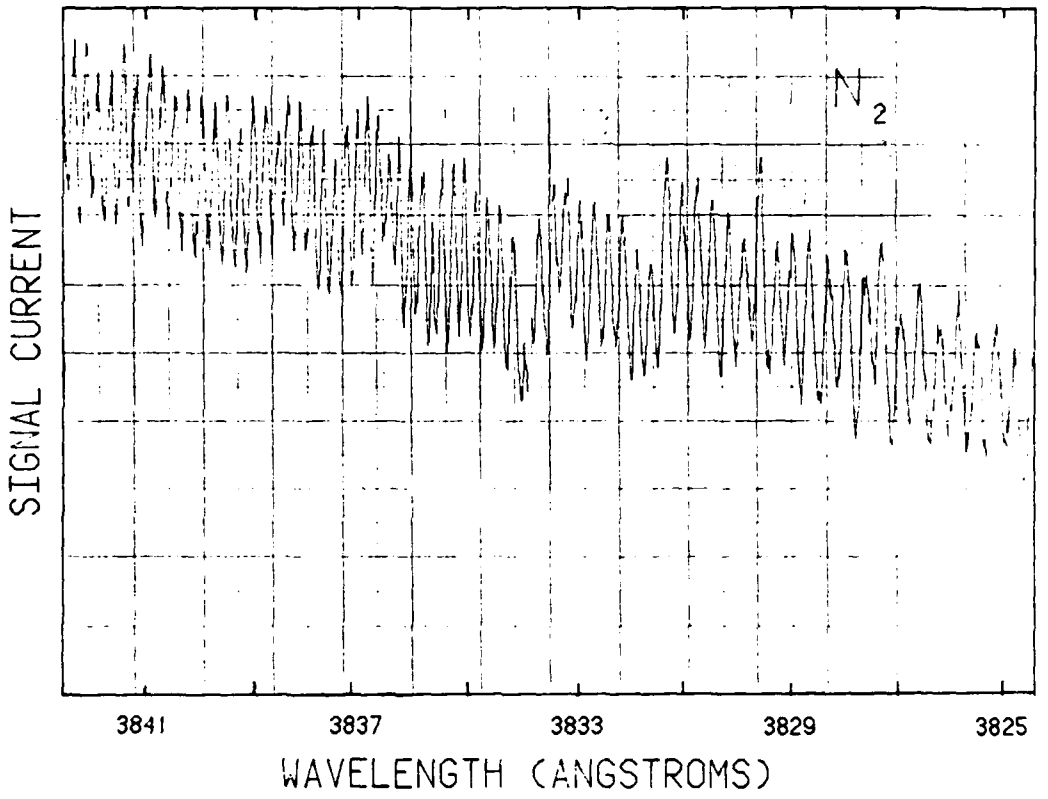

Fig. 4 Multiphoton ionization spectrum in N_2. The spectrum continues for approximately 50 Å on either side.

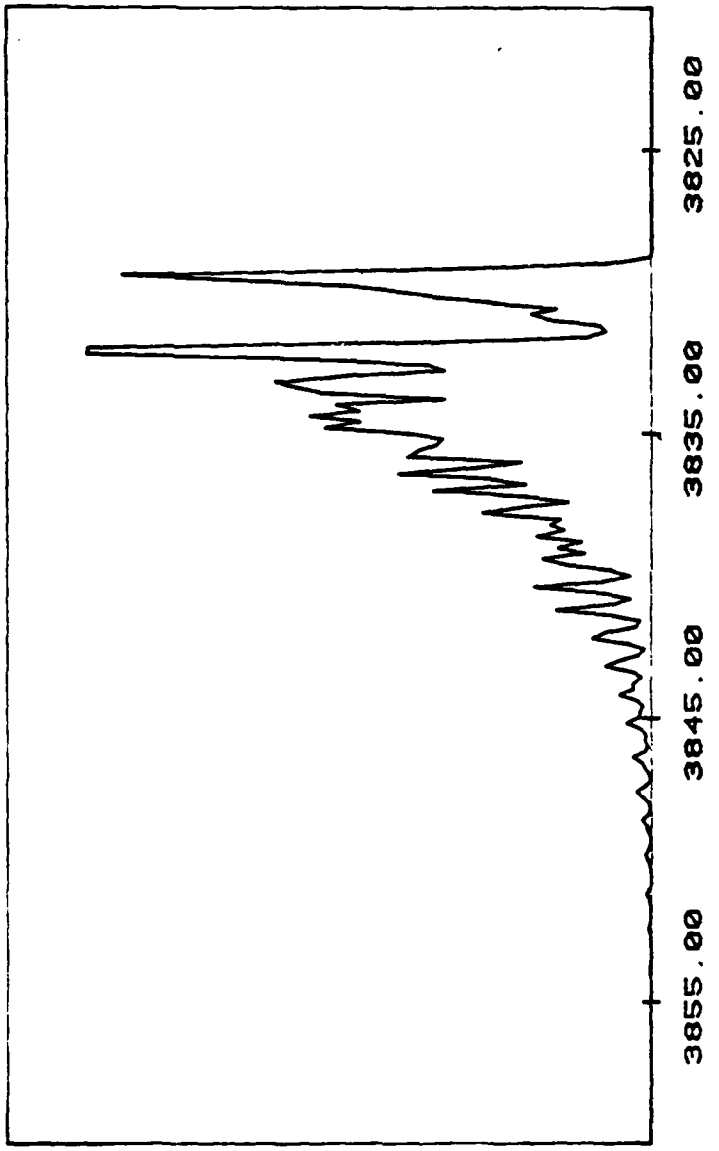

Fig. 5 Synthetic multiphoton ionization spectrum resulting from a four photon transition to a hypothetical state lying within 3eV of the ionization continuum.

ticular rotational-vibrational line resulting from a transition between v=0,J to v',J', should be proportional to a product of factors, given by [15]

$$I(J,J') \propto (2J+1)N(J)\ F(0,v')\ M(J,J')\ P(J',v')$$

where N(J) is the number of molecules in the laser beam in rotational state J (we assume only the v=0 level of the ground state has significant occupation), F(0,v') is the squared magnitude of a vibrational matrix element for the $0 \rightarrow v'$ transitions, M(J,J') is the squared magnitude of the rotational matrix element for a J to J' transition, and P(J',v') is the probability that the laser will ionize a molecule once it reaches the excited state.

To estimate the appearance of a spectrum we have taken the ionizing transition to be saturated, as was the case with Xe. Therefore P(J',v) = 1. The factor N(J) is simply given by the Boltzman factor, $N(J) = N_0 e^{-BJ(J+1)/kT}$, where B is the rotational constant for ground state N_2. The quantity M(J,J') is analagous to the Hönl-London factors for two-photon transitions [16]. In principle it may be calculated from tables of Clebsch-Gordon coefficients and from detailed knowledge of the symmetry of the electronic states involved in the transition [17]. In any case, for a homonuclear diatomic molecule, it will introduce a dipole selection rule of $\Delta J = \pm 4, \pm 2, 0$. Since we can only guess at the identity of the upper state, we have taken M(J,J') = 1 if the J-selection rule is satisfied, and M(J,J') = 0 if not. This assumption may introduce large errors into the relative intensities of the $\Delta J = \pm 4$, ± 2, and branches, but within a branch, only the low-J transitions should be subject to significant error. Finally, since the vibrational matrix elements are

completely unknown, we took them all to be equal to one. Since bands belonging to different vibrational manifolds are reasonably well separated spectrally, this assumption should not affect local structure.

From the synthetic spectrum in Fig. 5, it is clear that the structure we observe in N_2 cannot be explained in terms of a simple rotational model. There are too few strong rotational lines associated with each vibrational level. We do not presently understand this structure. Efforts are currently underway to ensure that the structure is not the result of some impurity in the gas fill mixture. We have carefully checked the wavelength dependence of the output power of our dye laser for any regular structure such as we see in the multiphoton ionization spectra, but we have seen no evidence of such an effect. Work is continuing to understand better this structure.

3. Monitoring of Ejected Electrode Material

We investigated the use of laser-induced fluorescence to monitor the migration of vaporized aluminum alloy electrode material into the gap region following a low energy spark in nitrogen. Among the lines evident in the emission spectrum of ground state aluminum are a doublet at 3944 and 3961 Å, resulting from transition from the $4s^2S$ state to the split $J = \frac{3}{2}$ and $J = \frac{1}{2}$ levels of the ground state, respectively, as shown in Fig. 6. In an earlier report we discussed the monitoring of Al atom migration during and shortly after the spark by observing the intensity of these lines in emission [12]. As we pointed out, this technique suffers from the difficulty that it monitors an excited state population, not the ground state population, whereas after the spark

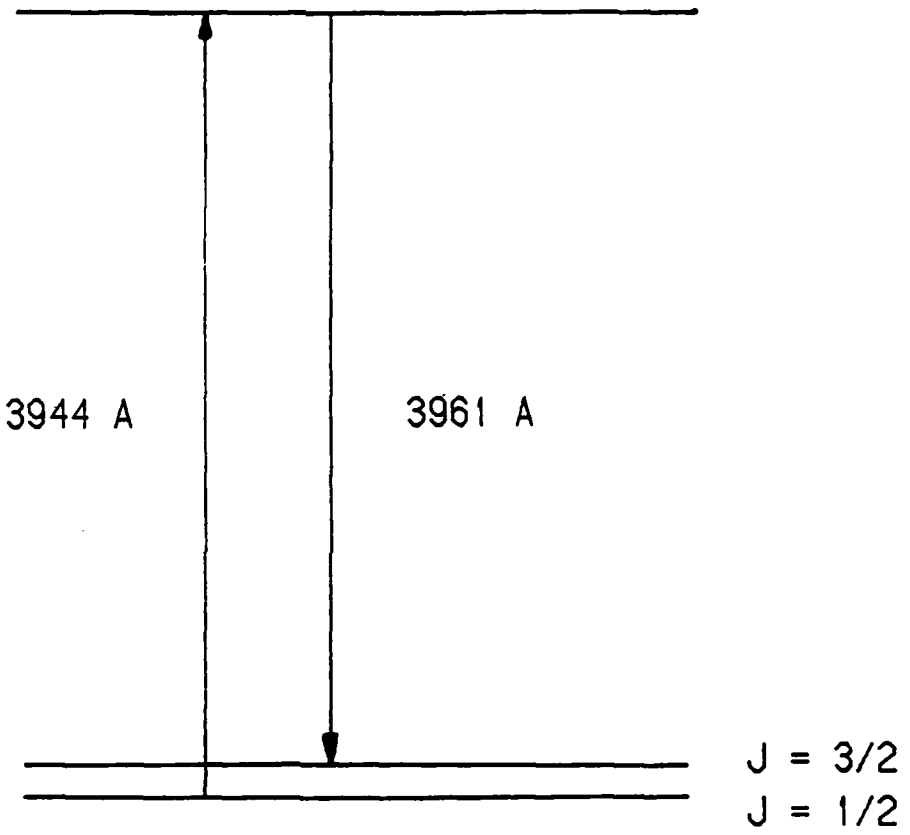

LASER-INDUCED FLUORESCENCE IN ALUMINUM

Fig. 6 Schematic diagram of energy level structure of atomic aluminum relevant to our laser-induced fluorescence studies.

most atoms quickly relax to the gound state and are therefore not detected with this technique.

Laser-induced fluorescence can be used to monitor the ground state population. In our experiments the output of a nitrogen laser-pumped dye laser tuned to 3944 Å, was used to excite ground state atoms to the $4s^2S$ upper state, and the subsequent emission resulting from transitions back to either of the split ground state levels was monitored. The intensity of this emission is directly proportional to the ground state Al atom density in the volume sampled by the intersection of the exciting beam and the collection viewport of the spectrometer.

The results of our experiments were quite encouraging. Figures 7a, 7b, and 7c, show typical spectra we obtained with only the spark, only the laser, and both the spark and the laser. Note the intensity scale difference in Fig. 7c. These are time resolved spectra taken 20 μs after the spark extinguished. Figure 7a shows the conventional emission in the afterglow, Fig. 7b shows the intensity of scattered laser light, and Fig. 7c clearly shows the laser-induced fluorescence.

We used this technique to monitor the density of Al atoms as a function of time at a fixed point in the gap. The cell was filled with N_2 at 200 Torr, and the 0.5 cm gap was charged to 5.5 kV through a coaxial cable system which produced a clean current pulse of 1 μs duration into a 50 Ω load. The gap was triggered to breakdown with a 3 mJ pulse of 3371 Å radiation from an NRG Model 0.7-5-200/m laser.

A set time after the gap was triggered, the dye laser was fired and the gate on the OMA detector was opened. The dye laser output was approximately 30 μJ and the 2 mm dia. unfocused beam was passed through the spark gap in a direction transverse to the axis of the gap and to

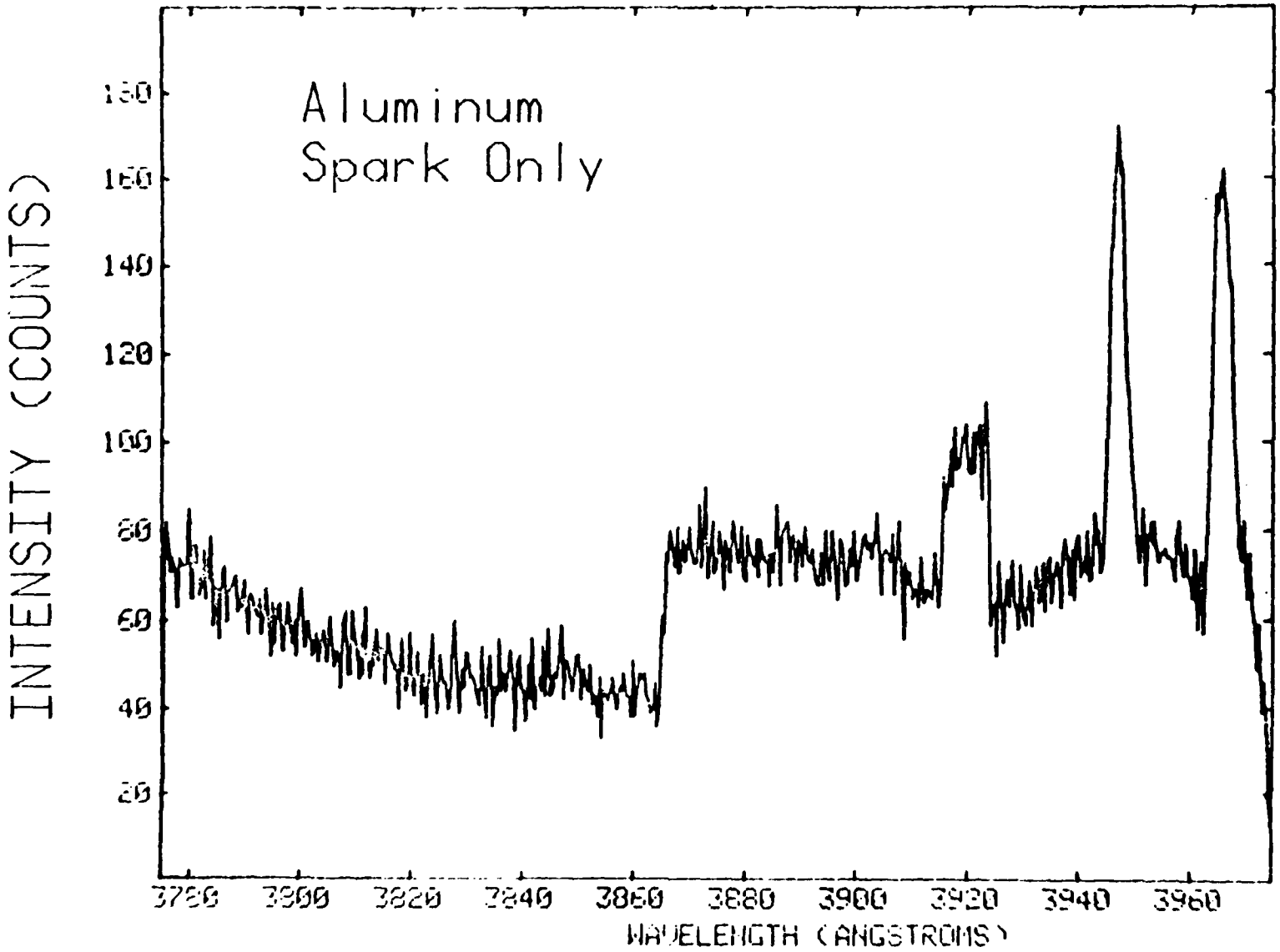

Fig. 7a Spectrum obtained from the L.I.F. experiment without the exciting laser, 20μs after the spark extinguished. The doublet is due to emission from Al vapor. The abrupt apparent intensity changes at 3864, 3915, and 3922 Å are due to a digital data transmission problem and are not real.

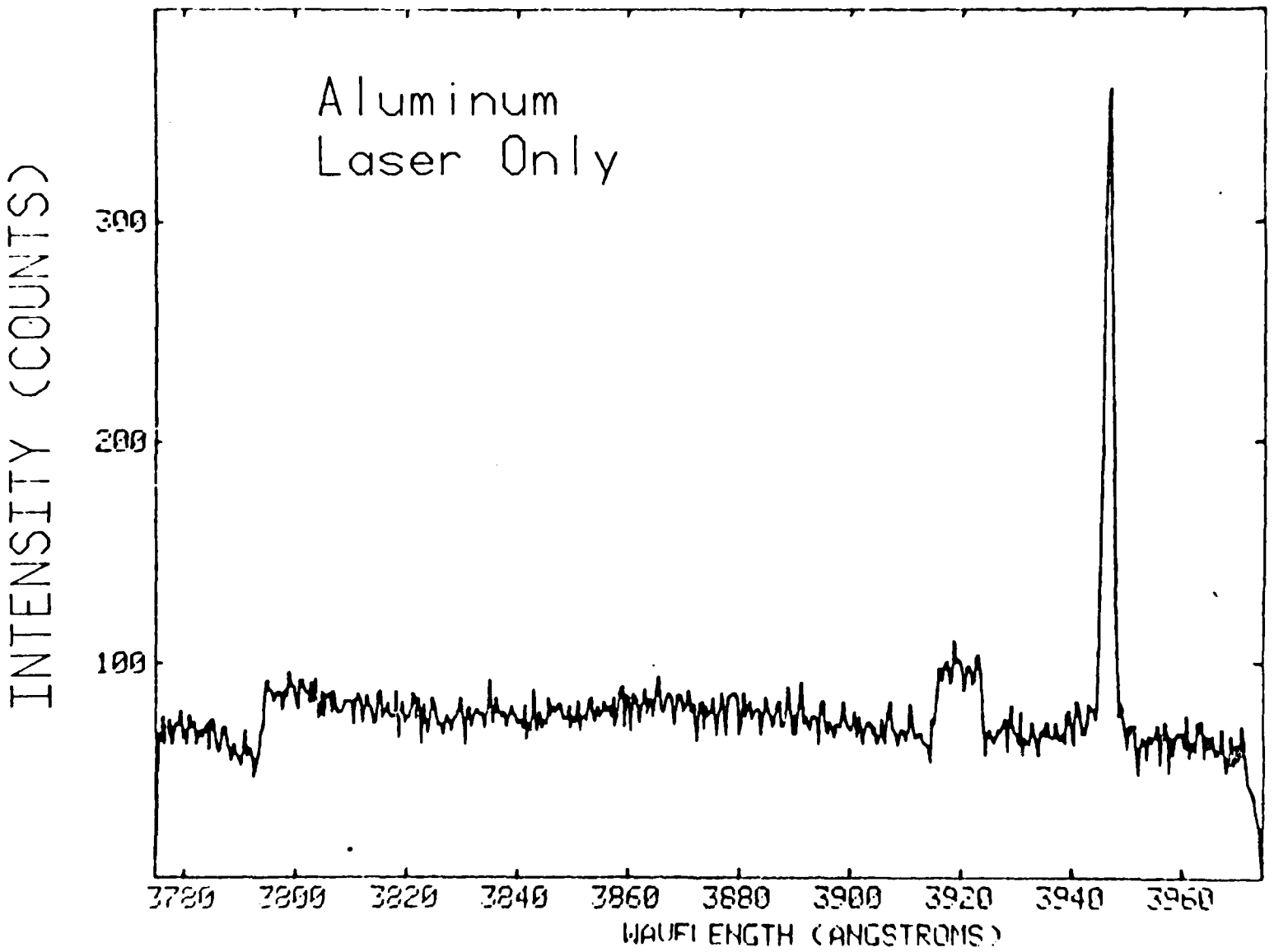

Fig. 7b Spectrum obtained from the L.I.F. experiment with the excitation laser, but with no voltage applied to the gap. The line is due to scattered light from the exciting laser. The abrupt apparent intensity changes at 3795, 3918, and 3923 Å are due to a digital data transmission problem and are not real.

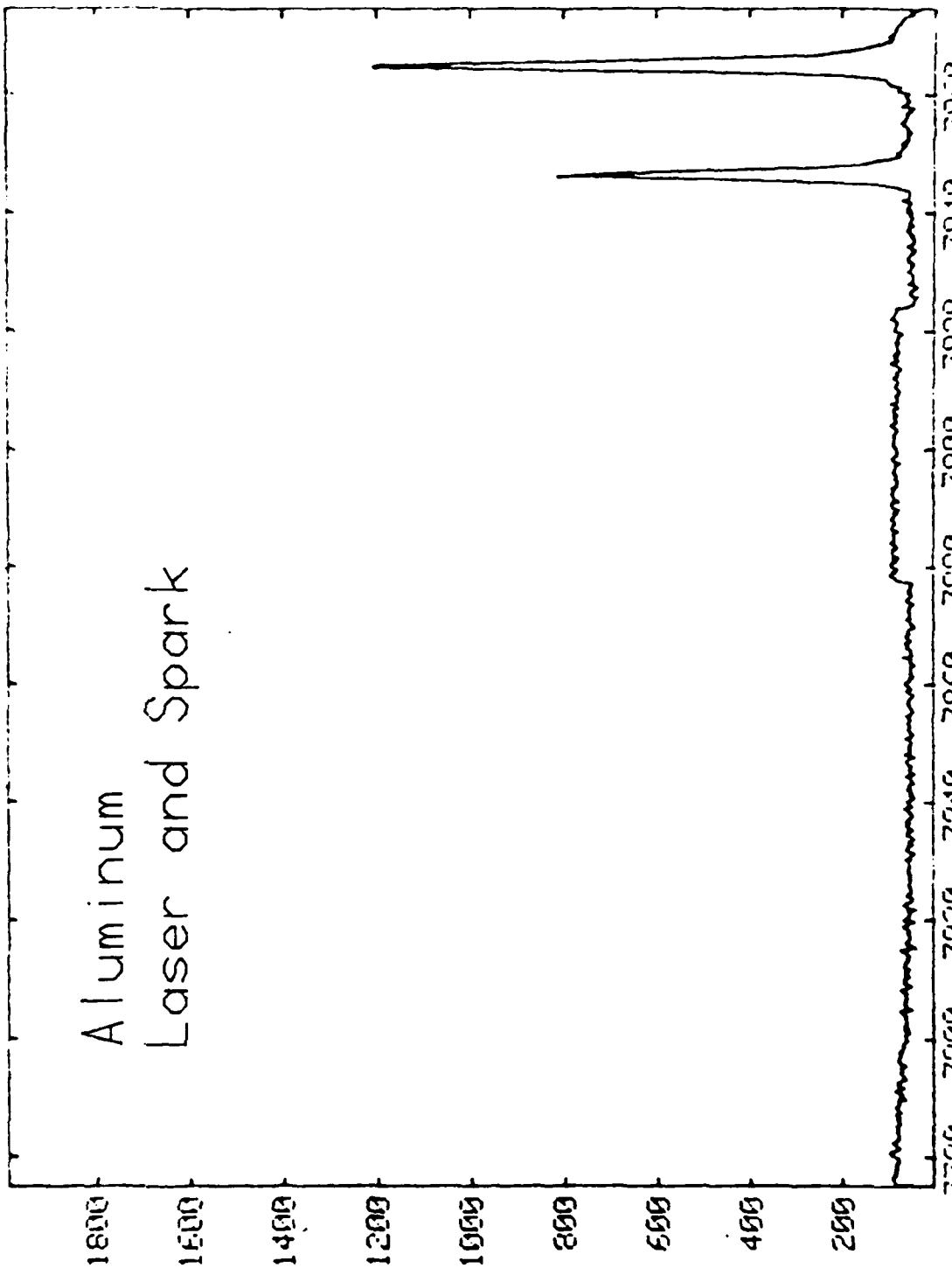

Fig. 7c Laser-induced fluorescence spectrum observed with the excitation laser, 20 μs after the spark extinguished. Note the difference in the intensity scale as compared with Figs. 7a and 7b. The abrupt apparent intensity changes at 3877, and 3924 Å are due to a digital data transmission problem and are not real.

the viewing port. Emission was collected and dispersed with an 0.5 m spectrograph and then detected with a gated OMA SIT vidicon detector.

The results of the preliminary study are shown in Fig. 8. Here the intensity of the laser-induced emission from a small volume, 1.5 mm above the lower, struck electrode, is plotted as a function of time after the spark. Because of the cable system used to charge the gap, the current pulse cuts off clearly after 1 μs and these data describe the outward diffusion of Al vapor during the after-glow part of the breakdown cycle.

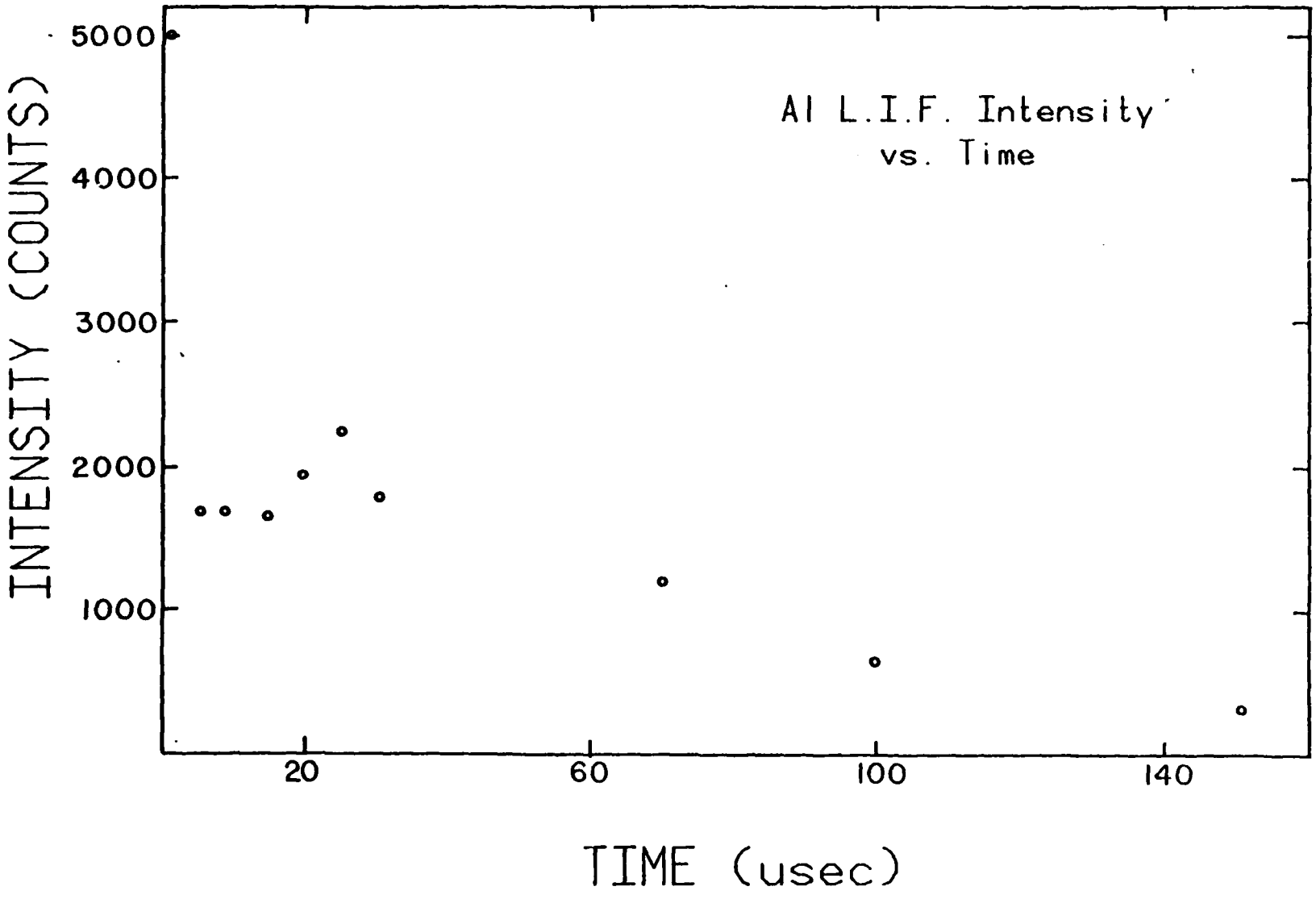

Fig. 8 Results of preliminary measurement of time dependence of the Al vapor density at a point 1.5 mm above the struck electrode using the laser-induced fluorescence technique discussed in the text.

C. REFERENCES

1. J. R. Woodworth, C. A. Frost, and T. A. Green, "U. V. Laser Triggered Switches", Third IEEE International Pulsed Power Conference, Albuquerque, N.M., June 1981.
2. L. C. Lee and W. K. Bischel, "Two-Photon Ionization Coefficients of Propane, 1-Butene, and Methylamines", Preprint, SRI International, Menlo Park, CA.
3. K. Aron and P. M. Johnson, J. Chem. Phys. 67, 5099 (1977).
4. R. Panock, R. R. Freeman, J. C. White, and R. H. Storz, Optics Lett. 5, 160 (1980).
5. P. M. Johnson, M. S. Bernan, and D. Zakheim, J. Chem. Phys. 62, 2500 (1975); D. Zakheim and P. M. Johnson, J. Chem. Phys. 68, 3644 (1978).
6. P. M. Johnson, J. Chem. Phys. 64, 4143 (1976).
7. C. B. Collins, et. al., Phys. Rev. A14, 1662 (1976).
8. J. C. Miller, R. N. Compton, M. S. Payne, and W. W. Gurrett. Phys. Rev. Lett. 45, 114 (1980).
9. D. M. Lubman, R. Naaman, and R. N. Zare, J. Chem. Phys. 72, 3034 (1980).
10. J. Murakamo, K. Kaya, and M. Ito, J. Chem. Phys. 72, 3034 (1980).
11. F. W. Dalby, G. Petty-Sil, M. H. L. Pryce, and C. Tai, Can. J. Phys. 55, 1033 (1977).
12. First Annual Report on Coordinated Program in Pulsed Power Physics, AFOSR Contract No. F49620-79-C-0191, Project No. 5, pp. 100-114, December, 1980.
13. H. C. Thomas, C. F. Griffin, W. E. Phillips, and E. C. Davis, Nuclear Physics 44, 268 (1963).
14. A. H. Guenther, J. R. Bettis, R. E. Anderson, and R. V. Webb, "Low Jitter Multigap Laser-Triggered Switching at 50 PPS",IEEE J. Quant. Elect. QE-6, 483 (1970).

15. G. Herzberg, Molecular Spectra and Molecular Structure, Vol. I Spectra of Diatomic Molecules, Chap. IV, (Reinhold, New York, 1950)

16. Ibid. p. 208.

17. M. Tinkham, Group Theory and Quantum Mechanics, Chap. 5, (McGraw-Hill, New York, 1966).

Project No. 6

Exploratory Concepts

(A. Donaldson, R. Curry, D. Johnson, H. Carper,
R. Pederson, M. Hagler, K. Schoenbach, and M. Kristiansen)

A. SUMMARY

Several exploratory concepts are being studied under this project. These are typically smaller investigations aimed at determining the feasibility and pay-off values of various ideas. The main purpose is to bring new ideas into the program. An example of this is that the investigations described under Project No. 10, "Opening Switches", were initiated under "Exploratory Concepts". Among the ideas and concepts under study are:

a) Schlieren and Interferometric Studies of Gas Blown Spark Gaps: A small experimental arrangement has been set up to study and compare breakdown in static and transversly blown gaps at 1 Atm of air. Some very interesting, fast (4200 frames/sec. exposure) film strips of the gas density variations in such gaps have been produced. It is felt that this experiment has excellent promise for obtaining valuable data about gas flow limitations and optimizations in gas blown gaps. Efforts are, therefore, being made to obtain separate funding for this project.

b) Arc Quenching: Investigations are underway to determine the relative effectiveness of various quenching materials for fuses. A modest experimental facility has been assembled and a few quenching materials have been compared with regard to quenching time, restrike time, and hold-off voltage.

c) Assessment of Switch Geometries: A computer field plotting code has been developed and used to analyze various switch geometries used in our laboratory. Among these are the electrodes used in the Optical Opening Switch experiment described in Project No. 10.

d) Field Effect Electrolyte Switch: The possibility of building an electrolyte switch which operates similar to a solid state field effect transistor has been studied and a small experiment is being planned.

e) Magnetic Switching: A small experiment, primarily aimed at gaining experience with magnetic switching, has been assembled and is being studied.

B. SCHLIEREN AND INTERFEROMETER STUDIES OF GAS BLOWN SPARK GAPS

(H. Carper and R. Pederson)*

Members of the faculty of the Department of Mechanical Engineering at Texas Tech University have recently been conducting some exploratory work on the application of optical techniques to the study of the fluid mechanics aspects of gas blown spark gap switches. Their interest is in the limitations imposed on the spark gap rep-rate by the fluid mechanics and related heat transfer processes in the interelectrode region of these switches. Some modest support and help, primarily with regard to the electric discharge system, has been provided by Project No. 6, Exploratory Concepts.

---

* Department of Mechanical Engineering, Texas Tech University

Both schlieren and interferometer systems have been used, along with high-speed photography, to observe the post arc effects on the gas density in the interelectrode region. A simple electrode configuration consisting of two 1-in. diameter brass electrodes with spherical ends was used. The minimum gap spacing was approximately 0.1 in. A small, D.C. charged, capacitor was used to drive the arc which had a self breakdown voltage of about 10 kV in ambient air. The arc had a maximum current of about 150 amps and a pulse width of about 3 μs.

For all experiments, the electrode assembly was placed in ambient air. Some experiments were conducted in which the gap was not flushed, and others were conducted in which the gap was continuously flushed by a jet of air issuing from a 2-in. diameter PVC pipe connected to a variable flow-rate blower. The axis of the jet was perpendicular to the electrode axes and to the path of the light source passing through the test section of the schlieren or interferometer system. The jet velocity used for all these initial experiments was 6.7 m/sec.

In the first set of experiments, the electrode assembly was placed in the test section of a schlieren system, and a Fastax, 16-mm, motion picture camera was used to obtain pictures of the effects on the air density in the interelectrode region, following the arc discharge. The camera speed was about 4,200 frames per second which is the maximum speed for the camera with the available power supply. Density gradients were clearly visible in the inter-electrode space for abour 14 ms after the discharge of the arc.

Following this first set of experiments, a subsequent set of experiments was conducted in which the gap was continuously flushed by the air jet. Figure 1 presents an example sequence of pictures obtained with

the Fastax camera at a camera speed of about 4,200 frames per second. These pictures are prints made from positive film and are therefore negatives. The camera speed of 4,200 frames per second results in an exposure time of about 80 μs. There was no synchronization between the arc and the camera, thus the time when the arc occurred cannot be referenced to the film. However, it appears that the first picture of the sequence contains the arc discharge itself. There are about 480 μs between each picture of the sequence. The 80 μs exposure time is relatively long for the motion being photographed, and the resulting pictures are not of the highest quality. Nevertheless, the temperature gradients in the air can be clearly discerned. The orientation of the knife edge of the schlieren was such that temperature gradients in the direction of air flow are indicated on the photographs. Areas lighter or darker than the background intensity of the photograph indicate regions of temperature gradient. The magnitude and sign of the gradient can be determined by analysis of the intensity variation. In principle, the density can be obtained by integration if the reference density and certain optical characteristics of the schlieren system and the flow are known. However, schlieren results are generally more useful qualitatively than quantitatively.

From these schlieren experiments, it was found that all evidence of any temperature gradients in the air contained within the space bounded by the diameter of the electrodes had vanished within about 4 ms. On the other hand, based on the volocity of the jet, a fluid particle would move from the location of the arc to the radius of the electrode in about 2 ms. The longer actual time required for the flushing process is indicative of the fact that the mean velocity in the interelectrode region is lower than the jet volocity. There is possibly also some effect of the upstream ex-

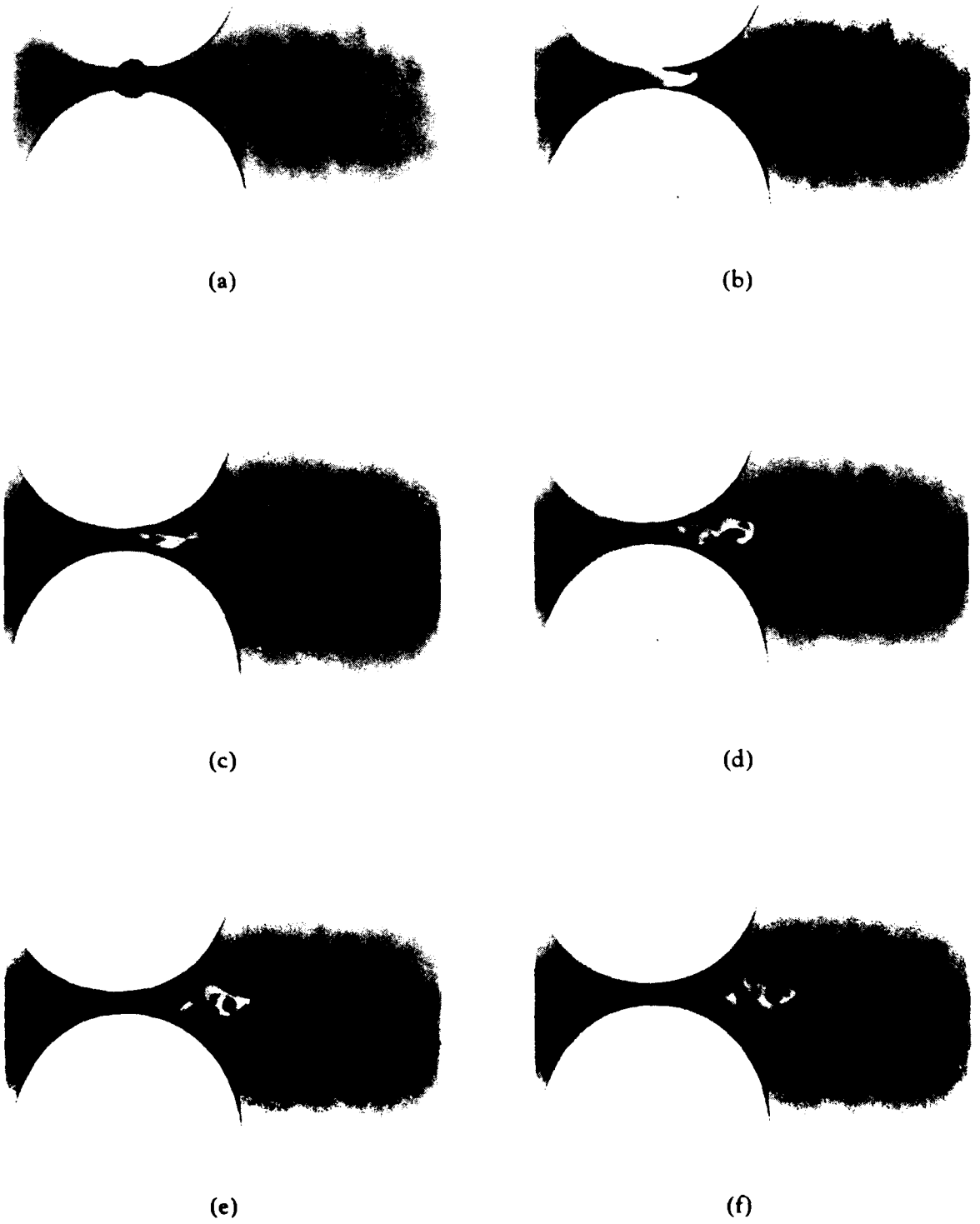

Figure 1. Schlieren Photographs of Flow between Electrodes following an Arc.

pansion of the air around the arc which opposes the velocity of the jet.

Another series of experiments was conducted with the electrode assembly placed in the test section of a Mach-Zehnder interferometer. Since the interferometer can be used to measure density directly, it is more suitable than the schlieren for making a quantitative determination of density. However, it is somewhat more difficult to use. In this series of experiments, high-speed motion pictures were obtained using both the infinite fringe and the fringe displacement techniques. Figure 2 presents an example sequence of pictures obtained with the infinite fringe technique using the 16-mm Fastax camera at a speed of about 4,200 frames per second. The first picture of the sequence was obtained at a time shortly after the arc discharge, and there are approximately 240 μs between each picture in the sequence. These pictures are also negative prints made from the positive 16-mm film. The dark area contained within the light ellipse, as seen in the first few pictures of the sequence, represents slightly over one complete room-air wavelength phase shift of the light source, this shift being a measure of the density decrease of the air which was heated by the arc. It is interesting to note that this hottest region of the gas tends to remain rather well defined as it moves toward the electrode radius and then begins to break up as a result of the turbulent mixing. Also noteworthy is the dark area surrounding the light ellipse, an area of intermediate density, which elongates into the shape of a fish with the tips of the tail fin tending to remain attached to the electrodes. This shows the effect of the reduced velocity in the boundary layers near the electrodes, which will inhibit the flushing process.

The results of these preliminary experiments show that schlieren and

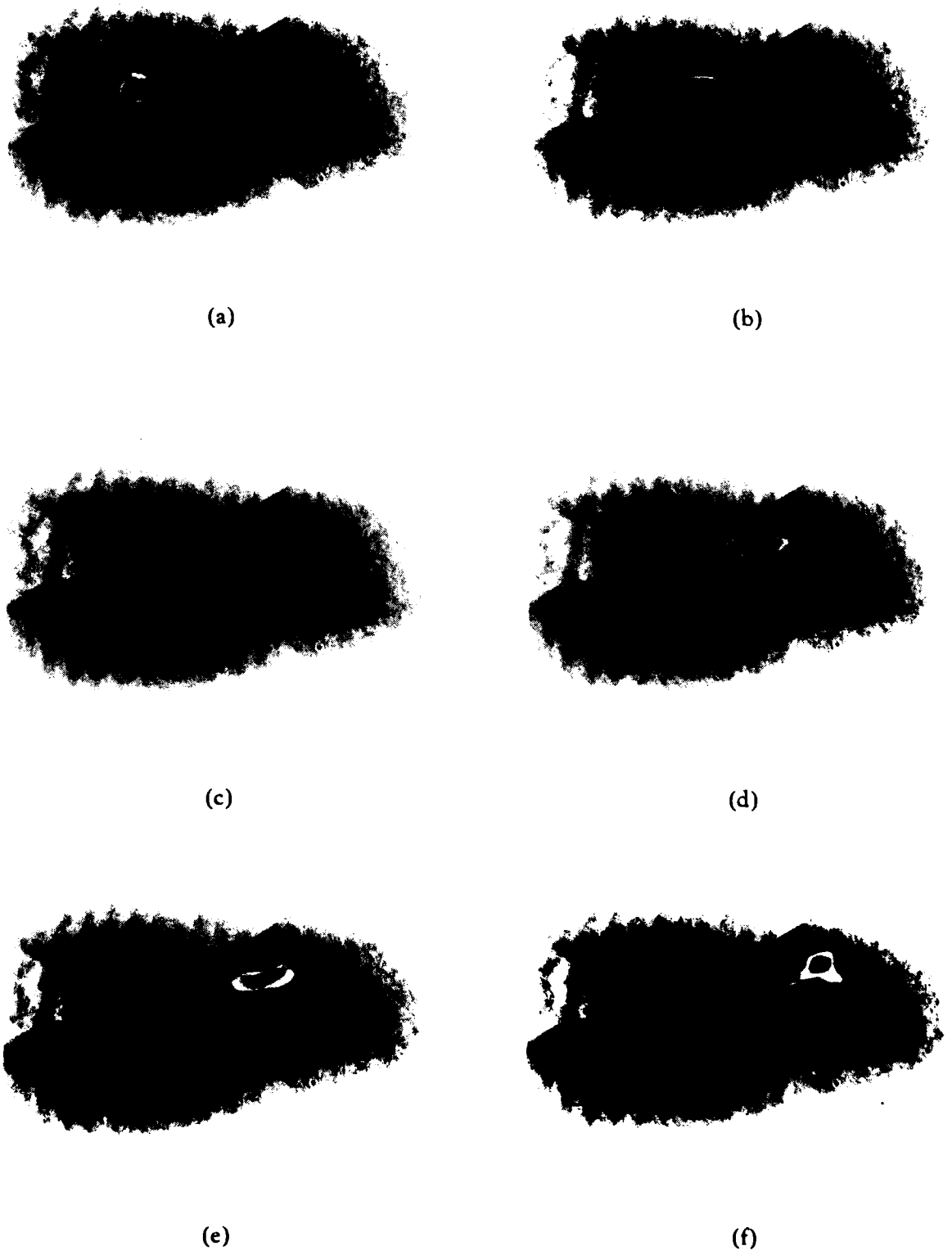

Figure 2. Interferometer Photographs of Flow between Electrodes following an Arc.

interferometer techniques coupled with high-speed photography can indeed be used to observe the effects of the arc on the density of the gas in a gas blown spark gap. It is believed that studies of the type reported here can provide useful quantitative information on switch recovery time, as limited by the gas flow, for various electrode configurations, flow rates, gas types, etc.

To define the density field completely, additional work is needed to address the three-dimensional nature of the density field in the gap, which makes the density determination from the schlieren and interferometer pictures more difficult than for two-dimensional flows. However, even without an accurate interpretation of the density field from the schlieren and interferometer pictures, useful data can still be obtained. For example, with electrodes of uniform spacing, as long as any post arc effects on density can be observed there is doubt as to whether the gap can be considered to be fully recovered. Along this line of reasoning, future experiments are planned with the electrode configuration described above where attempts will be made to photograph a restrike of the arc which might be expected to occur through the low density post arc gas rather than at the minimum gap spacing. If this occurs and can be observed, then the possibility exists that useful relationships between flow rate, electrode geometry, power transmitted, etc. and recovery time can be developed.

C. ARC QUENCHING

The material which surrounds an arc, e.g. from an exploding wire, influences the plasma recombination and the voltage recovery rate. In regular gas discharges, such as in a gas spark gap, additions of electro-

negative gases, such as SF_6, may increase the recombination rate.* In terms of voltage hold-off it is also important to cool the gas as fast as possible. It appears that an admixture of He may help in this regard, but no information has been found of such an investigation. The He gas may, however, have certain other undesirable effects related to UV radiation and resulting insulator damage, as well as reduced dielectric strength.

In terms of exploding wire (fuse) discharges various arc quenching materials have been investigated [1,2]. It has generally been found that quartz sand is one of the best such materials. Very few investigations with solid tamping materials have been reported. Epoxy has been tried with marginal success [3] as a wire tamp. Other materials might work better. A glass wool medium has, for instance, been reported to work quite well as a quenching material for a reprated arc discharge [4] and it may be of interest to investigate various solid synthetic materials which can emit large quantities of suitable quenching gases.

The basic experimental arrangement shown in Fig. 3 has been assembled and is being used for some preliminary investigations. At the present time we are comparing silicon beads, sugar, salt, alumina, silica gel, sodium silicate, potassium chloride and sodium carbonate. It is planned to reach a conclusion with regard to the proposed future of this experiment by the end of this calendar year.

---

* This hypothesis, however, not supported by the results reported under Project No. 3 for SF_6.

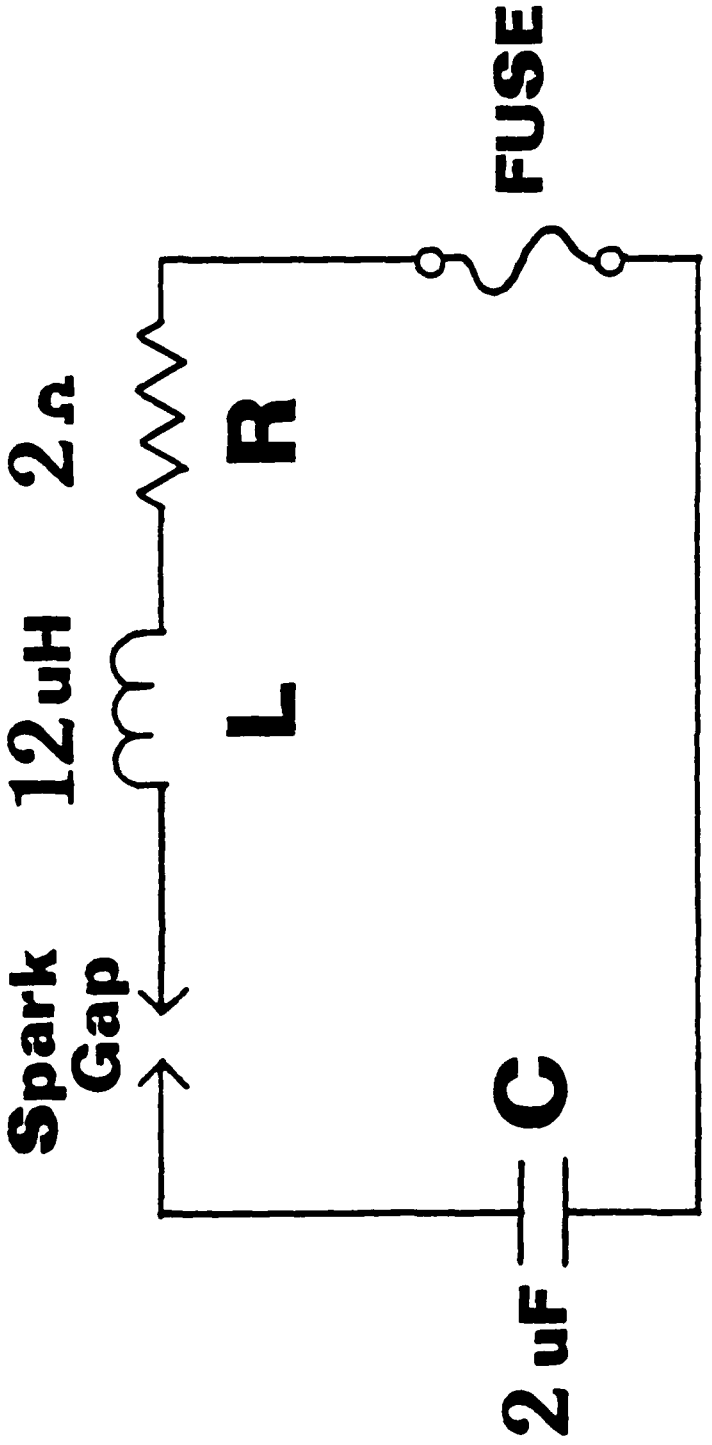

Fig. 3 Arc Quenching
Test Circuit

D. ASSESSMENT OF SWITCH GEOMETRIES

This project involves more of a strenthening of the basic technical capability of our group than an exploratory concept. In the design of high performance spark gaps it is important to be able to calculate the exact field geometry. Large field enchancements are often introduced by gas flow holes in the electrodes or by splash shields which protect the insulator surface. The solution of the field equations for irregular geometries with mixed boundary conditions (conductors and insulators) must be done numerically. We have implemented a computer code for such analysis and have used it to design electrode shapes for Project No. 10. The code was also used to design the electrodes in an earlier experiment on spark gap laser triggering through fiber optics. The availability of such a code and the ability to apply it to its fullest capability is felt to be most important to present and future work, e.g. in regard to gas and liquid flow considerations and in regard to insulator protection schemes. A rule-of-thumb in spark gap design is to avoid surface-induced effects. Gaps which are gas volume dominated usually are more reliable and repeatable. To ensure such behavior it is imperative to know the exact field geometry of the gap. The code is presently being documented so that it will be more generally useful to other researchers.

E. FIELD EFFECT ELECTROLYTE SWITCH

Electrolytes [5] are electrical conductors in which the charge carriers are positively or negatively charged ions rather than, as in metals and semiconductors, electrons. Acids, bases and salt solutions can all be electrolytes. The application of electrolytes in pulsed power, so far, has been mainly in water resistors, which use a solution of, for instance, copper sulphate in water. The mobilities of the positive and negative ions in an electrolyte can be quite different. In very dilute nitric acids, for example, the positive (Hydrogen) ion has a relatively high mobility [5] of 36.2×10^{-4} $cm^2/Vsec$ although the negative (nitrate) ion has a mobility [5] of only 7.4×10^{-4} $cm^2/Vsec$. The situation is reversed in sodium hydroxide where the positive (sodium) ion has a mobility [5] of only 5.19×10^{-4} $cm^2/Vsec$ and the negative (hydroxyl) ion has a relatively higher mobility [5] of 20.5×10^{-4} $cm^2/Vsec$. The differences in mobility in these examples suggests that some electrolytes may act somewhat like p or n type semiconductors. In particular, it may be possible to develop electrolytic devices that operate much like solid-state field effect transistors [6]. Potential advantages of electrolytic devices for pulsed power applications include 1) opening switch operation, 2) construction of large (high power) devices from inexpensive non-crystalline materials, 3) repair of electrical damage by flow replacement of the electrolyte, and 4) cooling of the device by circulating flow of the electrolyte. We have initiated the study of such a switch. Initial results are somewhat disappointing and indicate that the switch may be too slow for most applications of interest to the pulsed power community. We are planning a small experiment to check this out.

F. MAGNETIC SWITCHING

Lately there has been much renewed interest [7-9] in the area of magnetic switching (saturable reactors). With the development of Metglass*, with its high permeability and low conductivity, it appears that the state-of-the-art in magnetic switching can be advanced significantly. We are in the process of doing some simple experiments, primarily aimed at gaining some experience in this field and assessing its future vis-à-vis spark gap switches. It is also planned to study the possible use of magnetic switching and pulse compression in connection with the electromechanical pulse amplifier described in Project No. 7.

G. REFERENCES

[1] V.A. Burtsev, et.al., Sov. Phys.-Tech. Phys. 22 (8), 950 (1977).

[2] V.A. Burtsev, et.al., Sov. Phys.-Tech. Phys. 22 (8), 957 (1977).

[3] J. Salge, Tech. Univ. Braunschweig, Personal Communication.

[4] M. Dufour, Rev. Sci. Inst. 47, 1552 (1956).

[5] Samuel Glasstone, Physical Chemistry, (D. Van Nostrand, New York, 1946), pp. 884-921.

[6] Ben G. Streetman, Solid State Electronic Devices, (Prentice Hall, Englewood Cliffes, N.J., 1972) pp. 285-301.

[7] J.P. Vandevender, et.al., paper 13.1, 3rd IEEE International Pulsed Power Conf., Alb., N.M., June 1-3, 1981.

[8] D.L. Birx, et.al., paper 13.2, 3rd IEEE International Pulsed Power Conf., Alb., N.M., June 1-3, 1981.

[9] W.C. Nunnally, paper 10.2, 3rd IEEE International Pulsed Power Conf., Alb., N.M., June 1-3, 1981.

---

* A product of Allied Chemical

Project No. 7

Electromechanical Pulse Amplifier

(B.H. Dunlap and J.P. Craig)

A. SUMMARY

A theory for the operation of a novel electromechanical pulse amplifier has been developed. Design criteria have been worked out and preliminary, proof-or-principle, designs worked out with the help of a computer analysis. The input pulse forming network and the electronic control system have been designed, constructed, and tested. The electromechanical pulse amplifier has been constructed and is near testing.

B. INTRODUCTION

The electromechanical pulse amplifier is a lumped parameter transmission line which will delay, compress, and amplify an input pulse. Its advantages are that it uses compact inertial energy storage, it does not require switching, it has a potentially long life time, the rise times of the output pulses are an order of magnitude faster than for other electromechanical energy converters and the control of its output repetition rate is relatively easy.

From a practical point of view, the most promising version of the device is a design using static capacitors, and time varying inductors. Previous work has established the design criteria to prescribe the proper values of capacitance and inductance for each section of the artificial transmission line for a particular set of pulse parameters.

These criteria include the result that the inductances must vary in the manner $L_o(1-At)^2$ where L_o and A are constants that depend upon the delay, compression, and amplification for which the amplifier is designed, and $t_1<t<t_2$ is the time interval that the pulse travels through the particular inductor. Of course, t_1 and t_2 are different for each inductor in the amplifier. The inductances may vary in an arbitrary manner outside those specific time intervals. This makes it possible to design the variable inductors in the form of a rotating device with the inductors varying periodically between maximum and minimum values.

C. PROGRESS

A proof-of-concept model of the amplifier has been designed. It is designed for a 150 μs, 7.5 kW output pulse, with a rise time of approximately 10 μs. It is designed for a power gain of 9 and a maximum pulse rate of 83.3 pulses per second. The pulse rate can be reduced by 1/n, where n is any positive integer, by omitting input pulses.

The time consuming and most difficult part of the construction of the model is, of course, the construction of the variable inductors. The concept used in the design of the variable inductors was that of a variable reluctance. Standard "C" cores of Silectron material of 1 mil thick laminations were incorporated in the design with 1/2 of each core on the rotor and the other half on the stator of a rotating machine. A 30 mil air gap was used with aluminum shielding to decrease the pulsed leakage flux. The shapes and tolerances involved are close to the limit of our machine shop capabilities, but the parts have been machined and the assembly is near completion.

To test and evaluate the model, a pulse forming network has been designed, constructed and tested. This PFN will deliver the input pulses to the electromechanical pulse amplifier. An electronic control system with an electro-optical syncronizing transducer has also been designed, constructed and tested. Testing, evaluation and any necessary modification of the main device should take place in the near future.

One of the most promising applications for this device is expected to be as a pulse charger for faster type pulsers. Since magnetically switched pulse compressors are expected to have satisfactory switch life-times for repetitive pulse applications, the next year's work on this project will include a study of using the electromechanical pulse amplifier in conjunction with magnetically switched systems as mentioned in Project No. 6, Section F.

Projects No. 8 and 9

8. Multiple Ionization Cross Section Measurements*

9. Microscopic Processes in Spark Discharge Initiation*

(L.C. Lee, W.K. Bischel, and D.C. Lorents
SRI, International)

(F. Williams, K.H. Schoenbach, G. Schaefer, and M. Kristiansen
Texas Tech University)

INTRODUCTION AND COMMENTS TO THE SRI REPORT

In response to the request of F. Williams and M. Gundersen of Texas Tech University in June 1980, the group at SRI, International first undertook a study of multi-photon ionization in several gases. Initially we were interested in accurate measurements of the absolute ionization efficiency for comparison with our multiphoton ionization results obtained with a proportional counter. Since the multiphoton process is a non-linear one, accurate knowledge of the spatial dependence of the laser intensity is essential for precise absolute measurements. For this reason, the SRI group studied the process using an unfocused laser with uniform intensity. They also used a charge detection scheme which did not involve charge gain (as in a proportional counter) to minimize uncertainties due to gain calibration. These constraints, however, seriously limited the sensivity of their measurements, and they, therefore, initially studied two-photon ionization processes in several organic molecules using an excimer laser excitation source. These experiments are presented in Apendix A of the SRI report.

---

* Subcontractor Report (SRI, International) with Introduction and Comments from Texas Tech University staff.

The results of the SRI work have been helpful to pulsed power research in several ways. Multi-photon ionization undoubtedly plays a role in some aspects of electrical breakdown of gases, and a considerable body of evidence suggests that it may play a dominant role in low-jitter, laser-triggered breakdown, and in fast streamer propagation in over-volted breakdown. The SRI work has corroborated our work on multiphoton ionization in Xe by showing that substantial ionization can be produced with the process. The initial work probably preceeded the work of Woodworth, Frost, and Green at Sandia [1] on using multiphoton ionization as a trigger for voltage spark gaps. Also, the discovery and interpretation of the recombination-induced saturation of the ionization efficiency, as illustrated in Figs. 3 and 4 of Appendix A, is important in that it describes a limiting mechanism on the maximum charge density that can be produced with the process.

During the visit of L. Lee from SRI to Texas Tech in November 1980, a first concept for a gas mixture for an optically controlled opening switch was worked out. Based on previous investigations on gas mixtures for an excimer laser at SRI, a system was proposed containing N_2 and an admixture of NO to produce a high density of excited NO molecules via near-resonant energy transfer collisions with metastable N_2 molecules. These excited NO molecules were supposed to be ionized by a one step photoionization process with near UV laser light (dye laser with frequency doubling).

During the visit of K.H. Schoenbach and G. Schaefer at SRI in February 1981, in discussions with L. Lee and D. Lorents this concept was modified to use a two step photoionization from the excited NO state via an additional intermediate state using visible laser light. In

addition, information about basic data on NO and N_2 have been provided by SRI. Also, at this meeting, further experimental studies were discussed to provide missing data. Since NO is a weak attacher with a maximum cross section at high electron energies we suggested that NO might show an increasing attachment rate at the E/N values occuring in a diffuse self-sustained discharge. Therefore, an experiment was proposed to measure the electron decay rate in N_2 with admixtures of NO depending on the E/N value. Because of experimental limitations, only measurement with E/N values below the values for a self sustained discharge were performed. In this E/N region a decrease of the decay rate, k, with increasing E/N was observed although the measurement already seems to indicate a minimum at E/N $\approx 18 \times 10^{-17}$ V-cm^2 (see Fig. 6, Appendix B of SRI report). In order to get general information about the decay behavior in the E/N range necessary for our experiment we instead proposed to use N_2O as a model additive with an attachment cross section at much lower energies (NO: $\sigma_{max} = \sigma$ (8.0 eV); N_2O; $\sigma_{max} = \sigma$ (2.1 eV)). The measurements with N_2O were then performed and show the suggested properties (see Fig. 7, Appendix B of the SRI report). These measurements are very helpful for our ongoing project. They allow us to compare experimental and calculated attachment rates and to predict the attachment behavior of other molecules. The measurements of the electron decay rate in N_2 with admixtures of NO or N_2O are presented in Appendix B of the SRI report.

REFERENCES

[1] M. Tinkham, Group Theory and Quantum Mechanics, Chap. 5, (McGraw-Hill, New York, 1966).

November 24, 1981

Technical Report No. MP 81-201
Covering the Period 1 September 1980
to 31 October 1981

MULTIPHOTON IONIZATION CROSS SECTION MEASUREMENTS AND MICROSCOPIC PROCESSES IN SPARK DISCHARGE INITIATION

By: L. C. Lee, W. K. Bischel, and D. C. Lorents

Prepared for:

AIR FORCE OFFICE OF SCIENTIFIC RESEARCH
Bolling AFB
Washington, D. C. 20332

Submitted through:

Coordinated Research Program in Pulsed Power Physics
Department of Electrical Engineering
Texas Tech University
Lubbock, Texas 79409

AFOSR Contract No. F49620-79-C-0191
SRI Project No. PYD-1341

INTRODUCTION

This report describes the result obtained in the period from September 30, 1980 to October 30, 1981. In this project, SRI was designated to provide fundamental atomic and molecular data and to carry out experimental measurements for the Pulse Power Research Progam.

To the best of our ability, we have provided the cross sections and reaction rate constants related to N_2 and NO to Texas Tech University for the development of opening switches. In the meantime, we have measured the two-photon-ionization coefficients of organic molecules using excimer laser photons and also measured the decay rate constants of electron conduction current using a high energy e-beam to excite N_2 and the gas mixtures of Cl_2, NO, and N_2O in N_2.

RESEARCH ACCOMPLISHED

A. Multiphoton Ionization Cross Section Measurements

The two-photon-ionization coefficients of propane, 1-Butene, monomethylamine, dimethylamine, and trimethylamine were measured at the excimer laser wavelengths of 193 nm (ArF) and 248 nm (KrF). The results are summarized in a paper attached as Appendix A. This paper will appear in the Journal of Applied Physics in the January, 1982, issue.

In this investigation, we find that at low charge density, the ion current is proportional to the product of gas pressure and the square of laser intensity. At high gas pressure and high laser intensity, the ion current saturates. The saturation effect is well interpreted by a model including electron attachment and charge recombination processes. The two-photon-ionization coefficients were determined from the low ion current data. Among the molecules studied, the trimethylamine has the highest coefficient of 3.6×10^{-26} cm^4/W at the KrF laser wavelength of 248 nm. Such a high photo-ionization coefficient indicates that trimethylamine could be used to produce a high density of initial electrons for laser controlled switches. The present results could also be used to develop new techniques for investigating electron attachment and charge recombination processes at high gas pressures.

B. Microscopic Processes in Spark Discharge Initiation

This research task is to measure cross sections and rate constants for the molecular processes occurring in switch discharges as initiated late this year at the request of Texas Tech University. We began measurements on the decay rates of the electron conduction current in an atmosphere of N_2 mixed with Cl_2, NO, and N_2O using a high energy e-beam to initiate the ionization. The time dependent current was measured as a function of E/N and N. These results are summarized in a paper attached as Appendix B. Because of the time constraints the results are very preliminary and not fully understood.

The N_2^+ ions produced by e-beam excitation are quickly converted to N_4^+, which are then recombined with electrons to form N_2^*. These N_2^* species may be ionized by the discharge electrons to sustain the electron conduction current. The decay rate constants of the electron conduction current with the addition of Cl_2, NO, and N_2O to N_2 were measured at various E/N. The decay rate constants decrease with E/N for Cl_2 and NO, but increase for N_2O. The decay rate is a result of either electron attachment or quenching of N_2^* by the additive gases. This preliminary model is important for understanding the gaseous electronic kinetics involved in the N_2 discharge phenomena. However, it is subject to confirmation by more experimental data.

The results that the decay rate constants of electron conduction current by N_2O increase with E/N suggest that N_2O is a useful molecule for shortening the opening time of discharge switches.

PRESENTATIONS AND PUBLICATIONS DURING THIS FUNDING PERIOD

1. "Two-Photon-Ionization Coefficients of Propane, 1-Butene, Methylamines," L. C. Lee and W. K. Bischel, presented at the XII International Conference on the Physics of Electronic and Atomic Collisions, Gatlinburg, Tennessee, July 15-21, 1981; also paper accepted for publication in the Journal of Applied Physics, January, 1982.

2. "Electron Attachment and Charge Recombination Following Two-Photon-Ionization of Methylamines," L. C. Lee and W. K. Bischel, presented at the 34th Gaseous Electronics Conference, Boston, Massachusetts, October 20-23, 1981.

TWO-PHOTON-IONIZATION COEFFICIENTS OF PROPANE, 1-BUTENE, AND METHYLAMINES

by

Long C. Lee and William K. Bischel

Molecular Physics Laboratory
SRI International
Menlo Park, California 94025

ABSTRACT

Ion currents produced by two-photon ionization were investigated for several organic molecules. At low charge density, the ion current is proportional to the product of gas pressure and the square of laser intensity. At high gas pressure and high laser intensity, the ion current saturates. The saturation effect is well interpreted by a model including electron attachment and charge recombination processes. The two-photon-ionization coefficients were determined from the low ion current data. Among the molecules studied, trimethylamine has the highest coefficient of 3.6×10^{-26} cm^4/W at the KrF laser wavelength of 248 nm. Such a high photoionization coefficient indicates that trimethylamine could be used to produce a high density of initial electrons for laser-controlled switches. The present results could also be used to develop new techniques for investigating the electron attachment and charge recombination processes at high gas pressures.

MP 81-59
07/20/81

I. INTRODUCTION

Research in the multiphoton ionization of atoms and molecules has generated much interest during the past few years. The first applications were to the spectroscopy of atoms[1,2] and molecules[3] using pulsed dye lasers as the uv photon source. Recently, the development of excimer lasers has provided a new photon source for multiphoton ionization experiments, and the resonant enhancement of two-photon ionization cross section can now be investigated for many molecules. In addition, research using these uv lasers has been stimulated by the realization that resonantly enhanced two-photon ionization of molecules holds promise for both the sensitive detection of molecules[5] and the creation of a spatially uniform ionization volume, which could be potentially useful in the development of high power discharge switches.[6] Recent experiments using excimer lasers have investigated the fragmentation[7-9] of molecules following multiphoton ionization, as well as relative two-photon ionization cross sections.[9,10] However, there has been little work on characterizing the absolute multiphoton ionization cross sections at any wavelength or laser intensity.

A knowledge of the absolute multiphoton ionization cross section as a function of laser intensity and wavelength is essential for any application in which it is necessary to have an accurate model of the ion density. The work presented here is one of the first attempts to address this problem by measuring the absolute two-photon ionization cross section for several organic molecules. The goals of our experiments were two-fold: (1) to determine the dependence of the absolute two-photon ionization cross section as a function of laser intensity for two different uv wavelengths (193 nm and 248 nm) and (2) to survey the absolute cross sections for a class of molecules that might have large cross sections due to resonant enhancement from a nearby excited

state. For this purpose, the methylamines were chosen to be investigated first since a recent experiment[11] indicated that trimethylamine had a large resonantly enhanced two-photon ionization cross section. In addition, two smaller organic molecules, C_3H_8 and C_4H_8, were chosen to provide a comparison of the results for the methylamines to two-photon ionization cross sections for molecules that had no resonant enhancements. The results of these studies are described below.

II. EXPERIMENTAL

The experimental apparatus is illustrated in Fig. 1. A Lambda Physik EMG 101 excimer laser operating at 193 nm (ArF) or 248 nm (KrF) was used to photoionize the molecules under study in a collimated beam geometry. The excimer laser beam size was approximately 9×26 mm^2 for KrF and 7×26 mm^2 for ArF operation, and the intensity was relatively uniform over that dimension. A 3.2-mm-diam aperature limited the laser beam cross section in the experimental volume. Because only a small part of the incident laser was sampled, the laser intensity was assumed to be spatially uniform for the experiment. The laser energy per pulse through the aperature was measured after the exit window of the cell using a Laser Precision pyroelectric energy meter, which had been recently factory calibrated relative to NBS standards. The laser intensity was varied by inserting up to 12 quartz plates in the beam in front of the defining aperature. In this manner, the laser energy/pulse transmitted by the aperature could be varied from 0.05 to 5 mJ for KrF and 0.05 to 2 mJ for ArF.

The experimental cell was constructed from 8-in.-diam stainless steel pipe and connected to a high vacuum system that pumped out the cell to less

than 10^{-6} torr. The pressure in the cell was measured using an MKS Baratron capacitive manometer (1 torr), which had a last digit resolution of 10^{-4} torr. The gas under study was allowed to slowly flow through the cell to ensure that systematic errors due to outgassing and photodissociation of the parent molecule were minimized. Typical pressures used in the experiment varied from 1.0 to 500 mtorr.

The ionization detector was constructed from two parallel plates 3.5×7.5 cm^2 separated by 2 cm. The bottom plate had a 2.54×2.54 cm^2 hole in the central region covered by a fine screen (98% transmitting) and the ion collector was mounted 0.75 cm below the screen. The top plate was typically biased at +80 V, the middle plate at +22 V, and the ion collector was grounded through a Keithley 602 electrometer. The output of the electrometer was displayed on a strip chart recorder. Typical ion currents varied from 10^{-13} to 10^{-7} A.

When the experiment was first started, two sources of background current had to be reduced to allow the recording of ion currents in the range of 10^{-13} to 10^{-10} amps. The first background signal arose from residual gas in the cell even after the cell had been baked and pumped out to less than 10^{-6} torr. This background current was about 10^{-11} A for 1 mJ laser energy through the aperature. (This background is similar to one observed by Rockwood et al., Ref. 7). This problem was solved by mounting a cold finger in the cell and using a mixture of dry ice/acetone (-78°C) to cryopump the cell during an experiment when high sensitivity was needed.

The second source of background was electrons produced by scattered uv laser photons hitting the ion collection plate. It was determined that most of the scattering was caused by reflections from the exit window. This window was replaced with a window mounted at Brewster's angle, with the reflected

light being reflected into a Woods horn. Combining these steps with the use of a cold finger in the cell reduced the total background to below 10^{-13} A.

Typical experimental parameters measured during the experiment were the ion current as a function pressure, laser intensity, and plate voltage. These results are described in the next section.

III. RESULTS

The collection efficiency of the ion collector for positive ions produced by two-photon ionization was investigated by varying the bias plate voltages. The upper plate was biased at a positive voltage equal to or higher than the middle plate (biased at +22 V). The ion collector was run at ground potential. The reason for a positive bias on the middle plate was to prevent positive ions from terminating at the metal mesh. The ion current collected by the plate underneath the mesh is shown in Fig. 2, where a 5.2 mtorr of 1-Butene was photoionized by an ArF laser of 0.88 mJ/pulse. The ion current quickly reaches a plateau when the voltage of the upper plate is higher than the middle plate. The plateau ensures that the photoions are totally collected. As shown in Fig. 2, the ion current slightly increases with the applied voltage. However, for the present measurements the voltage is set at +80 V to avoid the interference of secondary ions produced by energetic electrons that are accelerated by the electric field.

The photoion currents versus the laser intensities were investigated for all the gases reported here. As an example, the results for trimethylamine of pressures at 3.0, 9.4, and 59.5 mtorr are shown in Fig. 3. The ion current was the total current produced by 10-Hz laser pulses. The laser area is 0.079 cm^2 and the collection plate is 2.54 cm long. When the ion current is

lower than 10^{-9} A, it increases with the square of laser instesity I^2. The laser intensity is obtained from the laser energy/pulse divided by the laser cross section area and laser pulse duration. However, at higher ion currents, the signal is no longer proportional to I^2, but instead to I^n where $n < 2$. Note that as the gas pressure is increased, the rate of ion current with increasing laser intensity decreases from the square law observed at low pressure. For the gas pressure of 59.5 mtorr, the ion current obviously approaches a constant at high laser intensity.

The dependence of ion current on pressure was also investigated for every gas studied. As an example, the results for trimethylamine measured at laser energies/pulse of 0.16, 0.32, 0.63, 1.6, and 3.03 mJ are shown in Fig. 4. The pressure dependence has a general character that it increases linearly at low pressure, reaches a maximum, then decreases at high pressure. The pressures for the maximum ion current decrease with increasing laser intensity.

At low laser energy and low gas pressure, the photoionization can be well described by a two-photon-ionization process. The number of electrons produced by each laser pulse is given by

$$N_e(0) = \alpha \int I^2(t)dt \cdot nA\ell/h\nu \qquad (1)$$

where α is the coefficient for two-photo-ionization (cm^4/W), I is the laser intensity (W/cm^2), n is the gas concentration (cm^{-3}), A is the laser beam cross section (cm^2), ℓ is the length of collection plate (cm), and $h\nu$ is the photon energy (joule). $I^2(t)$ is integrated over laser duration (s) and can be approximated by $\int I^2(t)dt = \Sigma I_i^2 \Delta t$ where I_i is the laser intensity at every $\Delta t = 2.5 \times 10^{-9}$ s. The pulse duration is 13×10^{-9} s for the KrF laser and 11×10^{-9} s for the ArF laser.

The two-photon-ionization coefficients for propane (C_3H_8), 1-butene (C_4H_8), monomethylamine (CH_3NH_2), dimethylamine [$(CH_3)_2NH$], and trimethylamine [$(CH_3)_3N$] are measured and given in Table I. The α values measured at different laser intensities and gas pressures vary within 20% of the given values. The systematic errors, which include the ion collection efficiency, the uniformity of laser intensity, and the detector response, may make the experimental uncertainties as high as 50%. Nevertheless, since only a small central portion of laser beam was used in the measurements, the laser beam may be reasonably uniform, as is verified by the reproducibility of the α values at various laser intensities.

Photoabsorption cross sections were measured for several molecules and were also given in Table I. They were determined by the attenuation of laser intensity, i.e.,

$$\sigma = \ell n(I_o/I)/n\ell \qquad (2)$$

The uncertainties for the absorption cross sections are estimated to be 15% of the given values. The σ values given by Tannenbaum et al.[13] are also listed in Table I for comparison. The present values measured at high laser intensities are systematically smaller than the previous values measured by weak uv light sources, but they are consistent within experimental uncertainties. The small differences indicate that the absorption cross sections do not significantly depend on light intensity.

The α and σ values for trimethylamine at the KrF laser wavelength are quite high. These high values may be the result of resonance absorption. An anti-Stokes Raman-shifted double-dye laser (bandwidth 0.3 cm^{-1}) was used to measure the absorption cross sections in the 246 to 250 nm region to look for resonance structure. However, no discrete structures were found in this wavelength region.

IV. DISCUSSION

The slow increase rate of ion current at high laser energy/pulse as shown in Fig. 3 and the decrease of ion current at high gas pressures shown in Fig. 4 can be caused by the recombination of positive ions with electrons and negative ions. The negative ions are formed by electron attachment to molecules. This hypothesis is supported by the observation that the negative charged current obtained with negative potentials applied on the upper plate shows a fast pulse with a long slow decay component as indicated in Fig. 5. The fast pulse results from electrons, because electrons have a high mobility. The slow component presumably results from the negative ions. The electron current shown in Fig. 5 was taken at a pressure of 7 mtorr. The ratio of the slow to the fast component increases with gas pressure, which indicates that the negative ions are produced from electron attachment.

With the assumption that the charges initially produced by the laser can be neutralized by recombination, the number of positive ions, N_+, electrons, N_e, and negative ions, N_-, which reach the electrodes for each laser pulse can be written as

$$N_+ = N_+(0) - \int\int \sigma_{+-} n_+(x,y,z) n_-(x,y,z) dzdv - \int\int \sigma_{+e} n_+(x,y,z) n_e(x,y,z) dzdv \qquad (3)$$

$$N_e = N_e(0) - \int\int \sigma_{+e} n_+(x,y,z) n_e(x,y,z) dzdv - \int\int \sigma_{oe} n n_e(x,y,z) dzdv \qquad (4)$$

$$N_- = N_+ - N_e \qquad (5)$$

where $N_+(0) = N_e(0)$ are the initial number of positive ions and electrons produced by laser ionization [see equation (1)]; σ_{+-} and σ_{+e} are the

recombination cross sections of positive ion with negative ion and electron, respectively; σ_{oe} is the electron attachment cross section; and n_+, n_-, and n_e are the densities of positive ions, negative ions, and electrons, respectively. The x-coordinate is chosen along the laser beam; z is along the applied electric field. The main contribution to the integrals results from the overlaps within the laser volume, v, and the laser dimension in the direction of electric field, ℓ.

For a qualitative understanding of the dependence of ion current on laser flux and gas pressure, we make the approximation that the positive ions are assumed to be uniformly distributed over the laser volume. This approximation will simplify Eq. (3) to

$$N_+ = N_+(0) - \sigma_{+-} N_+ N_-/A - \sigma_{+e} N_+ N_e/A \tag{6}$$

Assuming that the negative ions are mainly determined by electron attachment and the electrons are mainly the initial photoelectrons, i. e., $N_- \approx \sigma_{oe} n \ell N_e$ and $N_e \approx N_e(0)$, we have

$$N_+ \approx \frac{\alpha \bar{I}^2 T_p nve^{-2n\sigma L}/h\nu}{1 + \left(\frac{\sigma_{+-}\sigma_{oe}\ell}{A} n + \frac{\sigma_{+e}}{A}\right) \alpha \bar{I}^2 T_p nve^{-2n\sigma L}/h\nu} \tag{7}$$

where $\bar{I}^2$ is the square of the laser intensity before entering the gas cell and is averaged over the pulse duration T_p, L is the laser path length from window to the center of the ion collection plate, and $e^{-n\sigma L}$ is the attenuation of laser intensity from window to the center of the collection plate.

Eq. (7) indicates that the ion currents will increase linearly at low pressure and will decrease at high pressure. This description agrees with the experimental data, as shown in Fig. 4. The dependence of the gas pressure at

the maximum ion current on the laser intensity can also be described by Eq. (7). Since the absorption cross section of trimethylamine is not large at the KrF laser wavelength (7.6×10^{-19} cm^2), the attenuation factor of $e^{-2n\sigma L}$ in Eq. (7) can be neglected for the gas pressure less than 100 mtorr. By setting $\partial N_+/\partial n = 0$, we have the gas pressure at maximum ion current to be

$$n_{max} = \left(\frac{\sigma_{+-}\sigma_{oe}\ell\alpha T_p V}{Ah\nu}\right)^{-1/2} / \bar{I} \qquad (8)$$

This shows that the product of n_{max} and $\bar{I}$ is nearly a constant. This relation is true, as shown in Fig. 4 in which the constant for $n_{max}\bar{I}$ is about 15 mtorr • mJ. If we approximate A = 0.08 cm^2 and ℓ = 0.3 cm as the area and dimension of the laser beam, then $\sigma_{+-}\sigma_{oe} \sim 1.5 \times 10^{-27}$ cm^4. For a typical ion recombination cross section of $\sigma_{+-} \sim 10^{-12}$ cm^2, we obtain $\sigma_{oe} \sim 1.5 \times 10^{-15}$ cm^2.

When the laser fluxes become high, we have

$$N_+ \rightarrow \left(\frac{\sigma_{+-}\sigma_{oe}\ell}{A} n + \frac{\sigma_{+e}}{A}\right)^{-1} \qquad (9)$$

This indicates that the ion currents will approach a constant at high laser fluxes. The constant will decrease with gas pressure. This description agrees well with the experimental data as shown in Fig. 3.

The good agreements between modeling description and experimental data lead us to conclude that the slow increase of ion current at high laser fluxes and the decrease of ion current at high gas pressure are caused by the processes of charge recombination. The data can be used to derive the cross sections for the electron attachment and charge recombination processes.

V. CONCLUSION

The two-photon-ionization coefficients of propane, 1-butene, monomethylamine, dimethylamine, and trimethylamine have been measured using the data of low gas pressures and low laser intensities. The ion currents are saturated at high laser intensities and high gas pressures. A model including the electron attachment and charge recombination processes has been developed to explain the dependence of ion current on laser power and gas pressure. The agreement between the predictions of this simple model and experimental data is very good, which offers promise for the success of more detailed analysis of future experiments.

The present results indicate that trimethylamine can possibly be used to produce large numbers of initial electrons for laser controllable switches. For example, for a typical KrF laser pulse of 100 mJ (10 ns duration and 2 cm^2 cross section area) and a gas pressure of 1 torr, the initial electron density can be 10^{15} electrons/cm^3. Also, this molecule can be used to produce a high density of ions in a high gas pressure environment, so the cross sections for the electron attachment and charge recombination processes can be measured in the high pressure ranges that are of interest in the development of high power and fast discharge switches.

ACKNOWLDEGMENT

The authors wish to thank Professor F. Williams at Texas Tech University and Professsor M. Gundersen at the University of Southern California for initiating this program and also for their helpful suggestions. We also thank Dr. D. L. Huestis, Dr. D. C. Lorents, and Dr. J. R. Peterson at SRI, and

Professor G. Schaefer and Professor K. Schoenbach at Texas Tech University for helpful discussions. This work is supported by AFOSR under Contract No. F49620-79-C-0191, and the research program is coordinated by the Department of Electrical Engineering, Texas Tech University.

FIGURE CAPTIONS

Fig. 1. Schematic diagram for experimental apparatus.

Fig. 2. The dependence of ion current on the voltage applied to the top plate that collects electrons. The middle plate is biased at + 22V.

Fig. 3. Ion current versus laser energy for trimethylamine excited by a KrF laser. The data were measured at 3.0, 9.4, and 59.5 mtorr. Note that the ion current are proportional to the square of laser intensities at the ion current less than 10^{-9} amp.

Fig. 4. Ion current versus gas pressure for trimethylamine excited by a KrF laser. Note that the ion currents increase linearly with low gas pressures, and the products of the pressures for maximum currents and the laser energies/pulse are approximately a constant of 15 mtorr • mJ.

Fig. 5. Time dependence of negative charge current. The sharp pulse results from electrons, and the slow decay component presumably results from negative ions.

REFERENCES

1. G. S. Hurst, M. G. Payne, S. D. Kramer, and J. P. Young, Rev. Mod. Phys. 51, 767 (1979); and references therein.

2. G. Mainfray and C. Manus, Appl. Opt. 19, 3934 (1980); and references therein.

3. Philip M. Johnson, Appl. Opt. 19, 3920 (1980); Philip M. Johnson, Acc. Chem. Res. 13, 20 (1980).

4. D. H. Parker, J. O. Berg, M. A. El-Sayed, Advances in Laser Chemistry, Springer Series in Chemical Physics (Springer, Heidelberg, New York, 1978).

5. Charles Klimcak and John Wessel, Appl. Phys. Lett. 87, 138 (1980).

6. W. R. Rapoport, J. Goldhar, and J. R. Murray, to be published.

7. S. Rockwood, J. P. Reilly, K. Hohla, and K. L. Kompa, Opt. Comm. 28, 175 (1979).

8. V. S. Antonov, V. S. Ketokhov, and H. N. Shibanov, Appl. Phys. 22, 293 (1980).

9. Mark Seaver, J. W. Hudgens, and J. J. DeCorpo, Int. J. Mass Spectros. Ion Phys., June, 1980.

10. R. V. Hodges, L. C. Lee, and J. T. Moseley, to be published in Int. J. Mass Spectroc. Ion Phys. (1981).

11. W. Zapka and F. P. Schäfer, Appl. Phys. 20, 287 (1979).

12. M. B. Robin, Highly Excited States of Polyatomic Molecules, Vol. I and II (Academic Press, New York, 1974).

13. E. Tannenbaum, E. M. Coffin, and A. J. Harrison, J. Chem. Phys. 21, 311 (1953).

TABLE 1 The two-photon-ionization coefficients, α, and the photoabsorption absorption cross sections, σ, for various molecules.

Laser Wavelengths		193 nm			248 nm		
			This Work	Previous Work[b]		This Work	Previous Work[b]
	I.P.[a]	α	σ	σ	α	σ	σ
Molecules	(eV)	(cm^4/W)	(cm^2)	(cm^2)	(cm^4/W)	(cm^2)	(cm^2)
C_3H_8	11.4	3.0×10^{-31}					
C_4H_8	9.29	6.6×10^{-30}	1.1×10^{-18}		3.3×10^{-32}	$< 1\times10^{-20}$	
CH_3NH_2	9.70	6.8×10^{-28}	1.9×10^{-18}	2.1×10^{-18}	1.7×10^{-28}	$< 2\times10^{-20}$	
$(CH_3)_2NH$	8.90	2.4×10^{-27}	8.4×10^{-18}	1.25×10^{-17}	1.5×10^{-28}	2.4×10^{-20}	
$(CH_3)_3N$	8.50	1.5×10^{-27}	1.04×10^{-17}	1.34×10^{-17}	3.6×10^{-26}	6.3×10^{-19}	7.6×10^{-19}

[a] Ref. 12
[b] Ref. 13

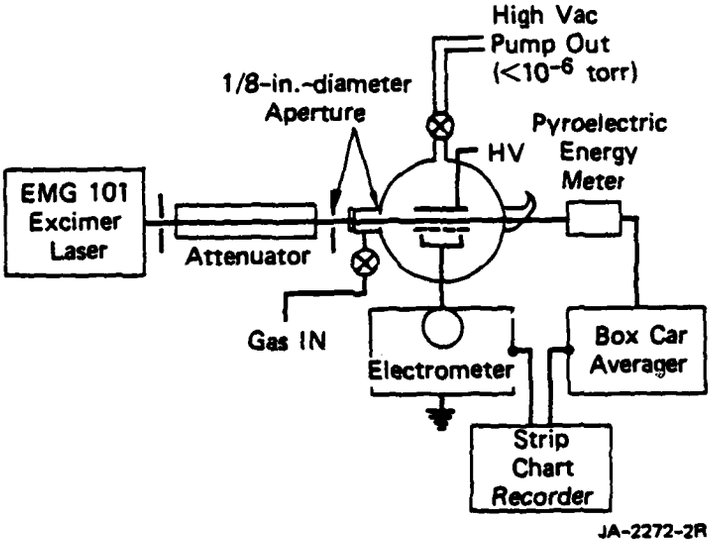
High Vac
Pump Out
(<10⁻⁶ torr)
1/8-in.-diameter
Aperture
Pyroelectric
Energy
Meter
HV
EMG 101
Excimer
Laser
Attenuator
Gas IN
Box Car
Averager
Electrometer
Strip
Chart
Recorder
JA-2272-2R

Fig. 1

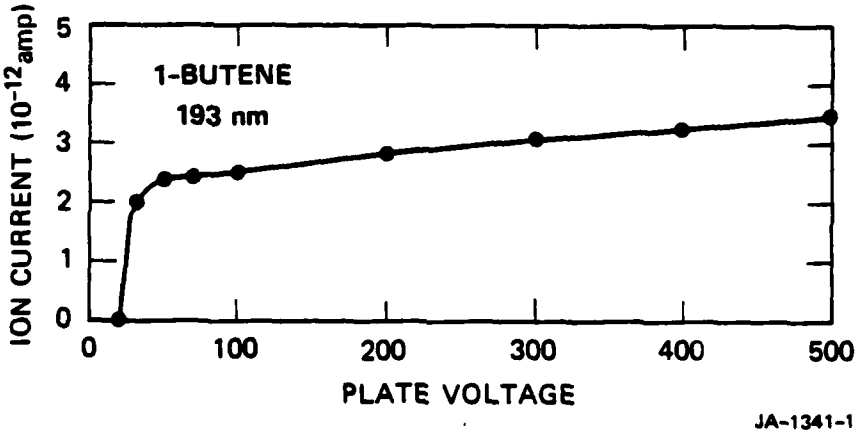
ION CURRENT (10^{-12}amp)
5
4
3
2
1
0
1-BUTENE
193 nm
0
100
200
300
400
500
PLATE VOLTAGE
JA-1341-1

Fig. 2

DEPENDENCE OF ION CURRENT ON LASER FLUX

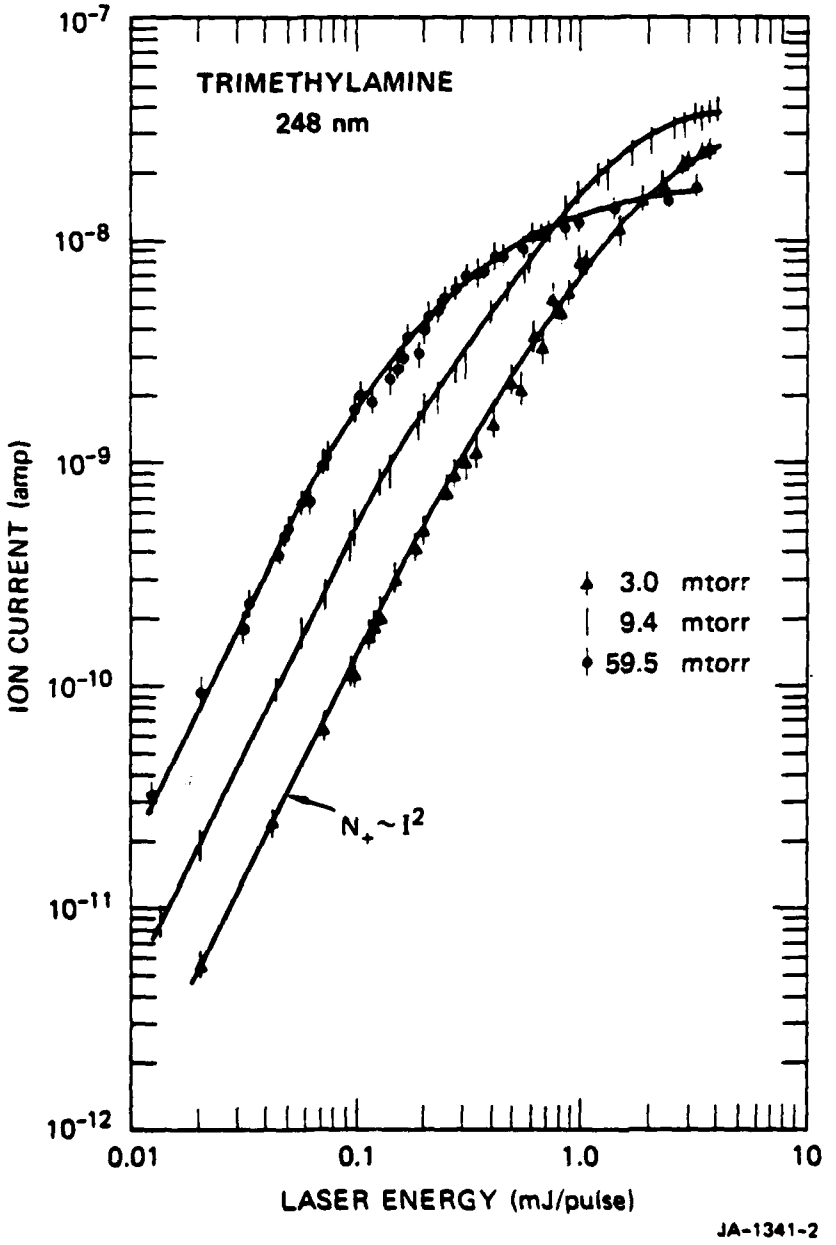

At low ion current

$$N_+ = \alpha \int I(t)^2 dt \; n \; v/h\nu$$

$$= \alpha \; I^2 \; \Sigma\beta_i^2 \; \Delta t \; n \; v/h\nu$$

Fig. 3

DEPENDENCE OF ION CURRENT ON GAS PRESSURE

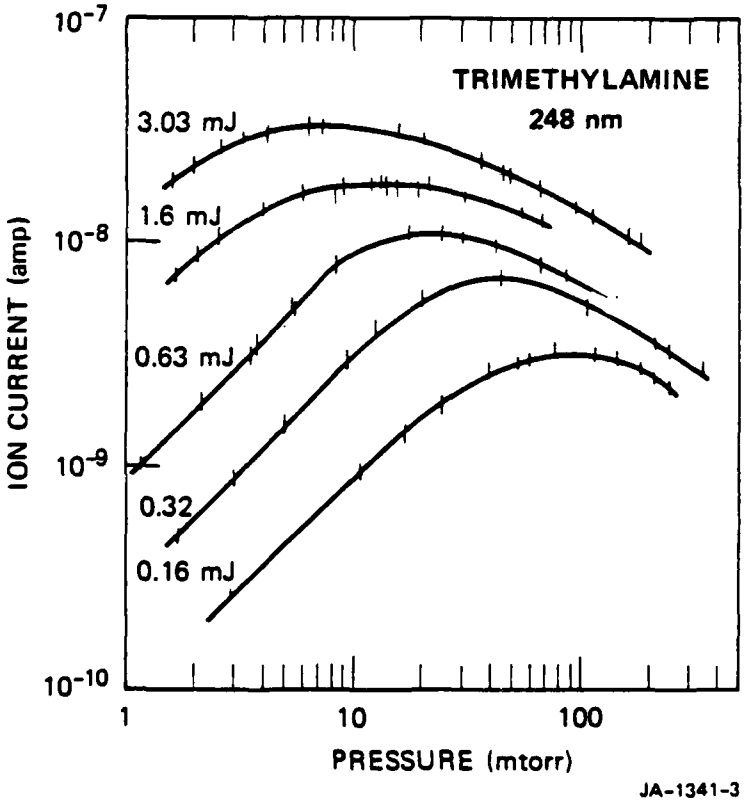

At low gas pressure

$$N_+ = [\alpha \int I(t)^2 dt \; v/h\nu]^n$$

Fig. 4

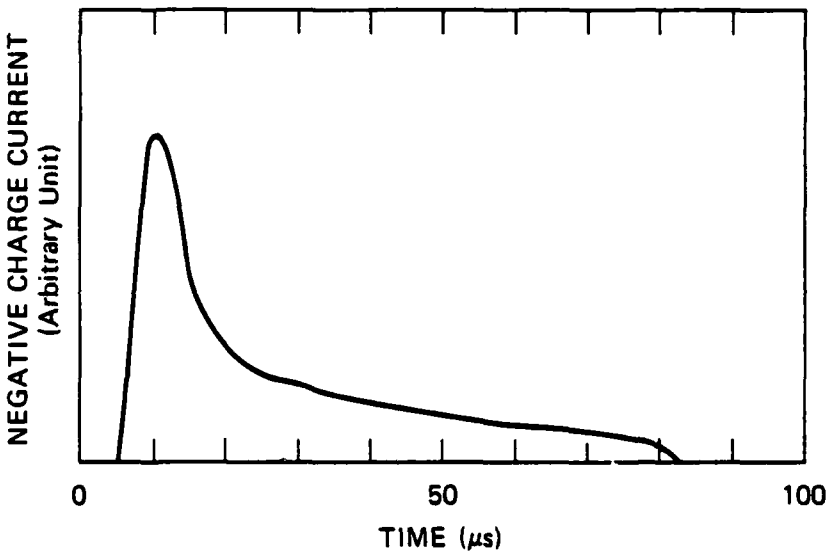
NEGATIVE CHARGE CURRENT
(Arbitrary Unit)
0
50
100
TIME (μs)
JA-1341-6

Fig. 5

GASEOUS ELECTRONIC KINETICS FOR e-BEAM EXCITATION OF Cl_2, NO, AND N_2O in N_2

L. C. Lee, C. C. Chiang, K. Y. Tang,
D. L. Huestis, and D. C. Lorents

Molecular Physics Laboratory
SRI International
Menlo Park, California 94025

ABSTRACT

The electron conduction current produced by a 600 keV electron excitation of N_2 and gas mixtures is investigated. The results are interpreted by a tentative gaseous electronic model. The N_2^+ ions produced by e-beam excitation are quickly converted to N_4^+, which are then recombined by electron to form N_2^*. These N_2^* species amplify electrons to form the electron conduction current. The decay rate constants of the electron conduction current by adding Cl_2, NO, and N_2O to N_2 are measured at various E/N. The decay rate constants decrease with E/N for Cl_2 and NO, but increase for N_2O. The decay rate is a result of either electron attachment or quenching of N_2^* by adding gases.

MP 81-194
11/24/81

AD-A110 409 TEXAS TECH UNIV LUBBOCK DEPT OF ELECTRICAL ENGINEERING F/G 20/3
COORDINATED RESEARCH PROGRAM IN PULSED POWER PHYSICS.(U)
DEC 81 M KRISTIANSEN, M O HAGLER F49620-79-C-0191
UNCLASSIFIED AFOSR-TR-82-0018 NL

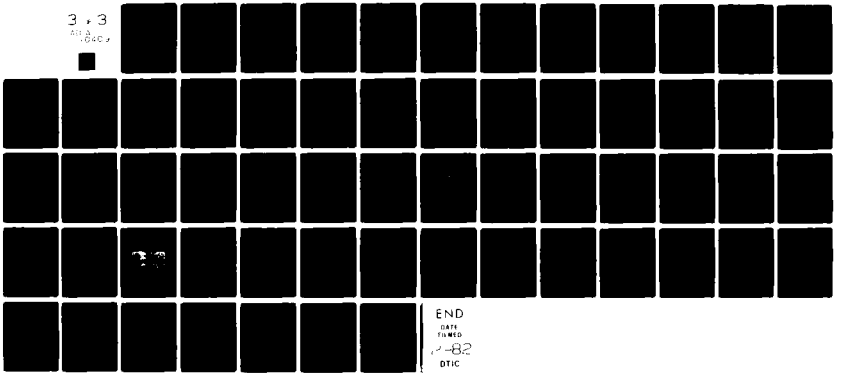

END
DATE FILMED
2-82
DTIC

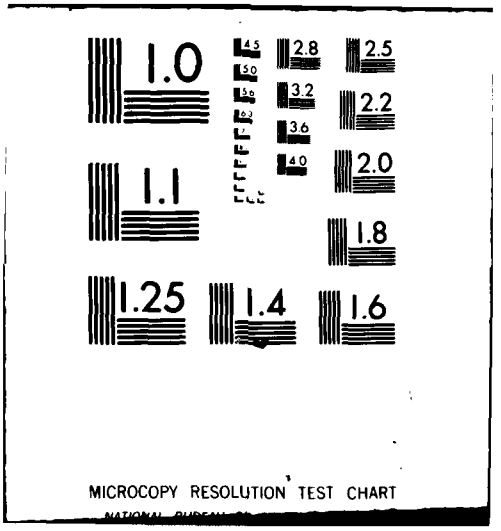
1.0
1.1
1.25
1.4
1.6
1.8
2.0
2.2
2.5
2.8
3.2
3.6
4.0
4.5
5.0
5.6
6.3
MICROCOPY RESOLUTION TEST CHART

I. INTRODUCTION

Recent developments in high technology areas, such as lasers, fusion, and particle beam experiments, require electrical switching capabilities beyond those currently available. For the advancement of this field, it is necessary to improve our understanding of the physics of externally controlled high current discharge and the associated recovery phenomena.

N_2 is often used in high pressure discharge switches as a buffer gas; its excitation and charge recombination processes are fundamentally interesting for characterization of discharge switching. In this paper, we report an experiment that used a high energy e-beam to irradiate an atmosphere of N_2 at various E/N and measured the electron conduction current produced by the excitation. The experiment results give some clues for understanding the electron decay mechanism following an e-beam excitation of N_2.

The enhancement of the decay rates of conduction current by adding small amounts of electron attaching gases (such as Cl_2, NO, and N_2O) to the N_2 buffer gas is also investigated in this experiment. The decay rates of the electron conduction current can be increased by the processes: (1) electron attachment by the added gases and (2) the excited species that generate electron conduction current quenched by the added gases. Our observations of the enhanced decay rates of conduction current at various E/N are tentatively described by a model involving the ion kinetics.

II. EXPERIMENTAL

The experimental setup is shown in Figure 1. A Febetron e-beam machine (Model 706) gives a 600 keV electrons of 6×10^3 A in a cross section area of 2 cm^2 in 3 ns (or 5.6×10^{13} electrons/cm^2) for each pulse. The gas cell is made of a plastic tubing (4" dia × $4\frac{1}{2}$" length) with a stainless steel plate on the front end and a plastic plate on the back end. A power supply (± 10 kV) was used to apply an electric field to the gas in the cell. The electron conduction current was detected by a grid of $\frac{3"}{4}$ diameter, which was guarded by a separated and grounded ring. The electron conduction current, which was converted to voltage by a 50 Ω resistor, was measured by a transient digitizer and a fast oscilloscope.

The gases of research grade supplied by Matheson were admitted into the gas cell without further purification. The gas in the cell was slowly pumped, and the pressure in the cell was kept constant by feeding in fresh gas. This flow system minimizes the build up of impurities produced from outgasing and from chemical reactions induced by e-beam excitation. The experiment was performed at room temperature.

III. RESULTS AND DISCUSSION

A. N_2

When an atmosphere of N_2 under an E/N of 18 Td (1 Td = 10^{-17} Vcm^2) in the gas cell is irradiated by the 600 keV e-beam, it generates electron conduction current as shown in Figure 2. The first sharp large pulse is a result of the e-beam electrons stopped on grid and the secondary electrons produced by e-beam ionization of N_2. A second pulse appears 25-50 ns after the first pulse decays.

The time duration of the second pulse depends on E/N. At low E/N, the second pulse quickly arises from a low current and then maintains at a constant amplitude for some time as shown in Figure 3, where 350 torr of N_2 is under an electric field of E/N = 5.6 Td. The pulse has a sharp drop after the constant amplitude and then decays with a long tail. The inverse of the long tail amplitude increases linearly with time suggesting that the decay is dominated by electron-ion recombination.

The higher the E/N, the shorter the time duration, τ, which is measured between the halves of maximum amplitude as shown in Figure 3. The data of τ^{-1} measured at 350 and 700 torr of N_2 are plotted in Figure 4 for various E/N. The distances between the end plate and grid were set at 6 and 2.25 cm for the N_2 pressures of 350 and 700 torr, respectively, in order to make E/N in the same range for both gas pressures. The data show that τ^{-1} depends solely on E/N.

The origin of the second pulse is not yet fully understood. It is possible that the second pulse is in fact not an increase in conductivity but a recovery of the electric field in the plasma between the grid and the end plate after the initial extremely large current pulse from the e-beam.

Because of the interpretation of the origin of the rising portion of the second pulse is not certain we can only interpret the decaying portion of the pulse at long time when we are confident the circuit potentials are well behaved.

When N_2 is irradiated by high energy electrons, it will be ionized by

$$e(600\ \text{keV}) + N_2 \rightarrow N_2^+ + e + e(600\ \text{keV}) \tag{1}$$

$$S = \frac{J}{W}\frac{dE}{dx} = 6 \times 10^{23}\ e/cm^3\ \text{sec atm}$$

where S equals the ionization rate during the e-beam pulse with J being the current density, W the energy per ion pairs and $\frac{dE}{dx}$ the stopping power. The N_2^+ ion concentration produced by the e-beam excitation of an atmosphere of N_2 is estimated to be $10^{15}\ cm^{-3}$.

The N_2^+ ions will be quickly converted to N_4^+ by the process

$$N_2^+ + N_2 + N_2 \rightarrow N_4^+ + N_2 \tag{2}$$

The reaction rate constant[3] for this process is $5 \times 10^{-29}\ cm^6/sec$. At 1 atmosphere of N_2 pressure, the time for converting N_2^+ to N_4^+ is 3.6×10^{-10} sec. N_4^+ will recombine with electrons by

$$N_4^+ + e \rightarrow N_2^* + N_2 \tag{3}$$

$$\rightarrow 2N_2 \tag{4}$$

The N_2^* may be in various electronically excited states and the $X^1\Sigma_g^+$ vibrationally excited states. The rate constant[4] for the recombination

process is $2 \times 10^{-6} \left(\frac{T_e}{300}\right)$ cm^3/s for electrons. During the e-beam pulse the electron temperature is on the order of 1 eV and the recombination rate coefficient is 5×10^{-8} cm^3/s. For an electron concentration of 10^{15} cm^{-3} initially produced by e-beam excitation the recombination rate is 5×10^7 sec^{-1}. Because of such high reaction rates for the processes (2) and (3), the ions and electrons initially produced by e-beam excitation will be converted to N_2^* within about 20-30 ns. A column of uniform N_2^* density between the end plate and grid is thus created which will be on order of 10^{15} cm^{-3}. The conduction current may be sustained by secondary ionization of these N_2 excited states by the following reaction:

$$e + N_2^* \rightarrow N_2^+ + 2e \qquad (5)$$

The residual electrons accelerated by the electric field may sustain the conductivity by the cyclic process of reactions (5), (2), and (3). However, at the low E/N values used in this experiment, the electrons lose energy on each cycle and are soon unable to sustain the ionization. At low N_2^* concentration, the amplification process will stop, and the electron conduction current will decay through recombination process (4). This is consistent with the experimental observation that the current decreases with time as a function of $(1 + \alpha t)^{-1}$ after the sharp drop in electron current.

Under this proposed model, the electron conduction current should be decreased by adding gases either to attach the electrons or to quench the N_2^* species. The results for adding Cl_2, NO, and N_2O to N_2 are reported below.

B. Cl_2 in N_2

When Cl_2 is added to N_2, the electron conduction current (Figure 3) at long times (> 100 ns) shows an exponential decay with time. This decay is interpreted as electron attachment of Cl_2,

$$e + Cl_2 \rightarrow Cl^- + Cl \qquad (6)$$

The decay may also be caused by quenching of N_2^* by Cl_2,

$$N_2^* + Cl_2 \rightarrow N_2 + Cl_2 + \Delta E \qquad (7)$$

As shown in Figure 5, the decay rates increase with the Cl_2 pressure in 1 atmosphere of N_2 under E/N = 18 Td, where the distance between the end plate and the grid is set at ℓ = 2.25 cm. The rate constant derived from this plot is $(1.6 \pm 0.5) \times 10^{-10}$ cm^3/sec. When E/N decreases to 9 Td, the rate constant increases to $(2.6 \pm 0.8) \times 10^{-10}$ cm^3/sec. These results are consistent with the measurements of Rokni, Jacob, and Mangano[5] within experimental uncertainties.

Since the cross section[6,7] for process (6) is peaked at the electron energy ~ 0, the attachment rate constants of Cl_2 are expected to increase with decreasing E/N. The results that the observed decay rate constants increase with decreasing E/N suggest that the decay is mainly a contribution of process (6). However, process (7) may also have a non-negligible contribution. By linear extrapolation of our data to E/N = 0, the decay rate constant is at least $(4.2 \pm 1.3) \times 10^{-10}$ cm^3/sec. This is slightly larger than the attachment rate constant of Cl_2 for thermal electrons at 300 K measured by Christodoulides, Schumacher, and Schindler[8] of 3.1×10^{-10} cm^3/sec. The rate

constant for process (7) is not known, but it seems reasonable that it be on the order of 10^{-10} cm^3/sec.

C. NO in N_2

When NO is added to N_2, the electron conduction current also has an exponential decay with time. The decay rates increase linearly with NO pressure in N_2. Figure 6 shows the decay rate constants for adding NO to an atmosphere of N_2 versus various E/N. The rate constants decrease with increasing E/N.

For E/N values applied in this experiment, the mean electron energy[9] is not more than 1 eV. This electron energy is much lower than the threshold energy[10] of 6.7 eV for the dissociative attachment process of NO,

$$e + NO \rightarrow N + O^- \qquad (8)$$

Thus, the decay of the electron conduction current is not expected to be caused by the dissociative electron attachment of NO. Instead, the decay is more likely a contribution of the quenching of N_2^* by NO,

$$N_2^* + NO \rightarrow NO + N_2 \qquad (9)$$

The rate constants[11] for quenching $N_2^*(A^3\Sigma_u^+)$ by NO depends on the vibrational energy of $N_2^*(A)$. The rate constants[11-14] are in the range of (2-10) $\times$ 10^{-11} cm^3/sec for various vibrational levels. About half of the quenching results in $NO^*(A^2\Sigma^+)$.[12-14] This excited species is also subject to ionization similar to N_2^*, so it does not contribute to the decay of electron conduction current. Thus, the effective quenching rate constant of $N_2(A^3\Sigma_u^+)$ by NO is in the range of (1-5) $\times$ 10^{-11} cm^3/sec. The decay rate

constant at E/N → 0 is about 2×10^{-11} cm^3/sec (see Figure 6), which is within the range of the rate constants of N_2^* quenching by NO. These results indicate that the decay of electron conduction current is likely caused by the quenching of N_2^* by NO, where N_2^* is most likely to be in the $A^3\Sigma_u^+$ state.

The ionization efficiency of N_2^* by electrons increases[15] with increasing electron energy. Thus, N_2^* will be more rapidly ionized by electrons at higher E/N, which makes the quenching of N_2^* by NO become less effective. This may be the reason that the decay rate constants of the electron conduction current decrease with increasing E/N (see Figure 6).

It is also possible that the decrease of the electron conduction current is partly contributed by the three body electron attachment process,

$$e + NO + M \rightarrow NO^- + M \qquad (10)$$

The rate constant for this process is not known for M = N_2, but it may be in the range[16] of 10^{-32}–10^{-31} cm^6/sec. At 1 atmosphere of N_2, the effective two body rate constant is $2.7 \times (10^{-13}$–$10^{-12})$ cm^3/sec. This is smaller than the observed decay rate constant of 2×10^{-11} cm^3/sec.

D. N_2O in N_2

When N_2O is added to N_2, the electron conduction current shows an exponential decay with time. The decay rates increase linearly with the N_2O pressure added to N_2. The decay rate constants at various E/N are shown in Figure 7 for N_2O added in 350 torr of N_2. The decay rate constant starts to become significant at E/N = 3 Td and increases linearly with higher E/N.

The rate constant[17] for $N_2^*(A^3\Sigma_u^+)$ quenched by N_2O is 6.4×10^{-12} cm^3/sec at temperature 300 K. This rate constant is much smaller

than the decay rate constants shown in Figure 7. The decay rate is thus mainly contributed by the dissociative electron attachment process,

$$e + N_2O \rightarrow N_2 + O^- \qquad (11)$$

This process has an electron energy threshold about 0.3 eV, and its cross section increases with electron energy to a maximum value of 8.4×10^{-18} cm^2 at 2.2 eV.[10] The average electron energy in 1 atmosphere of N_2 at E/N = 6 Td is 0.87 eV.[9] At this electron energy the cross section for process (11) is 2.2×10^{-18} cm^2. Taking the electron velocity of 5.5×10^7 cm/sec calculated from $\frac{1}{2}mv^2 = 0.87$ eV, we have the rate constant for process (11) to be 1.2×10^{-10} cm^3/sec. This value checks very well with the observed decay rate constant of 1.3×10^{-10} cm^3 as shown in Figure 7. This good agreement confirms that the decay is indeed a result of the dissociative electron attachment.

IV. CONCLUDING REMARKS

The measured data are tentatively described by a gaseous kinetic model involving formation and charge recombination of N_4^+, which is converted from N_2^+ initially produced from the e-beam excitation of N_2. N_4^+ is quickly recombined with an electron to form N_2^*. The N_2^* excited species sustain the residual electrons and extend in time for the electron conduction current. This tentative model is subject to confirmation by obtaining more experimental data.

The decreases of the electron conduction current by adding Cl_2, NO, and N_2O to N_2 are attributed to the processes of both dissociative electron attachment and quenching of the excited N_2^* species. The rate constants of these processes measured in this experiment are consistent with the values given by previous measurements or by estimation from other parameters.

Acknowledgement

The authors are grateful to Professors Schoenbach, Schaeffer and Williams at Texas Tech University for their useful suggestions and discussions. This work is supported mainly by AFOSR and partly by ARO under contract no. F49620-79-C-0191. The research project is a part of the Pulse Power Program coordinated by the Department of Electrical Engineering, Texas Tech University.

REFERENCES

1. L.G.H. Huxley and R. W. Crompton, The Diffusion and Drift of Electrons in Gases, (John Wiley and Sons, New York, 1974).
2. B. L. Schram, Thesis, University of Amsterdam (1966).
3. T. M. Miller, J. T. Moseley, D. W. Martin, and E. W. McDaniel, Phys. Rev. Lett. 21, A3 (1968).
4. W. H. Kasner and M. A. Biondi, Phys. Rev. 137, A317 (1965).
5. M. Rokni, J. H. Jacob, and J. A. Mangano, Appl. Phys. Lett. 34, 187 (1979).
6. W. C. Tam and S. F. Wong, J. Chem. Phys. 68, 5626 (1978).
7. M. V. Kurepa and D. S. Belic, J. Phys. B: Atom. Molec. Phys. 11, 3719 (1978).
8. A. A. Christodoulides, R. Schumacher, and R. N. Schindler, J. Chem. Phys. 79, 1904 (1975).
9. D.L.M. McCorkle, A. A. Christodoulides, L. G. Christophorou, and I. Szamrej, J. Chem. Phys. 72, 4049 (1980).
10. D. Rapp and D. D. Briglia, J. Chem. Phys. 43, 1480 (1965).
11. J. W. Dreyer, D. Perner, and C. R. Roy, J. Chem. Phys. 61, 3164 (1974).
12. R. A. Young and G. A. St. John, J. Chem. Phys. 48, 895, 898 (1968).
13. R. A. Young, G. Black, and T. G. Slanger, J. Chem. Phys. 50, 303 (1969).
14. A. B. Callear and P. M. Wood, Trans. Faraday Soc. 67, 272 (1971).
15. P. B. Armentrout, S. M. Tarr, A. Dori, and R. S. Freund, J. Chem. Phys. 75, 2786 (1981).
16. G. E. Caledonia, Chem. Rev. 75, 333 (1975).
17. T. G. Slanger, B. J. Wood, and G. Black, J. Photochem. 2, 63 (1973/74).

FIGURE CAPTIONS

Figure 1. Schematic diagram for the experimental apparatus.

Figure 2. Electron conduction current produced by a 3 ns and 600-keV e-beam excitation of 760 torr N_2 under E/N = 18 Td.

Figure 3. Electron conduction current produced by e-beam excitation of 350 torr N_2 under E/N = 5.6 Td.

Figure 4. τ^{-1} versus E/N for N_2 pressures at 350 and 700 torr. τ is the time duration between the halves of maximum amplitude.

Figure 5. The decay rates of the electron conduction current for various Cl_2 pressures added in 1 atmosphere of N_2 under E/N = 18 Td.

Figure 6. The decay rate constants of the electron conduction current by adding NO in 1 atmosphere of N_2 at various E/N.

Figure 7. The decay rate constants of the electron conduction current by adding N_2O in 350 torr of N_2 at various E/N.

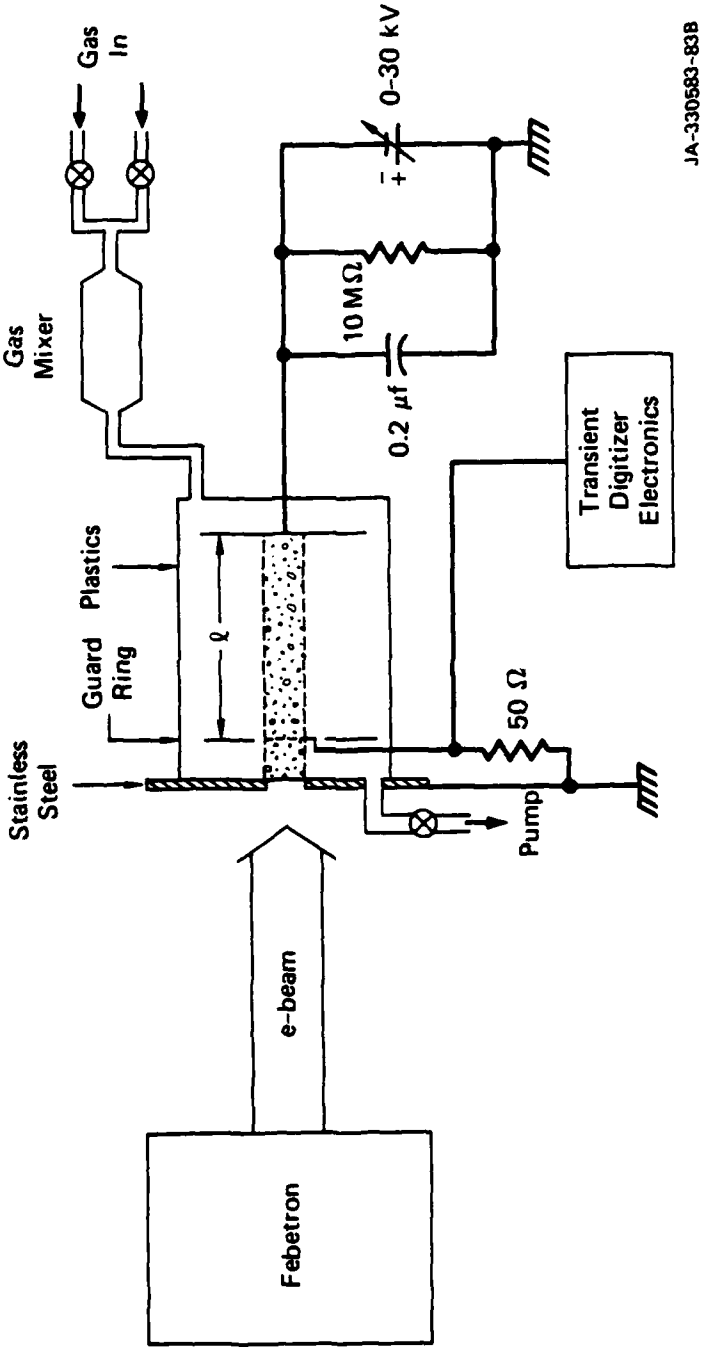
Gas In
0-30 kV
Gas Mixer
10 MΩ
0.2 μf
Transient Digitizer Electronics
Plastics
Guard Ring
ℓ
50 Ω
Stainless Steel
Pump
e-beam
Febetron
JA-330583-83B

Fig. 1

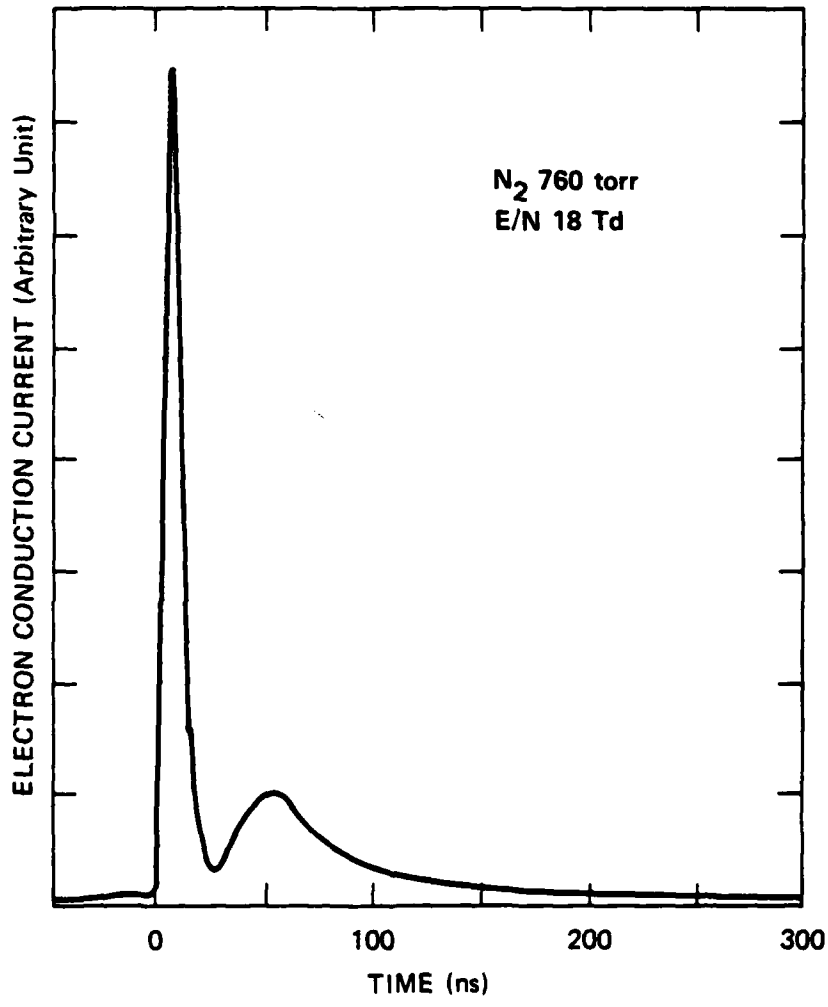
ELECTRON CONDUCTION CURRENT (Arbitrary Unit)
N_2 760 torr
E/N 18 Td
0
100
200
300
TIME (ns)
JA-330522-54

Fig 2

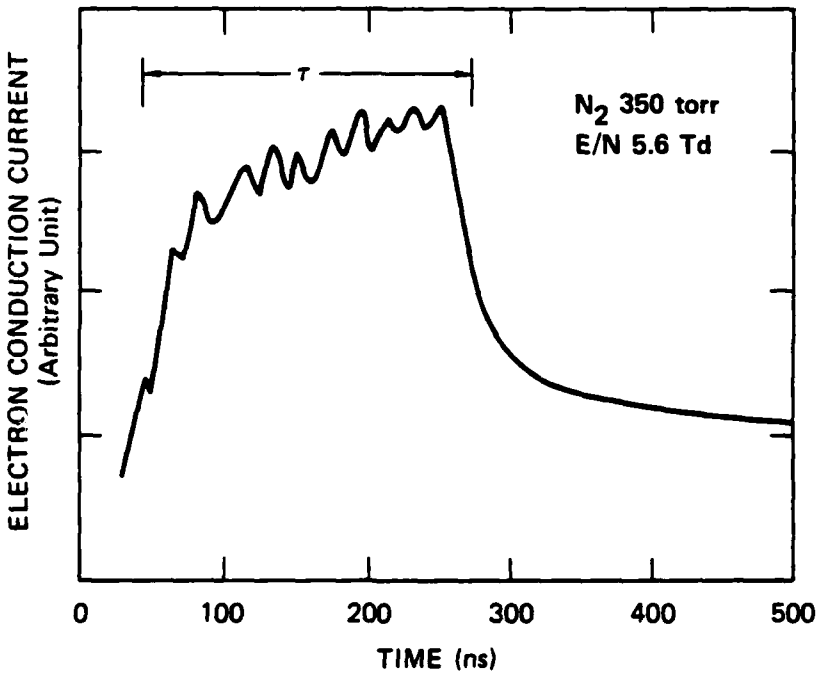
ELECTRON CONDUCTION CURRENT
(Arbitrary Unit)
τ
N2 350 torr
E/N 5.6 Td
0
100
200
300
400
500
TIME (ns)
JA-330522-53

Fig 3

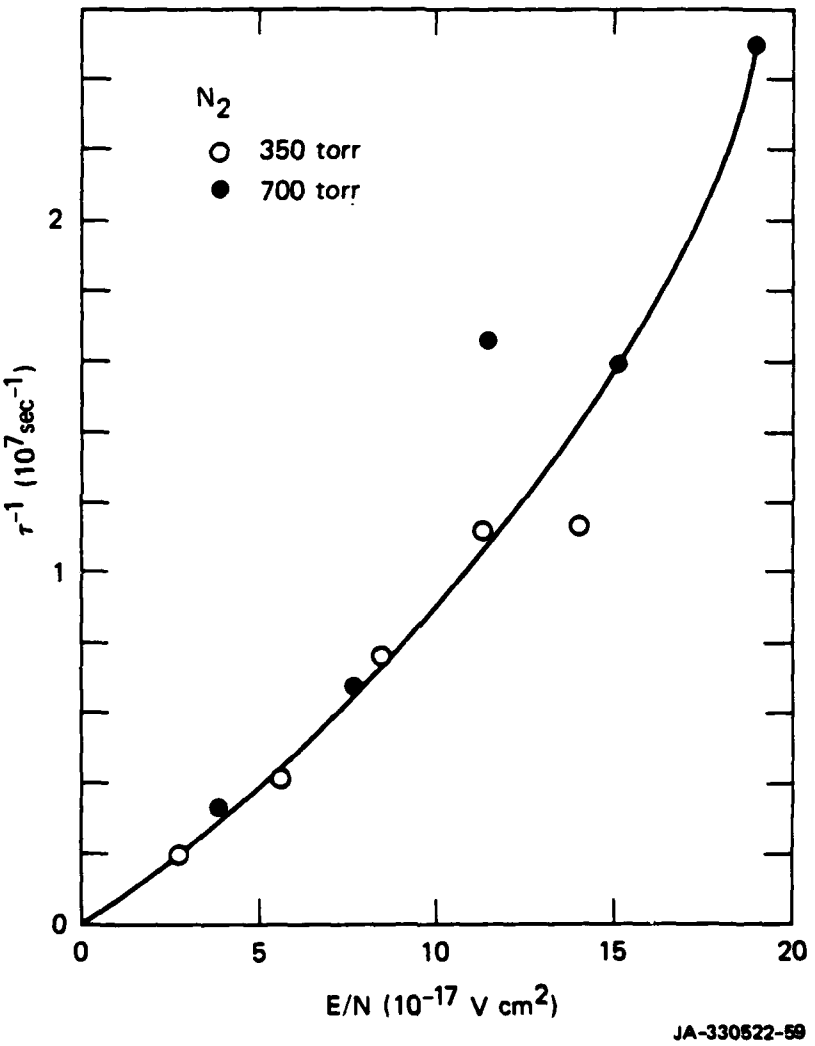
N2
350 torr
700 torr
τ⁻¹ (10⁷sec⁻¹)
E/N (10⁻¹⁷ V cm²)
0
1
2
0
5
10
15
20
JA-330522-59

Fig 4

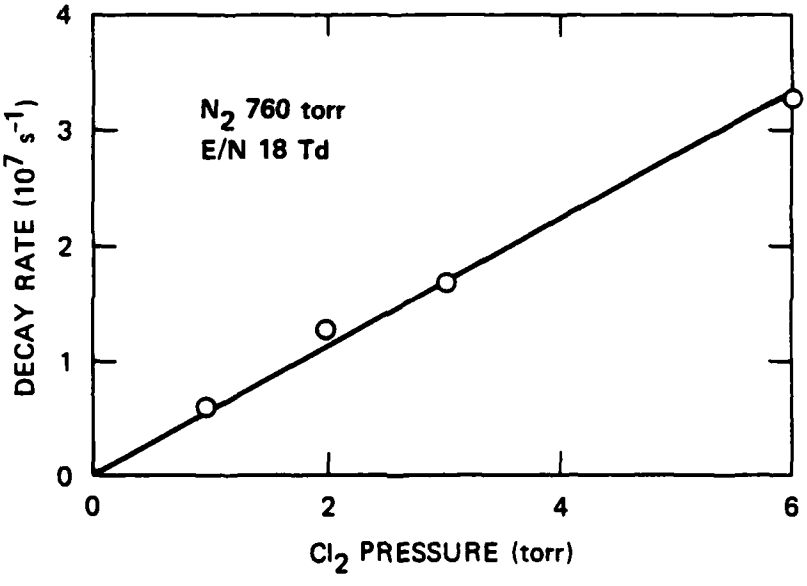
N_2 760 torr
E/N 18 Td
DECAY RATE (10^7 s^{-1})
0
1
2
3
4
0
2
4
6
Cl_2 PRESSURE (torr)
JA-330522-56

Fig 5

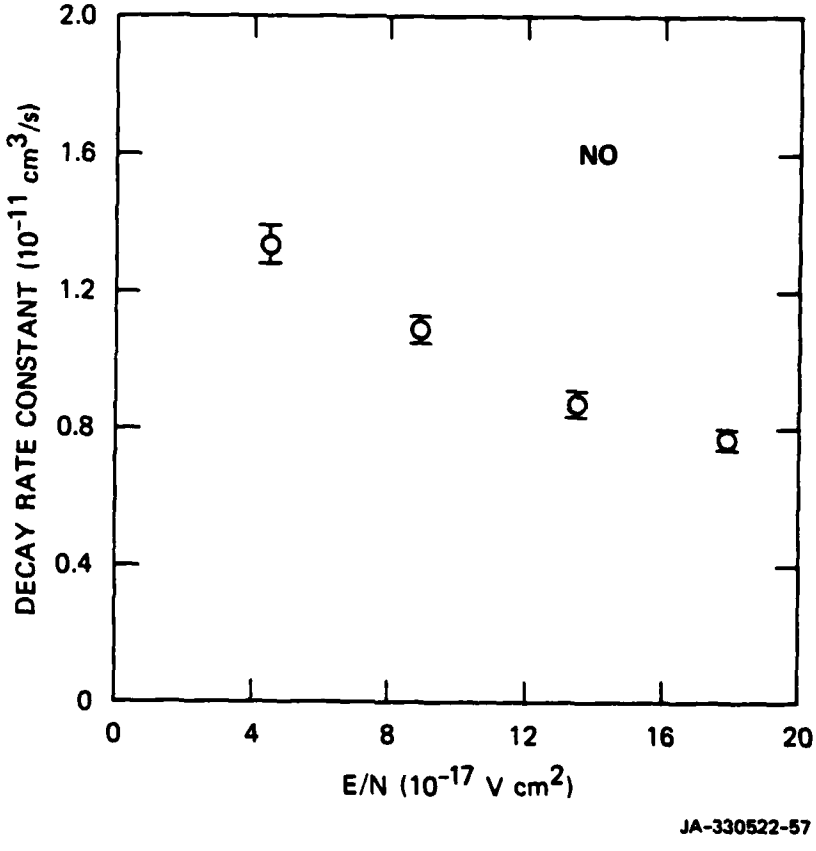
2.0
1.6
1.2
0.8
0.4
0
DECAY RATE CONSTANT (10^{-11} cm^3/s)
NO
0
4
8
12
16
20
E/N (10^{-17} V cm^2)
JA-330522-57

Fig 6

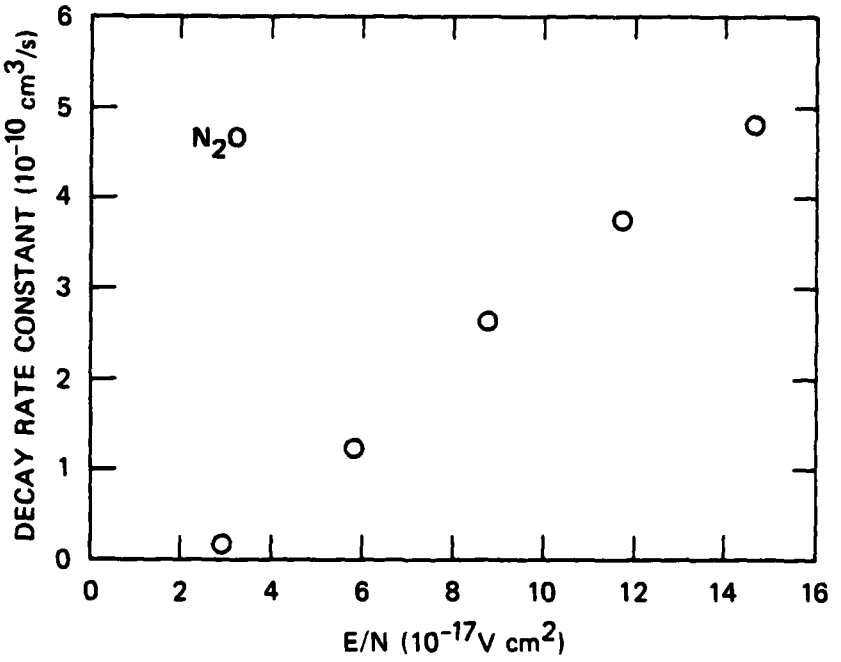

JA-330533-58

Fig 7

Project No. 10

Supplementary Funded Research on

Opening Switches*

(H. C. Harjes, G. Hutchinson, G. Leiker,
K.H. Schoenbach, G. Schaefer, L. Hatfield,and M. Kristiansen)

A. SUMMARY

The primary objective of this work is to study the processes in externally sustained or controlled diffuse discharges, with respect to their application as opening switches. Experimental set-ups are designed to investigate the applicability of two concepts for diffuse discharge opening switches:

a) the electron-beam sustained diffuse discharge

b) the optically controlled diffuse discharge where optical control either means sustainment of the discharge by means of laser radiation or optical stimulation of loss processes in self sustained discharges

For the investigation of electron-beam sustained discharges an apparatus is designed which consists of an electron gun with a thermionic cathode which generates an electron current of approximately 100 A at electron energies $E_e > 200$ keV and a discharge cell for high pressure gases ($p \leq 10$ atm). For diagnostics a voltage probe with ns time-resolution was developed.

---

* This research was funded based on two separately submitted proposals and is funded partly by AFOSR and partly by Army Research Office. In the current, 1982, budget year, this research is identified by Project No's. 8 (AFOSR) and 9 (ARO). Projects 8 and 9 in this annual report are not continued into the 1982 Budget Year.

For investigations of optically controlled discharges, a discharge cell was designed and is presently tested at charging voltages of $V_c \approx 100$ kV. Diagnostic techniques for voltage and current measurements with ns time resolution were developed.

Topics for initial studies include:

a) production of stable diffuse discharges in N_2 with admixtures of attachers

b) increase of conductivity by resonant two-step photoionization of NO in N_2 as buffer gas.

A rate equation code was developed which describes the behavior of discharge parameters in a diverter circuit. The program is tested presently for a N_2/NO gas mixture.

Several other exploratory opening switch concepts have also been examined for potential use as opening switches. Among these are the dense plasma focus, wall stabilized discharges, and a novel solid state opening switch.

B. ELECTRON-BEAM CONTROLLED SWITCH

1. Introduction

The feasibility of using an electron-beam to control the conductivity of the gas volume between two charged electrodes has been studied experimentally [1,2] and theoretically [3,4]. By suitable choice of gas and electron-beam parameters, the conductivity of the gas may be rapidly changed over a wide range of values.

An electron-beam controlled discharge circuit has been designed and is presently under construction to study the behavior of an e-beam sustained, attachment dominated discharge

a) at high discharge current densities,

b) in gases which are suitable for low loss, fast opening operation,

c) for rep-rated operation.

The objective of the investigation is to determine a set of criteria concerning electrical and gas parameters of an e-beam sustained discharge, which will guide the design of a rep-rated electron-beam controlled opening switch.

2. Experimental Arrangement Design

The experimental arrangement consists of an evacuated electron gun which is an integral part of a capacitive discharge circuit. The circuit itself contains as a controllable resistive element a discharge chamber filled with a high pressure gas mixture, whose conductivity is e-beam controlled. In particular, the following constraints were imposed on the design of the experimental arrangement:

a) E-Beam

1. The electron energy should be greater than E = 150 keV to minimize losses in the anode foil, which separates the e-beam gun and discharge chamber.
2. The electron beam current density should be relatively high with a switch current density of at least 1-2 orders of magnitude higher than the beam current density. The electron current density should be varied to values up to 1 A/cm^2 at a cross section of $A \simeq 100\ cm^2$.
3. The e-beam should be turned off in times shorter than the desired switch opening time.
4. The electron emitter must be able to deliver electron currents over a long period of time to allow rep-rated operation.

b) Switch

1. The chamber has to stand pressures up to p = 10 atm, a requirement which especially concerns the construction of the foil for the e-beam entry.
2. The electrode shape should allow the establishment of an uniform electric field in the gap.
3. The gas mixture should satisfy the following conditions:
   - high mobility at low E/N
   - low attachment rate at low E/N
   - high attachment rate at high E/N
   - high dielectric strength

c) Diagnostics

1. Voltage and current probes should have a time resolution of < 10 ns.

2. Optical access to the switch chamber is required for streak and time integrated photography of the discharge.

3. Construction of the Experimental Arrangement

With the above constraints in mind, the e-beam controlled switch of Fig. 1 was designed and is presently being constructed. The FRP-250 pulse generator is used to supply the e-beam accelerating voltage. The pulser is capable of delivering a 250 kV pulse which rises in 10 ns and decays expontially with a 1 μs time constant. The FRP-250 is designed to drive a 100 Ω stripline. The evacuated e-beam chamber is placed between the stripline plates with the positively charged plate on top and the grounded plate on bottom. The chamber is a 12" I.D. Pyrex tube and is connected to the vacuum system through a hole in the grounded plate (Fig. 1). The vacuum system (shown in Fig. 2) consists of a mechanical roughing pump and 280 liter/sec diffusion pump and is designed to give a pressure of 10^{-5} Torr in the e-beam chamber. The e-beam cathode is mounted on a tube which is connected to the grounded plate. The square foil window is located just above the cathode on the positively charged plate. The 10 cm x 10 cm wide e-beam passes from the vacuum chamber into the switch chamber through this foil.

A cross section of the e-beam cathode is shown in Fig. 3. The thermionic cathode consists of an array of electrically heated thoriated tungsten filaments. A heating power of 4.5 kW is required to raise the filament temperature to 1900° K. The output current density from the e-beam can be varied by changing either the filament temperature, the cathode to plate spacing, or the accelerating voltage, V_A. The maximum output current density should be 1 A/cm^2. Beam control is accomplished by using a control grid above the filaments and a spreader plate below

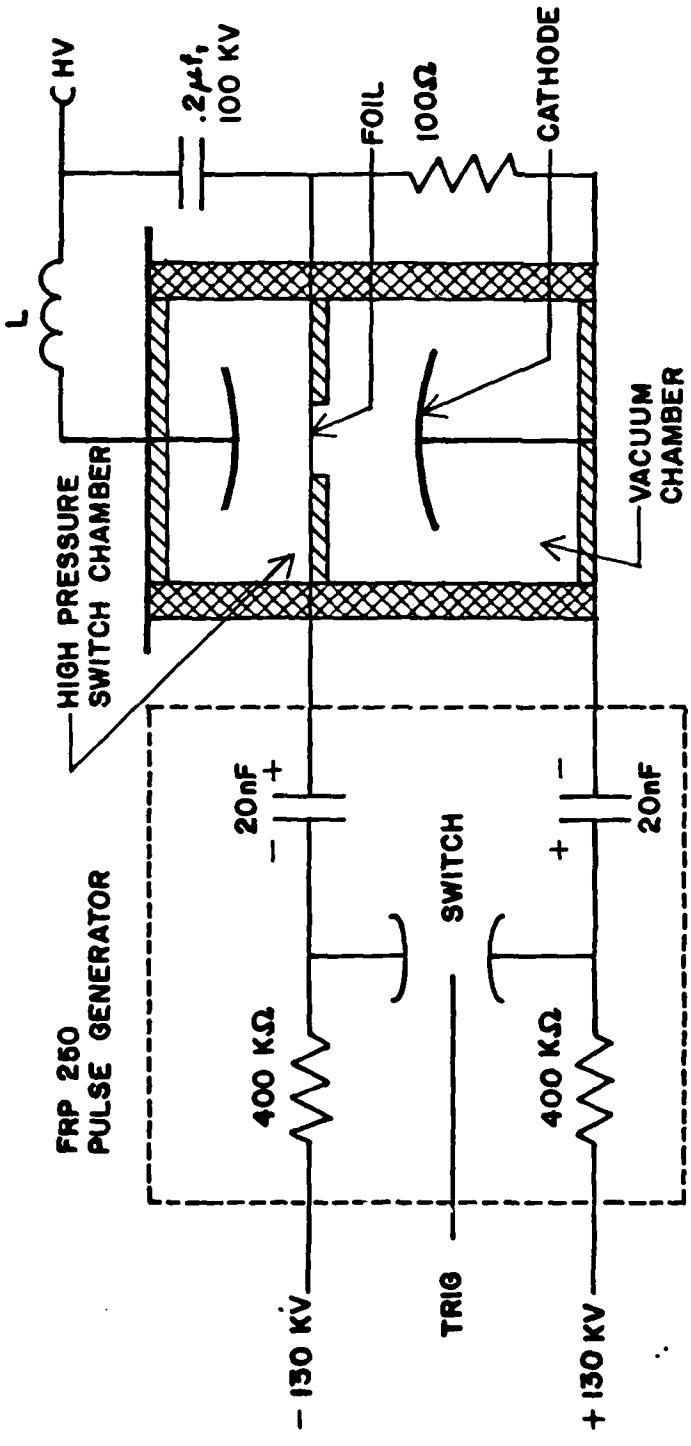

Fig. 1 Experimental Arrangement

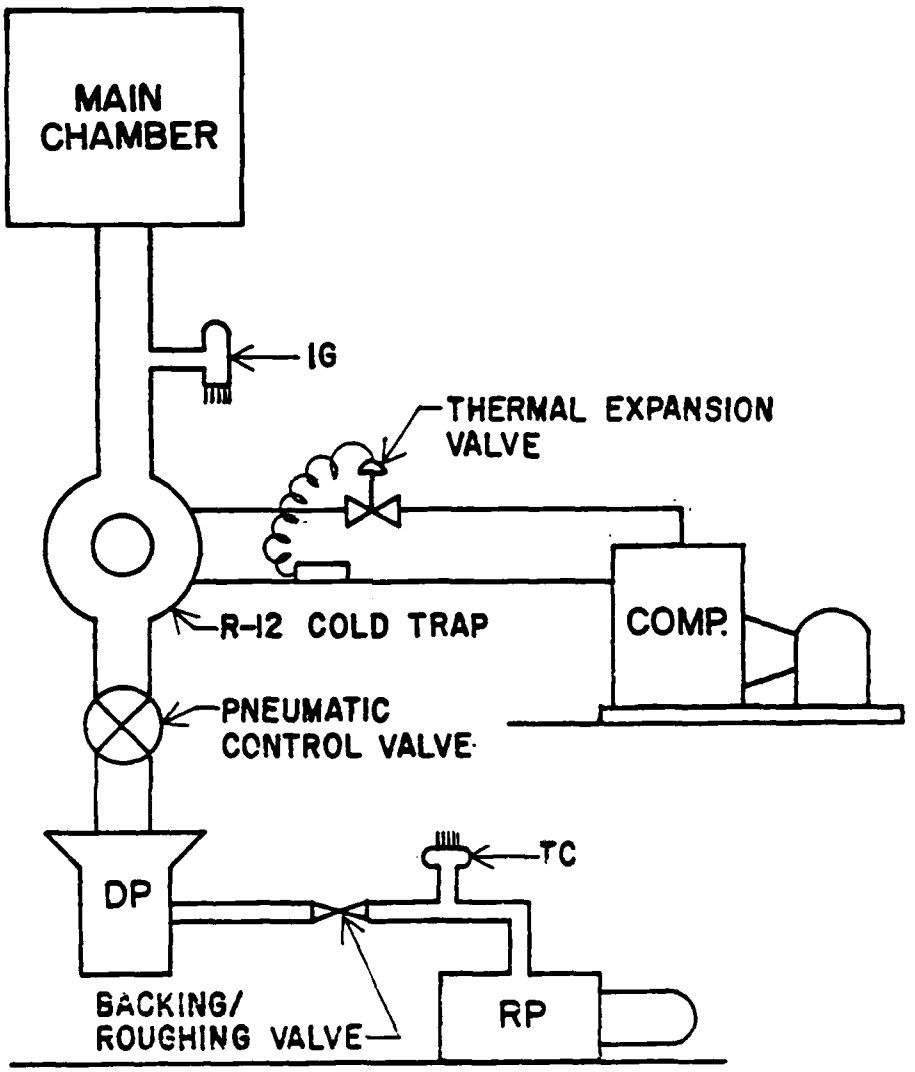

Fig. 2 Vacuum System

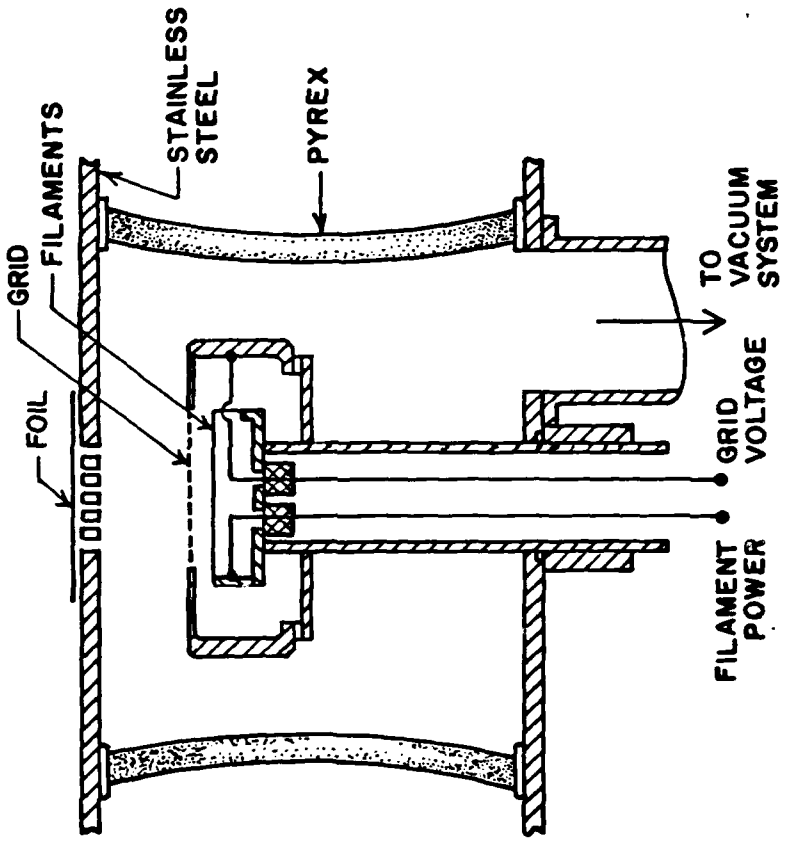

Fig. 3 Cross Section of the e-Beam Diode

the filament [5]. The beam current can be controlled by applying a modest negative voltage to these two conductors.

The switch chamber is located just above the e-beam chamber, as shown in Fig. 1. A cross section of the switch circuit is shown in Fig. 4. The contour of the top electrode is calculated to give a uniform E-field in the discharge region by using a computer field plotting code. The walls of the chamber are made of 1" thick plexiglass and the foil is protected from possible arcs by a coarse metallic grid, as shown. When the switch is closed, the .2 μf capacitor is partially discharged through the switch.

Resistive voltage dividers are used to measure the voltages, as shown in Fig. 5, and Rogowski coils are used to measure the currents. The switch voltage can be determined from the difference of the outputs of the two voltage probes. Voltage probe #1 serves as a 100 Ω terminating load for the FRP-250 stripline and has already been tested with the FRP-250. The response time of the probe is less than 10 ns.

C. OPTICALLY CONTROLLED DIFFUSE DISCHARGES

For the optical control of a diffuse discharge, in general two types of processes may be influenced by the use of a laser: the generation processes and the depletion processes for the electrons.

1. Electron Depletion:

An electron depletion rate that can be strongly influenced by radiation is electron attachment. Some possible influence mechanism are summarized in Table 1. The only data concerning rates or cross sections are available for rotationally and vibrationally excited molecules like SF_6

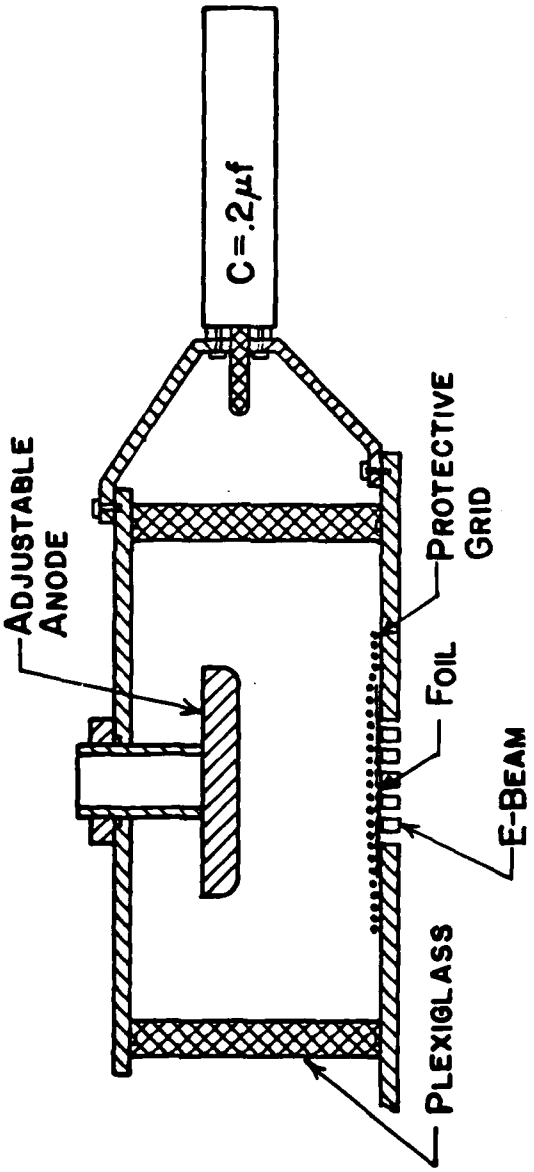

Fig. 4 Cross Section of the Switch Circuit

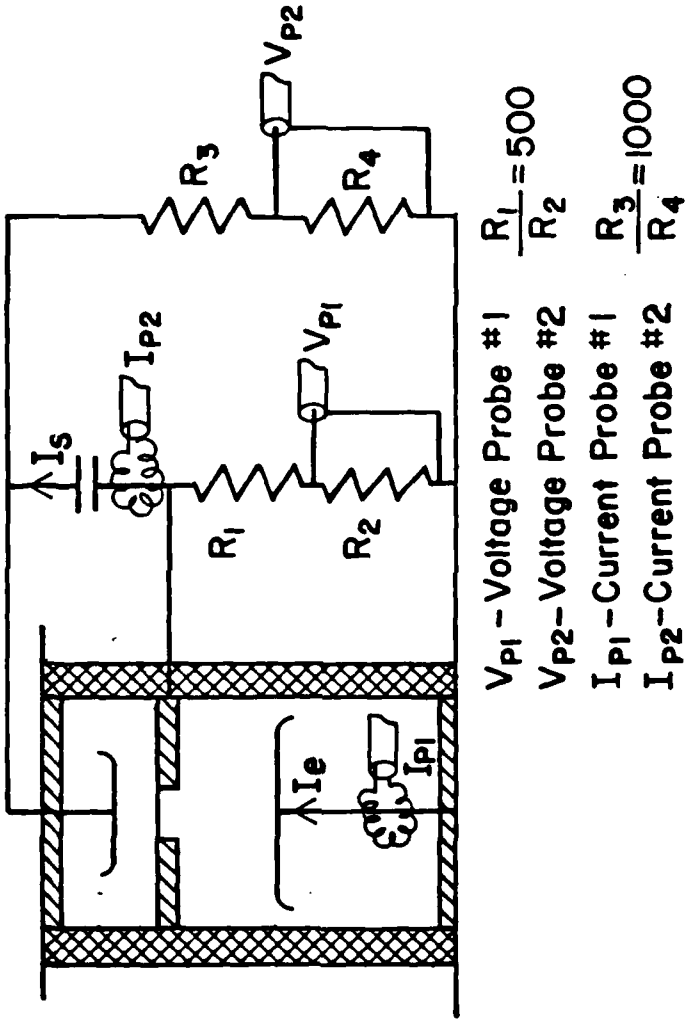

Fig. 5 Electrical Diagnostics

[6] and HCl [7]. Calculations of Norman Bardsley [8] showed that the vibrational excitation of HCl (v=0) to the HCl (v=2) state increases the attachment rate at room temperature and the E/N values, as used for diffuse discharges, by nearly two orders of magnitude. To avoid a strong competition with electron impact vibrational excitation, mainly those molecules may be used where the attachment rate increases strongly for highly excited states where the rotational-translational energy $E_{R,T} \gtrsim 1$ eV.

Table 1 Optically Controlled Electron Depletion

Process	Example	Control	Comment
a) Photoenhanced Attachment		laser to decrease conductivity (short pulse)	
1. rotational excitation	HCl;HF		small shift and increase of $\sigma(E)$
2. vibrational excitation	SF_6:HCl		strong shift and increase of $\sigma(E)$
3. electronic excitation			
4. photochemical reaction	unimolecular decompositions		
b) Photodetachment	O^-;F^-	laser to increase conductivity	

Another promising process is the photodecomposition (either UV or multiphoton IR decomposition) of molecules to produce fragments with much higher attachment cross sections and rates than the starting products. The available data and the feasibility of this mechanism have not yet been investigated in detail.

2. Electron Generation

The influence of the electron generation rate by radiation is used in optogalvanic spectroscopy. Some processes that may be used to change the impedance of a diffuse discharge are summarized in Fig. 6 and Table 2 Processes (1-5) increase the conductivity by increasing the electron generation rate, while process (6) decreases the electron generation rate. The two photon ionization from an intermediate excited or metastable state (5) has the advantage that flashlamp pumped dye lasers, without frequency doubling, may be used for several systems.

An atomic system may contain mercury as shown in Fig. 7. From the metastable state 6^3P_o or the resonance state 6^3P_1 resonant, two photon ionization via the 7^3S_1 state is possible.

A molecular system (Fig. 8) may work with N_2 with a small admixture of NO [9]. By energy transfer collisions of NO with metastable $N_2(A^3\Sigma_u^+)$ molecules the NO $(A^2\Sigma^+)$ state can be populated efficiently. From this state a resonant two photon excitation via the NO $(E^2\Sigma^+)$ state is possible. The wavelength for this transition is approximately 600 nm, depending on the rotational states of NO.

For first calculations to investigate the feasibility of the two photon ionization from an intermediate state, the N_2: NO system has been chosen. The rate equations for this system include all processes menioned in Fig. 8. The rate constants for the electron collision processes have been evaluated depending on E/N. The rate equation shall be solved including the influence of the circuit on the E/N value of the discharge.

Table 2 Optically Controlled Electron Generation
(one frequency)

	Process	Example	Type of Control	Comment
(1)	one photon ionization from ground state	Alkali	externally sustained	UV, chemically agressive
(2)	two photon ionization from ground state	$(CH_3)_3N$	laser to increase conductivity (long pulse)	UV
(3)	one photon excitation from ground state	Alkali;Hg	externally controlled	UV-Vis resonance trapping
(4)	one photon ionization from excited state	Alkali;NO		UV-Vis
(5)	two photon ionization from excited state	Hg;NO		Vis
(6)	one photon excitation from metastable state to non-metastable state	He;Ne	laser to decrease conductivity (short pulse)	Vis-IR resonance trapping

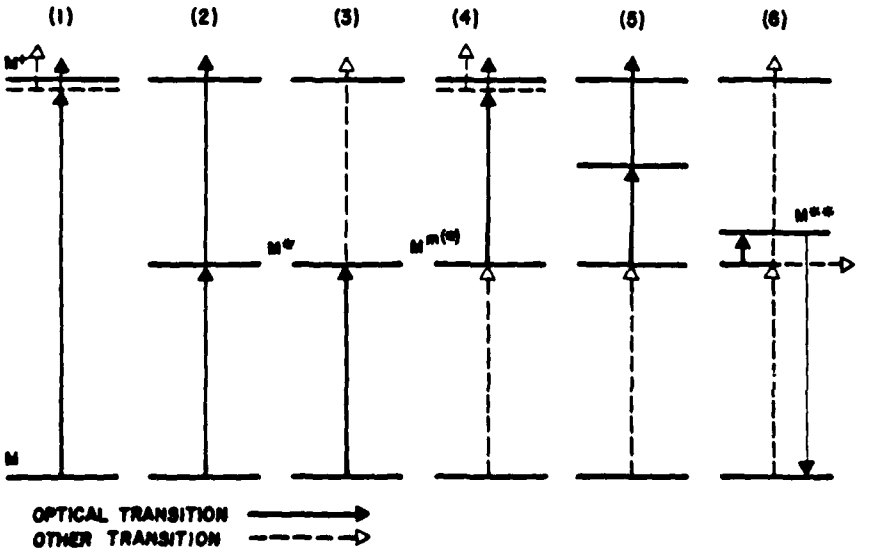

Fig. 6: Optically Controlled Electron Generation
(one frequency)

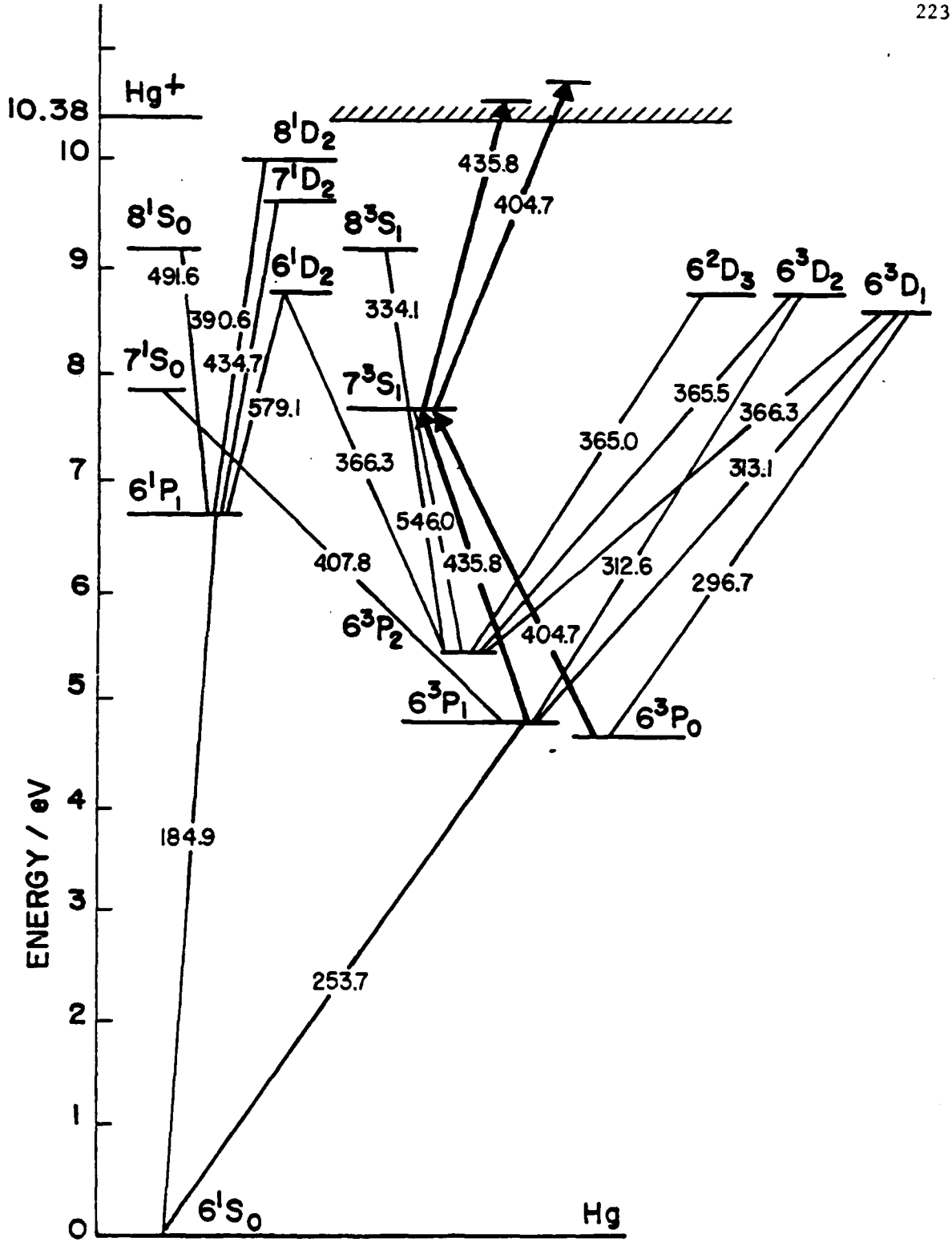

Fig. 7 Energy level diagram of Hg with proposed two step photo-ionization from excited states

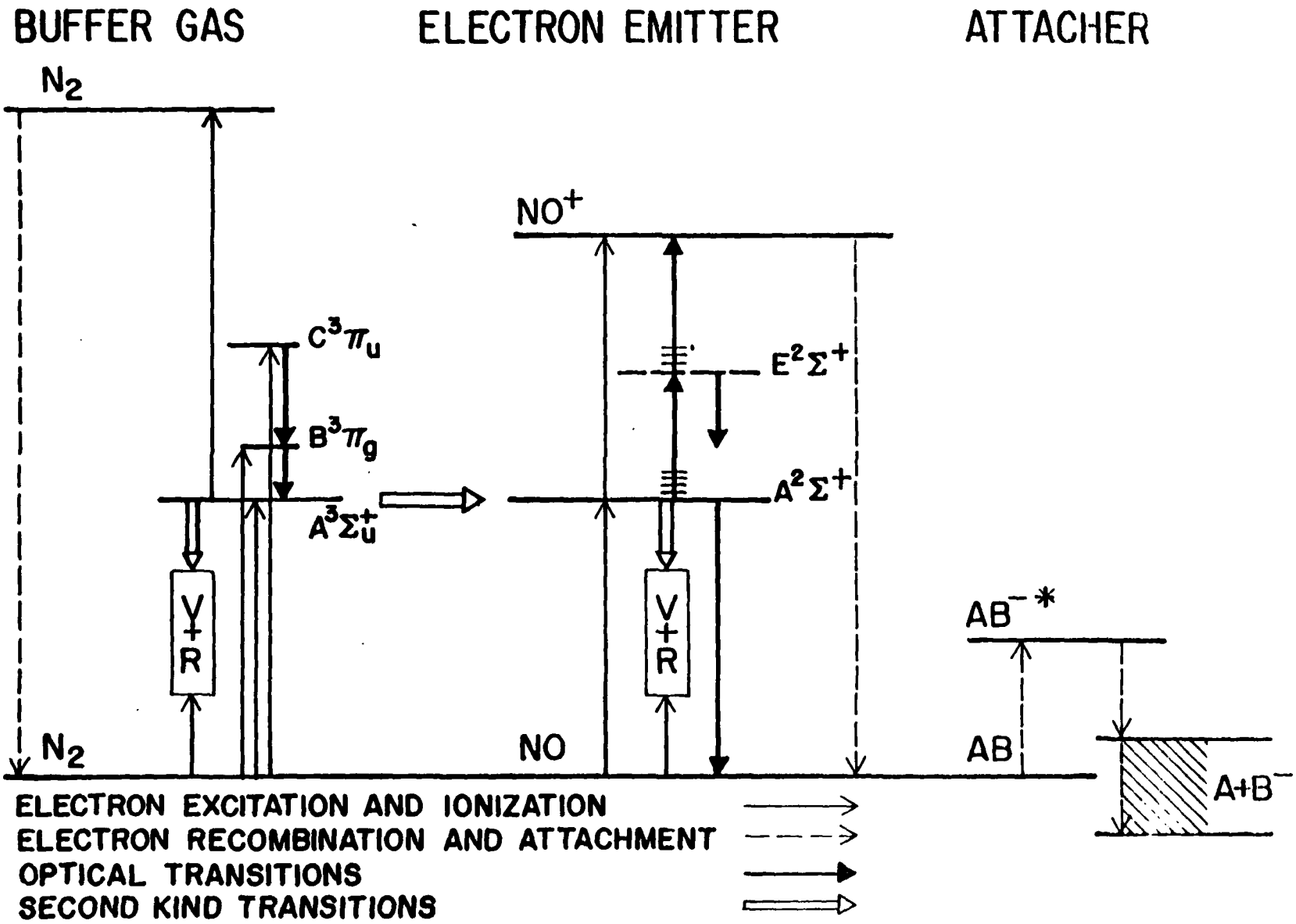

Fig. 8 Energy level for the N_2, NO system with transitions used for calculations

3. Experimental Arrangement

An experimental set-up has been designed (Fig. 9) for investigation of optogalvanic effects in a diffuse plasma. The system consists of an oil filled, 50 Ω-line, a laser-triggered closing switch, C, and a discharge chamber, O, where the diffuse discharge is produced. The closing switch serves to apply the charging voltage across the main discharge gap. The discharge current can be controlled by a water resistor array with variable resistance.

Voltage and current probes allow the measurements of the electrical parameters of the discharge. Additional optical measurements (time integrated and streak photographs) give information on position and onset time of arcs in the diffuse discharge. Together with electrical data they allow a rough estimate of electron densities, if the drift velocity is known: $n_e = \frac{I}{qA} \frac{1}{v(E/N)}$

where: n_e = electron density

I = current

A = cross section of diffuse discharge

$v(E/N)$ = drift velocity

A flashlamp is used to provide for preionization of the fill gas which is supposed to satisfy the following conditions:

a) high mobility at low E/N

b) low attachment rate at low E/N

c) high attachment rate at high E/N

d) high dielectric strength

The conductivity of the diffuse plasma is to be changed by means of optogalvanic effects (see previous paragraph), using a laser.

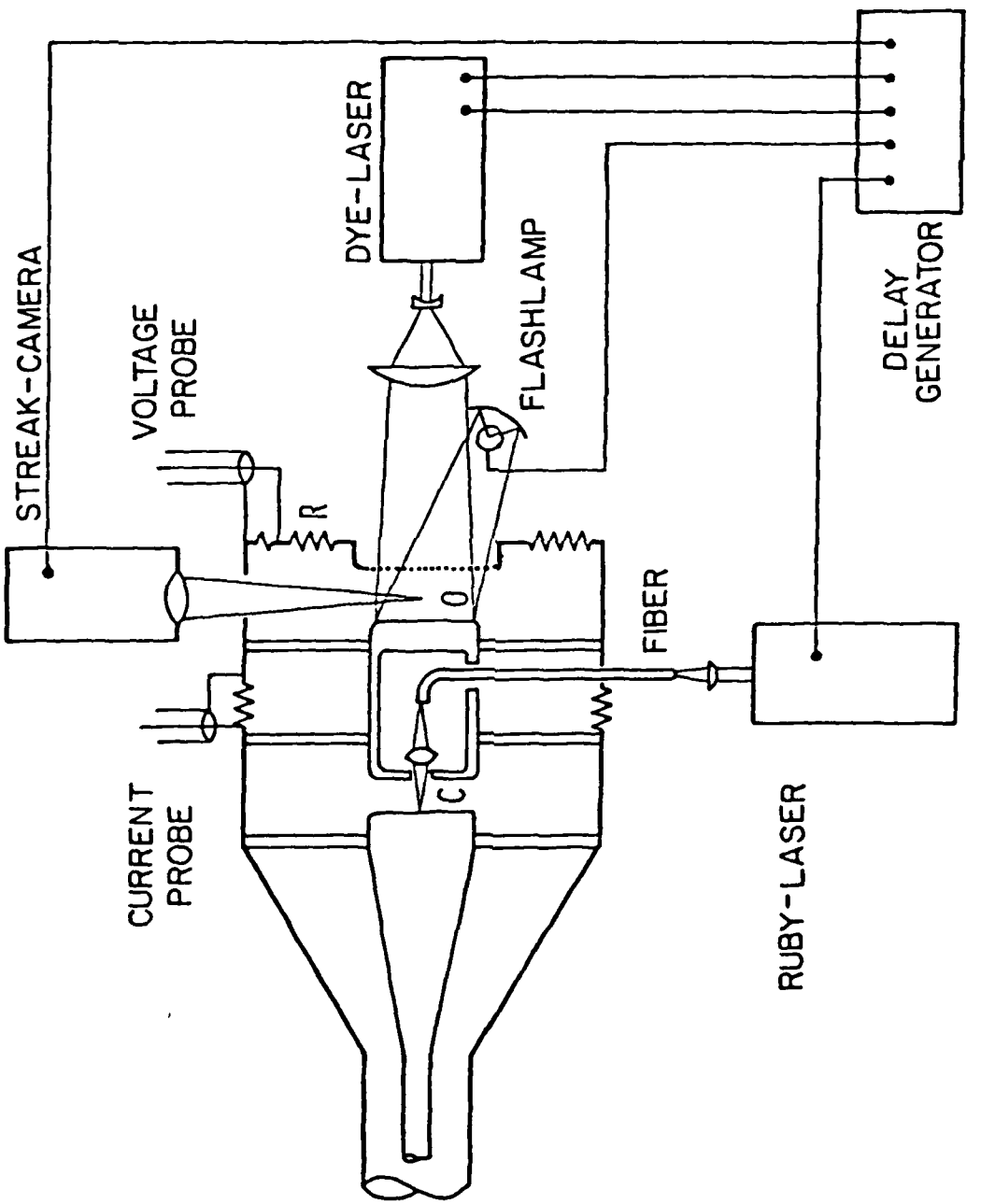

Fig. 9 Functional Experimental Set-up for Optically Controlled Diffuse Discharge

a) Constraints on Design

In particular, the following constraints were imposed on the design of the experimental arrangement.

A. Conditions for the production of a high pressure diffuse discharge

1. option to use gases with boiling point above T = 300° K
2. voltage across the main gap (O) large compared to breakdown voltage of gas mixture (large overvoltage)
3. fast voltage rise (dV/dt > 10 kV/ns)
4. uniformity of preionization
5. uniformity of initial electric field
6. possibility to vary discharge current

B. Conditions for optical control of the diffuse discharge

1. optical access to the diffuse discharge
2. tunability of laser
3. possibility to cut laser pulse in times shorter than the desired opening time of the diffuse discharge switch

C. Conditions for diagnostics

1. ns-time resolution of voltage and current measurements
2. optical access side-on and end-on

b) Construction of Experimental Arrangement (Fig. 10)

The option to use any gas, that means also gases with a boiling point above T = 300 °K, requires a heating system for the discharge cell. Hence, all materials used in this cell were selected according to their ability to withstand temperatures of 450° K without changing their properties. The heating system uses hot oil as heat carrier. To prevent large losses by conduction, the discharge cell is to a large extent

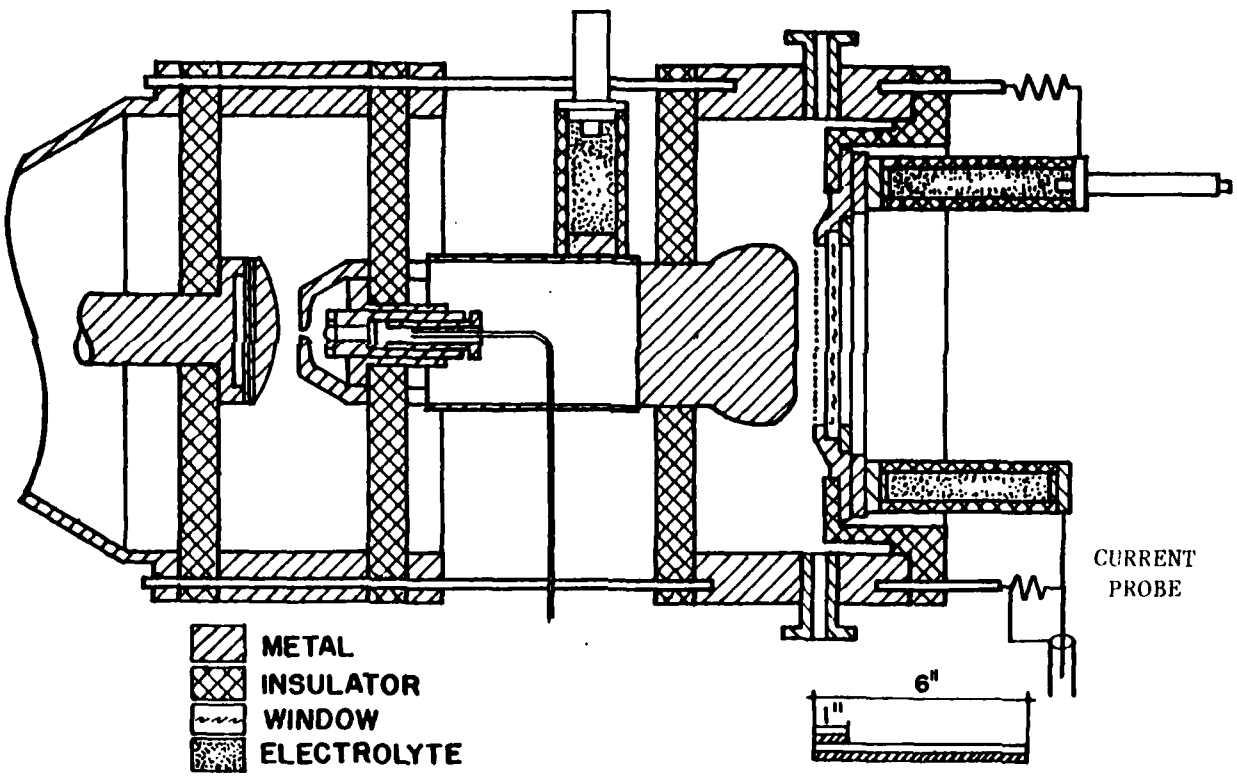

Fig. 10 Experimental Arrangement

thermally decoupled from the remaining system. That part of the inner conductor which connects the discharge cell and closing switch is a thin metal foil (low thermal conduction), the outer conductor consists of 6 brass rods.

In order to produce a diffuse discharge in a gas mixture suitable for an opening switch, the voltage initially applied across the main gap should be large compared to the breakdown voltage of the filler gas. For N_2 as a filler gas and an electrode separation of d = 1 cm, the breakdown voltage is $V_{br} \simeq 40$ kV [10]. The line was tested up to a charging voltage of 110 kV.

A second conditior is a fast voltage rise across the main gap. A voltage rise of $dV/dt > 10$ kV/ns should be attempted. In other words, the risetime of a 100 kV pulse should be less than 10 ns. To obtain this value, a method will be used which provides for risetimes in the order of nanoseconds; namely laser triggering of spark gaps [11].

The third condition is a uniform initial electron density, either in a plasma layer parallel to the electrodes or in the entire volume between the electrodes. It is planned to use a method which is based on uniform irradiation of the cathode by means of a flash lamp [12].

A fourth condition for the ignition and sustainment of a diffuse discharge is a uniform electric field in the gap, especially at the electrodes. A cathode was calculated by means of a field plotting computer code and constructed. It satisfies the requirements of constant field streng over a large cross section and no field enhancement at the edges. The anode consists of a Ni-mesh with a transparency of approximately 75%.

The current amplitude and the current density, respectively, in the

diffuse discharge can be varied independently of voltage by a variable external resistance (6 water resistors in parallel). This variation of the external resistance allows us to find the current-voltage characteristics of the diffuse discharge independent of the initial conditions (e.g. % overvoltage).

c) Laser

Initial studies of optogalvanic effects will use two-photon ionization from an intermediate excited or metastable state (process #5). For this process, a flash lamp pumped dye-laser will be used which is tunable in the entire visible range of the spectrum. The laser is a Phase-R laser, model DL-2100B, with an output energy of 5 J and a pulse duration of 500 ns, corresponding to a maximum power of 10 MW. To provide for short decay times of the laser pulse a chopping device is used, which allows us to cut parts out of the laser pulse, with chopping times in the order of 10 ns.

d) Diagnostics

It is planned to measure the discharge current by measuring the voltage drop across a set of carbon resistors in series with the water resistor. Voltage measurements will be performed between the closing switch and the discharge chamber and at the current controlling water resistors.

For voltage measurements, two types of voltage dividers were designed and tested:

a) A purely resistive divider, similar to the one which is used in the electron beam controlled switch (see Section B)

b) A capacitive-resistive divider. Both voltage dividers are connected to water resistors which serve as a first stage, resistive voltage divider.

Fig. 11 shows the capacitive-resistive divider with test results. The risetime of the monitor pulse is proportional to the resistance of the water times the series capacitance in the capacitive voltage devider. For a water resistor of R_w = 50 Ω and a capacitance C = 24 pF the risetimes is approximately 2 ns.

D. OTHER OPENING SWITCH CONCEPTS

1. Optical Control of Excess Carrier Lifetime in Solids (W.M. Portnoy)*

a) Introduction

The possibility of developing a solid-state, optically controlled opening switch has been considered. The operation is somewhat analogous to the optically controlled,gaseous switches we discussed in Section D. The basic features of such a switch are described.

b) Discussion

Recombination of excess carriers in silicon occurs by two important mechanisms: via transitions to intermediate deep levels, or through band-to-band processes, in which the energy of the recombining hole-electron pair is taken up by a third carrier which is excited to a more energetic state in the energy band structure. Such band-to-band, or Auger, recombination, is a third-order process, inasmuch as three carriers are involved, whereas recombination by way of traps is a first-order process. In power semiconductor switches, where injected carrier densities exceed background concentrations and charge neutrality is valid, the effective recombination rate can be represented by

---

* Dept. Elec. Engr., Texas Tech University

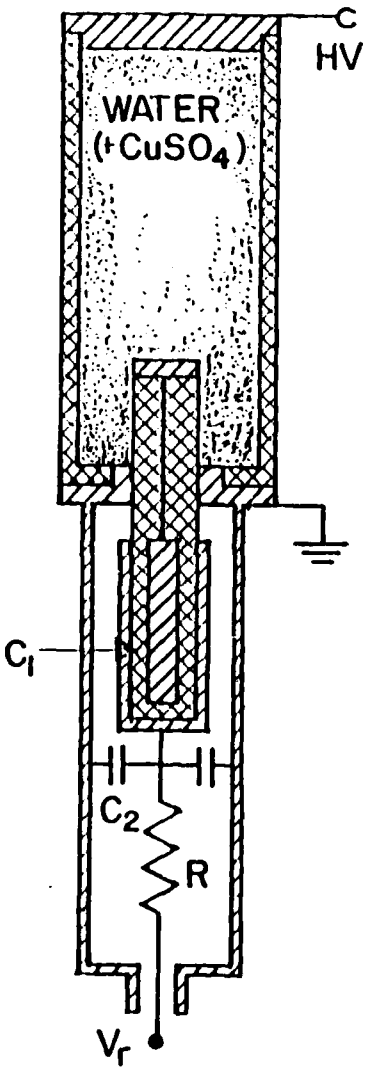

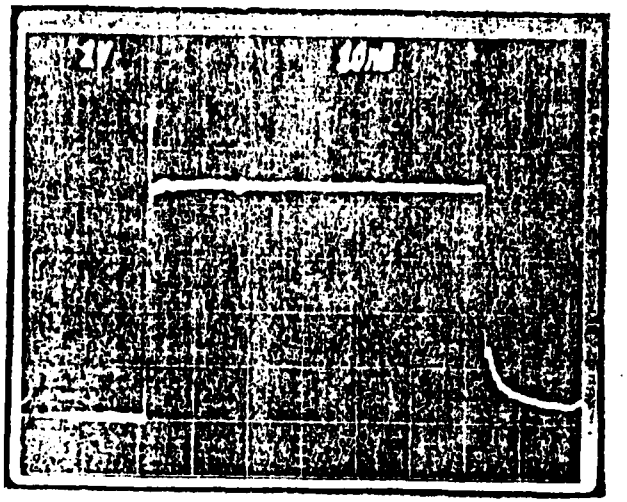

TEST PULSE

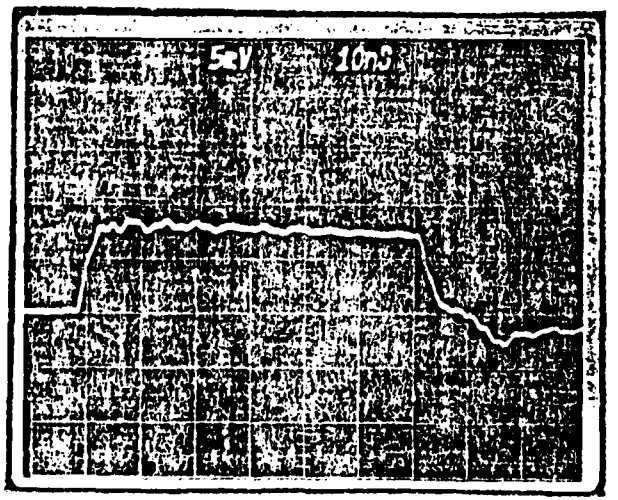

MONITOR PULSE

DIVIDER RATIO
HV/V_r = GOOD

Fig. 11 Voltage Probe with Test Results

$$R = \gamma_1 n + \gamma_3 n^3$$

where n is the average injected carrier density. At low to moderate injected carrier concentrations (low-level), the effective lifetime is dominated by the first-order term, hence by deep traps. At very high injected carrier concentrations (high-level), the third order term is more important, unless γ_1, which depends on the density of deep recombination centers, is large.

During forward conduction in a semiconductor switch, the injected carrier density in the switch base region, which is lightly doped to obtain a high blocking voltage, greatly exceeds the background doping density. The effectiveness of the conductivity modulation is determined by the diffusion length, so that the forward voltage drop, and forward power dissipation, is governed by the high level lifetime in the base region. When the device is switched off, part of the excess charge in the base is removed initially by reverse current which flows before a depletion region forms at the injection junction. After a reverse voltage begins to build up at the depletion region, further excess carrier removal proceeds by recombination. This recombination occurs late in the reverse recovery process, so that excess carrier decay occurs predominately at low levels, and turn-off time is controlled by the low level lifetime in the base. Ideally, for lowest forward drop and fastest turn-off, a high density of recombination centers should be introduced during turn-off and removed during forward conduction. This is not possible in a real device, so that a compromise between forward voltage drop and turn-off time is conventionally obtained by adjusting the lensity of deep-lying (lifetime killer) states, usually introduced by gold-doping.

The effectiveness of a recombination center depends on its capture cross section, which is related to its charge state, or occupation. It is then possible, in principle, to alter the effectiveness of deep traps as recombination sites by changing their occuption by appropriate photo-excitation. As an example, a deep acceptor-type trap (such as gold) will capture electrons from the conduction band and the negatively charged acceptor will have a large capture cross section for holes. As soon as a hole is trapped on a site, an electron from the conduction band will drop into the center, and recombination takes place. If the traps are kept empty by photoexcitation of trapped electrons back to the conduction band during the on-state state of the switch, recombination is inhibited; when the switch is turned off, excitation is stopped, the traps become effective and turn-off proceeds rapidly. There are several problems associated with this phenomenon which will require examination. For example, typical n-bases in high power switches are doped with phosphorus to around 5×10^{14} cm^{-3}. A gold concentration of about 8×10^{15} cm^{-3} is required for a 10 ns lifetime, so that considerable compensation can take place, increasing the resistivity, hence the forward drop and also the possibility of punch-through and a possible reduction in blocking voltage. This relationship, and the general effect of concentrations of deep traps high with respect to background doping levels must be considered. Some of these effects may be compensated by a suitable choice of energy of the deep trap; there are many possible useful dopants in this respect.

2. Sheath-Controlled Low Pressure Discharges as Opening Switches

Techniques as developed in the semiconductor technology can often be applied to low pressure discharges if slightly modified. Processes which determine the behavior of Field Effect Transistors (FET) are probably usable to control the conductance of low pressure wall-stabilized gas discharges, if the ion mobility can be neglected.

In a junction FET the resistance of the device is controlled by varying the depletion region of two reversed biased junctions (Fig.12), which determine the size of a conducting channel. Control is performed by variation of drain-source voltage and gate voltage (Fig.13). A similar effect, namely control of resistance by variation of wall-sheath thickness should be possible in wall-stabilized discharges using an auxiliary electrode transverse to the discharge column (Fig.14). Using Poisson's equation the voltage V_p necessary to deplete the entire plasma column of electrons is given by

$$V_p = \frac{q}{2\varepsilon_o} n_e \left(\frac{d}{2}\right)^2$$

where d is the wall to wall distance and $n_e = n_i$ the density of electrones and ions, respectively. For $n_i = 10^{14}\ cm^{-3}$ and $d = 0.2$ mm, $V_p \simeq 10$ kV. The voltage V_p is identical with the gate voltage only as long as the voltage drop between cathode and anode is small compared to the gap voltage. In opening switches large voltages across the switch are generated. In this case, the voltage necessary to deplete the plasma column so that the sheet region covers the entire discharge volume is gate voltage plus switch voltage.

To operate low pressure discharges in a high current mode, one possibility is to use a large number of small diameter discharge channels (Fig.15). The capacitance of such a system of channels may be rather high, in the order of nF. To provide for fast control, that means fast opening, the gate pulse has to be applied in times of nanoseconds. Fast voltage across the system capacitance probably can be obtained by using a stripline with low impedance.

It should be possible to calculate such systems using models such as developed for semiconductor devices. One important difference, however, between FET and low pressure discharges is the fact that in discharges the remaining charge carriers in the "depleted" discharge column are mobile ions. Their mobility is smaller than that of electrons but negligible only for times small compared to the drift time.

So far these considerations are only relying on analogy consideration. To prove the feasibility of such concepts, which may include other FET-technologies (e.g. MOSFET, corresponding to gas discharges with an auxiliary electrode coupled capacitively to the plasma) careful studies are necessary.

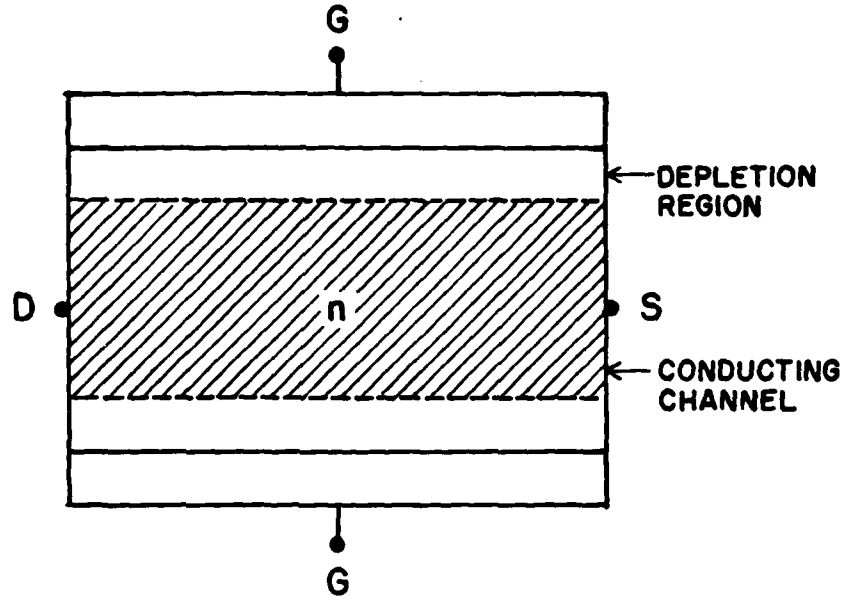

Fig. 12 Simplified Cross-Sectional View of a Junction FET

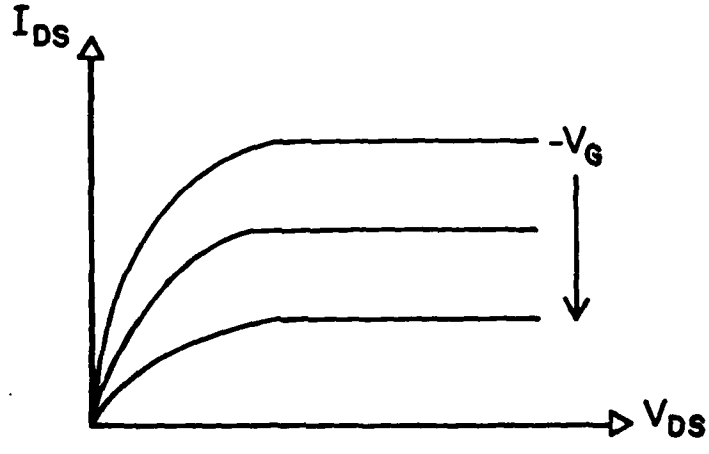

Fig. 13 Characteristic Current-Voltage Curves for a JFET

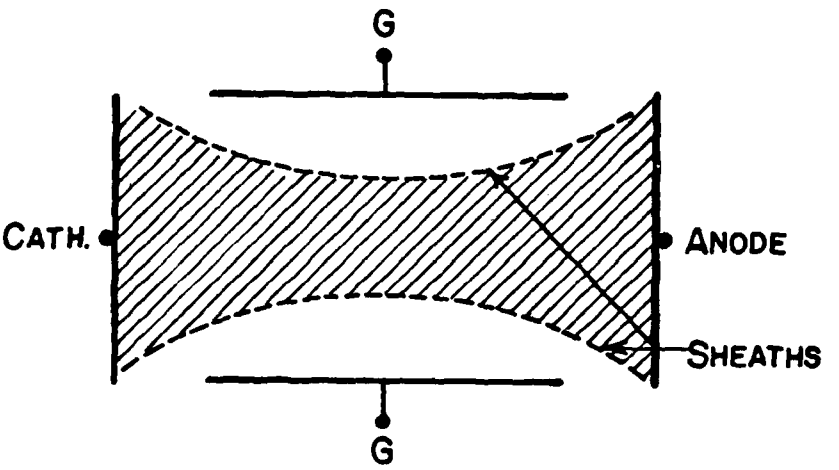

Fig. 14 Simplified Cross-Sectional View of a Sheath-Controlled Gas Discharge

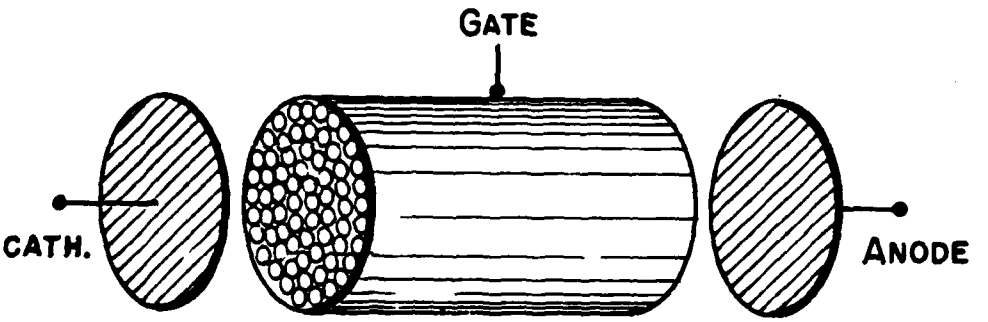

Fig. 15 Example for a Functional Design of a Sheath-Controlled Discharge

E. REFERENCES

1. B.M. Kovaltchuk and G.A. Mesyats, Proc. of 1st International Pulsed Power Conf., Lubbock, Texas (1976), paper 1C-7

2. R.O. Hunter, Proc. of 1st International Pulsed Power Conf., Lubbock, Texas (1976), paper 1C-8.

3. R.F. Fernsler, D. Conte, and I.M. Vitkovitsky, IEEE Trans. on Plasma Science, PS-8, 76 (1980).

4. J.W. Dzimianski and L.E. Kline, Aero Propulsion Lab, Rept. DYD-55585-AA (1979).

5. G.A. Thioahanis, J.H. Jacob and S.J. Sackett, Avco-Everett Rept. F29601-73-C-0116.

6. C.L. Chen and P.J. Chantry, J. Chem. Phys. 71, 3879 (1979).

7. W.L. Morgan and M.J. Proud, 33rd Gaseous Electronics Conf., Norman, Okla. Oct. 1980, Abstract FB-3.

8. J.N. Bardsley, private communication.

9. D. Lorentz and L. Lee, private communication.

10. T.W. Dakin, G. Luxa, G. Opperman, J. Vigreux, G. Wind and H. Winkelnkemper, Electra 32, 61 (1974).

11. H.C. Harjes, K.H. Schoenbach, M. Kristiansen, A.H. Guenther and L.L. Hatfield, IEEE Trans. on Plasma Science, PS-8, 170 (1980).

12. J. Koppitz, J. Phys. D6, 1454 (1973).

JOURNAL PAPERS AND CONFERENCE PROCEEDINGS PAPERS, 1979-81

(Published with AFOSR/ARO Support)

1. E. Chu, R. Druce, M. Kristiansen, M. Hagler, and R. Bengston, "Beat Heating in Plasmas Using CO_2 Lasers", Journal de Physique, Colloque C7, supplement No. 7, 40, C7-747, (1979).

2. K. McDonald, M. Newton, E. Kunhardt, M. Kristiansen, and A.H. Guenther "An Electron beam Triggered Spark Gap", IEEE Transactions on Plasma Science, PS-8, 181 (1980).

3. S. Levinson, E. Kunhardt, M. Kristiansen, and A.H. Guenther, "Simulation of Inductive and Electromagnetic Effects Associated with Single and Multichannel Triggered Spark Gaps", Proc. 2nd IEEE International Pulsed Power Conference, Lubbock, Texas, 433, (1979).

4. K. McDonald, M. Newton, E.Kunhardt, M. Kristiansen, and A.H. Guenther, "An Electron-Beam-Triggered Spark Gap", Proc. 2nd IEEE International Pulsed Power Conference, Lubbock, Texas,437 (1980).

5. M. Newton, K. McDonald, E. Kunhardt, M. Kristiansen, and A.H. Guenther, "Applications of Electron Beams for Precise Switching of High Voltages", Proc. 3rd International Topical Conference on High Power Electron and Ion Beam Research and Technology, Novosibirsk, USSR, 1979.

6. M. Kristiansen and A.H. Guenther, "Digest of Technical Papers", 2nd IEEE International Pulsed Power Conference, Lubbock, Texas.

7. M. Kristiansen and B. Miedzinski, "Investigations of Reed Switch Dynamics When Switching Heavy Loads", Proc. 10th International Conf. Contact Phenomena, Bucharest, Hungary, Aug. 25-29, 1980.

8. R.J. Crumley, P.F. Williams, M. Gundersen and A. Watson, "Electron Densities in Laser-Triggered Spark Gap Discharges", Proc. 2nd IEEE International Pulsed Power Conference, 119 (1979).

9. R.J. Crumley, P.F. Williams, and M. Gundersen, "Studies of the Basic Processes Responsible for Laser-Triggered Breakdown in Gases", Journal de Physique, Colloque C7, Supplement No. 7, 40, 27-305 (1979).

10. R.J. Crumley, P.F. Williams, and M. Gundersen, "Temporal Behavior of Electron Densities in Laser-Triggered Gaps", IEEE Trans. Plasma Sci., PS-8, 164 (1980).

11. *E. Kunhardt and W.W. Byszewski, "Development of Overvoltage Breakdown in High Pressure Gases", Physical Review, A, 21, 2069 (1980).

12. J.P. Craig, "Multi-Megajoule Energy Storage and Conversion Device", Proc. Conf. on Electromagnetic Guns and Launchers, San Diego, CA, Nov. 1980.

---

*Also partially supported by NSWC.

13. IEEE Trans. Plasma Science, Special Issue on Plasma Switches, Sept., 1980, A.H. Guenther and M. Kristiansen, Guest Editors.

14. R.L. Druce, M. Kristiansen, and M.O. Hagler, "An Experimental and Numerical Investigation of Laser-Plasma Interactions", submitted to Journal of Applied Physics.

15. K.H. Schoenbach, G. Schaefer, E.E. Kunhardt, M. Kristiansen, L.L. Hatfield, and A.H. Guenther, "An Optically Controlled Diffuse Discharge Switch", Proc. 3rd IEEE International Pulsed Power Conference, Albuquerque, N.M., June 1981. (Invited Paper)

16. Y.H. Tzeng, E.E. Kunhardt, M. Kristiansen and A.H. Guenther, "The Effect of Electron Beam Induced Space sharge on Spark Gap Breakdown", Proc. 3rd IEEE International Pulsed Power Conference, Albuquerque, N.M., June 1981. (Invited Paper)

17. M. Kristiansen, A.H. Guenther, J. Ungvarsky, F.C. Brockhurst, R.D. Franklin, A.K. Hyder and R.L. Gullickson, "Modular Instructional Material in Pulsed Power Technology", Proc. 3rd IEEE International Pulsed Power Conference, Albuquerque, N.M., June 1981.

18. H.C. Harjes, E.E. Kunhardt, M. Kristiansen, L.L. Hatfield and A.H. Guenther, "Space Charge Effects in a Laser-Fiber Optics Triggered Multichannel Spark Gap", Proc. 3rd IEEE International Pulsed Power Conference, Albuquerque, N.M., June 1981.

19. B.H. Dunlap and J.P. Craig, "Time Varying Inductors for Electromechanical Pulsers", Proc. 3rd IEEE International Pulsed Power Conference, Albuquerque, N.M., June 1981.

20. L.B. Gordon, M.O. Hagler, M. Kristiansen and H.C. Kirbie, "Investigations of a 60 KV, 5 CM Spark Gap for Several Electrode, Insulator, and Gas Types", Proc. 3rd IEEE International Pulsed Power Conference, Albuquerque, N.M., June 1981.

21. G.L. Jackson, Kai-Chi Yuan, L.L. Hatfield and M. Kristiansen, "Surface Damage of Dielectrics in a Spark Gap", Proc. 3rd IEEE International Pulsed Power Conference, Albuquerque, N.M., June 1981.

22. K.H. Schoenbach, G. Schaefer, H.C. Harjes, G. Leiker, and M. Kristiansen, "Opening Switches", Proc. 3rd IEEE International Pulsed Power Conference, Albuquerque, N.M., June 1981.

21. S. Dhali and P.F. Williams, "Multiphoton Ionization - A Potential Trigger and/or Control for Electrical Breakdown", Proc. 3rd IEEE International Pulsed Power Conference, Albuquerque, N.M., June 1981.

22. M. Kristiansen, et. al., "Report of Workshop on Repetitive Opening Switches", Proc. 3rd IEEE International Pulsed Power Conference, Albuquerque, N.M., June 1981. (Invited Paper)

23. K. Schoenbach, G. Schaefer, M. Kristiansen, L.L. Hatfield, and A.H. Guenther, "Diffuse Discharge Opening Switches", Proc. NATO Advanced Study Institute: Electrical Breakdown and Discharges in Gases, Les Arcs, France, July 1981.

24. M. Kristiansen and A.H. Guenther, "Plasma Applications" Proc. NATO Advanced Study Institute: Electrical Breakdown and Discharges in Gases, Les Arcs, France, July 1981.

25. B. Miedzinski and M. Kristiansen, "Investigations of Reed Switch Dynamics and Discharge Phenomena When Switching Intermediate and Heavy Loads", accepted for publication in IEEE Trans. on Components, Hybrids and Manf. Technology, 1981.

26. Proceedings of Workshop on "Repetitive Opening Switches", Tamarron, Colorado, January 1981, M. Kristiansen and K.H. Schoenbach, Editors.

27. K.H. Schoenbach, M. Kristiansen, E.E. Kunhardt, L.L. Hatfield, and A.H. Guenther, "Exploratory Concepts of Opening Switches", Proc. Workshop on Repetitive Opening Switches, Tamarron, Colorado, January 1981, p 65.

28. S.K. Dahli and P.F. Williams, "Multiphoton Ionization Efficiency in Xe", Submitted to Appl. Phys. Lett., 1981.

INTERACTIONS

(Oct. 1, 1980 - Sept. 30, 1981)

a) Papers Presented

1. J.P. Craig, "Multi-Megajoule Energy Storage and Conversion Device", Conference on Electromagnetic Guns and Launchers, San Diego, CA, November 1980.

2. E.E. Kunhardt, "Development of Overvoltage Breakdown at High Gas Pressure", and "Nanosecond-Pulse Breakdown in Gases at High Overvoltages", 33rd Gaseous Electronics Conference, Norman Oklahoma, October, 1980.

3. P.F. Williams, M.A. Gundersen and A. Watson, "Pre-Spark Channel Phenomena in Laser-Triggered Breakdown", 33rd Gaseous Electronics Conference, Norman, Oklahoma, October 1980.

4. S.R. Dhali, R.J. Crumley, P.F. Williams, E.E. Kunhardt, and M.A. Gundersen, "Electron Densities in Laser-Triggered Hydrogen Sparks", 33rd Gaseous Electronics Conference, Norman, Oklahoma, October 1980.

5. R.J. Crumley, P.F. Williams, and M. Gundersen, "Studies of the Basic Processes Responsible for Laser-Triggered Breakdown in Gases", 14th International Conference Phenomena in Ionized Gases, Grenoble, France, 1979.

6. K.H. Schoenbach, G. Schaefer, E.E. Kunhardt, M. Kristiansen, L.L. Hatfield, and A.H. Guenther, "An Optically Controlled Diffuse Discharge Switch", 3rd IEEE International Pulsed Power Conference, Albuquerque, N.M., June 1981.

7. Y.H. Tzeng, E.E. Kunhardt, M. Kristiansen, and A.H. Guenther, "The Effect of Electron Beam Induced Space Charge on Spark Gap Breakdown", 3rd IEEE International Pulsed Power Conference, Albuquerque, N.M., June 1981.

8. M. Kristiansen, A.H. Guenther, J. Ungvarsky, F.C. Brockhurst, R.D. Franklin, A.K. Hyder and R.L. Gullickson, "Modular Instructional Material in Pulsed Power Technology", 3rd IEEE International Pulsed Power Conference, Albuquerque, N.M., June 1981.

9. H.C. Harjes, E.E. Kunhardt, M. Kristiansen, L.L. Hatfield, and A.H. Guenther, "Space Charge Effects in a Laser-Fiber Optics Triggered Multichannel Spark Gap", 3rd IEEE International Pulsed Power Conference, Albuquerque, N.M., June 1981.

10. B.H. Dunlap and J.P. Craig, "Time Varying Inductors for Electromechanical Pulsers", 3rd IEEE International Pulsed Power Conference, Albuquerque, N.M., June 1981.

11. L.B. Gordon, M.O. Hagler, M. Kristiansen and H.C. Kirbie, "Investigations of a 60 KV, 5 CM Spark Gap for Several Electrode, Insulator, and Gas Types", 3rd IEEE International Pulsed Power Conference, Albuquerque, N.M., June 1981.

12. G.L. Jackson, Kai-Chi Yuan, L.L. Hatfield and M. Kristiansen, "Surface Damage of Dielectrics in a Spark Gap", 3rd IEEE International Pulsed Power Conference, Albuquerque, N.M., June 1981.

13. K.H. Schoenbach, G. Schaefer, H.C. Harjes, G. Leiker, and M. Kristiansen, "Opening Switches", 3rd IEEE International Pulsed Power Conference, Albuquerque, N.M., June 1981.

14. S. Dhali and P.F. Williams, "Multiphoton Ionization - A Potential Trigger and/or Control for Electrical Breakdown", 3rd IEEE International Pulsed Power Conference, Albuquerque, N.M., June 1981.

15. K. Schoenbach, G. Schaefer, M. Kristiansen, L.L. Hatfield, and A.H. Guenther, "Diffuse Discharge Opening Switches", NATO Advanced Study Institute: Electrical Breakdown and Discharges in Gases, Les Arcs, France, July 1981.

16. M. Kristiansen, et. al., "Report of Workshop on Repetitive Opening Switches", 3rd IEEE International Pulsed Power Conference, Albuquerque, N.M., June 1981.

17. M. Kristiansen and A.H. Guenther, "Plasma Applications", NATO Advanced Study Institute: Electrical Breakdown and Discharges in Gases, Les Arcs, France, July 1981.

18. M. Kristiansen, "Review of the 3rd IEEE International Pulsed Power Conference", Institute Nuclear Physics, Novosibirsk, USSR, July 1981.

19. M. Kristiansen, "Pulsed Power Technology", Presented at:
    1) Chinese Academy of Science, Peking, PRC, November 1980.
    2) Plasma Research Center, Heifei, PRC, November 1980.
    3) Bahba Atomic Research Center, Bombay, India, December 1980.
    4) Physical Research Center, Ahmedabad, India, December 1980.
    5) Indian Institute of Science, Bangalore, India, December 1980.

20. K.H. Schoenbach, "Opening Switches", Air Force/Texas Tech Pulsed Power Lecture Series, July 23, 1981, Wright-Patterson Air Force Base, Ohio; July 24, 1981, Kirtland Air Force Base, Albuquerque, N.M.

21. M. Hagler, "Gas Insulated Spark Gaps", Air Force/Texas Tech Pulsed Power Lecture Series, June 11, 1981, Wright-Patterson Air Force Base, Ohio; June 12, 1981, Kirtland Air Force Base, N.M.

22. W.M. Portnoy, "Solid State Switching", Air Force/Texas Tech Pulsed Power Lecture Series, February 19, 1981, Wright-Patterson Air Force Base, Ohio; February 20, 1981, Kirtland Air Force Base, N.M.

23. E.E. Kunhardt, "Gas Breakdown", Air Force/Texas Tech Pulsed Power Lecture Series, January 22, 1981, Wright-Patterson Air Force Base, Ohio; January 23, 1981, Kirtland Air Force Base, N.M.

24. M. Kristiansen, "The AFOSR/ARO Supported "Coordinated Research in Pulsed Power Physics" at Texas Tech University", Navy PUPTAG Meeting, Los Alamos National Laboratory, February 1981.

b. Consultative and Advisory Functions

1. Prof. M. Kristiansen coordinates the AFOSR sponsored Pulsed Power Lecture Series together with Dr. A.H. Guenther of the Air Force Weapons Lab and Professors E. Kunhardt, M. Hagler, K. Schoenbach, and W.M. Portnoy have lectured in this series at the AFWL and WPAFB.

2. Prof. M. Kristiansen served as a consultant to NASA on space plasmas on Oct. 8-10, 1980 at Goddard Space Flight Center, MD.

3. Prof M. Kristiansen was appointed to the Air Force Scientific Advisory Board and attended the orientation meeting at the Pentagon on Sept. 15, 1981 and the Fall meeting at Eglin Air Force Base, FL, on Nov. 4-5, 1981.

4. Professors E. Kunhardt and M. Kristiansen served on the organization Committee for the 1981 NATO Advanced Study Intsitute on Gas Breakdown together with Dr. A.H. Guenther, AFWL, and Mr. L. Luessen, NSWC.

5. Professors M. Kristiansen and K.H. Schoenbach organized a Workshop on Repetitive Opening Switches for the USARO at Tamarron, CO on January 29-30, 1981.

6. Professor M. Kristiansen serves as a Visiting Staff Member at Los Alamos National Laboratory and supervises a Ph.D. Thesis program on repetitive opening switches, conducted by one of their staff members.

c. Other Interactions

1. The following visits were made to Sandia National Laboratories for the purpose of discussing common pulsed power rese ch problems with the Sandia Pulsed Power Research Group:

   a) Aug. 18, 1981: Dr. M. Kristiansen and Mr. C. Harjes
   b) Aug. 14, 1981: Dr. P.F. Williams (also Los Alamos National Labs)
   c) Sept.24, 1981: Dr. M. Hagler and Mr. A. Donaldson

2. Professor M. Kristiansen and Mr. C. Harjes visited the Naval Surface Weapons Center at White Oaks, MD on Sept. 13-14, 1981 to discuss electron beam opening switches with Dr. E. Nolting. Mr. Harjes also visited NRL on Sept. 15, 1981 to discuss opening switches with Mr. I. Vitkovitsky and Dr. Kristiansen visited the Naval Surface Weapons Center at Dahlgren, VA on Sept. 15, 1981 to discuss magnetic switching and gas spark gap switching with Dr. Frank Rose and others.

3. Dr. A. Guenther from the AFWL and Dr. A. Engelhardt from LANL served on Ph.D. committees for our graduate students.

4. Professors K.H. Schoenbach and G. Schaefer visited the subcontractor, SRI, International, on January 11-14, 1981 and discussed their work with Dr's. L. Lee and D. Lorents.

5. Dr. L. Lee from SRI, International visited Texas Tech University on November 5-17, 1980 to discuss the selection of suitable gases for diffuse discharge opening switches.

6. Prof. J. Moseley of the University of Oregon visited Texas Tech University on May 21-22, 1981 to discuss future cooperation concerning experimental determination of various basic data needed for our work.

7. Prof. M. Kristiansen met with General R. Mathis in the Pentagon on Sept. 14, 1981 to discuss Air Force educational programs.

8. M. Kristiansen attended the NRL Review of Homopolar Generator Research in Washington, D.C. on April 30, 1981.

9. A special meeting of leading expects on gas discharges was called at Texas Tech University on September 23-24, 1981. The purpose of the meeting was to seek possible cooperative research efforts and define needed research areas for repetitive opening switch development. A summary of the meeting and a list of the attendants is given at the end of this report,in the Appendix.

ADVANCED DEGREES AWARDED (1980-81)

1. Alex K. Auyeung, "A Computer Based Data Acquisition System for Fast Pulsed Power Experiments", MSEE Thesis, 1981.

2. S.K. Dhali, "Muliphoton Ionization Spectroscopy in Xe", MSEE Thesis, 1981.

3. George L. Jackson, "Ultraviolet Radiation Damage to Dielectrics in Spark Gaps", MSEE Thesis (Physics), 1981.

4. Kenneth F. McDonald, "An Electron Beam Triggered Spark Gap", MSEE Thesis, 1981.

5. Yonhua Tzeng, "The Effect of Space Charge Induced by an Electron Beam on Spark Gap Operation", MSEE Thesis, 1981.

6. Kai-Chih Yuan, "Ellipsometric Studies of Surface Damage on Dielectrics", MSEE Thesis, 1981.

APPENDIX

Summary of Meeting On

"Diffuse Discharge Opening Switches"

K. Schoenbach and M. Kristiansen

A meeting on "Basic Processes in Diffuse Discharge Opening Switches" was held in Lubbock on September 23-24, 1981. It brought together 20 atomic and plasma physicists and electrical engineers. The goal of the meeting, set up especially to discuss the opening switch concepts developed at Texas Tech, was:

a) to identify the limitations of diffuse discharge switch concepts

b) to identify the unresolved problems

c) to identify research areas that must be supported to resolve the problems

d) to identify where the needed research expertise resides

e) to establish cooperative, coordinated research efforts.

The meeting was opened with a brief review on the state-of-the-art of repetitive opening switches with special emphasis on concepts developed at Texas Tech. Discussion sessions on "Production of High Pressure Diffuse Discharges", "Optical Control of Diffuse Discharges", "Basic Data" and "Diffuse Discharge Modeling" followed. The results of the discussions were summarized in a final session:

1. Limitations on current density and time of conduction in atmospheric pressure diffuse discharges are due to instabilities which are mainly developing on the electrode surface. To prevent instabilities or, at least, to delay their onset, the establishment of a high uniformity of pre-ionization and electric field in the gap and of the controlling e-beam or laser power has to be attempted. With respect to the applications as rep-rated switches, where excessive

heating of the gas must be avoided, gas exchange systems have to be considered.

2. The conditions for gas mixtures, usable in attachment dominated diffuse discharge switches are:

   a) High mobility at low E/N

   b) Low attachment rate at low E/N

   c) High attachment rate at high E/N

   d) High dielectric strength

   Whereas agreement on these general features existed, the opinion about the "best" gases differed. As appropriate attachers for opening switches NO, N_2O, I_2, some halogenated hydro-carbons, and HCl in buffer gases like N_2, CH_4, and noble gases were considered. Basic data for commonly used gases (N_2, noble gases) are fairly complete, whereas they are limited for the other gases. Predictions about the behavior of gas mixtures containing ions, radicals, and excited molecules, however, (a research object of plasma chemistry) are rather vague for most opening switch gas mixtures. It is therefore important to increase the appropriate plasma chemical investigations.

3. An effort which should also be increased is modeling of diffuse discharges in diverter circuits. Rate equation codes and Boltzmann equation codes are available or under development. A major obstacle for using the codes in opening switch calculations is the lack of data for appropriate gases. Experiment-theory comparisons could fill gaps in the data base.

4. Generally, the importance of experiments for both e-beam and optically controlled diffuse discharges was emphasized together with development of fast diagnostic techniques. Special atten-

tion should be payed to experimental investigations of laser induced effects (opto-galvanic effects).

To proceed in the field of diffuse discharge opening switches further interaction of the three communities present at this meeting (scientists, engineers, "appliers") was highly recommended.

List of Attendees:

M.A. Biondi	University of Pittsburgh
P. Chantry	Westinghouse Research Lab
L.G. Christophorou	Oak Ridge National Laboratory
D.H. Douglas-Hamilton	Avco Everett Research Lab
A. Garscadden	Air Force Wright Aeronautical Laboratories
A.H. Guenther	Air Force Weapons Laboratory
B.D. Guenther	U.S. Army Research Office
A.K. Hyder	Air Force Office of Scientific Research
B. Junker	Office of Naval Research
L.E. Kline	Westinghouse Research Lab
J.E. Lawler	University of Wisconsin
W.H. Long, Jr.	Northrop Research and Technology Center
J.T. Mosely	University of Oregon
A.V. Phelps	Joint Institute for Laboratory Astrophysics
L. Pitchford	Sandia National Laboratories
M.F. Rose	Naval Surface Weapons Center
G. Schneider	Air Force Wright Aeronautical Laboratories
M. Kristiansen	Texas Tech University
E.E. Kunhardt	" " "
G. Schaefer	" " "
K. Schoenbach	" " "